HIGH PRESSURE: A CHALLENGE FOR LAB-ON-A-CHIP TECHNOLOGY

This research has been supported by the Dutch Technology Foundation STW, applied science division of NWO, and by NanoNed, a national nanotechnology program coordinated by the Dutch Ministry of Economic Affairs.

Benito López, Fernando
High Pressure: a Challenge for Lab-on-a-Chip Technology, Ph.D. thesis, University of Twente, Enschede, The Netherlands
ISBN 978-90-365-2482-7

Publisher: Wöhrmann Print Service, Zutphen, The Netherlands

Cover design by Fernando Benito López. Front page: microreactor channel (70 μm width), which contains herringbone mixers with <<< design. The picture was taken during a flow behavior study of a mixture of ethanol and liquid carbon dioxide at high pressures and temperatures. Water droplets condensed in between the mixers; herewith it was found out that ethanol was contaminated with water. Never ever an undesirable result was so beautiful to observe. Back page: Bright-red mist pattern of a mixture of ethanol and liquid carbon dioxide at 90 bars and 60 °C in the microreactor channel, which contains herringbone mixers with \\\ design.

HIGH PRESSURE: A CHALLENGE FOR LAB-ON-A-CHIP TECHNOLOGY

PROEFSCHRIFT

ter verkrijging van
de graad van doctor aan de Universiteit Twente,
op gezag van de rector magnificus,
prof.dr. W. H. M. Zijm,
volgens besluit van het College voor Promoties
in het openbaar te verdedigen
op donderdag 5 April 2007 om 13.15 uur

door

Fernando Benito López

Geboren op 30 Mei 1978
te Madrid, Spanje

Dit proefschrift is goedgekeurd door:

Promotor:	Prof.dr.ir. D. N. Reinhoudt
Assistent Promotor:	Dr. W. Verboom

Success is going from failure to
failure without loss of enthusiasm.

Winston Churchill

A mi familia.

Contents

1

General Introduction

The first experiments where elevated pressures were successfully used for a chemical transformation, the acid-catalyzed inversion of sucrose, have been carried out by Röntgen in 1892 using pressures of 500 bar.[1] However, in chemistry elevated pressures were hardly used at that time, mainly because of instrumentation problems. In the twentieth century high pressure became a very important tool for chemical synthesis and analysis. For instance, Carl Bosch and Friedrich Bergius received the Nobel Prize in Chemistry in 1931 for their contributions to high pressure chemical methods, while Percy Williams Bridgman received the Nobel Prize in Physics in 1946 for the invention of an apparatus to produce extremely high pressures up to 100 kbar and for the discoveries he made with it.[2]

Nowadays, high pressure is used for the preparation of new compounds as well as studying organic and inorganic reactions.[3-6] It is particularly useful for controlling/influencing the course of competitive and consecutive reactions[7] as well as improving the chemo-, regio- and stereoselectivity of chemical reactions.[8]

Despite the fact that high pressure techniques have been proven valuable in many fields (*e.g.* materials science, physics and food science), the application of high pressure in chemistry has been limited almost exclusively to academic research. High pressure is usually generated in very sophisticated, expensive and closed systems, thus operations such as mixing or the incorporation of probes for chemical analysis are difficult. In general, it is regarded as a technique that requires specialized equipment with strict safety precautions.

Considering the mentioned disadvantages of high pressure equipment, miniaturization of such systems would be a good alternative, because smaller and portable systems relax safety issues, save costs, materials and increase performances of high pressure systems by integrating miniaturized components.[9] Micro total analysis systems (μTAS)[10-13] have extended the concept of miniaturization to organic chemistry.[14] The benefits of microreactors in chemistry - small systems with high surface-to-volume ratios, high heat and mass transfer rates and operated in continuous flow mode[15,16] - combined with the advantages of high pressure open a bright future for the field of high pressure microreactor technology (Figure 1-1).

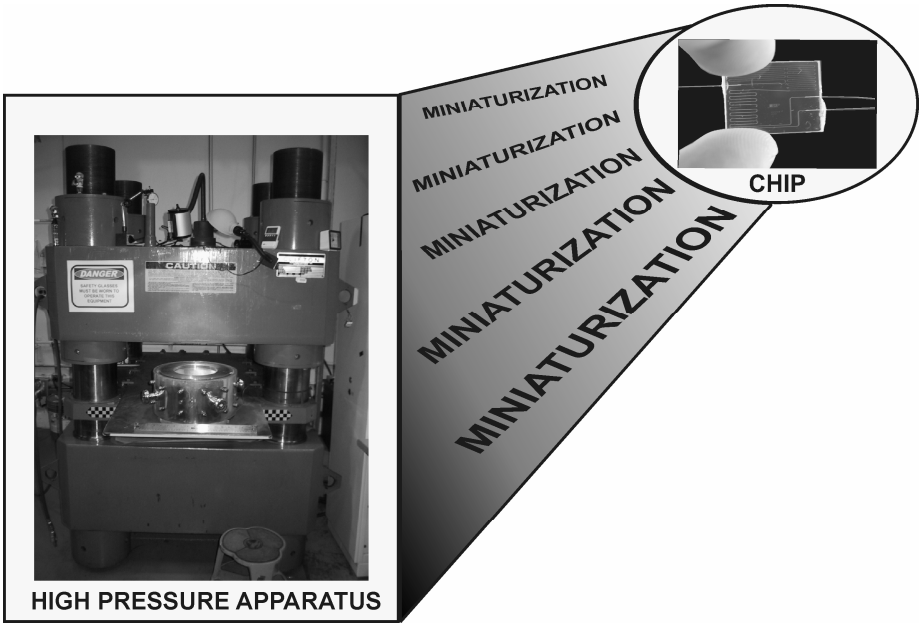

Figure 1-1: Artistic impression of the research described in this thesis.[17]

This thesis contributes to incorporate elevated pressures as a common technique in miniaturized systems. New microreactor-based platforms were developed to perform organic chemistry at high pressure. Systems like capillaries and microreactor chips were designed, fabricated and tested and it was proven that these systems are suitable for studying the influence of pressure on organic reactions. Below an overview of the contents of each Chapter of this thesis is given.

Chapter 2 gives an introduction to high pressure, its effects and the available high pressure instrumentation for organic reactions. On the way to miniaturization, pressure technology is described, going from continuous flow pipes and capillaries to lab-on-a-chip systems.

In Chapter 3 a capillary-based microreactor platform with fiber optics for on-line UV/Vis spectroscopy is discussed. This technique is used to investigate chemical reaction kinetics under pressures up to 600 bar and to determine activation volumes for a number of organic reactions.

Chapter 4 deals with the design, fabrication and performance of several in-plane fiber-based interface geometries to glass microreactor chips for high pressure chemistry.

In Chapter 5 microfluidic high pressure chips are used for studying fluid phase transitions in multi-component mixtures (CO_2-alcohol) under conditions close to the critical point of the mixtures by means of optical microscopy.

Chapter 6 describes the esterification reaction of phthalic anhydride with methanol in a continuous flow microreactor at pressures up to 110 bar as well as using supercritical CO_2 as a co-solvent.

In Chapter 7 a set-up (up to 150 bar) is described, that allows independent sampling of reagents into the microreactor. It is used to study the influence of pressure on the Diels-Alder reactions of cyclopentadiene with methyl-, phenyl- and benzylmaleimides.

In Chapter 8 the fabrication of a microreactor with an integrated microcoil NMR for NMR spectroscopy analysis (60 MHz NMR apparatus) is presented. The rate constant of the imine formation of the reaction of benzaldehyde and aniline is determined with this NMR microreactor operated in a continuous flow mode. This μTAS is meant to be used for on-line monitoring of high pressure organic reactions.

1.1 References

1. Röntgen, W. C., *Ann. Phys. Chem.* **1892**, *45*, 91-97.
2. http://nobelprize.org/nobel_prizes/lists/all/.
3. Jones, R. V.; Godorhazy, L.; Varga, N.; Szalay, D.; Urge, L.; Darvas, F., *J. Comb. Chem.* **2006**, *8*, 110-116.
4. McMillan, P. F., *Chem. Soc. Rev.* **2006**, *35*, 855-857.
5. Ghaziaskar, H. S.; Daneshfar, A.; Calvo, L., *Green Chem.* **2006**, *8*, 576-581.
6. Kotsuki, H.; Kumamoto, K., *J. Synth. Org. Chem. Japan* **2005**, *63*, 770-779.
7. Klärner, F. G.; Wurche, F., *J. Prakt. Chem.* **2000**, *342*, 609-636.
8. Jenner, G., *Tetrahedron* **1997**, *53*, 2669-2695.
9. Thorsen, T.; Maerkl, S. J.; Quake, S. R., *Science* **2002**, *298*, 580-584.
10. Reyes, D. R.; Iossifidis, D.; Auroux, P. A.; Manz, A., *Anal. Chem.* **2002**, *74*, 2623-2636.
11. Auroux, P. A.; Iossifidis, D.; Reyes, D. R.; Manz, A., *Anal. Chem.* **2002**, *74*, 2637-2652.

12. Vilkner, T.; Janasek, D.; Manz, A., *Anal. Chem.* **2004**, *76*, 3373-3385.
13. Dittrich, P. S.; Tachikawa, K.; Manz, A., *Anal. Chem.* **2006**, *78*, 3887-3907.
14. Jähnisch, K.; Hessel, V.; Löwe, H.; Baerns, M., *Angew. Chem., Int. Ed.* **2004**, *43*, 406-446.
15. Ehrfeld, W.; Hessel, V.; Löwe, H., *Microreactors: New Technology for Modern Chemistry*. Wiley-VCH: Weinheim, (Germany), **2000**.
16. Brivio, M.; Verboom, W.; Reinhoudt, D. N., *Lab Chip* **2006**, *6*, 329-344.
17. http://epswww.unm.edu/highp/move.html.

2

High Pressure in Organic Reactions; on the Way to Miniaturization

This Chapter offers an overview of the research area of high pressure organic reactions. In the first part, an introduction to high pressure and its instrumentation for chemical applications is given. Subsequently, the advantages as well as the disadvantages of high pressure over standard laboratory methodologies are described and illustrated by a number of organic reactions. The last part deals with the possibility to miniaturize high pressure systems, going from continuous flow pipes and capillaries to lab-on-a-chip systems.

2.1 Introduction

High pressure is a phenomenon that can be found everywhere in the universe, for example in the deep sea, inside the earth and on other planets.[1,2] From a geological point of view high pressure is the principal parameter in the formation of coal and oil deposits. In the 1950s the use of extreme conditions such as ultra high pressure in material sciences and industry led to the successful preparation of synthetic diamonds, rubies and borazones.[3,4] Figure 2-1 shows a schematic representation of pressure in nature, pressures reached in laboratories and some applications.

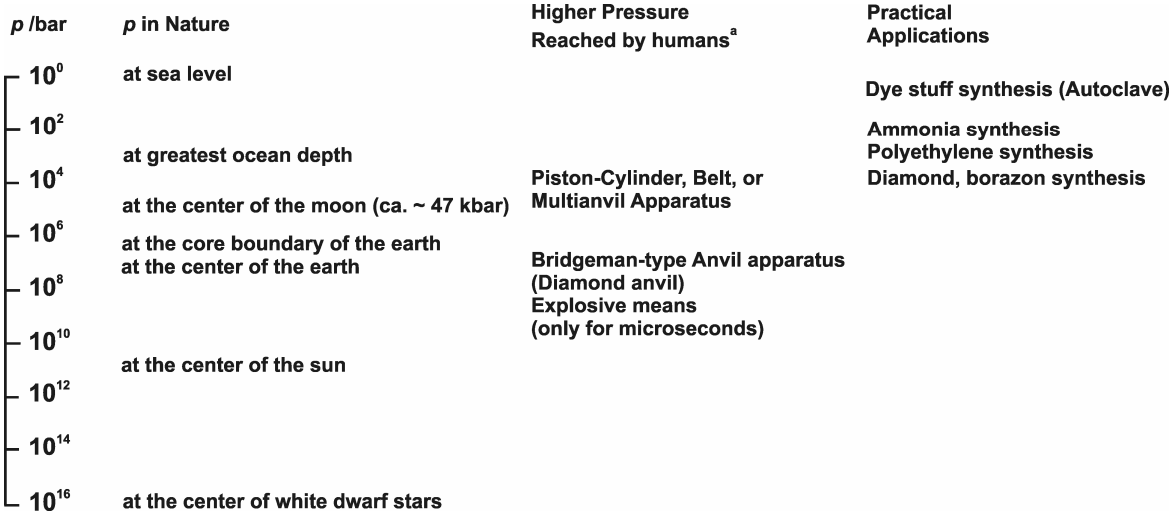

Figure 2-1: Pressures and applications.[1] [a]Other factors such as temperature and inside volume are not considered.

It has been known since the origin of mankind that pressure is a fundamental physical parameter. However, high pressure chemistry is a relatively recent field. The first example of a reaction under pressure, *viz.* the acid-catalyzed inversion of sucrose, has been reported by Röntgen in 1892.[5] Nevertheless, high pressure as a tool in synthetic chemistry was almost not explored, despite its great potential. Until the 1980s, autoclaves were not even commonly used apparatus for high pressure reactions.[6-13]

When a chemical reaction is performed at high pressure, it would be convenient to know the effect of pressure on the electronic, steric, thermal and photochemical properties of the reacting molecules. To optimize chemical reactions it is also important to know how catalysts, phase transfer reagents, sonochemistry,

microwave and solvent-free organic syntheses, are influenced by pressure.[11,12,14] An example is the use of supercritical fluids as alternatives to organic solvents.[15-17]

In the literature the term "high pressure" is used for different conditions. High pressure in organic reactions generally means reactions at 1 - 20 kbar.[18] High pressure in microreactor technology can mean 4 bar.[19] In this Chapter we use the following definitions:

- Ultra high pressures (> 100 kbar). These pressures require special equipments[20] and are used to study, among others, new materials,[21,22] and solid state chemistry.[23,24] In this Chapter this research area is not reviewed, because it is not within the scope of this thesis.
- High pressures (1 - 20 kbar). This pressure range is commonly used for studying the pressure influence on organic reactions (section 2.5.1).
- Medium pressures (20 - 1000 bar). Processes involving heterogeneous catalysts and liquid/gas reactions like hydrogenations are performed in this pressure range in continuous flow operation (section 2.5.2).
- Pressure in microreactors 2 - 80 bar (section 2.5.3).

In this Chapter an overview is given of the instrumentation for high pressure chemistry as well as the most representative and recent examples of organic reactions under these conditions. Finally, pressure at microscale, going from continuous flow systems, tubes and pipes, *via* capillaries to lab-on-a-chip systems will be discussed.

2.2 Pressure in chemistry

2.2.1 General principles

Pressures in the range of 1 - 20 kbar (strongly) influence the rate and equilibrium of many chemical reactions. In general, reactions accompanied by a decrease in volume, such as C-C bond formation, are accelerated by pressure (activation volume $\Delta V^{\neq} < 0$) and the equilibria are shifted towards the side of the products (reaction volume $\Delta V < 0$). Other processes, such as concentration of charge

and ionization, are also accelerated by pressure. Considering these aspects, the reactions in which rate enhancements are expected, when pressure is applied, are the following.[1,25]

- Reactions in which the stoechiometry decreases in the products; *e.g.* cycloadditions and condensations.
- Reactions which proceed *via* cyclic transition states; *e.g.* Claisen and Cope rearrangements.
- Reactions which take place through dipolar transition states; *e.g.* the Menschutkin reaction and electrophilic aromatic substitution reactions.
- Reactions with steric hindrance.

2.2.2 Advantages of pressure in organic chemistry

Like catalysis, microwave or ultrasonic techniques, pressure is considered an efficient tool to overcome the activation barrier of reactions.[26-28] Pressure is a very mild and non-destructive activation method for reactions that at atmospheric pressure either require too high temperatures or are hindered by steric or electronic factors.

As already briefly mentioned in section 2.2.1, pressure affects equilibria and rates in chemical reactions, especially those with a large negative activation volume ($\Delta V^{\neq}$). Rate acceleration is particularly useful in controlling competitive and consecutive reactions.[29] High pressure kinetics is a powerful tool in mechanistic investigation of reactions in solution,[4] for instance in the self-assembly of supramolecular structures.[30]

When the activation volumes of the individual reaction steps for different reaction products are different, high pressure can lead to an improvement of the chemo-, regio- and stereoselectivity.[31] It is also used in multicomponent reactions and combinatorial chemistry, since pressure has no negative effects on the reactivity of resin-bound reactants in solid phase reactions.[32-34]

The application of high pressure has been proven to be advantageous in many catalytic processes, although due to the mechanistic complexity of such reactions it is not easy to predict the net effect of pressure in general terms.[35] The physical properties of matter, such as boiling and melting point, density, viscosity, solubility, dielectric constant, or conductivity, are affected by pressure. The different properties of a solvent at high pressure compared with those at atmospheric conditions have

been used to improve chemical reactions.[36] Ultra high pressure experiments (> 100 kbar) provide new phenomena and materials.[37]

2.2.3 Drawbacks of pressure in organic chemistry

High pressure operation has now reached maturity in scientific fields like food science or separation technology. In chemistry the application of high pressure has been confined almost exclusively to laboratory experiments, although it is possible to find some industrial polymer process where pressure is diary used. One of the reasons is related to the small rate increase in a pressure range between 1 bar and 3 kbar, even for fairly pressure-dependent reactions.

High pressure is usually generated in closed systems *e.g.* autoclaves, thus operations such as mixing or the incorporation of probes for chemical analysis are difficult. Visualization inside a high pressure apparatus is possible only *via* view cells, which are difficult and time consuming to clean, expensive and prone to leakage around the window-cell interface.[38]

In general, high pressure chemistry is regarded as a technique that requires specialized equipment with strict safety precautions. Since explosion damage is approximately proportional to the energy content of the system, which in a pressurized system is basically the product of pressure and volume, large production processes in industry at high pressure are hardly used.

2.2.4 Activation and reaction volume, the main parameters

The effect of pressure on chemical equilibria and reaction rates can be described using thermodynamic principles.[39,40] The relations between pressure (p) and the Gibbs free energy of reaction and activation (ΔG, $\Delta G^{\neq}$, respectively), are the most important parameters (equations (2-1) and (2-2)).

$$\Delta V = \left(\frac{\partial \Delta G}{\partial p}\right)_T = \left(\frac{-\partial \ln K_p}{\partial p}\right)_T \cdot RT \qquad \text{eq. (2-1)}$$

$$\Delta V^{\neq} = \left(\frac{\partial \Delta G^{\neq}}{\partial p}\right)_T = \left(\frac{-\partial \ln k_p}{\partial p}\right)_T \cdot RT \qquad \text{eq. (2-2)}$$

The reaction and activation volumes (ΔV, $\Delta V^{\neq}$) can be determined from the pressure dependence of the equilibrium constant (K) and the rate constant (k), respectively. The effect of pressure on the equilibrium constant of a reaction directly follows the Le Chatelier-Braun principle.[41] If $\Delta V < 0$, upon the application of pressure the equilibrium shifts toward the product (Figure 2-2). These effects are originating from the different influence of pressure on the chemical potentials of the reactants and products (equilibrium), or reactants and transition state (kinetic).

Within the scope of the transition state theory,[42] the activation volume ($\Delta V^{\neq}$) can accordingly considered to be a measure of the partial molar volume of the transition state with respect to the partial molar volumes of the reactants. These can be determined, together with ΔV, from the pressure dependence of the equilibrium constant and rate constant, respectively.[43] ΔV also corresponds to the difference between the partial molar volumes of reactants and products and is usually determined experimentally. The activation and reaction volumes are itselves pressure-dependent.[44] Therefore, several empirical equations are employed to fit the pressure dependencies of rate and equilibrium constants.[45] In general, $\Delta V^{\neq}$ and ΔV are constituted from intrinsic factors as well as solvation components (equations (2-3) and (2-4)).

$$\Delta V^{\neq} = \Delta V_{\text{int}}^{\neq} + \Delta V_{solv}^{\neq} \qquad \text{eq. (2-3)}$$

$$\Delta V = \Delta V_{\text{int}} + \Delta V_{solv} \qquad \text{eq. (2-4)}$$

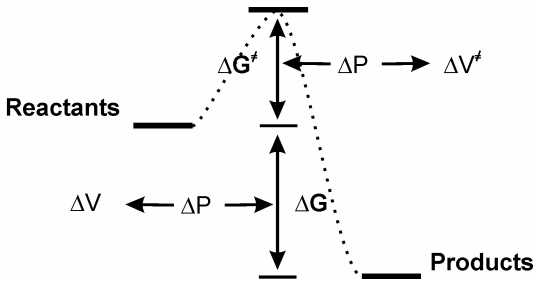

Figure 2-2: Reaction free energy profile: effect of pressure on free energies.[18]

The intrinsic volumes of a ground or transition state are defined by the space occupied by the Van der Waals spheres and can be calculated from the cartesian coordinates of the molecular structure resulting from experimental data, molecular mechanics, or quantum mechanical calculations and from the Van der Waals radii of the different types of atoms derived from crystallographic data.[46] They can also be calculated from the group contribution tables like those published by Bondi in 1964.[47]

The solvation effect is significant in reactions in which there is a change in charge or the polar character in forming the activated complex. All these processes give rise to a decrease or an increase of $\Delta V^{\neq}$ or ΔV.

Sometimes $\Delta V^{\neq}_{solv}$ or ΔV_{solv} can be estimated using the Drude-Nernst equation (eq. (2-5)), which describes the relation between the electrostriction volume ($\Delta V^{\neq}_{solv}$ and ΔV_{solv}), the newly generated or neutralized charges (q) in products or transition state, the radius (r), the dielectric constant (ε) of the solvent and its pressure dependence:[36]

$$\Delta V^{\neq}_{solv},\ \Delta V_{solv} = -\frac{N_0 \cdot q^2}{2r \cdot \varepsilon^2} \cdot \left(\frac{\partial \varepsilon}{\partial p}\right)_T \qquad \text{eq. (2-5)}$$

where N_0 is the Avogadro number.

Pressure effects should be explained considering both parameters. For instance, in a heterolytic bond dissociation the attractive interaction between the newly generated ions and the solvent molecules leads to a volume contraction that is, generally, much larger than the volume expansion resulting from the dissociation. Thus, the overall effect, called electrostriction, leads to negative activation and reaction volumes ($\Delta V^{\neq} < 0$, $\Delta V < 0$).[29] Table 2-I provides a survey of the expected contribution of several chemical processes to the activation volume.

Table 2-I: Possible contributions to the activation volume of various chemical processes.[48]

Mechanistic feature	**Contribution in cm^3 mol^{-1}**
Homolytic bond cleavage	~ +10
Homolytic association	~ -10
Bond deformation	~ 0
Ionization	~ -20[a]
Neutralization	~ +20[a]
Change concentration	~ -5
Change dispersal	~ +5
Displacement	~ -5
Steric hindrance	(-)
Diffusion control	> +20

[a] Dependent on the solvent polarity.

2.3 Instrumentation for high pressure chemistry

The effect of pressure on compressed fluids, solids and reactions is frequently investigated by simple hydraulic pumps that operate in the range of 1 to 20 kbar (***no-flow methods***). The pump is equipped with a pressure intensifier, a pressure vessel where the reaction takes place, a gauge to measure the pressure and several valves to separate the reaction vessel from the pressure generator and to release the pressure after the reaction has been completed. In ***flow methods***, amounts of sample are continuously injected in the reaction vessel. Product is collected, while pressure is maintained constant over the system by pressure controllers and valves.

In kinetic studies the rate of the reaction, the composition and the equilibrium depending on time must be determined at several different pressures. For this purpose, on-line spectroscopic measurements are performed using high pressure cells that allow Fourier-transform infrared (FT-IR),[49-51] ultraviolet-visible (UV-Vis),[51,52] nuclear magnetic resonance (NMR)[53-55] techniques, *etc.* (Figure 2-3). It is also possible to maintain a constant pressure in the reaction vessel with an electric pump controller, to collect small samples with a microspindle sampler and analyze them by gas chromatography (GC) or High-Performance Liquid Chromatography (HPLC).

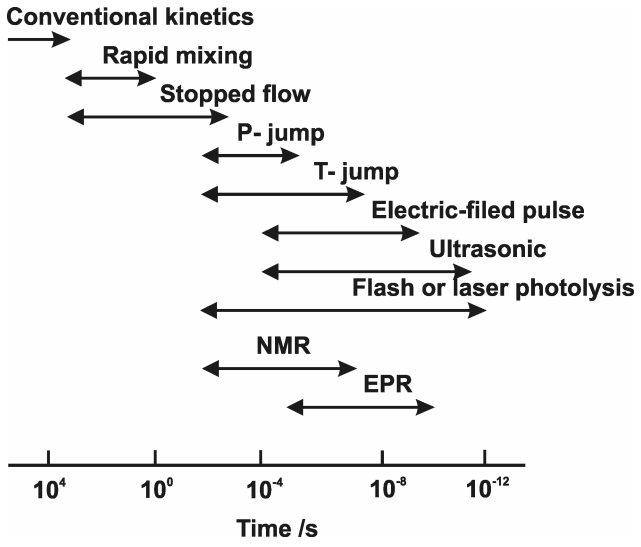

Figure 2-3: Applicability of high pressure kinetic techniques for different time ranges.[56]

Depending on the method used for generating the pressure (no-flow or continuous flow) and on the analytical technique used to monitor the process, there

are different types of high pressure instrumentation, these are described in the following section,[42,56,57] most of these instruments are "home-made".

Manual hydraulic pumps are able to generate pressures up to 3 kbar without the necessity of a pressure intensifier. Figure 2-4a shows a general scheme of the apparatus where pressure is obtained through mechanical compression of a liquid. A high pressure cell is used for direct analysis by an optical technique.[36,58]

Slow reactions (half-lives > 15 min) can be performed either in autoclaves, or high pressure cells equipped with spectroscopic or conductometric detection. The samples are introduced in the vessel, usually made of polytetrafluoroethylene (PTFE) by syringes[59] or cylinders with a movable piston.[58] These systems need a large amount of sample, so more compact versions have been constructed in such a way that components are placed in separated chambers and mixed after pressure and temperature equilibration.[60] In these systems UV-Vis is the most used spectroscopic technique coupled to these high pressure cells (Figure 2-4b).[52] Similar high pressure cells use IR and Raman spectroscopy.[36] Conductometry,[61] optical rotation, or refractive index determinations are other on-line techniques used.

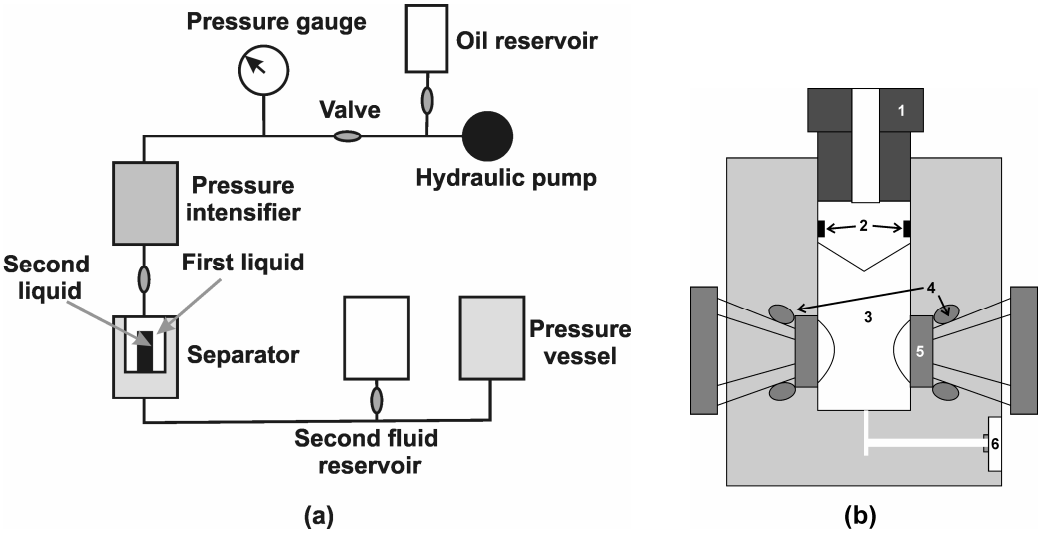

Figure 2-4: (**a**) Schematic drawing of a manual high pressure apparatus.[36,58] (**b**) Schematic cross section of a high pressure cell for UV-Vis optical measurements. **1** pressure plug, **2** O-ring, **3** sample holder with cell, **4** ring system, **5** sapphire window, **6** connection to pressure line.[52]

Fast reactions (half-lives < 15 min) can be performed in high pressure cells equipped with spectroscopic analysis detection, as well as continuous flow systems. These systems are classified as function of the time span of the applicability of each method.[62]

- Flow methods in which the reactions are so slow that they can be initiated by physical mixing.
- Equilibrium perturbation methods for reactions which are so rapid that they are studied by perturbation of an equilibrium condition.
- Radiation induced methods that are initiated by a very rapid burst of radiation.

Equipment that involves mixing systems allows studying fast reactions by spectrophotometry or conductometry. The first instrument of this kind has been developed by Heremans and Rijkenberg for pressures up to 12 kbar.[63] More recently, Ishihara *et al.*[64,65] designed a high pressure stopped flow apparatus with spectrophotometric detection for the study of organic reactions in the millisecond range. White *et al.*[66] used the same concept for biological purposes (photoactivated biological processes, photosynthesis) using FT-IR spectroscopy.

More recently, continuous flow systems have been used to study fast chemical reactions at supercritical conditions[67,68] and involving catalysis.[69-71] Figure 2-5 shows a novel continuous flow hydrogenation reactor integrated with a liquid handler as a fully automated high-throughput hydrogenation system.

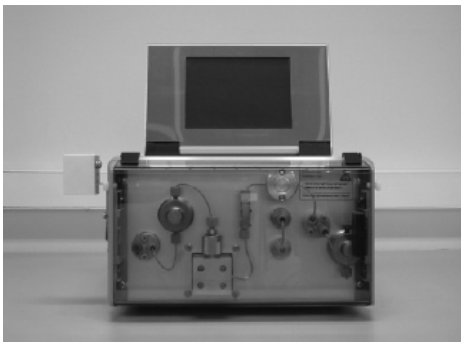

Figure 2-5: Continuous flow reactor for hydrogenation reactions.[69]

One of the most significant advances for high pressure in the last decade was the development of NMR, temperature jump (T-jump) and pressure-jump (P-jump) relaxation methods for pressures up to 3 kbar.

High pressure NMR techniques[72] have been reviewed by Jonas,[73] Merbach,[74] and Moore[75] and recently by Ando and Webb,[76] as well as by Damoense *et al.*[77] for inorganic chemistry, and by Yonken and Linehan[78] for supercritical fluids. Such NMR probes must be non-magnetic and of high mechanical strength: titanium and Be-Cu alloys, glass or quartz capillaries and sapphire give excellent results.

Furthermore, a compromise between the probe size, sample size and the sensitivity has to be found. The construction and introduction of high pressure probes into the spectrometer are highly specialized and costly activities.

Temperature-jump technique is used to study kinetics of rapid equilibration processes in solution on a microsecond time scale. Various high pressure T-jump instruments have been constructed, in which either laser excitation or an electrical discharge (Joule heating) is used to cause the temperature jump.[72] T-jump instrumentation is used successfully for studying fast complex formation and bioinorganic processes.[79] Nowadays the application of T-jump combined with FT-IR spectroscopy is also an important tool in polymer chemistry.[80]

Pressure-jump technique has been used by Brower[81] to perform measurements at pressures up to 15 kbar using a deformable sample cell to separate the sample solution from the pressurizing medium. In general, such systems can be employed to study fast complex formation reactions that are accompanied by large volume changes, so that a pressure jump will initiate a relaxation process.

Photochemical and photophysical measurements at elevated pressures include the determination of quantum yields of chemical and physical processes, as well as the measurement of excited state lifetimes and spectral properties as a function of pressure.[56] High pressure electrochemical studies have led to a better understanding of a variety of processes under non-classical conditions with potential applications in today's industrial environment.[82] This method is also suitable for systems that use supercritical fluid media.[18] Dilatometric and density measurements are essential in order to construct volume profiles or to determine reaction volumes from the pressure dependence of the equilibrium constant.

The different types of high pressure equipment discussed in this section enable the investigation of a wide range of organic reactions. Future developments will involve the miniaturization of the systems in such a way that pressure becomes a normal tool in chemistry, easily available and cheap.[52,83,84] Some of these systems are already on the market, offering advantages such as portability (small size) and the integration of analytical techniques (on-line analysis). In conclusion, microreactors are a good alternative for high pressure instrumentation and chemistry.

2.4 Influence of high pressure on physical properties

As a thermodynamic parameter, pressure modifies the physical and physicochemical properties of liquids considered as media for organic synthesis. Among others, pressure affects the solubility, freezing, melting and boiling points, density or viscosity, thus the organic reaction itself.[85] Pressure increases the solubility of solids and gases in liquids and also increases the miscibility of liquids. This is important, since it influences the homogeneity of the medium.[86] With rare exceptions, the melting points of most liquids increase with pressure (*ca.* 15 - 20 °C per 1 kbar).[87] Pressure increases the viscosity of all liquids in an exponential way (equation 2-6), where γ is the pressure coefficient.

$$\eta = \eta_0 \cdot \exp(\gamma \cdot p) \qquad \text{eq. (2-6)}$$

For the majority of organic solvents, at 25 °C the pressure coefficient (γ) is 3-6 × 10^{-4} bar^{-1}, whereas for more viscous liquids γ is much higher and can exceed 4 × 10^{-3} bar^{-1}.

Kiselev *et al.*[88] showed how the solvent viscosity affects the rate constant of the Diels-Alder reaction of 9,10-dimethylanthracene (**1**) with maleic anhydride (**2**) (Scheme 2-1) at elevated pressures. When the pressure increases 1 kbar, the viscosities of MeCN, toluene and silicon oil increase by 1.4, 1.6 and 20 times, respectively. In toluene the reaction rate smoothly increases over the whole pressure range. In the more viscous silicon oil a similar dependence is observed up to 3 kbar. The reaction rate sharply decreases upon further increase of the pressure, because the process becomes diffusion controlled. More generally, Diels-Alder reactions, 1,3-dipolar cycloadditions and Claisen rearrangements show a viscosity-related acceleration at elevated pressures (kbar range).[89]

Pressure causes also changes in the dielectric constant according to the description of the Owen-Brinkley empirical equation (equation 2-7).

$$\varepsilon_{p_0} \Big/ \varepsilon_p = 1 - A Ln\left[\frac{(B+p)}{(B+1)}\right] \qquad \text{eq. (2-7)}$$

In equation 2-7 A and B are characteristic parameters for a liquid. The dielectric constant increases slowly, but significantly with pressure. It determines the magnitude

of the electrostriction induced by the solvent in the vicinity of charged species, which is a very important parameter for activation volume calculations (see section 2.2.4).[85]

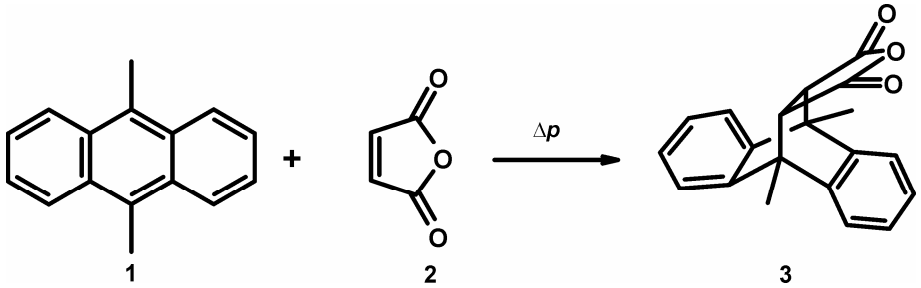

Scheme 2-1: Reaction of 9,10-dimethylanthracene (**1**) with maleic anhydride (**2**) at high pressures.

Other physical solvent properties are also affected by pressure, such as refractive index, compressibility, thermal conductivity, electrical conductivity, specific heat and surface tension.[36]

A supercritical fluid (SCF) is defined as a substance above its critical temperature (T_c) and pressure (p_c), called the critical point, but below the pressure required to condense it into a solid.[90] Figure 2-6 shows a hypothetic phase diagram where the supercritical region is visible. SCFs are very interesting media to carry out organic reactions. They represent an alternative solvent, because they are not in the liquid state.[91] Reactions in a SCF may offer advantages like controlling the phase behavior increasing the reaction rates and giving rise to specific reaction paths.

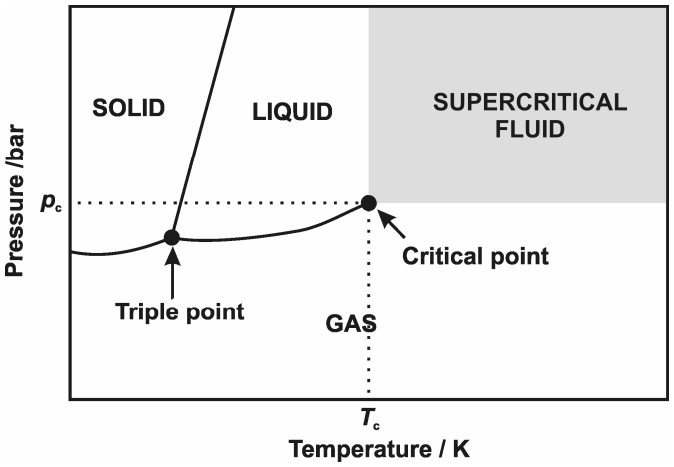

Figure 2-6: A typical phase diagram showing the supercritical region.[17]

SCFs have many physical properties that are between those of a liquid and a gas.[92] For instance, the density of a SCF is typically less than half of the liquid state,

but two orders of magnitude larger than that of a gas. Properties may change dramatically with pressure near the critical region. SCFs have no surface tension and, like gases, rapidly diffuse to occupy the entire volume of the system. In many publications the SCF properties are used for synthetic purposes.[17,62,93-100]

Supercritical CO_2 (*sc* CO_2) as a reaction medium is of particular interest in organic synthesis.[101] Its physical properties are very interesting mainly because it has a relatively accessible critical point (T_c = 31.1 °C, p_c = 73 bar). As a "green solvent" it is non-flammable, relatively non-toxic, inert and inexpensive. It can be recycled and has low solvent disposal costs. *sc* CO_2 also leaves less solvent residues in products and consequently a lower environmental impact.

Ionic liquids are organic liquids (only) consisting of ions.[102] Since their physical properties can be affected by pressure, their possible use as high pressure media must be taken into account[95]

2.5 Pressure in organic reactions

There are several monographs and reviews on chemical reactions at high pressure,[6,9,103,104] covering the literature of the past decade.[18,29,31,105-108] Recent reviews of Klärner and Wurche,[29] as well as a monograph by Van Eldik and Klärner[18] cover recent progress in high pressure organic synthesis up to the first half of 2001. Matsumoto *et al.* published a review about cycloaddition reactions under high pressure in 2005.[109] Very recently, Chemical Society Reviews published a special issue with ten reviews on high pressure, expressing the importance that high pressure nowadays has in chemistry, biology and engineering.[110]

2.5.1 Reactions in closed systems

Most of the high pressure chemistry during the past four years was carried out in closed systems like autoclaves in which pressures range from 1 to 20 kbar.

There are some general aspects in which high pressure is expected to have an effect on organic reactions which have been explained in detail in section 2.2. The effect of pressure on chemical reactions, especially, the change in the packing coefficient during cyclization of chains and the effect of electrostriction on reactions, in which charged species are generated, contribute substantially to a volume

contraction leading to a powerful pressure-induced acceleration of such reactions.[22] In organic chemistry, high pressure is used to enhance reaction rates when the reactions show large negative reaction or activation volumes. In many instances yields are increased and reaction times are shortened, in addition the product ratios may be altered. Some reactions that do not or cannot proceed at atmospheric pressure, occur smoothly under pressure. In this section the latest developments in high pressure organic chemistry are reviewed.

Cycloadditions are typical examples of pressure-accelerated reactions being the most extensively investigated because their activation ($\Delta V^{\neq}$) and reaction volumes (ΔV) are highly negative (*e.g.* $\Delta V^{\neq} \approx$ -25 to -50 $cm^3\ mol^{-1}$).[109] Pressure particularly improves or even promotes cycloaddition reactions that are reluctant to occur due to steric hindrance or electronic reasons.[8]

Diels-Alder reactions

The Diels-Alder reaction of a variety of electron-rich 2*H*-pyran-2-ones (**4**) with alkynes (**5**) to give aniline derivatives (**6**) is affected by pressure (13-15 kbar)[111,112] (Scheme 2-2). The substituents at the 3- and 5- positions in 2*H*-pyran-2-one (**4**) induce a different reactivity and regioselectivity. This different reactivity was qualitatively explained on the basis of electron demand and also by the formation of zwitterionic intermediates. High pressure affects the regioselectivity of the reactions because they are governed by different factors than those at normal pressure. Stereoelectronic factors influence the activation volume as well as changes in the reaction mechanism.

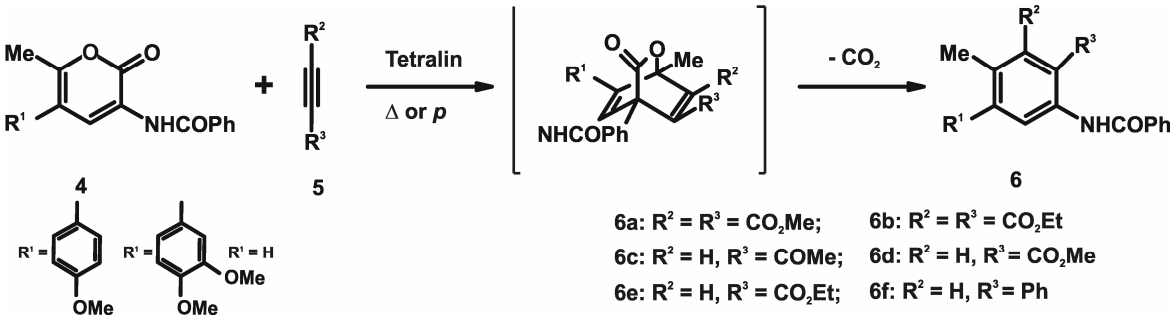

Scheme 2-2: Diels-Alder reactions of 2*H*-pyran-2-ones (**4**) with alkynes (**5**) yielding aniline derivatives (**6**).

Fujita *et al.*[113] studied the Diels-Alder reaction of 2(1*H*)-quinolones having an electron-withdrawing group at the 3-position with alkyl- and silyloxy-1,3-butadienes to

give regio- or stereoselectively functionalized phenanthridones under atmospheric as well as high pressure conditions (10 kbar).

The regio- and stereoselectivity in the reaction of the enantiopure diene **7** with prochiral cyclohexadienones (**8**) to give the cycloadduct (**9**) was studied at high pressure (up to 14 kbar) (Scheme 2-3). The resulting [4+2] cycloadducts (**9**) allowed the preparation of new polyfunctional cyclohexenone derivatives.[114]

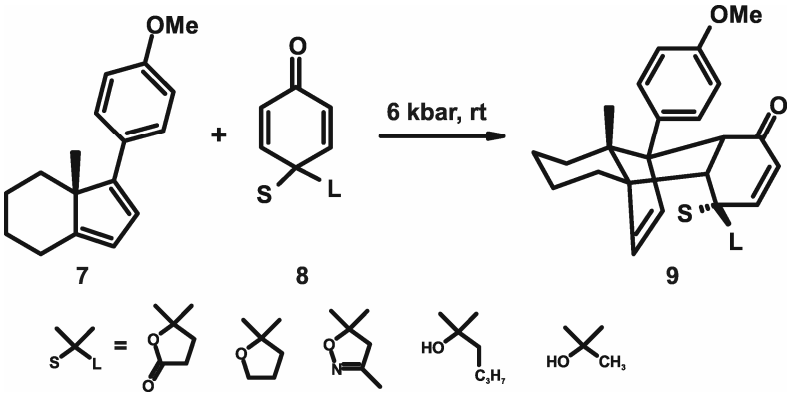

Scheme 2-3: Reaction of prochiral cyclohexadienones (**8**) and the diene (**7**) to give the cycloadducts **9**.

In the last few years the combination of high pressure (12 kbar) and catalysis has been extensively used for the improvement of the selectivity of organic reactions. It has been proven that this combination has a profound influence on the chemoselectivity of the [4+2] cycloaddition reaction of pyrrole derivative (**10**) with electron-rich diene (**11**) (Scheme 2-4).[115] Both the structural and electronic nature of the substituents on the *N*-tosylpyrrole nucleus play a crucial role in the course of the reaction directing both the reactivity and the chemoselectivity of the cycloaddition reaction. Activation by high pressures and a Lewis acid leads to increased yields.

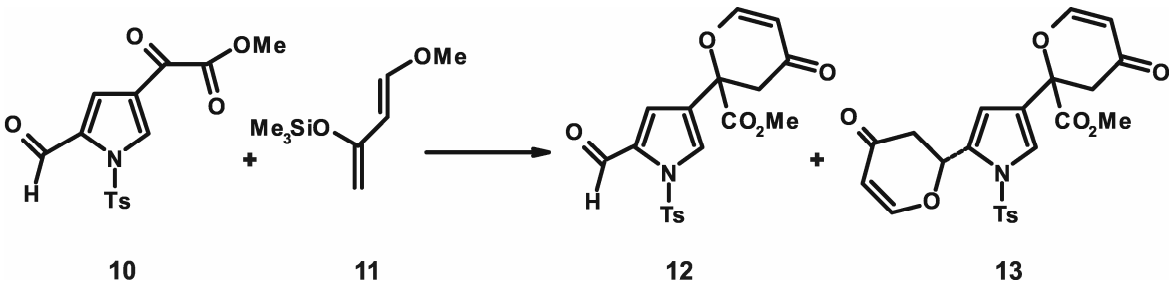

Scheme 2-4: Cycloaddition reaction between pyrrole derivative (**10**) and diene (**11**).

(Salen)-chromium(III) chiral Lewis acids have been used for the [4+2] cycloaddition reactions of buta-1,3-diene with chiral or achiral glyoxylates at high

pressures giving rise to high enantioselectivities.[116-118,119] At pressures of 10 kbar, the Diels-Alder reaction of 1-methoxybuta-1,3-diene with *n*-butyl glyoxylate in the presence of a Co(II)-catalyst gave very high enantioselectivities (70 - 90% ee) and yields.[120,121] Minuti *et al.*[122] have studied the Diels-Alder reactions between (+)-nopadiene and 2-cyclopenten-1-one, 2-cyclohexen-1-one, 4-oxo-2-cyclopentenyl-acetate and two indenone derivatives under high pressure conditions in combination with Et_2AlCl as a catalyst. The reactions were totally regioselective and anti-endo diastereoselective, providing a new approach to optically active polycyclic compounds that were obtained in very high yields. Kosior *et al.*[116] have studied the stereochemistry of the Diels-Alder reaction of buta-1,3-diene with chiral and achiral glyoxylates in the presence of (salen) chromium(III) complexes at high pressure. The chemical yields and the diastereoselectivities were not very high, probably due to the steric requirements both of the catalyst and the dienophile. Much better results have been obtained for the enantioselective mode of this reaction using achiral glyoxylates. A similar Diels-Alder reaction, the [4+2] cycloaddition reaction of 1-methoxybuta-1,3-diene and glycolaldehyde-derived heterodienophiles in the presence of chiral metallosalen complexes, gave good yields (up to 90%), very good diastereoselectivities (up to 92%) and enantioselectivities (up to 93% ee).[117]

Under high pressure (11-15 kbar) 3-methyl- and 3-phenylsulfanylfuran (**14**) undergo a facile, regioselective and stereoselective Diels-Alder cycloadditions reaction with a variety of cycloalkenones (*e.g.* **15**) to give the corresponding annulated 7-oxabicyclo[2.2.1]-heptene derivatives (**16**) in good yields (Scheme 2-5) using zinc iodide as catalyst.[123] More examples of Diels-Alder reactions affected by high pressure, when catalysts are involved, are summarized in references 124-131. Others have used high pressure for the synthesis of Diels-Alder cycloadducts in a regio- and stereoselective way.[113,122,128,132-138]

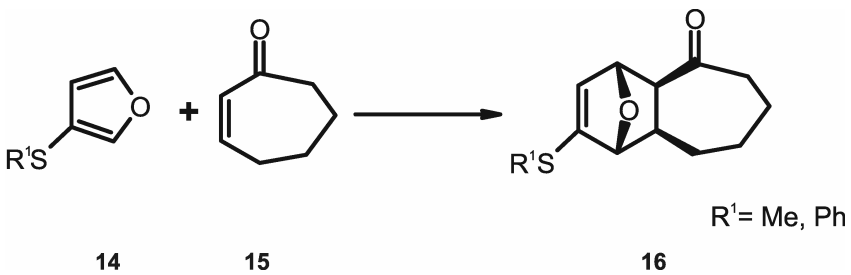

Scheme 2-5: Diels-Alder reaction of 3-methyl- and 3-phenylsulfanylfuran (**14**) and 2-cyclohepten-1-one (**15**) at 15 kbar.

In solid phase organic synthesis, high pressure conditions eliminate the need for stirring and heating, which can damage the resin. It also eliminates the use of a catalyst, which may deposit residues in the polymeric matrix. High pressure also allows the use of reactants of relatively low reactivity or that are sensitive toward heat or (Lewis acid) catalysts. A very interesting example has been presented by the group of Scheeren in the synthesis of spirohydantoins and spiro-2,5-diketopiperazines *via* resin-bound cyclic *a*,*a*-disubstituted α-amino esters (Scheme 2-6).[139]

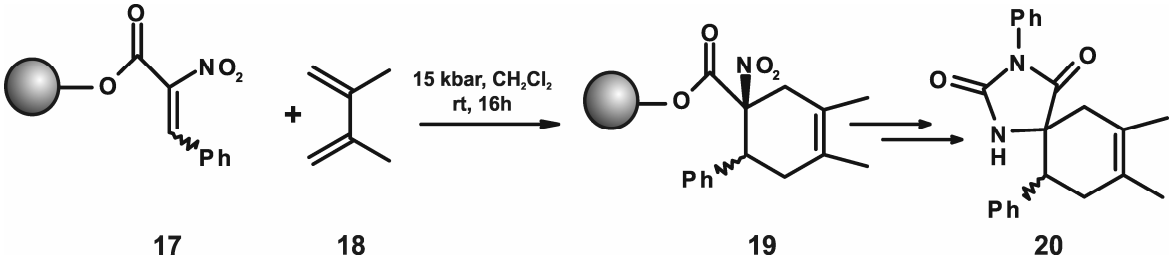

Scheme 2-6: One step in the synthesis of spirohydantion (**20**).

Pressures of 8 kbar and solvent free conditions have successfully been used for the Diels-Alder reaction of thiophene (**21**) and maleic anhydride (**22**) (Scheme 2-7). The remarkable effects of the combination of high pressure and solvent-free conditions led to a significant lowering of the pressure required for this reaction, but also to a considerable improvement in yield (almost quantitative) compared with the same reaction carried out in solution (19% in CH_2Cl_2 and 23% in tetrachloro-ethylene).[140]

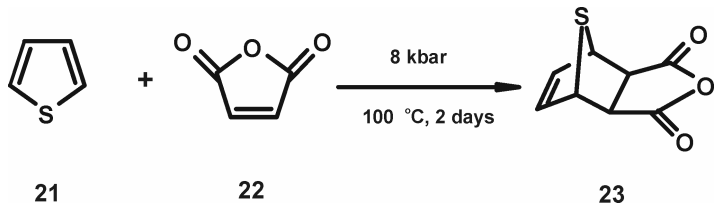

Scheme 2-7: High pressure Diels-Alder reaction of thiophene (**21**) with maleic anhydride (**22**).

Pressure can also give rise to a reduction of the number of reaction steps. An example is the synthesis of cantharidin (**27**) (Scheme 2-8). At 15 kbar the reaction of furan (**24**) and thieno[3,4-*c*]furan-1,3(4*H*,6*H*)-dione (**25**) proceeds in only two steps and the product is obtained quantitatively. Before, ten steps were necessary and poor yields were obtained.[141,142] Nowadays more research groups are using high pressure for

reducing synthesis steps for the stereochemical synthesis of natural and/or pharmaceutical compounds with high potential industrial application.[143-148]

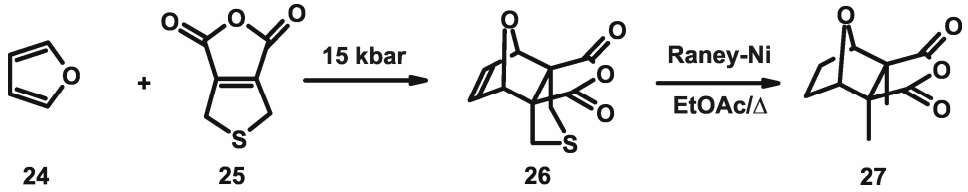

Scheme 2-8: Synthesis of cantharin (**27**) at high pressure.

1,3-Dipolar cycloadditions

1,3-Dipolar cycloadditions usually occur stereospecifically with retention of configuration in the dienophiles. Activation and reaction volumes[149] are in the range of $\Delta V^{\neq}$ = -21 cm^3 mol^{-1}, smaller than those of Diels-Alder reactions. The reason might be the dependence on the ring size in the volume changes during the cycloadditions.[150]

High pressure decreased the reaction time of the cycloaddition reactions of chiral nitrones derived from *L*-valine with methyl acrylate to give the corresponding diastereomeric 3,5-disubstituted isoxazolidines. The stereoselectivity was dependent on the substituent being attached on the nitrogen atom in the starting nitrone and reaction conditions.[151]

In the cycloaddition reaction of organic azides (**29**) with morpholinobuta-1-en-3-yne (**28**) a pressure of 7 kbar considerably improved the yield of some of the cycloadducts (Scheme 2-19).[152]

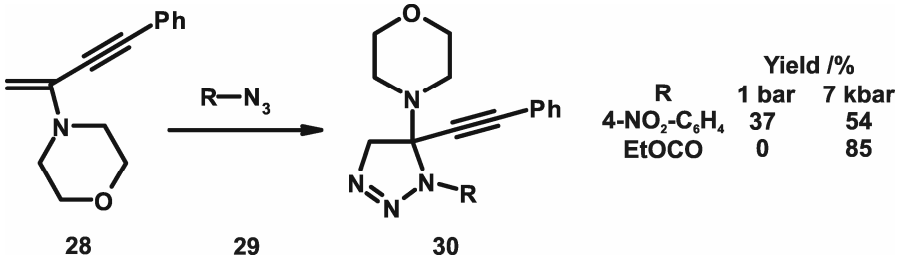

Scheme 2-9: Reaction of 2-morpholinobut-1-en-3-yne (**28**) with azides (**29**) at high pressure.

[2 + 2] Cycloadditions

The activation volumes of [2 + 2] cycloadditions reactions are highly negative ($\Delta V^{\neq}$ = -22 to -52 cm^3 mol^{-1}). Thus, the effect of pressure leads to a considerable acceleration of these reactions comparable to that of Diels-Alder reactions. For instance, under high pressure conditions (15 kbar) 4-methylphenyl-1,2-propadienyl sulfones and enol ethers undergo a regioselective [2 + 2] cycloaddition reaction to give

(3-alkoxycyclobutylidene)methyl 4-methylphenyl sulfones in good yields, while at atmospheric pressure the reaction does not take place.[153]

Another interesting example reported by Aben *et al.*[154] involves the reaction of enol ethers and alkyl 3-aryl-2-cyano-2-propenoates at high pressure to give the cycloadducts in high yields and stereoselectivities. The obtained products are attractive scaffolds for use in combinatorial chemistry due to the presence of a sulfonyl group, a methylene function and an alkoxy group, while the cyclobutane ring can either be left as a basic structural unit or can be involved in further conversions.

As explained in section 2.2, pressure is generally effective in increasing yields and giving better selectivities for reactions that involve an ionization process like, among others, condensations, additions and nucleophilic reactions.

Condensation reactions

The Knoevenagel reaction of (a)cyclic ketones with ethyl cyanoacetate to produce hindered alkenes is accelerated by a pressure of 3 kbar compared with the reaction at 1 bar.[155]

High pressure (3 kbar) was used as a simple and efficient synthetic method for the condensation of phenols with aromatic aldehydes using TfOH as a strong acid catalyst.[156] *L*-proline was used as a catalyst by Kutsoki *et al.*[157] for the direct asymetric aldol reaction between ketones and aldehydes.

The first example of a diastereoselective nitro-aldol reaction of *a*-amino aldehydes under high pressure without a catalyst has been reported by Misumi and Matsumoto.[158] Although the diastereoselectivities did not rival those of reactions with highly sophisticated catalysts, the experimental procedure was extremely simple.

Unsymmetrical ureas have been synthesized *via* the direct condensation of Troc-carbamates with primary or secondary amines under high pressure conditions (6 kbar) where pressure replaces the catalyst.[159] Kumamoto *et al.* have developed a method to prepare a variety of *N*-pyridinothiourea derivatives using the high pressure promoted, uncatalyzed condensation of isothiocyanates with aminopyridines at pressures up to 6 kbar.[160]

A new practical method for ketalization or oxy-Michael/ketalization involves the high pressure promoted condensation of *a,β*-unsaturated ketones with alcohols in the presence of trialkyl orthoformates as water scavenger. This method is considered as an environmentally friendly process.[161]

An exotic and smart way to generate high pressure is by water freezing. As the volume of water increases by about 10% on freezing, a high pressure, up to 2 kbar, can be easily created when water is frozen in a sealed autoclave at -20 °C. The catalytic asymmetric three-component List-Barbas-Mannich reaction has been performed in such a system (Scheme 2-10) giving rise to higher yields and better enantioselectivities than at room temperature and 1 bar.[162] The same method has successfully been used for the catalytic asymmetric aldol reaction,[163] and the Baylis-Hillman reaction.[164]

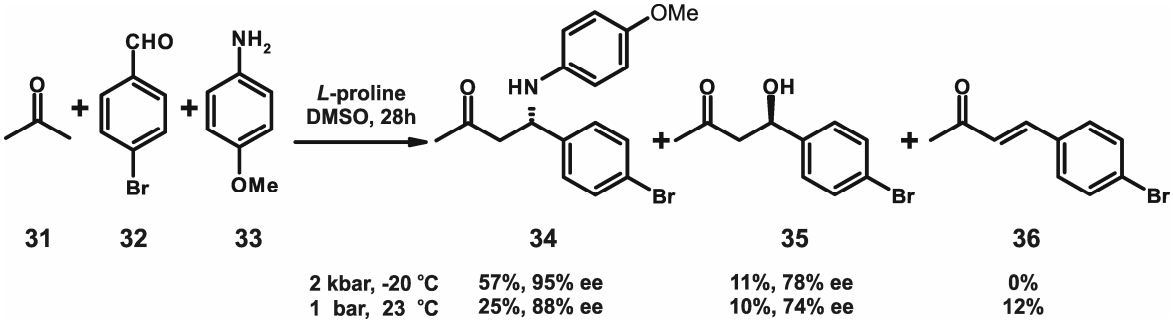

Scheme 2-10: List-Barbas-Mannich reaction of acetone (**54**), *p*-bromobenzaldehyde (**55**) and *p*-anisidine (**56**) using *L*-proline as catalyst at high pressure.

Nucleophilic reactions

Since charge development in the transition state invariably results in a rate increase on application of pressure, most nucleophilic reactions have a negative $\Delta V^{\neq}$. In particular, the Menshutkin reaction has large negative values (*e.g.* $\Delta V^{\neq}$ = -58.2 cm^3 mol^{-1} in *n*-hexane).

Pressure benefits organic reactions which due to steric hindrance (steric effects) have low rate constants.[165] This is due to the fact that steric interactions are repulsive interactions leading to the destabilization of the system (see also additions and miscellaneous reactions). From this point of view, pressure contributes to reduce the destabilization. The Menshutkin reaction of buttressed pyridines (**37**) (Scheme 2-11) is a good example,[166] where the rate constant under ambient pressure conditions decreases with increasing bulkiness of the Y and the Z substituents (Table 2-II). In general, the more hindered reactions are more accelerated by pressure up to 2 kbar, meaning more negative activation volumes ($\Delta V^{\neq}$), thus when pressure is applied, the reactions with higher steric hindrance (more negative $\Delta V^{\neq}$) will be positively affected.

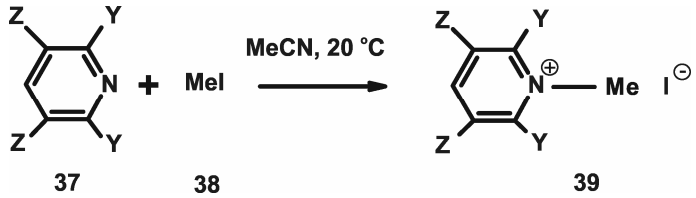

Scheme 2-11: Menshutkin reaction of buttressed pyridines (**37**) with methyl iodide (**38**).

Table 2-II: Menshutkin reactions of methyl iodide (**38**) with buttressed pyridines (**37**).[166]

Z	Y	Rate constant ratio[a]	$\Delta V^{\neq}$ /cm^3 mol^{-1}
H	H	1	-28.2
H	Me	0.0354	-30.8
t-Bu	Me	0.0036	-32.5

[a] In acetonitrile at 20 °C and 1 bar.

Addition and elimination reactions

Additions of nucleophiles or electrophiles to olefinic compounds have negative activation volumes.[1] The 1,4-addition of alcohols to activated alkenes catalyzed by tri-*n*-butylphosphine is activated by pressure in the case of crotonic compounds with a hindered β reaction center while the corresponding additions of alcohols to methacrylic analogs are hardly affected.[167,168] The phosphine-catalyzed nucleophilic addition of alcohols to unsaturated nitriles is also affected by pressure (3 kbar), when either the alcohol or the nitrile have bulky groups.[169] In this particular reaction, geometrical and electrostatic interactions (steric hindrance to ionization) are presented as the main reasons for the positive pressure effects.

For the reaction of 2-methylfuran (**40**) with alkyl glyoxylates (**41**), the cobalt catalyst (**42**) afforded at high pressure the Friedel-Craft products (**43**) and (**44**) in yields up to 70% with enantioselectivities up to 72% ee (Scheme 2-12).[170]

The enantioselective addition of allylstannanes to glyoxylates and glyoxals, as well as simple aromatic and aliphatic aldehydes, catalyzed by chiral (salen)Cr(III) complexes has given good yields and moderate enantioselectivities when high pressure (up to 10 kbar) was applied.[171-173] In the case of the asymmetric Michael reaction of chiral imines with alkyl and aryl crotonates, pressure accelerates the reaction as well as increases the regio- and stereoselectivities (90 - 98% ee).[174]

As already explained in section 2.4, solvent effects should be considered[175] upon the application of pressure. The rate constants of some Michael-like and [4+2] cycloaddition reactions are less affected by pressure in water than in organic

solvents.[176] For the Michael addition reaction the effect of pressure is partially due to the reduction of the electrostriction volume, while for the Diels-Alder reaction in water pressure positively affects the rate constants. Pressure alters the intensity of solvophobic and polarity parameters, but the effects vary for each reagent.

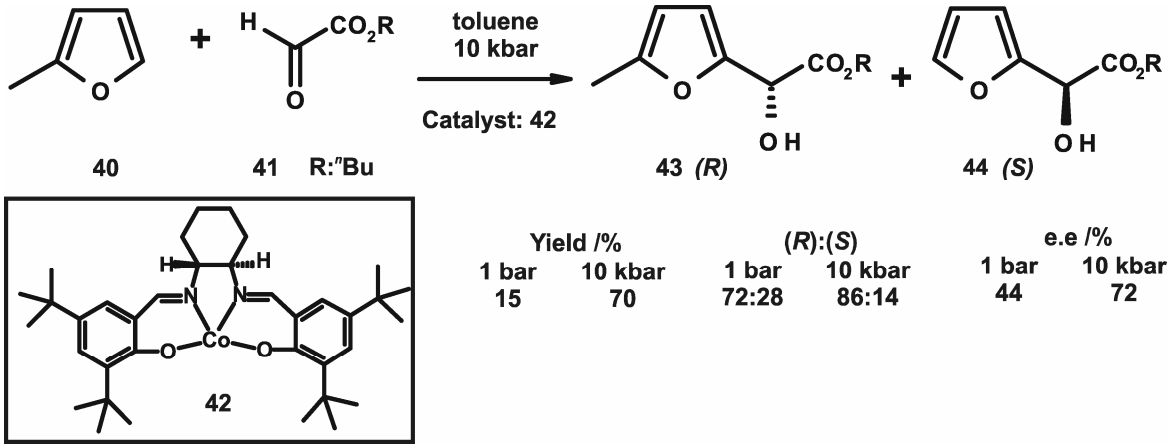

Scheme 2-12: Reaction of 2-methylfuran (**40**) and *n*-butyl glyoxylate (**41**) at 10 kbar using a (salen) Co(II) complex (**42**) as catalyst.

Other non-conventional media like fluorophobic solvents have been used to study their effect in the conjugate addition of amines to acrylonitrile at high pressures as well as in Diels-Alder reactions in the range of 2 - 10 kbar.[177] In this case the pressure effect is lower than in other media (water, ethylene glycol). Finally, the freezing water method described above has also been successfully applied to a high-yield Michael reaction of alcohols and *a*,*β*-unsaturated ketones.[178]

Domino reactions

The activation ($\Delta V^{\neq}$) and reaction volumes (ΔV) of domino reactions are of the same order of magnitude as those of the Diels-Alder reactions and thus are positively affected by pressure. Nevertheless, the effects depend on the type of reactions that are involved. For example, the Horner-Wadsworth-Emmons reaction (alkenylation of carbonyl compounds with phosphonates) of aldehydes with phosphonates proceeds at room temperature in the presence of triethylamine without Lewis acids if high pressure (8 kbar) is applied to the system.[179] Another type of domino reaction, the 6π-electrocyclization/Diels-Alder reaction of 1,6-disubstituted (*E*,*Z*,*E*)-1,3,5-hexatriene (**45**) affords at pressures up to 10 kbar good yields (36 - 76%), whereas there is no reaction at atmospheric pressure (Scheme 2-13).[180] The domino Knoevenagel hetero Diels-Alder reaction of sugar derived *δ*,*ε*-unsaturated aldehydes has also been studied,

yielding to new polyhydroxylated carbocycle-dihydropyran fused ring systems.[181] Scheeren *et al.* studied both the reaction of 2-methoxybuta-1,3-diene in an one-pot domino [4+2]/[4+2]/[3+2] cycloaddition at high pressure to form structurally diverse multicyclic nitroso acetals in good yields and stereoselectivities[182,183] and the synthesis of polycyclic alkaloids.[184]

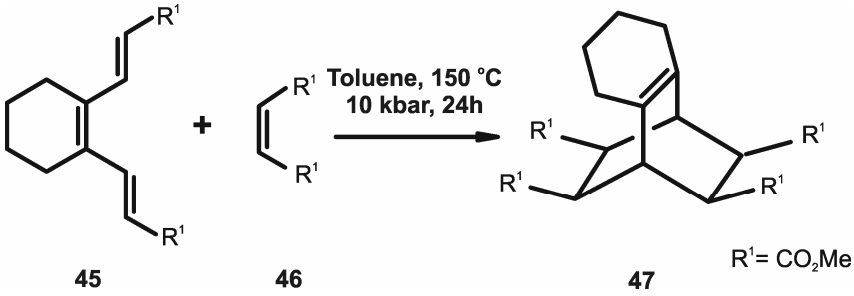

Scheme 2-13: 6π-Electrocyclization of a (*E*,*Z*,*E*)-1,3,5-hexatriene (**45**) ensuring the Diels-Alder reaction with dimethyl maleate (**46**), as a one pot-procedure.

Miscellaneous reactions

There are many other interesting applications of high pressure in organic synthesis. High pressure techniques have been used to accelerate Heck reactions before,[185] one of the most versatile C-C bond forming processes. The mechanism of the Heck reaction of iodobenzene with methyl, ethyl and *t*-butyl acrylate and of both 4-nitrophenyl iodide and 4-nitrophenyl triflate with methyl acrylate, has been studied by quantitative on-line FT-IR spectroscopy at pressures up to 3 kbar.[186] The results suggested that the rate-determining step of the overall reaction is not the oxidative addition, but either the alkene coordination or the subsequent carbopalladation.

Sterically demanding reactions like the Passerini reaction[187] show an enhanced sensitivity to pressure, small when moderately hindered reactants are involved, but very large when bulky isocyanates (**50**) are used (Scheme 2-14).

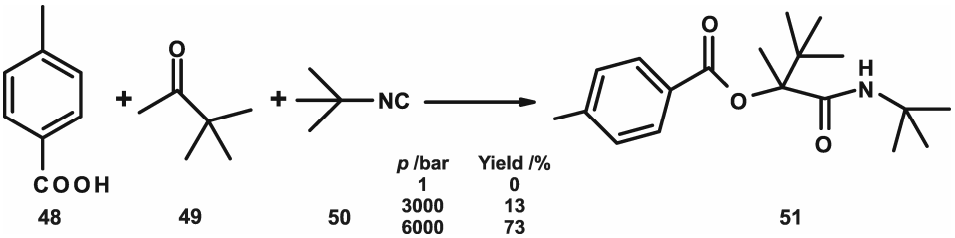

Scheme 2-14: Passerini reaction of 4-methylbenzoic acid (**48**) with the highly sterically hindered ketone (**49**) and isocyanate (**50**) at high pressures.

The three-component Strecker synthesis of *a*-aminonitriles (**55**) starting from ketones (**52**), aromatic amines (**53**) and trimethylsilyl cyanide (TMSCN) (**54**) has been studied at high pressures (up to 6 kbar) in the absence of a catalyst. In this particular reaction pressure replaces the catalyst. The effect of pressure increases with higher steric hindrance (Scheme 2-15).[188-190]

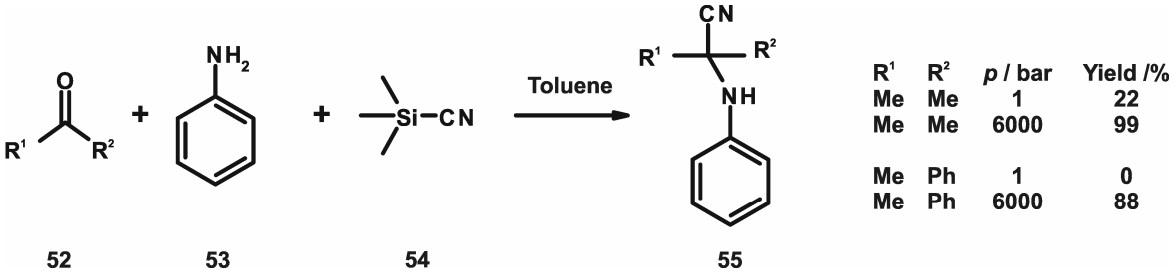

Scheme 2-15: Strecker reaction of ketones (**52**) with aniline (**53**) and TMSCN (**54**) in toluene for 24 h at 6 kbar.

When bulky groups are present the Stetter reaction of bulky aliphatic acyloins and *γ*-ketonitriles[191] as well as the Biginelli reaction (a multicomponent reaction involving a α-ketoester, an urea and an aldehyde to give 3,4-dihydro-2(1*H*)-pyrimidinones) are promoted by high pressure.

The Baeyer-Villinger oxidation of aliphatic ketones (**56**) only exhibits a small pressure effect, which it is reflected in slightly negative activation volumes (-2 to -8 $cm^3\ mol^{-1}$, Scheme 2-16).[192]

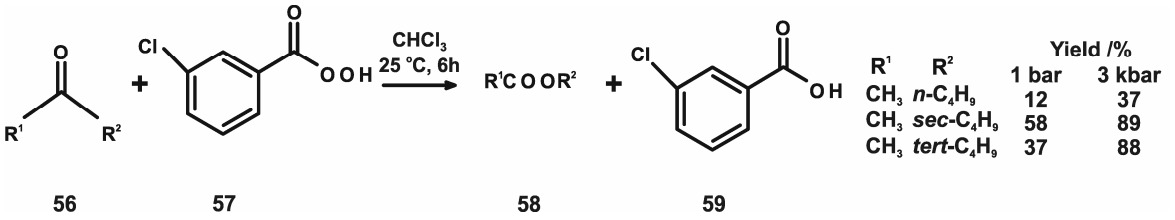

Scheme 2-16: Baeyer-Villiger oxidation of aliphatic ketones (**56**) with *m*-chloroperbenzoic acid (MCPA) (**57**) at 3 kbar.

During the synthesis of complex target molecules, selective deprotection of sensitive functionalities is of crucial importance. The deprotection of *t*-butyldiphenylsilyl (TBDPS) groups at very sterically hindered positions has successfully been performed at 10 kbar, using HF/pyridine in DMF.[193]

Chiral macrocyclic tetraamines derived from α-amino acids have been synthesized in good yields at 10 kbar.[194] These macrocycles were used for the study of

metal complexation (Li^+, Na^+, K^+, Rb^+ and Cs^+).[195,196] The Jurczak group studied the implementation of high pressure in many other reactions like the cleavage of sterically hindered steroid esters[197] and the synthesis of crown ethers, cryptands,[198,199] azacoronands,[200] and herbicidals.[201] Matsumoto *et al.* have studied the influence of pressure on several heterocyclic organic reactions.[202-205]

In this section it is shown that high pressure finds more and more successful applications as a useful methodology in synthetic chemistry.

2.5.2 Reactions in continuous flow systems

Chemical transformations under continuous flow operation are now carried out in laboratories and in industry at atmospheric pressure conditions.[206] Flow-through processes using reactors that contain immobilized reagents or catalysts deliver compounds with high purities.[207] Continuous flow is mainly used in combinatorial and parallel-synthetic methods for pharmaceutical purposes.[208,209]

In such systems pressures from 20 - 700 bar are commonly applied. Higher pressures are hardly used because to combine pressure and continuous flow operation requires sophisticated and expensive instrumentation as well as severe safety measurements. Only one example of a continuous flow system that operates at high pressure (> 1 kbar) has been reported in the past four years.[210] In this field, miniaturization of the system is a good option, because it relaxes safety issues. Kirschning *et al.*[211] filled a fiber (about 110 mm in length and 5 mm diameter) with a functionalized monolithic material based on a glass/polymer composite. Using standard HPLC connections a "PASS-Flow reactor" was built, (Figure 2-7) that operates up to 20 bar.

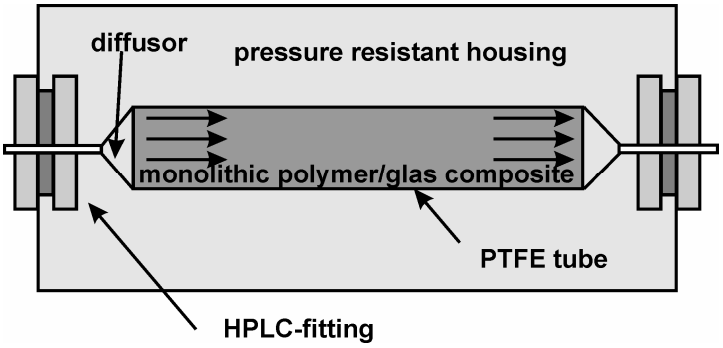

Figure 2-7: Schematic set up of the PASS-Flow reactor; PTFE: polytetrafluoroethylene. [211]

These chemically functionalized flow-through reactors have first been tested for basic transformations, such as substitution, oxidation, reduction and Horner-Wadsworth-Emmons (HWE) olefinations. The products were isolated in high yields by simple removal of the solvent.

The use of continuous flow operation in high pressure systems is still in its infancy, but a bright future is predicted. This section summarizes the literature on continuous flow systems, mainly microreactor chips, which are used for chemical applications at high pressures.

2.5.2.1 Autoclaves

Zhao *et al.*[212] designed a pressure reaction cell autoclave for kinetics and *in-situ* infrared reflection spectroscopic measurements on model catalysts at pressures up to 3 bar. The cell could be operated both as batch reactor and as flow reactor with a defined gas flow. Following the same principle, Jansen and Niemeyer improved greatly the system developing an automated high pressure plant with a continuous flow through a fixed silica gel bed was constructed for pressures up to 3.5 kbar.[210]

A continuous flow laboratory-scale device for heterogeneous hydrogenations using Pd/C and Raney-Ni as catalysts has successfully been applied for the reduction of aromatic nitro groups, deprotection of benzyl groups and desulfurization reactions of selected dihydropyrimidine analogues at pressures up to 100 bar.[213] Jones *et al.*[69] incorporated a liquid handler to the system resulting in a fully automated high-throughput hydrogenation system for library synthesis. The reactor, (the H-Cube, Figure 2-8)[214] combines endogenous hydrogen generation from the electrolysis of water with a continuous flow-through system. The reduction of a series of functional groups at 70 °C and 70 bar, has been performed in this reactor.

In a continuous flow, fixed-bed microreactor the competitive hydroconversion of *n*-heptane and *n*-nonane and its mixture using a Pt/H-Y zeolite as a catalyst has been carried out at 230, 250 and 270 °C at 100 bar, at these pressure the zeolite configuration changes.[215]

Experiments with supercritical fluid (SCF) require pressures higher than 100 bar, nevertheless the pressures are generally much lower than those associated with the high pressure experiments mentioned in section 2.5.1. Typical supercritical experiments are carried out at pressures below 400 bar in autoclaves or reaction

vessels. Their low viscosity and good thermal and mass transport properties make SCFs particularly interesting for continuous flow experiments. Nowadays, the developments in the SC-field concern the fabrication of new apparatus as well as studies in continuous flow systems.[216,217] The main studied topics are the behavior of supercritical fluids as well as their mixtures with other fluids (alcohols) and solubility and separation studies.[17,218]

The selective oxidation of benzyl alcohol to benzaldehyde with molecular oxygen in supercritical carbon dioxide (scCO$_2$) over a Pd/Al$_2$O$_3$ catalyst using toluene as a co-solvent[219,220] and the catalytic esterification of 2-ethylhexanoic acid with 2-ethyl-1-hexanol in scCO$_2$[68] are reactions carried out in these systems. Other examples are the fabrication of highly crystalline anatase TiO$_2$ nanoparticles[67] in less than 1 min in a supercritical propanol-water mixture and the inhibition of enzymatic processes by pressure and scCO$_2$ conditions.[70]

2.5.2.2 Tubes and pipes

Conventional liquid chromatography (LC)-type steel tubing (volume of 2 mL and an inner diameter of 1.27 mm and 1.5 m length) has been used to study reactions up to 700 bar.[221] Tubes and capillaries have also been filled with catalysts for carrying catalytic reactions in continuous flow. A tube reactor packed with Pd/C catalyst performs as an efficient hydrogenation system, which converts 4-cyanobenzaldehyde (**60**) to the benzyl alcohol derivatives (**54**-**56**) at 25 °C, (Scheme 2-17). Such systems are already implemented in pilot plants for industrial production.[222]

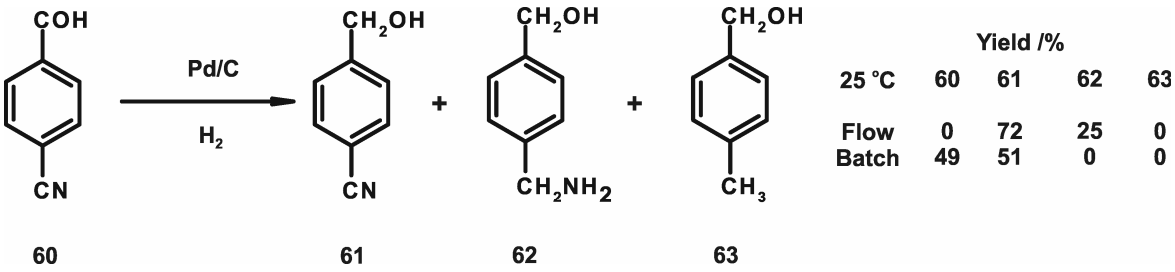

Scheme 2-17: Hydrogenation reaction of 4-cyanobenzaldehyde (**60**) in the flow and batch reactor systems at 25 bar.

2.5.2.3 Capillaries

The first miniaturization step in the construction of continuous flow systems for pressure applications are capillary reactors. The pressure range used in these systems is very wide, going from a few bar in capillary like HPLC columns to 400 bar in metal microtubes for supercritical water applications. The capillaries follow the same principle as the columns used in HPLC or GC systems, but are here used for synthetic purposes. One of the first examples of such a reactor consists of a PTFE capillary (1.0 mm diameter, 1 - 8 m length) surrounded by a thermostatted jacket (60 - 120 °C) operating at a pressure of 4 bar.[215,223,224] The pressure is regulated by a needle valve. It is especially suitable for investigating two-phase liquid-liquid reactions, *e.g.* the nitration of aromatic compounds.

Ratka and Berndt[225] have developed a simple flow system based on a low-cost diaphragm pump that operates at pressures up to 6 bar (Figure 2-8). By employing these diaphragm pumps in flow systems, the pressure gap between conventional HPLC pumps (20 - 400 bar) and peristaltic pumps (< 2 bar) was filled. This system has been used for on-line trace pre-concentration and detection with flame atomic absorption spectroscopy (FAAS) and inductively coupled plasma-optical emission spectrometry (ICP-OES), but could also be used for chemical synthesis with minor modifications.

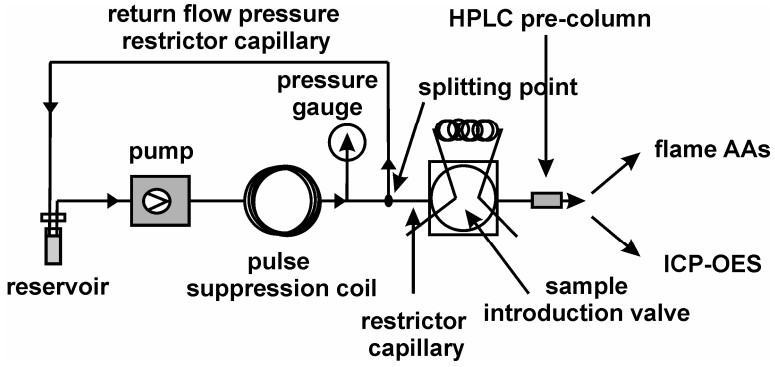

Figure 2-8: Set-up of a damped diaphragm pump system (carrier circulation flow of 100 mL min^{-1} at 6 bar with an analytical split off flow of 0.1 - 50 mL min^{-1}) applied to on-line trace pre-concentration/matrix separation in FAAS and ICP-OES.[225]

A continuous flow-type hydrothermal reaction system based on a reaction loop (stainless-steel tubing with an internal diameter of 0.5 mm and 10 m length) has been reported by Tsuda *et al.* (Figure 2-9).[226] The temperature and the pressure are rapidly

and dynamically controlled in the system and the reaction products are analyzed with liquid chromatography. Using this system, methyl benzoate has been hydrolyzed and analyzed at four conditions (pressure, temperature) in the liquid and supercritical phase (404 °C, 235 bar).

Wakashima *et al.*[227] reported a microtube made from a Ni-base alloy operating in continuous flow at supercritical water conditions (> 221 bar, > 374 °C), however, no synthetic application has been reported yet.

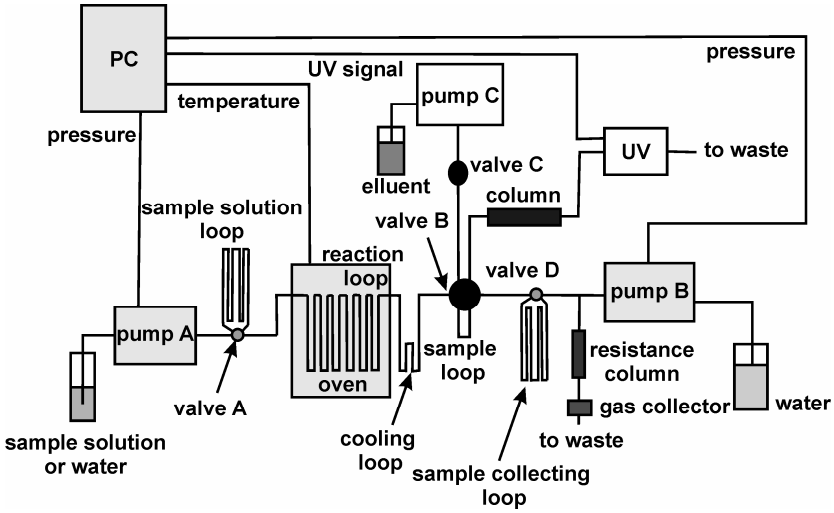

Figure 2-9: Schematic diagram for a high temperature and pressure reaction system with continuous flow hyphenated with liquid chromatograph (RT-HighTP-LC).[226]

2.5.3 Miniaturized systems (microreactors)

2.5.3.1 Introduction

The concept of lab-on-a-chip technology[228,229] is becoming more and more important, in particular for chemical analysis[230] and biotechnology[231,232] applications. Morover, this technology has shown its utility in organic chemistry.[233] From the first miniaturized analytical device, a glass chromatographic analyzer presented by Terry *et al.* at the end of the 1970s[234,235] to the most sophisticated micro Total Analysis Systems (μTAS),[236] the trend is the incorporation of analytical techniques. The design, fabrication, flow control, analysis and connection techniques are under continuous development improving among others, the throughput and the automation,[230,237,238] at the same time leading to reduced costs.[239]

Microreactors, defined as miniaturized reaction vessels fabricated by using, methods of microtechnology and precision engineering,[240] can nowadays be used to study chemical reactions at the microscale scale.[240] Microreactors consist of three-dimensional structures (microchannels) with diameters typically in the range of 10 - 500 μm, which are used to manipulate reagent solutions. Microreactors are usually fabricated in glass, quartz, silicon, polymers, or metals. For synthetic applications glass is the most popular, nevertheless, metals are often used for high pressure applications.[241]

There are many reactions that have been carried out in microreactors and in many cases yield, selectivity and purity are improved, in a continuous flow at the microscale as compared to the conventional lab-scale equipment.[233,242-244] Additionally, continuous flow operation in microreactors enables real-time measurements and consequently fast analysis protocols. Recently, the aim of microdevice experiments are changing from simply proving the feasibility of one chemical reaction towards more in-depth scientific studies and industrial piloting (chemicals-producing industry).[245,246] For the improvement of chemical processes it is very convenient to make use of microreactors,[247] as well as for the production of new or specialty products that are difficult to produce in conventional macroscale reactions.

2.5.3.2 Properties of microreactors

The small characteristic dimensions of microreactors result in small internal volumes and high surface-to-volume ratios, which lead to improved heat and mass transfer rates.

The applications of microreactors in chemistry are very promising because it is possible to optimize conventional chemical processes by improving the selectivity, product quality and safety.

Microreactors intensify mixing and mass transport; this advantage is particularly important in multi-phase reaction systems (gas/liquid or liquid/liquid) and in reactions that are sensitive to temperature. Furthermore, use of microreactors significantly reduces the hazards in for instance fluorinations,[248] chlorinations,[249] nitrations,[250] hydrogenations,[251] and oxygenations.[252,253]

2.5.3.3 Connections for pressure microreactors

To connect microreactors to the "macro world" standard connections can be used such as Swagelok® and metal blocks,[254] silicone *o*-ring couplers,[255] injection-molded plastic couplers,[256] polydimethyl siloxane (PDMS) elastomer based press-fit-type interconnectors.[257] Alternatively a polymer (polyethylene) tube can be fused by melting to the microreactor at the connection point and permanently bonded using epoxy glue.[258]

For pressure and supercritical fluid applications in microreactors the development of interconnectors which can reliably operate under severe operating conditions is crucial. This section presents a summary of the materials used for interconnecting microdevices with pressure systems. A holder (socket) made of polyether ether ketone (PEEK) has been reported by Yang and Maeda.[259,260] With this socket, twenty channels can be easily connected at 2 bar. Another type of holder, also made of PEEK, has been designed for the (non-permanent) coupling of standard capillary tubing to silicon/glass micromixer chips[261] and it resists around 6 bar (Figure 2-10a).

Interconnectors based on polydimethylsiloxane (PDMS) have been introduced by Li and Chen.[262] The maximum working pressures reach 5 - 7 bar, depending on reusable or non-reusable interconnectors (Figure 2-10b). PDMS has also been used for the fabrication of an interconnector that resists up to 10 bar.[263]

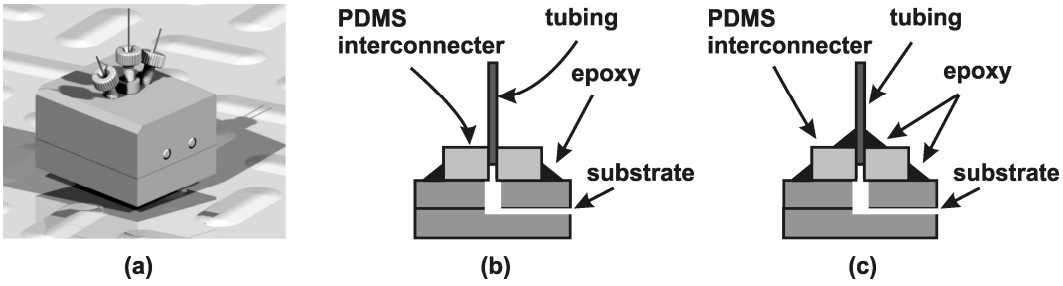

Figure 2-10: (a) Scheme of the assembled chip interface (external dimensions 38 × 35 × 30 mm),[261] (b) schematic representation of an epoxy-glued reusable PDMS interconnector and (c) a nonreusable PDMS interconnector bonded to a silicon substrate using UV-curable epoxy glue.[263]

Plastic tubing connections to microreactors are not very resistant to pressure; for instance Lee *et al.*[264] could not achieve pressures higher than 2 bar. Similar

pressures were obtained with adhesive-free interconnectors fabricated by sealing the silicon inlets of the device with silastic tubes *via* heat treatment.[265]

Metal connections have been used by many research groups. Chen *et al.*[266] combined silicon microreactors with stainless steel for pressures up to 1.5 bar. Pattekar and Kothare[267] improved the pressure range to 21 bar by sealing the inlet/outlets *via in-situ* melting of the metallic fiber and subsequent reinforcement with high pressure epoxy glue. The combination of PDMS and quartz microreactors ("PDMS connection method") for HPLC-chip[268] applications created a very resistant device, with good seals resisting 50 bar.[269] Puntambekar and Ahn[270] increased the durability of the connections to 66 bar by using serial or parallel self-aligning interconnectors. Even better results have been obtained by Szekely and Freitag[271] who fabricated a microreactor, based on clamping of two ceramic plates, which is able to resist pressures up to 150 bar.

From this section it is clear that the main limitation for carrying out pressure experiments in microdevices is the interface with the "macro world". Different materials like plastic, PDMS, or metals have been investigated as well as the way the connectors are attached to the devices (glue, heat and clamp). Nevertheless, only pressures up to 150 bar can be reached and in many cases with poor reproducibility.

2.5.3.4 Reactions under pressure in microreactors

Already in 1962 Shorr *et al.*[272] have described a "high pressure microreactor" for chemical applications. The "microreactor" that consisted of a metallic coil-tube of 2.1 mm inner diameter, resists pressures up to 2 kbar. This principle has been used by Cerveny and Weitkamp[273] for their low volume (14 cm^3, 2 kbar) magnetically stirred high pressure "microreactor" in 1972.

To date there is not yet a real concept of high pressure μTAS. In general, solution reactions in microsystems involve gases and catalysts coated on the channel surface and use pressures of max. 25 bar to improve the miscibility of the gas and the liquid phase.[274,275] Reactions like the oxidation of ammonia,[276] ethylene, 1-butene, methanol, propene, isoprene, methane, carbon monoxide, formamides,[241] and hydrogenations [240,277] were performed in microreactors at pressures of a few bar. A ceramic microreactor with catalytic coatings reported by Menschke *et al.*[278] had high

heat transfer rates and was stable at pressures up to 10 bar and temperatures above 800 °C.

Gas/liquid or gas/liquid/solid reactions in microreactors[279] use pressure (max. 30 bar) to mix gas and liquid,[280] by generating two phases[281] or forming bubbles.[282] Kobayashi *et al.*[283] recently described a microfluidic device for hydrogenation reactions under continuous flow conditions using *sc* CO_2 as a solvent up to 90 bar. In this microreactor substrate solutions and external hydrogen gas are pumped through a microchannel with immobilized palladium (*ca.* 100 - 200 μm in width and depth), utilizing the large specific interfacial area of the microchannel reactor. A high conversion within 1 second can be achieved.

Abdallah *et al.*[284] used a microstructured mesh for gas/liquid/solid hydrogenations and gas/liquid asymmetric hydrogenations (Figure 2-11). The microreactor is able to operate at pressures up to 30 bar in continuous flow mode with residence times of several minutes.

Recently, a modified version of this type of microreactor, with longer residence times (up to hours), has been used to synthesize chiral compounds by hydrogenation of *e.g.* (1*S*, 2*R*)-*cis*-1-amino-2-indanol with Pt deposited at the channel surface using pressures up to 45 bar.[285]

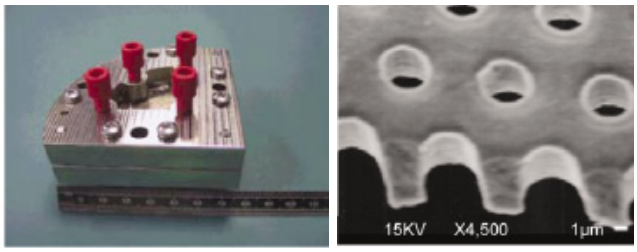

Figure 2-11: Photographs of the mounted mesh microreactor with fluid connectors and the micro-holes (5 μm) (SEM image).[284]

Only a few publications refer to pressure as a tool to perform liquid and liquid/liquid-phase reactions in microreactors. Mae described a micromixer reactor[286] operating at temperatures up to 110 °C and pressures of 6 bar. In this reactor the selectivity of the Friedel-Crafts reaction of aromatic and heteroaromatic compounds is increased with respect to the batch-scale.

An electrochemical microreactor coupled to a continuous chromatographic separation process has been fabricated with a pressure resistance over 30 bar at flow rates of 10 mL min^{-1}. The electrochemical synthesis of 4-methoxybenzaldehyde (**66**)

starting from 4-methoxytoluene (**64**) was chosen as a model reaction. The conversion and selectivity depend on the cell voltage, (Scheme 2-18).[287]

The aqueous Kolbe-Schmitt synthesis of 2,4-dihydroxybenzoic acid from resorcinol has been performed in a microreactor containing a microstructured cooler and a microstructured mixer (Figure 2-12).[288] For temperatures up to 220 °C and pressures up to 74 bar the reaction time was reduced from 2 hours to a few seconds. Compared to standard laboratory operation, the space-time yield increased by a factor of 440.

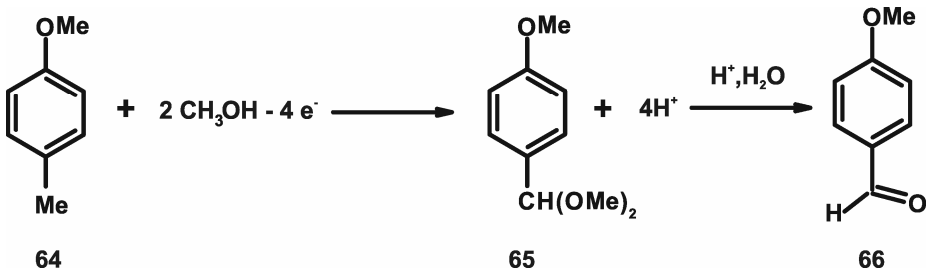

Scheme 2-18: The electrochemical synthesis of 4-methoxybenzaldehyde (**66**) starting from 4-methoxytoluene (**64**) in an electrochemical microreactor. Oxidation in acidified (pH 1, sulfuric acid) methanolic solution containing 0.01 M potassium fluoride at a glassy-carbon electrode.

Using similar instrumentation, the Michael addition reaction of amines to *a,β*-unsaturated carbonyl compounds gave very good yields (> 85%) of the Michael adducts in a very short period of time.[289]

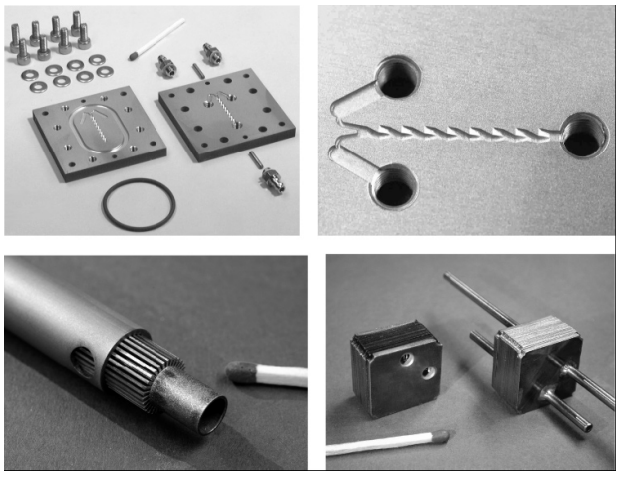

Figure 2-12: Microstructured device used for the Kolbe-Schmitt reaction. Top left: the two microstructured housing plates. Top right: up-down curved ramp-type microstructured channel in the mixer. Bottom left: electrically stirred liquid microstructured pre-heater. Bottom right: fluidically driven liquid microstructured cooler. [288]

The results summarized in this section show that microreactors are not suitable yet for high pressure operation, their highest operative pressure is lower than 150 bar. Investigation in this field is still in its infancy; nevertheless, researchers in microfluidic technology as well as chemists are interested in the development of new systems for performing high pressure at small scale and in continuous flow operation.

2.6 Conclusions and Outlook

High pressure can be an important tool for synthetic chemistry both at laboratory as well as industrial scale. Nevertheless, high pressure is considered to be dangerous and severe safety regulations must be applied.

The benefits of microreactors (among others, continuous flow operation, high surface-to-volume ratio, efficient heat transfer) combined with the advantages of high pressure in organic reactions render high pressure microreactor technology attractive.

Development of miniaturized systems may lead to a situation at which pressure becomes a normal tool in chemistry.

This thesis deals with organic reactions at elevated pressures in glass microreactors. In Chapter 3 organic reactions are carried out in a capillary microreactor, up to 600 bar. The design and fabrication of new microreactors suitable for pressure applications are described in Chapter 4. An important physical property of solvent mixtures, *viz.* phase transition, is investigated in the new microreactors when involving carbon dioxide and alcohols under conditions near the critical point of the mixture (Chapter 5). The effects of the small characteristic dimensions of microreactors, surface-to-volume ratio, thus improves heat and mass transfer and pressure operation on organic reactions are studied when carried out in the microreactors (Chapters 6 and 7). Finally, on-line monitoring of a chemical reaction by NMR spectroscopy is presented, for the first time, using an NMR microreactor (Chapter 8).

2.7 References

1. Matsumoto, K.; Sera, A.; Uchida, T., *Synthesis* **1985**, 1-27.
2. Sharma, A.; Scott, J. H.; Cody, G. D.; Fogel, M. L.; Hazen, R. M.; Hemley, R. J.; Huntress, W. T., *Science* **2002**, *295*, 1514-1516.
3. Bridgman, P. W., *The Physics of High Pressure*. G. Bell and Sons: London (UK), **1952**.
4. Hammann, S. D., *Physico-Chemical Effects of Pressure*. Butterworth: London (UK), **1987**.
5. Röntgen, W. C., *Ann. Phys. Chem.* **1892**, *45*, 91-97.
6. Matsumoto, K.; Acheson, R. M., *Organic Synthesis at High Pressure*. John Wiley and Sons: New York (USA), **1991**.
7. Matsumoto, K.; Ibata, T., *Organic Synthesis under Ultra High Pressure ['Chokoatsu Yuki Gosei']*. Nakanishiya Shuppan Co., Ltd.: Tokyo (Japan), **1999**.
8. Ciobanu, M.; Matsumoto, K., *Liebigs Ann./Recueil* **1997**, 623-635.
9. Matsumoto, K.; Sera, A., *Synthesis* **1985**, 999-1028.
10. Matsumoto, K.; Uchida, T.; Acheson, R. M., *Heterocycles* **1981**, *2*, 103-120.
11. Perreux, L.; Loupy, A., *Tetrahedron* **2001**, *57*, 9199-9223.
12. Lew, A.; Krutzik, P. O.; Hart, M. E.; Chamberlin, A. R., *J. Comb. Chem.* **2002**, *4*, 95-105.
13. Jenner, G., *Tetrahedron* **2002**, *58*, 5185-5202.
14. Tanaka, K.; Toda, F., *Chem. Rev.* **2000**, *100*, 1025-1074.
15. Arai, Y.; Sako, T.; Y., T., *Distinctive Techniques for Organic Synthesis*. World Scientific, Toh Tuck Link: Singapore, **1981**.
16. Savage, P. E., *Chem. Rev.* **1999**, *99*, 603-621.
17. Arai, Y.; Sako, T.; Y., Takebayashi., *Supercritical Fluids: Molecular Interactions, Physical Properties and New Applications*. Springer-Verlag: Berlin (Germany), **2002**.
18. Van Eldik, R.; Klärner, F.-G., *High Pressure Chemistry*. Wiley-VCH: Weinheim (Germany), **2002**.
19. Chen, Z.; Wang, P.; Chang, H. C., *Anal. Bioanal. Chem.* **2005**, *382*, 817-824.
20. McMillan, P. F., *Chem. Soc. Rev.* **2006**, *35*, 855-857.
21. San-Miguel, A., *Chem. Soc. Rev.* **2006**, *35*, 876-889.
22. Horvath-Bordon, E.; Riedel, R.; Zerr, A.; McMillan, P. F.; Auffermann, G.; Prots, Y.; Bronger, W.; Kniep, R.; Kroll, P., *Chem. Soc. Rev.* **2006**, *35*, 987-1014.
23. Santoro, M.; Gorelli, F. A., *Chem. Soc. Rev.* **2006**, *35*, 918-931.
24. Wilding, M. C.; Wilson, M.; McMillan, P. F., *Chem. Soc. Rev.* **2006**, *35*, 964-986.
25. Thies, H., *Chimia* **1978**, *32*, 79-84.
26. Le Noble, W. J., *Chem. unserer Zeit* **1983**, *17*, 152-162.

27. Klärner, F.-G., *Chem. unserer Zeit* **1989**, *23*, 53-61.
28. Stranks, D. R., *Pure Appl. Chem.* **1974**, *38*, 303-323.
29. Klärner, F. G.; Wurche, F., *J. Prakt. Chem.* **2000**, *342*, 609-636.
30. Saudan, C.; Dunand, F. A.; Abou-Hamdan, A.; Bugnon, P.; Lye, P. G.; Lincoln, S. F.; Merbach, A. E., *J. Am. Chem. Soc.* **2001**, *123*, 10290-10298.
31. Jenner, G., *Tetrahedron* **1997**, *53*, 2669-2695.
32. Van Berkom, L. W. A.; Kuster, G. J. T.; Scheeren, H. W., *Mol. Divers.* **2003**, *6*, 271-282.
33. Kuster, G. J.; Scheeren, H. W., *Tetrahedron Lett.* **2000**, *41*, 515-519.
34. Kuster, G. J.; Scheeren, H. W., *Tetrahedron Lett.* **1998**, *39*, 3613-3616.
35. Reiser, O., *Top. Catal.* **1998**, *5*, 105-112.
36. Isaacs, N. S., *Liquid Phase High Pressure Chemistry*. John Wiley: Chichester (UK), **1981**.
37. Hemley, R. J., *Annu. Rev. Phys. Chem.* **2000**, *51*, 763-800.
38. Hunt, F.; Ohde, H.; Wai, C. M., *Rev. Sci. Instrum.* **1999**, *70*, 4661-4667.
39. Atkins, P. W., *Physical Chemistry, 5rd Ed.* Oxford University Press: Oxford (UK), **1994**.
40. Moore, J. W.; Pearson, R. G., *Kinetic and Mechanism, 3rd Ed.* John Wiley: New York (USA), **1981**.
41. Bruice, P. Y., *Organic Chemistry, 3rd Ed.* Prentice Hall: London (UK), **2001**; p 367-369.
42. Hubbard, C. D.; Van Eldik, R., *Instrumentation Sci. Tech.* **1995**, *23*, 1-41.
43. Stearn, A. E.; Eyring, H., *Chem. Rev.* **1941**, *29*, 509-523.
44. Viana, C. A. N.; Reis, J. C. R., *Pure Appl. Chem.* **1996**, *68*, 1541-1551.
45. Asano, T.; Okada, T., *J. Phys. Chem.* **1984**, *88*, 238-243.
46. Yoshimura, Y.; Osugi, J.; Nakahara, M., *J. Am. Chem. Soc.* **1983**, *105*, 5414-5418.
47. Bondi, A., *J. Phys. Chem.* **1964**, *68*, 441-451.
48. Asano, T.; Le Noble, W. J., *Chem. Rev.* **1978**, *78*, 407-489.
49. Buback, M., *Angew. Chem., Int. Ed.* **1991**, *30*, 641-653.
50. Buback, M., *J. Mol. Struct.* **1995**, *347*, 113-129.
51. Buback, M.; Klingbeil, S., *Chem. Ing. Tech.* **1995**, *67*, 493-495.
52. Spitzer, M.; Gartig, F.; Van Eldik, R., *Rev. Sci. Instrum.* **1988**, *59*, 2092-2093.
53. Frey, U.; Helm, L.; Merbach, A. E., *High Pressure Res.* **1990**, *2*, 237-243.
54. Alezra, V.; Bernardinelli, G.; Corminboeuf, C.; Frey, U.; Kundig, E. P.; Merbach, A. E.; Saudan, C. M.; Viton, F.; Weber, J., *J. Am. Chem. Soc.* **2004**, *126*, 4843-4853.
55. Tietze, L. F.; Ott, C.; Frey, U., *Liebigs Ann.* **1996**, 63-67.
56. Kotowski, M.; Van Eldik, R., *Coord. Chem. Rev.* **1989**, *93*, 19-57.
57. Magde, D.; Van Eldik, R., *High Pressure Techniques in Chemistry and Physics: A Practical Approach*. Oxford University Press: Oxford (UK), **1997**.

58. Heydemann, P. L. M.; Kelm, H., *High Pressure Chemistry*. Reidel, Dordrecht (The Netherlands), **1978**.
59. Lentz, H.; Oh, S. O., *High Temp. - High Pressures* **1975**, *7*, 91-95.
60. Grieger, R. A.; Eckert, C. A., *Trans. Faraday Soc.* **1970**, *66*, 2579-2583.
61. Kotowski, M.; Palmer, D. A.; Kelm, H., *Inorg. Chem.* **1979**, *18*, 2555-2560.
62. Van Eldik, R.; Hubbard, C. D., *Chemistry under Extreme or Non-Classical Conditions*. John Wiley and Sons, Inc: New York (USA), **1997**.
63. Heremans, K.; Snauweaert, J.; Rijkenberg, J., *Rev. Sci. Instrum.* **1980**, *51*, 806-808.
64. Ishihara, K.; Funahashi, S.; Tanaka, M., *Rev. Sci. Instrum.* **1982**, *53*, 1231-1234.
65. Ishihara, K.; Kondo, Y.; Koizumi, M., *Rev. Sci. Instrum.* **1999**, *70*, 244-245.
66. White, A. J.; Drabble, K.; Wharton, C. W., *Biochem. J.* **1995**, *306*, 843-849.
67. Hald, P.; Becker, J.; Bremholm, M.; Pedersen, J. S.; Chevallier, J.; Iversen, S. B.; Iversen, B. B., *J. Solid State Chem.* **2006**, *179*, 2674-2680.
68. Ghaziaskar, H. S.; Daneshfar, A.; Calvo, L., *Green Chem.* **2006**, *8*, 576-581.
69. Jones, R. V.; Godorhazy, L.; Varga, N.; Szalay, D.; Urge, L.; Darvas, F., *J. Comb. Chem.* **2006**, *8*, 110-116.
70. Tanimoto, S.; Matsumoto, H.; Fujii, K.; Ohdoi, R.; Sakamoto, K.; Izuwa, S.; Yamane, Y.; Miyake, M.; Shimoda, M.; Osajima, Y., *Biosci. Biotechnol. Biochem.* **2005**, *69*, 2094-2100.
71. Takebayashi, Y.; Yoda, S.; Sugeta, T.; Otake, K. In *Continuous-Flow Reactor for Kinetic Analysis of Rapid Hydrothermal Reactions by Raman Spectroscopy*, The 14th International Conference on the Properties of Water and Steam (14th ICPWS), Kyoto (Japan), August 29 - September 3, **2004**.
72. http://www.hi-techsci.com/print/tj-tech-print.html.
73. Jonas, J., *Adv. Magn. Reson.* **1973**, *6*, 73-139.
74. Merbach, A. E., *Pure Appl. Chem.* **1987**, *59*, 161-173.
75. Moore, J. W., *Pure Appl. Chem.* **1985**, *59*, 345-355.
76. Ando, I.; Webb, G. A., *Magn. Reson. Chem.* **1995**, *24*, 557-567.
77. Damoense, L.; Datt, M.; Green, M.; Steenkamp, C., *Coord. Chem. Rev.* **2004**, *248*, 2393-2407.
78. Yonker, C. R.; Linehan, J. C., *Prog. Nucl. Magn. Reson. Spectrosc.* **2005**, *47*, 95-109.
79. Doss, R.; Van Eldik, R.; Kelm, H., *Inorg. Chem.* **1982**, *21*, 4108-4109.
80. Brill, T. B.; Brush, P. J.; James, K. J.; Shepherd, J. E.; Pfeiffer, K. J., *Appl. Spectrosc.* **1992**, *46*, 900-911.
81. Brower, K. R., *J. Am. Chem. Soc.* **1968**, *90*, 5401-5403.
82. Giovanelli, D.; Lawrence, N. S.; Compton, R. G., *Electroanalysis* **2004**, *16*, 789-810.
83. Stoll, N.; Hawali, I.; Thurow, K., *J. Autom. Methods Manag. Chem.* **2005**, 230-234.

84. Miura, K.; Nakagawa, H.; Nakai, S. I.; Kajitani, S., *Chem. Eng. Sci.* **2004**, *59*, 5261-5268.
85. Jenner, G., *Mini-Rev. Org. Chem.* **2004**, *1*, 9-26.
86. Aben, R. W.; Keijsers, J. A.; Scheeren, J. W., *High Pressure Res.* **1991**, *7*, 569-572.
87. Jenner, G., *New J. Chem.* **1999**, *23*, 525-529.
88. Kiselev, V. D.; Kashaeva, E. A.; Shihab, M. S.; Potapova, L. N.; Iskhakova, G. G., *Russ. Chem. Bull.* **2004**, *53*, 45-50.
89. Swiss, K. A.; Firestone, R. A., *J. Phys. Chem. A* **2000**, *104*, 3057-3063.
90. Jessop, P. G.; Leitner, W., *Chemical Synthesis Using Supercritical Fluids*. Wiley-VCH: Weinheim (Germany), **1999**.
91. Adams, D. J.; Dyson, P. J.; Tevener, S. J., *Chemistry in Alternative Reaction Media*. Willey: New York (USA), **2004**.
92. Garrabos, Y.; Leneindre, B.; Subra, P.; Cansell, F.; Pommier, C., *Ann. Chim. Sci. Mat.* **1992**, *17*, 55-90.
93. Paryjczak, T.; Lewicki, A., *Przem. Chem.* **2006**, *85*, 85-95.
94. Pasquali, I.; Bettini, R.; Giordano, F., *Eur. J. Pharm. Sci.* **2006**, *27*, 299-310.
95. Shariati, A.; Peters, C. J., *J. Supercrit. Fluids* **2005**, *34*, 171-176.
96. Andrade, C. K. Z.; Alves, L. M., *Curr. Org. Chem.* **2005**, *9*, 195-218.
97. Tang, Z.; Xie, W. H.; Zong, B. N.; Min, E. Z., *Chin. J. Chem. Eng.* **2004**, *12*, 498-504.
98. Perrut, M., *Stp Pharma Sciences* **2003**, *13*, 83-91.
99. Hauthal, W. H., *Chemosphere* **2001**, *43*, 123-135.
100. Prajapati, D.; Gohain, M., *Tetrahedron* **2004**, *60*, 815-833.
101. Beckman, E. J., *J. Supercrit. Fluids* **2004**, *28*, 121-191.
102. Welton, T., *Chem. Rev.* **1999**, *99*, 2071-2083.
103. Le Noble, W. J., *Organic High Pressure Chemistry*. Elservier: Amsterdam (The Netherlands), **1988**.
104. Van Eldik, R.; Asano, T.; Le Noble, W. J., *Chem. Rev.* **1989**, *89*, 549-688.
105. Buchanan, J.; Hamann, S. D., *Trans. Faraday Soc.* **1953**, *49*, 1425-1442.
106. Kappe, C. O.; Murphree, S. S.; Padwa, A., *Tetrahedron* **1997**, *53*, 14179-14233.
107. Borm, C.; Meibom, D.; Winterfeldt, E., *Chem. Commun.* **1996**, 887-894.
108. Boranowski, B.; Jurczak, J., *High Pressure Chemical Synthesis*. Elsevier: New York (USA), **1989**.
109. Matsumoto, K.; Hamana, H.; Iida, H., *Helv. Chim. Acta* **2005**, *88*, 2033-2234.
110. McMillan, P. F., *Chem. Soc. Rev.* **2006**, *35*, 855-857.
111. Kranjc, K.; Kocevar, M., *New J. Chem.* **2005**, *29*, 1027-1034.
112. Kranjc, K.; Stefane, B.; Polanc, S.; Kocevar, M., *J. Org. Chem.* **2004**, *69*, 3190-3193.

113. Fujita, R.; Watanabe, K.; Yoshisuji, T.; Kabuto, C.; Matsuzaki, H.; Hongo, H., *Chem. Pharm. Bull.* **2001**, *49*, 893-899.
114. Tran-Huu-Dau, M. E.; Wartchow, R.; Winterfeldt, E.; Wong, Y. S., *Chem. Eur. J.* **2001**, *7*, 2349-2369.
115. Chretien, A.; Chataigner, I.; Piettre, S. R., *Tetrahedron* **2005**, *61*, 7907-7915.
116. Kosior, M.; Kwiatkowski, P.; Asztemborska, M.; Jurczak, J., *Tetrahedron: Asymmetry* **2005**, *16*, 2897-2900.
117. Kwiatkowski, P.; Chaladaj, W.; Malinowska, M.; Asztemborska, M.; Jurczak, J., *Tetrahedron: Asymmetry* **2005**, *16*, 2959-2964.
118. Kwiatkowski, P.; Asztemborska, M.; Caille, J. C.; Jurczak, J., *Adv. Synth. Catal.* **2003**, *345*, 506-509.
119. Malinowska, M.; Salanski, P.; Caille, J. C.; Jurczak, J., *Synthesis* **2002**, 2707-2710.
120. Kwiatkowski, P.; Asztemborska, M.; Jurczak, J., *Tetrahedron: Asymmetry* **2004**, *15*, 3189-3194.
121. Malinowska, M.; Kwiatkowski, P.; Jurczak, J., *Tetrahedron Lett.* **2004**, *45*, 7693-7696.
122. Minuti, L.; Taticchi, A.; Marrocchi, A.; Broggi, A.; Gacs-Baitz, E., *Tetrahedron: Asymmetry* **2004**, *15*, 1187-1192.
123. Rao, H. S. P.; Murali, R.; Taticchi, A.; Scheeren, H. W., *Eur. J. Org. Chem.* **2001**, 2869-2876.
124. Palasz, A., *Org. Biomol. Chem.* **2005**, *3*, 3207-3212.
125. Aversa, M. C.; Barattucci, A.; Bonaccorsi, P.; Faggi, C.; Gacs-Baitz, E.; Marrocchi, A.; Minuti, L.; Taticchi, A., *Tetrahedron* **2005**, *61*, 7719-7726.
126. Lemiegre, L.; Stevens, R. L.; Combret, J. C.; Maddaluno, J., *Org. Biomol. Chem.* **2005**, *3*, 1308-1318.
127. Meibom, D.; Weinmann, H.; Winterfeldt, E., *Arkivoc* **2004**, 4-23.
128. Lomberget, T.; Chataigner, I.; Bouyssi, D.; Maddaluno, J.; Balme, G., *Tetrahedron Lett.* **2004**, *45*, 3437-3441.
129. Troisi, L.; De Vitis, L.; Granito, C.; Pilat, W.; Pindinelli, E., *Tetrahedron* **2004**, *60*, 6895-6900.
130. Knappwost-Gieseke, C.; Nerenz, F.; Wartchow, R.; Winterfeldt, E., *Chem. Eur. J.* **2003**, *9*, 3849-3858.
131. Hada, V.; Tungler, A.; Szepesy, L., *J. Catal.* **2002**, *209*, 472-479.
132. Fujita, R.; Watanabe, K.; Yoshisuji, T.; Hongo, H.; Matsuzaki, H., *Chem. Pharm. Bull.* **2001**, *49*, 900-904.
133. Ishikura, M.; Uchiyama, H.; Hino, A.; Katagiri, N., *J. Heterocycl. Chem.* **2001**, *38*, 675-678.
134. Biolatto, B.; Kneeteman, M.; Paredes, E.; Mancini, P. M. E., *J. Org. Chem.* **2001**, *66*, 3906-3912.

135. Fujita, R.; Watanabe, K.; Yoshisuji, T.; Matsuzaki, H.; Harigaya, Y.; Hongo, H., *Chem. Pharm. Bull.* **2001**, *49*, 407-412.
136. Fujita, R.; Oikawa, K.; Yoshisuji, T.; Okuyama, Y.; Nakano, H.; Matsuzaki, H., *Chem. Pharm. Bull.* **2003**, *51*, 295-300.
137. Drew, M. G. B.; Jahans, A.; Harwood, L. M.; Apoux, S., *Eur. J. Org. Chem.* **2002**, 3589-3594.
138. Minuti, L.; Taticchi, A.; Marrocchi, A.; Costantini, L.; Gacs-Baitz, E., *Tetrahedron: Asymmetry* **2001**, *12*, 1179-1183.
139. Kuster, G. J. T.; Van Berkom, L. W. A.; Kalmoua, M.; Van Loevezijn, A.; Sliedregt, L.; Van Steen, B. J.; Kruse, C. G.; Rutjes, F. P. J. T.; Scheeren, H. W., *J. Comb. Chem.* **2006**, *8*, 85-94.
140. Kumamoto, K.; Fukada, I.; Kotsuki, H., *Angew. Chem., Int. Ed.* **2004**, *43*, 2015-2017.
141. Danishefsky, S.; Tsuzuki, K., *J. Am. Chem. Soc.* **1980**, *102*, 6893-6894.
142. McCluskey, A.; Keane, M. A.; Walkom, C. C.; Bowyer, M. C.; Sim, A. T. R.; Young, D. J.; Sakoff, J. A., *Bioorg. Med. Chem. Lett.* **2002**, *12*, 391-393.
143. Attard, G. A.; Griffin, K. G.; Jenkins, D. J.; Johnston, P.; Wells, P. B., *Catal. Today* **2006**, *114*, 346-352.
144. Pichlmair, S.; Ruiz, M. D.; Basu, K.; Paquette, L. A., *Tetrahedron* **2006**, *62*, 5178-5194.
145. Yang, C.; Nakamura, A.; Fukuhara, G.; Origane, Y.; Mori, T.; Wada, T.; Inoue, Y., *J. Org. Chem.* **2006**, *71*, 3126-3136.
146. Grunwaldt, J. D.; Baiker, A., *Phys. Chem. Chem. Phys.* **2005**, *7*, 3526-3539.
147. Jarosz, S.; Gawel, A., *Eur. J. Org. Chem.* **2005**, 3415-3432.
148. Jarosz, S.; Szewczyk, K.; Gawel, A.; Luboradzki, R., *Tetrahedron: Asymmetry* **2004**, *15*, 1719-1727.
149. Van Eldik, R.; Asano, T.; Le Noble, W. J., *Chem. Rev.* **1989**, *89*, 549-688.
150. Diedrich, M. K.; Klärner, F. G., *J. Am. Chem. Soc.* **1998**, *120*, 6212-6218.
151. Blanarikova-Hlobilova, I.; Kubanova, Z.; Fisera, L.; Cyranski, M. K.; Salanski, P.; Jurczak, J.; Pronayova, N., *Tetrahedron* **2003**, *59*, 3333-3339.
152. Brunner, M.; Maas, G.; Klärner, F. G., *Helv. Chim. Acta* **2005**, *88*, 1813-1825.
153. Aben, R. W. M.; Braverman, S.; Scheeren, H. W., *Eur. J. Org. Chem.* **2003**, 894-897.
154. Aben, R. W. M.; De Gelder, R.; Scheeren, H. W., *Eur. J. Org. Chem.* **2002**, 3126-3132.
155. Jenner, G., *Tetrahedron Lett.* **2001**, *42*, 243-245.
156. Ohishi, T.; Kojima, T.; Matsuoka, T.; Shiro, M.; Kotsuki, H., *Tetrahedron Lett.* **2001**, *42*, 2493-2496.
157. Sekiguchi, Y.; Sasaoka, A.; Shimomoto, A.; Fujioka, S.; Kotsuki, H., *Synlett* **2003**, 1655-1658.
158. Misumi, Y.; Matsumoto, K., *Angew. Chem., Int. Ed.* **2002**, *41*, 1031-1034.

159. Azad, S.; Kumamoto, K.; Uegaki, K.; Ichikawa, Y.; Kotsuki, H., *Tetrahedron Lett.* **2006**, *47*, 587-590.
160. Kumamoto, K.; Misawa, Y.; Tokita, S.; Kubo, Y.; Kotsuki, H., *Tetrahedron Lett.* **2002**, *43*, 1035-1038.
161. Kumamoto, K.; Ichikawa, Y.; Kotsuki, H., *Synlett* **2005**, 2254-2256.
162. Hayashi, Y.; Tsuboi, W.; Shoji, M.; Suzuki, N., *J. Am. Chem. Soc.* **2003**, *125*, 11208-11209.
163. Hayashi, Y.; Tsuboi, W.; Shoji, M.; Suzuki, N., *Tetrahedron Lett.* **2004**, *45*, 4353-4356.
164. Hayashi, Y.; Okada, K.; Ashimine, I.; Shoji, M., *Tetrahedron Lett.* **2002**, *43*, 8683-8686.
165. Jenner, G., *Tetrahedron* **2005**, *61*, 3621-3635.
166. Cheung, C. K.; Wedinger, R. S.; Le Noble, W. J., *J. Org. Chem.* **1989**, *54*, 570-573.
167. Jenner, G., *Tetrahedron Lett.* **2001**, *42*, 4807-4810.
168. Jenner, G., *High Pressure Res.* **2004**, *24*, 163-168.
169. Jenner, G., *Tetrahedron* **2002**, *58*, 4311-4317.
170. Kwiatkowski, P.; Wojaczynska, E.; Jurczak, J., *Tetrahedron: Asymmetry* **2003**, *14*, 3643-3645.
171. Kwiatkowski, P.; Chaladaj, W.; Jurczak, J., *Tetrahedron* **2006**, *62*, 5116-5125.
172. Kwiatkowski, P.; Chaladaj, W.; Jurczak, J., *Synlett* **2005**, 2301-2304.
173. Kwiatkowski, P.; Jurczak, J., *Synlett* **2005**, 227-230.
174. Camara, C.; Keller, L.; Jean-Charles, K.; Joseph, D.; Dumas, F., *High Pressure Res.* **2004**, *24*, 149-162.
175. Tietze, L. F.; Henrich, M.; Rothert, I.; Kuchta, G.; Buback, M., *Pol. J. Chem.* **1997**, *71*, 1749-1762.
176. Jenner, G., *J. Phys. Org. Chem.* **1999**, *12*, 619-625.
177. Jenner, G.; Gacem, B., *J. Phys. Org. Chem.* **2003**, *16*, 265-270.
178. Hayashi, Y.; Nishimura, K., *Chem. Lett.* **2002**, 296-297.
179. Has-Becker, S.; Bodmann, K.; Kreuder, R.; Santoni, G.; Rein, T.; Reiser, O., *Synlett* **2001**, 1395-1398.
180. von Essen, R.; Frank, D.; Sunnemann, H. W.; Vidovic, D.; Magull, J.; De Meijere, A., *Chem. Eur. J.* **2005**, *11*, 6583-6592.
181. Gallos, J. K.; Koumbis, A. E., *Arkivoc* **2003**, 135-144.
182. Marrocchi, A.; Minuti, L.; Taticchi, A.; Scheeren, H. W., *Tetrahedron* **2001**, *57*, 4959-4965.
183. Kuster, G. J. T.; Steeghs, R. H. J.; Scheeren, H. W., *Eur. J. Org. Chem.* **2001**, 553-560.
184. Van Berkom, L. W. A.; Kuster, G. J. T.; Kalmoua, F.; De Gelder, R.; Scheeren, H. W., *Tetrahedron Lett.* **2003**, *44*, 5091-5093.
185. Voigt, K.; Schick, U.; Meyer, F. E.; Demeijere, A., *Synlett* **1994**, 189-190.
186. Buback, M.; Perkovic, T.; Redlich, S.; De Meijere, A., *Eur. J. Org. Chem.* **2003**, 2375-2382.

187. Jenner, G., *Tetrahedron Lett.* **2002**, *43*, 1235-1238.
188. Matsumoto, K.; Kim, J. C.; Hayashi, N.; Jenner, G., *Tetrahedron Lett.* **2002**, *43*, 9167-9169.
189. Jenner, G.; Ben Salem, R.; Kim, J. C.; Matsumoto, K., *Tetrahedron Lett.* **2003**, *44*, 447-449.
190. Matsumoto, K.; Kim, J. C.; Iida, H.; Hamana, H.; Kumamoto, K.; Kotsuki, H.; Jenner, G., *Helv. Chim. Acta* **2005**, *88*, 1734-1753.
191. Gacem, B.; Jenner, G., *High Pressure Res.* **2004**, *24*, 233-236.
192. Jenner, G., *Tetrahedron Lett.* **2001**, *42*, 8969-8971.
193. Matsuo, I.; Wada, M.; Ito, Y., *Tetrahedron Lett.* **2002**, *43*, 3273-3275.
194. Zielinski, T.; Achmatowicz, M.; Jurczak, J., *Tetrahedron: Asymmetry* **2002**, *13*, 2053-2059.
195. Szczepanska, A.; Salanskia, P.; Jurczak, J., *Tetrahedron* **2003**, *59*, 4775-4783.
196. Szczepanska, A.; Tarnowski, P.; Jurczak, J., *Pol. J. Chem.* **2005**, *79*, 1909-1917.
197. Kroszczynski, W.; Olszewska, E.; Salanski, P.; Jurczak, J., *Helv. Chim. Acta* **2004**, *87*, 1488-1492.
198. Tarnowska, A.; Jarosz, M.; Jurczak, J., *Synthesis* **2004**, 369-372.
199. Tarnowska, A.; Tarnowski, P.; Jurczak, J., *Tetrahedron Lett.* **2004**, *45*, 9553-9556.
200. Lipkowski, P.; Urbanczyk-Lipkowska, Z.; Jurczak, J., *Pol. J. Chem.* **2002**, *76*, 729-736.
201. Jezewski, A.; Jurczak, J.; Lidert, Z.; Tice, C. M., *J. Heterocycl. Chem.* **2001**, *38*, 645-648.
202. Kumamoto, K.; Iida, H.; Hamana, H.; Kotsuki, H.; Matsumoto, K., *Heterocycles* **2005**, *66*, 675-681.
203. Choi, M. C. K.; Chan, S. S.; Chan, M. K.; Kim, J. C.; Iida, H.; Matsumoto, K., *Heterocycles* **2004**, *62*, 643-653.
204. Choi, M. C. K.; Chan, S. S.; Chan, M. K.; Kim, J. C.; Matsumoto, K., *Heterocycles* **2002**, *58*, 645-654.
205. Misumi, Y.; Bulman, R. A.; Matsumoto, K., *Heterocycles* **2002**, *56*, 599-605.
206. Jas, G.; Kirschning, A., *Chem. Eur. J.* **2003**, *9*, 5708-5723.
207. Hafez, A. M.; Taggi, A. E.; Lectka, T., *Chem. Eur. J.* **2002**, *8*, 4114-4119.
208. Tundo, P., *Continuous Flow Methods in Organic Synthesis*. Wiley-Interscience: New York (USA), **1991**.
209. Jönsson, D.; Warrington, B. H.; Ladlow, M., *J. Comb. Chem.* **2004**, *6*, 584-595.
210. Jansen, J.; Niemeyer, B., *J. Supercrit. Fluids* **2005**, *33*, 285-293.
211. Kirschning, A.; Altwicker, C.; Drager, G.; Harders, J.; Hoffmann, N.; Hoffmann, U.; Schonfeld, H.; Solodenko, W.; Kunz, U., *Angew. Chem., Int. Ed.* **2001**, *40*, 3995-3998.
212. Zhao, Z.; Diemant, T.; Haring, T.; Rauscher, H.; Behm, R. J., *Rev. Sci. Instrum.* **2005**, *76*.
213. Desai, B.; Kappe, C. O., *J. Comb. Chem.* **2005**, *7*, 641-643.
214. http://thalesnano.com/H-Cube.

215. Denayer, J. F. M.; Ocakoglu, R. A.; Huybrechts, W.; Dejonckheere, B.; Jacobs, P.; Calero, S.; Krishna, R.; Smit, B.; Baron, G. V.; Martens, J. A., *J. Catal.* **2003**, *220*, 66-73.
216. Banister, J. A.; Howdle, S. M.; Poliakoff, M., *J. Chem. Soc., Chem. Commun.* **1993**, 1814-1815.
217. Burck, J.; Wiegand, G.; Roth, S.; Mathieu, H.; Kramer, K., *J. Near Infrared Spectrosc.* **2004**, *12*, 29-36.
218. DeSimone, J. M.; Tumas, W., *Green Chemistry Using Liquid and Supercritical Carbon Dioxide*. Oxford University Press: New York (USA), **2002**.
219. Caravati, M.; Grunwaldt, J. D.; Baiker, A., *Catal. Today* **2004**, *91-92*, 1-5.
220. Caravati, M.; Grunwaldt, J. D.; Baiker, A., *Appl. Catal., A* **2006**, *298*, 50-56.
221. Wille, C. *Entwicklung Und Charakterisierung Eines Mikrofallfilm-Reaktors Für Stofftransportlimitierte Hochexotherme Gas/Flüssig-Reaktionen*. PhD thesis. University Clausthal-Zellerfeld, 2002.
222. Yoswathananont, N.; Nitta, K.; Nishiuchi, Y.; Sato, M., *Chem. Commun.* **2005**, 40-42.
223. Dummann, G.; Quittmann, U.; Groschel, L.; Agar, D. W.; Worz, O.; Morgenschweis, K., *Catal. Today* **2003**, *79*, 433-439.
224. Burns, J. R.; Ramshaw, C., *Chem. Eng. Res. Des.* **1999**, *77*, 206-211.
225. Ratka, A.; Berndt, H., *Anal. Bioanal. Chem.* **2003**, *375*, 275-280.
226. Tsuda, T.; Kitagawa, S.; Umeyama, T.; Araki, S.; Hirashita, T.; Aoki, M.; Nakamura, K., *Anal. Sci.* **2006**, *22*, 479-481.
227. Wakashime, Y.; Hatakeda, K.; Suzuki, A. In *Microtube and Microchannel Devices for Continuous Supercritical Water Chemical Synthesis*, 9th International Conference on Microreaction Technology (IMRET 9), Postdam/Berlin (Germany), 6-8 Sept, **2006**, p 186-187.
228. Ehrfeld, W., *Microsystem Technology for Chemical and Biological Bioreactors*. Frankfurt (Germany), **1995**; Vol. 132, p 1-28.
229. Gravesen, P.; Branebjerg, J.; Jensen, O. S., *J. Micromech. Microeng.* **1993**, *3*, 168-182.
230. Vilkner, T.; Janasek, D.; Manz, A., *Anal. Chem.* **2004**, *76*, 3373-3385.
231. Thorsen, T.; Maerkl, S. J.; Quake, S. R., *Science* **2002**, *298*, 580-584.
232. Kopp, M. U.; De Mello, A. J.; Manz, A., *Science* **1998**, *280*, 1046-1048.
233. Brivio, M.; Verboom, W.; Reinhoudt, D. N., *Lab Chip* **2006**, *6*, 329-344.
234. Terry, S. C. *A Gas Chromatography System Fabricated on a Silicon Wafer Using Integrated Circuit Technology*. PhD thesis. Stanford University, Stanford, (USA), 1975.
235. Terry, S. C.; Jerman, J. H.; Angell, J. B., *IEEE Trans. Electron. Devices* **1979**, ED-26, 1880.
236. Dittrich, P. S.; Tachikawa, K.; Manz, A., *Anal. Chem.* **2006**, *78*, 3887-3907.
237. Reyes, D. R.; Iossifidis, D.; Auroux, P. A.; Manz, A., *Anal. Chem.* **2002**, *74*, 2623-2636.
238. Auroux, P. A.; Iossifidis, D.; Reyes, D. R.; Manz, A., *Anal. Chem.* **2002**, *74*, 2637-2652.
239. Kakuta, M.; Bessoth, F. G.; Manz, A., *Chem. Record* **2001**, *1*, 395-405.

240. Ehrfeld, W.; Hessel, V.; Löwe, H., *Microreactors: New Technology for Modern Chemistry*. Wiley-VCH: Weinheim, (Germany), **2000**.

241. Hessel, V.; Hardt, S.; Löwe, H., *Chemical Micro Process Engineering*. Wiley-VCH: Weinheim (Germany), **2004**.

242. Watts, P.; Haswell, S. J., *Chem. Eng. Tech.* **2005**, *28*, 290-301.

243. Erbacher, C.; Bessoth, F. G.; Busch, M.; Verpoorte, E.; Manz, A., *Mikrochim. Acta* **1999**, *131*, 19-24.

244. Ismagilov, R. F., *Angew. Chem., Int. Ed.* **2003**, *42*, 4130-4132.

245. Pennemann, H.; Hessel, V.; Löwe, H., *Chem. Eng. Sci.* **2004**, *59*, 4789-4794.

246. Pennemann, H.; Watts, P.; Haswell, S. J.; Hessel, V.; Löwe, H., *Org. Process Res. Dev.* **2004**, *8*, 422-439.

247. Jensen, K. F., *AIChE J.* **1999**, *45*, 2051-2054.

248. Chambers, R. D.; Holling, D.; Spink, R. C. H.; Sandford, G., *Lab Chip* **2001**, *1*, 132-137.

249. Jähnisch, K.; Hessel, V.; Löwe, H.; Baerns, M., *Angew. Chem., Int. Ed.* **2004**, *43*, 406-446.

250. Doku, G. N.; Haswell, S. J.; McCreedy, T.; Greenway, G. M., *Analyst* **2001**, *126*, 14-20.

251. De Mas, N.; Jackman, R. J.; Schmidt, M. A.; Jensen, K. F.; Matlosz, M.; Ehrfelt, W.; Baselt, J. P. In *Microchemical Systems for Direct Fluorination of Aromatics*, Proc. IMRET 5, Springer: Berlin (Germany), **2002**, p 60.

252. Veser, G., *Chem. Eng. Sci.* **2001**, *56*, 1265-1273.

253. Widmer, H. M., *Chimia* **1997**, *51*, 12-13.

254. Vandelli, N.; Wroblewski, D.; Velonis, M.; Bifano, T., *J. Microelectromech. Syst.* **1998**, *7*, 395-403.

255. Yao, T.; Lee, S.; Fang, W.; Tai, Y. In *Micromachined Rubber O-Ring Microfluidic Couplers*, 13th IEEE Int. Conf. on Micro Electro Mechanical Systems (MEMS '00), Miyazaki, Japan, 23-27 Jan., **2000**, p 624-625.

256. Gray, B. L.; Jaeggi, D.; Mourlas, N. J.; Van Drieenhuizen, B. P.; Williams, K. R.; Maluf, N. I.; Kovacs, G. T. A., *Sens. Actuators, A* **1999**, *77*, 57-65.

257. Armani, D.; Liu, C.; Aluru, N. In *Re-Configurable Fluid Circuits by Pdms Elastomer Micromachining*, 12th IEEE Int. Conf. on Micro electro Mechanical Systems (MEMS'99), Orlando, FL, USA, 17-21 January, **1999**, p 222-227.

258. Andersson, H.; Van der Wijngaart, W.; Enoksson, P.; Stemme, G., *Sens. Actuators, B* **2000**, *67*, 203-208.

259. Yang, Z.; Maeda, R., *Electrophoresis* **2002**, *23*, 3474-3478.

260. Yang, Z.; Maeda, R., *J. Chromatogr. A* **2003**, *1013*, 29-33.

261. Nittis, V.; Fortt, R.; Legge, C. H.; De Mello, A. J., *Lab Chip* **2001**, *1*, 148-152.

262. Li, S. F.; Chen, S. C., *IEEE Trans. Adv. Packaging* **2003**, *26*, 242-247.

263. Chiou, C. H.; Lee, G. B., *J. Micromech. Microeng.* **2004**, *14*, 1484-1490.

264. Lee, E. S.; Howard, D.; Liang, E.; Collins, S. D.; Smith, R. L., *J. Micromech. Microeng.* **2004**, *14*, 535-541.

265. Pan, T.; Baldi, A.; Ziaie, B., *J. Microelectromech. Syst.* **2006**, *15*, 267-272.

266. Chen, H.; Acharya, D.; Gajraj, A.; Meiners, J. C., *Anal. Chem.* **2003**, *75*, 5287-5291.

267. Pattekar, A. V.; Kothare, M. V., *J. Micromech. Microeng.* **2003**, *13*, 337-345.

268. Shintani, Y.; Hirako, K.; Motokawa, M.; Iwano, T.; Zhou, X. J.; Takano, Y.; Furuno, M.; Minakuchi, H.; Ueda, M., *J. Chromatogr. A* **2005**, *1073*, 17-23.

269. Shintani, Y.; Hirako, K.; Motokawa, M.; Takano, Y.; Furuno, M.; Minakuchi, H.; Ueda, M., *Anal. Sci.* **2004**, *20*, 1721-1723.

270. Puntambekar, A.; Ahn, C. H., *J. Micromech. Microeng.* **2002**, *12*, 35-40.

271. Szekely, L.; Freitag, R., *Anal. Chim. Acta* **2004**, *512*, 39-47.

272. Shorr, I. M.; Rogozinski, M.; Vearsanyi, A., *Rev. Sci. Instrum.* **1962**, *33*, 1468-1469.

273. Cerveny, W. J.; Weitkamp, W. J., *Rev. Sci. Instrum.* **1972**, *43*, 929.

274. Rebrov, E. V.; Seijger, G. B. F.; Calis, H. P. A.; De Croon, M.; Van den Bleek, C. M.; Schouten, J. C., *Appl. Catal., A* **2001**, *206*, 125-143.

275. Janicke, M. T.; Kestenbaum, H.; Hagendorf, U.; Schuth, F.; Fichtner, M.; Schubert, K., *J. Catal.* **2000**, *191*, 282-293.

276. Jenner, G., *AIChE. J* **1999**, *45*, 2051-2054.

277. Hawell, S. T.; Watts, P., *Green Chem.* **2003**, *5*, 240-249.

278. Meschke, F.; Riebler, G.; Hessel, V.; Schurer, J.; Baier, T., *Chem. Eng. Tech.* **2005**, *28*, 465-473.

279. Doku, G. N.; Verboom, W.; Reinhoudt, D. N.; Van den Berg, A., *Tetrahedron* **2005**, *61*, 2733-2742.

280. Ehrfeld, W.; Golbig, K.; Hessel, V.; Löwe, H.; Richter, T., *Ind. Eng. Chem. Res.* **1999**, *38*, 1075-1082.

281. Hessel, V.; Ehrfeld, W.; Herweck, t.; Haverkamp, V.; Löwe, H.; Shiewe, J.; Wille, C.; Kern, T.; Lutz, N. In *Gas/Liquid Microreactors: Hydrodynamics and Mass Transfer*, 4th Int. Conf. Microreaction Technology (IMRET 4), Atlanta, GA, (USA), 5-9 March, **2000**, p 174-186.

282. Haverkamp, V.; Emig, G.; Hessel, V.; Liauw, M. A.; Löwe, H. In *Characterization of a Gas/Liquid Microreactor, the Microbubble Column: Determination of Specific Interfacial Area*, 5th Int. Conf. Microreaction Technology (IMRET 5), Berlin (Germany), **2001**, Matlosz, M. E., W.; Baselt, J. P., Ed. Springer-Verlag: p 202-214.

283. Kobayashi, J.; Mori, Y.; Kobayashi, S., *Chem. Commun.* **2005**, 2567-2568.

284. Abdallah, R.; Meille, V.; Shaw, J.; Wenn, D.; De Bellefon, C., *Chem. Commun.* **2004**, 372-373.

285. Abdallah, R.; Meille, V.; Fumey, B.; De Bellefon, C. In *A Micro-Structured Mesh Contactor as a Tool for Screening of G/L/S Aymmetric Hydrogenations*, 9th International Conference on Microreaction Technology (IMRET 9), Postdam/Berlin (Germany), 6-8 Sept 2006, **2006**, Dechema e.V: p 58-59.

286. Mae, K. In *Advanced Chemical Processing Using Micro Space*, 9th International Conference on Microreaction Technology (IMRET 9), Postdam/Berlin (Germany), 6-8 Sept 2006, **2006**, Dechema e.V: p 53-54.

287. Küpper, M.; Hessel, V.; Löwe, H.; Stark, W.; Kinkel, J.; Michel, M.; Schmidt-Traub, H., *Electrochim. Acta* **2003**, *48*, 2889-2896.

288. Hessel, V.; Hofmann, C.; Löb, P.; Löhndorf, J.; Löwe, H.; Ziogas, A., *Org. Process Res. Dev.* **2005**, *9*, 479-489.

289. Löwe, H.; Hessel, V.; Löb, P.; Hubbard, S., *Org. Process Res. Dev.* **2006**, *10*, 1144-1152.

3

Pressure Chemistry in a Capillary Microreactor*

A miniaturized fiber-optics based platform for on-line measurement by UV/Vis spectroscopy of chemical reaction kinetics under pressure, up to 600 bar, was developed. The reaction rate constants, at different pressures and the activation volumes for a nucleophilic aromatic substitution and an aza-Diels-Alder reaction were determined. The influence of the pressure on the conversion and the stereoselectivity of the Diels-Alder reactions of 2- and 3-furylmethanol with methyl-, benzyl- and phenylmaleimide was studied in a capillary microreactor by ^{1}H NMR spectroscopy. In the case of 2-furylmethanol, pressure positively affected the formation of the *exo* isomer.

---

* Parts of this Chapter have been published in: Benito-López, F.; Verboom, W.; Kakuta, M.; Gardeniers, J. G. E.; Egberink, R. J. M.; Oosterbroek, R. E.; Van den Berg, A.; Reinhoudt, D. N., Optical fiber-based on-line UV/Vis spectroscopic monitoring of chemical reaction kinetics under high-pressure, in a capillary microreactor, *Chem. Commun.* **2005**, 2857-2859.

3.1 Introduction

Application of (high) pressure is an methodology to enhance the reaction rate of a variety of organic reactions.[1] In general, high pressure chemistry is regarded as a technique that requires specialized equipment with strict safety precautions as was shown in Chapter 2. The miniaturization of the reaction system that requires fewer amounts of sample is expected to relax safety regulations, so that high pressure experimentation will become more readily available.

A simple miniaturization step is the construction of capillary microreactors, which are suitable for studying chemical reactions.[2] The immobilization of metals[3] and enzymes[4] on the capillary inner surface has been used for heterogeneous catalysis and enzymatic processes, respectively. A further consideration is to make use of the intrinsic safety of a microreactor.

As a first step towards such an integrated system, in this Chapter a miniaturized experimentation platform is described based on a capillary microreactor coupled to conventional HPLC tools. This system is used to study the influence of pressure on organic reactions up to 600 bar. Although this pressure range does not give the full advantage of high pressure chemistry, the range is large enough to study the rate enhancement and to collect valuable information necessary to determine the molar activation volumes of reactions. To monitor the course of the reactions, a fiber-optic system for on-line UV spectroscopy is used.

UV-Vis detection is one of the most used techniques in this field owing to its versatility and ease of operation.[5] At atmospheric pressure, similar detection systems incorporated or even integrated in microscale reactors, such as capillaries and chips, are described in literature.[6-8] Also for high pressure systems and more in concrete HPLC,[9] coupled fiber-optic detection of a similar layout is well known. Other applications of fiber-optics coupled with high pressure equipments, related to HPLC apparatus, are the measurements of reactants solubility and chemical reactions in supercritical CO_2[10-12] and supercritical H_2O.[13]

The applicability of the miniaturized experimental platform for pressure kinetic studies is demonstrated for two types of reactions, *viz.* a nucleophilic aromatic substitution of three *p*-halonitrobenzenes with secondary amines and an aza-Diels-Alder reaction of the Danishefsky's diene with benzylidenaniline. Valuable kinetic parameters as rate constants and activation volumes were determined. The influence

of the applied pressure on the conversion and on the stereochemistry of the Diels-Alder reactions of 2- and 3-furylmethanol with methyl-, benzyl- and phenylmaleimide are also shown.

3.2 Results and Discussion

3.2.1 Set-up design

A schematic representation of the microreactor set-up used for the determination of activation volume values and rate constants at pressures up to 600 bar is given in Figure 3-1. It consists of a fused silica capillary, volume 3 μL, running through a stainless steel cross, a six-port valve for sample inlet and outlet and an HPLC pump as pressure generator. The course of the reactions was followed *via* an optical fiber, connecting the silica capillary and an UV/Vis spectrophotometer.

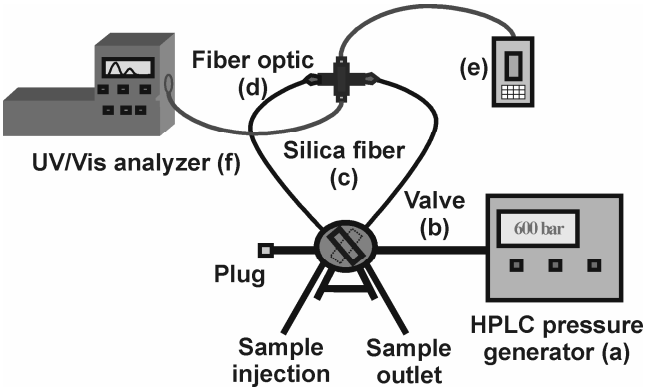

Figure 3-1: Schematic representation of the pressure UV capillary microreactor system: high pressure generator (a), six-port valve for injection (b), capillary microreactor (c), optical fiber (d), UV/Vis light source (e) and UV/Vis detector (f).

Pressure sources delivering pressures up to several hundreds of bar are generally available for HPLC, a rather common analytical method and can be used without the safety regulations that need to be fulfilled in "conventional" high pressure chemistry laboratories. Fluidic connections and valves for lab-on-a-chip systems reliable over a large pressure range (up to 800 bar) are not widely available yet.[14] Nevertheless, commercially available connections guaranteed to function properly up to 700 bar could be used in combination with the capillary microreactor without

adjustment. In this study fused silica capillaries with an inner diameter of 100 µm were used; larger inner diameters allow, however, the use of lower sample concentrations.

3.2.2 Determination of the reaction rate constants and activation volumes

3.2.2.1 Nucleophilic aromatic substitution reactions

About fifteen years ago Ibata *et al.*[15,16] reported that nucleophilic aromatic substitution reactions of aromatic halides containing electron-withdrawing groups with various amines can be accelerated by pressure. This type of reaction proceeds *via* a Meisenheimer dipolar intermediate. The effect of pressure on this reaction can be explained by the fact that both bond formation and charge separation occur in the transition state.[17]

These reactions were studied in the capillary microreactor since they have high negative activation volumes. Therefore *p*-halonitrobenzenes (**1**) (X = F, Cl, Br) were reacted with a ten-fold excess of pyrrolidine (**2a**), piperidine (**2b**) and morpholine (**2c**) in THF at 1, 200, 400 and 600 bar to give *p*-*N*,*N*-dialkylamino-nitrobenzenes (**3a-c**), Scheme 3-1. The product formation was monitored by following the increase of the absorption peak at 391 nm in the UV/Vis spectra.

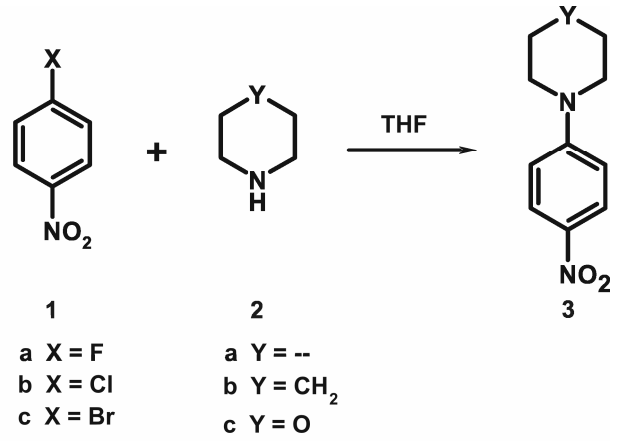

Scheme 3-1: Nucleophilic aromatic substitution reaction of *p*-halonitrobenzenes (**1**) with amines (**2**).

The rate constants k_{obs} of the different reactions at the mentioned pressures were calculated using a pseudo-first order kinetic equation 3-1, (see the Experimental

part). The rate constant k_{obs} has to be divided by the amine concentration to obtain the second order rate constant k. As an illustration, Figure 3-2 shows the rate constants k of the reaction of 1-fluoro-4-nitrobenzene (**1a**) *vs.* pressure for the three different amines (**2**). The rate constants k_{obs} and k at 600 bar are given in Table3-I.

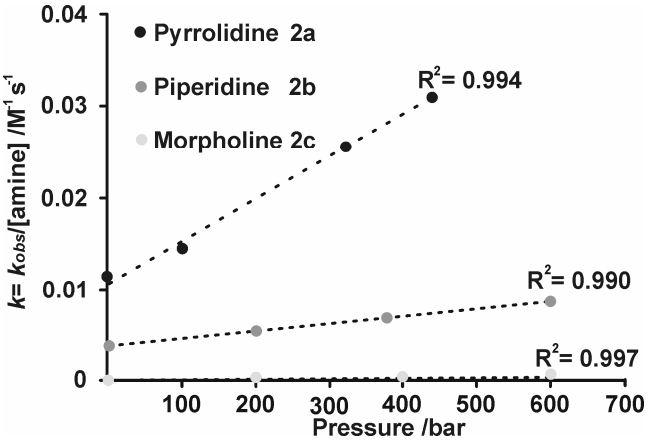

Figure 3-2: Rate constant k of nucleophilic aromatic substitution reaction of 1-fluoro-4-nitrobenzene (**1a**) (0.125 M) with amines (**2a-c**) (1.25 M) in THF at four different pressures.

The k values show the following reactivity order of the leaving groups: F > Cl > Br.[18] However, in the case of pyrrolidine (**2a**), 1-bromo-4-nitrobenzene (**1c**) reacts somewhat faster than the corresponding chloro derivative (**1b**) (6.60×10^{-4} M^{-1} s^{-1}, *vs.* 5.56×10^{-4} M^{-1} s^{-1} at 600 bar). A similar behavior has been observed in corresponding reactions using the methoxide ion as a nucleophile.[19]

Table 3-I: Rate constants k_{obs} and k for the nucleophilic aromatic substitution reaction of *p*-halonitrobenzenes (**1**) with amines (**2**) at 600 bar.

p-halonitrobenzene[a]	Amine[a]	k_{obs} /s^{-1}	k /M^{-1} s^{-1}
1a	**2a**	4.72×10^{-2}	3.78×10^{-2}
1b	**2a**	6.95×10^{-4}	5.56×10^{-4}
1c	**2a**	8.25×10^{-4}	6.60×10^{-4}
1a	**2b**	1.10×10^{-2}	8.80×10^{-3}
1b	**2b**	3.62×10^{-4}	2.89×10^{-4}
1c	**2b**	3.22×10^{-5}	2.57×10^{-5}
1a	**2c**	9.87×10^{-5}	7.89×10^{-5}
1b	**2c**	6.76×10^{-5}	5.41×10^{-5}
1c	**2c**	2.17×10^{-7}	1.74×10^{-7}

[a] Upon mixing 0.125 M *p*-halonitrobenzene (**1**) and 1.25 M amine (**2**).

For the reaction with 1-fluoro-4-nitrobenzene (**1a**), Figure 3-2 clearly shows the expected order in reactivity between the amines (**2**): pyrrolidine > piperidine > morpholine,[15,20] having rate enhancements of 2.7, 1.7 and 1.5, respectively at 600 bar. A batch reaction at atmospheric pressure resulted in k values comparable to those obtained with the capillary microreactor, thereby excluding microreactor wall effects.

The activation volumes were calculated from a plot of the second-order reaction rate constants *vs.* pressure using equation 3-2, (see the Experimental part). The $\Delta V^{\neq}$ values are presented in Table 3-II. The most negative activation volumes are found for the fastest reactions, *viz.* the reaction of 1-fluoro-4-nitrobenzene (**1a**) with pyrrolidine (**2a**). All $\Delta V^{\neq}$ values are in the same range as those reported in the literature for the nucleophilic aromatic substitution reactions of bromoquinolines and bromonaphthalenes with piperidine.[21]

Table 3-II: Activation volumes $\Delta V^{\neq}$ ($cm^3\ mol^{-1}$) for the reactions of *p*-halonitrobenzenes (**1a-c**) with amines (**2a-c**).

p-halonitrobenzene [a]	Amine [a]		
	Pyrrolidine (**2a**)	Piperidine (**2b**)	Morpholine (**2c**)
1a	-58.0[b]	-32.4[b]	-22.5
1b	-41.7	-23.3	-18.2
1c	-32.7	-17.3	-14.5

[a] Upon mixing 0.125 M *p*-halonitrobenzene (**1**) and 1.25 M amine (**2**).

[b] As an example: the errors for the reactions of **1a** with **2a** and **1b** with **2b** are 0.4 and 0.1 $cm^3\ mol^{-1}$, respectively (five different experiments).

It is known that nucleophilic aromatic substitution reactions of *p*-halonitrobenzenes with secondary amines can be base-catalyzed, with the amine being the catalyst.[22,23] Examples are the reactions of 2,4-dinitrohalobenzenes with morpholine,[24] piperidine,[25] and aniline.[26] To investigate this catalytic effect, the reactions of 1-fluoro-4-nitrobenzene (**1a**) with pyrrolidine (**2a**) and piperidine (**2b**) were performed at different amine concentrations. The second-order rate constants k and the activation volumes $\Delta V^{\neq}$ are shown in Table 3-III. The same approximations by pseudo-first order kinetics as described above were used. Although not in all cases the approximation is valid, in low amine concentration results, for instance, a deviation of 3 - 15 % was calculated depending on applied pressure), meaningful results were still obtained. Plots of the second-order rate constants *vs.* the pyrrolidine or piperidine

concentrations pass through the origin and have a positive slope, Figure 3-3 which indicates that the reactions are amine catalyzed.[27]

Table 3-III: Rate constants k and activation volumes $\Delta V^{\neq}$ for the base-catalyzed reaction of 1-fluoro-4-nitrobenzene (**1a**), 0.125 M upon mixing, with pyrrolidine (**2a**) and piperidine (**2b**).

2a /M	p /bar	k /M^{-1} s^{-1}	$\Delta V^{\neq}$ /cm^3 mol^{-1}	**2b** /M	p /bar	k /M^{-1} s^{-1}	$\Delta V^{\neq}$ /cm^3 mol^{-1}
1.2500	1	1.123×10^{-2}	-58.0	1.2500	1	3.91×10^{-3}	-32.4
	100	1.424×10^{-2}			200	5.22×10^{-3}	
	320	2.591×10^{-2}			400	6.72×10^{-3}	
	440	3.086×10^{-2}			600	8.80×10^{-3}	
0.6250	1	4.37×10^{-3}	-59.1	0.6250	1	1.95×10^{-3}	-33.4
	100	5.36×10^{-3}			200	2.50×10^{-3}	
	200	7.15×10^{-3}			400	3.35×10^{-3}	
	300	8.94×10^{-3}			600	4.43×10^{-3}	
0.3125	1	2.83×10^{-3}	-58.1	0.3125	1	1.11×10^{-3}	-33.0
	200	4.94×10^{-3}			200	1.44×10^{-3}	
	400	7.23×10^{-3}			400	1.84×10^{-3}	
	600	1.20×10^{-2}			600	2.54×10^{-3}	
0.1563	1	3.45×10^{-4}	-58.0	0.0325	1	1.88×10^{-4}	-32.2
					200	2.85×10^{-4}	
	320	7.48×10^{-4}			400	3.41×10^{-4}	
	440	9.90×10^{-4}			600	4.14×10^{-4}	

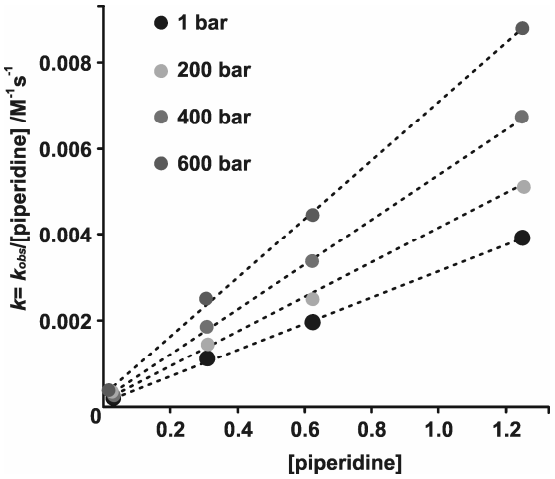

Figure 3-3: Piperidine (**2b**) concentration dependence at different pressures for the reaction with 1-fluoro-4-nitrobenzene (**1a**) in THF.

3.2.2.2 Aza-Diels-Alder reaction

Usually, Diels-Alder reactions[28-31] have rather high negative activation volumes typically in the range of -25 to -45 $cm^3\ mol^{-1}$, which make them sensitive to pressure.[32,33]

Recently, Yuan *et al.*[34] reported that at room temperature the aza-Diels-Alder reaction of Danishefsky's diene (**4**) with imines in methanol gave 2-substituted dihydro-4-pyridone derivatives in good yield. In our set-up the reaction of Danishefsky's diene (**4**) with imine (**5**) in methanol to give 1,2-diphenyl-2,3-dihydropyridin-4(1*H*)-one (**6**) was studied at different pressures, Scheme 3-2.

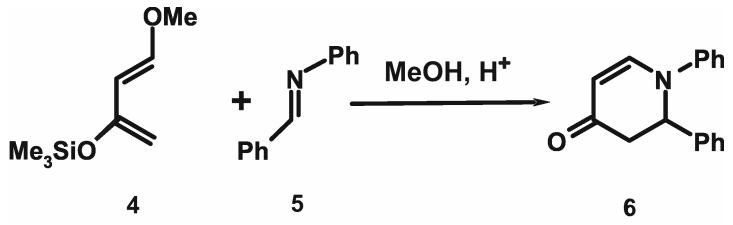

Scheme 3-2: Aza-Diels-Alder reaction of the Danishefsky's diene (**4**) with benzylidenaniline (**5**).

The product formation was monitored by the increase of the absorption at 335 nm in the UV/Vis spectrum; k_{obs} values of 1.5×10^{-4}, 1.8×10^{-4}, 2.2×10^{-4} and 2.8×10^{-4} s^{-1} were obtained at 1, 100, 200 and 300 bar, respectively. An activation value of -33 $cm^3\ mol^{-1}$ was calculated using equation 3-2. This value is in agreement with those of related Diels-Alder reactions, such as the reaction of furan with furan-2,5-dione ($\Delta V^{\neq}$ = -30.5 $cm^3\ mol^{-1}$) or 9-(hydroxymethyl)anthracene with *N*-ethylmaleimide ($\Delta V^{\neq}$ = -31.4 $cm^3\ mol^{-1}$).[35]

3.2.3 Pressure influence on the stereoselectivity of the reaction of 2- and 3-furylmethanol with methyl-, benzyl- and phenylmaleimide

In literature only a limited number of studies are known concerning the influence of pressure on the stereoselectivity of Diels-Alder reactions.[1,36-38] As a general rule, the most compact transition state structure is preferred under pressure. In cycloaddition reactions the *endo* transition structure usually has a smaller volume than

the *exo* one. For instance, in the homo-Diels-Alder reaction of norbornadiene with maleic anhydride the yield of the *endo* product varied from 81% at atmospheric pressure to 92% at 1 kbar. The difference in activation volume between the *endo* and the *exo* reaction products ($\Delta\Delta V^{\neq} = \Delta V^{\neq}_{endo} - \Delta V^{\neq}_{exo}$) was found to be -3.4 $cm^3\,mol^{-1}$.[38]

Arjona *et al.* have reported the reaction of 2- (**7a**) and 3-furylmethanol (**7b**) with *E*-1,2-bis(phenylsulfonyl)ethylene to give the *endo* and *exo* Diels-Alder cycloadducts.[39] In the capillary microreactor, the influence of pressure on the reaction of 2-furylmethanol (**7a**) and 3-furylmethanol (**7b**) with the maleimides (**8a-c**) was studied (Scheme 3-3). The *endo*/*exo* reaction product ratio (**9**/**10**) of the reaction of **7a** with **8a-c** was determined comparing the ^{1}H NMR spectra of the reaction mixtures. The intensities of the signals of the protons adjacent to the double bond at 5.25-5.35 ppm (double doublet) and 5.05-5.22 ppm (doublet)[40] of the *endo* and *exo* isomers, respectively give the *endo*/*exo* ratio. Likewise, the *endo*/*exo* reaction product ratio (**9**/**10**) of the reaction of **7b** with **8a-c** was determined comparing the intensities of the signals of the double bond protons at 6.26-6.35 ppm (doublet) and 5.95-6.30 ppm (doublet) for the *endo* and *exo* isomers, respectively.

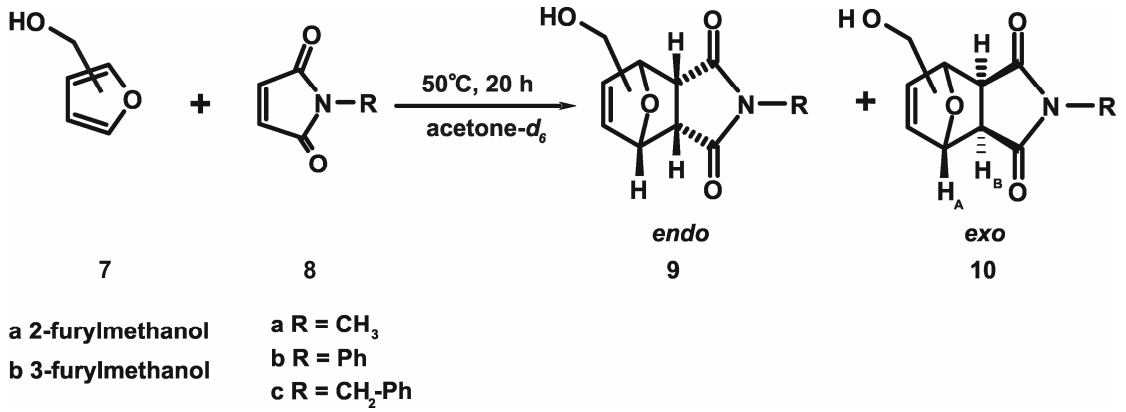

Scheme 3-3: Diels-Alder reaction of 2- and 3-furylmethanol (**7a,b**) with maleimides **8a-c**.

Table 3-IV shows that 3-furylmethanol (**7b**) is more reactive than 2-furylmethanol (**7a**) giving about a 1.6-fold higher conversion at 1 bar. The hydroxymethyl group at C-2 in **7a** reduces the atomic coefficient of the HOMO orbital on this carbon with respect to C-2 in furan (**11**), thereby decreasing the reactivity of the diene in the Diels-Alder reaction, Figure 3-4.[41]

It is known that the HOMO of 2-methylbutadiene (**13**) at C-1 has a higher atomic coefficient than that of butadiene (**12**), Figure 3-4.[42,43] Comparatively, the

hydroxymethyl group in **7b** at C-3 will also enlarge the coefficient of the HOMO orbital of the contiguous carbon (C-2), thereby increasing its reactivity during the Diels-Alder reaction.

Table 3-IV: Conversion (%) and *endo*/*exo* ratio of the Diels-Alder reactions of 2- and 3-furylmethanol (**7a**,**b**) with maleimides (**8a-c**) at 1 and 600 bar.

7+8	Conversion /% [a]		*endo* (**9**) /*exo* (**10**) ratio	
	1 bar [b]	600 bar	1 bar [b]	600 bar
aa	35	66	66: 34	59: 41
ab	35	55	55: 45	52: 48
ac	40	62	62: 38	57: 43
ba	57	57	57:43	57: 43
bb	55	54	40: 60	39: 61
bc	59	58	55: 45	54: 46

[a] The results are the average of three experiments (error ~ 1.5%).

[b] Batch-experiments carried out at 1 bar showed the same conversion and *endo*/*exo* ratio.

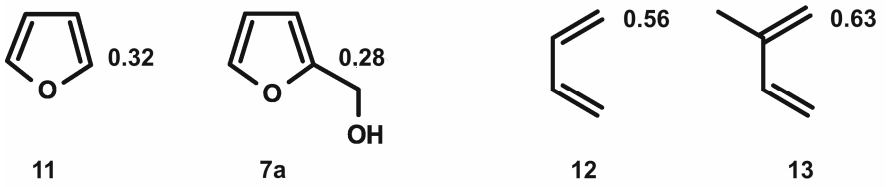

Figure 3-4: Atomic coefficients (eV) of the HOMO of furan (**11**),[41] 2-furylmethanol (**7a**),[41] butadiene (**12**),[41] and 2-methylbutadiene (**13**). [42, 43]

Increasing the pressure to 600 bar gave rise to a 1.7-fold higher conversion in the reactions of 2-furylmethanol (**7a**) with maleimides (**8a-c**). However, the corresponding reaction of 3-furylmethanol (**7b**) was not affected by pressure.

Reactions with the highest negative reaction volume ΔV ($\Delta V_{product} - \Delta V_{reactants}$) are more positively affected by pressure.[1] The ΔV's for the reactions of 2-furylmethanol (**7a**) and 3-furylmethanol (**7b**) with *N*-methylmaleimide (**8b**) were calculated using a PCModel program (Table 3-V). The volumes of the reactants are 69.6, 67.6 and 122.6 cm^3 mol^{-1} for **7a**, **7b** and **8b**, respectively. Figure 3-5 shows the minimized structures of the corresponding *endo* (**9ab**, **9bb**) and *exo* (**10ab**, **10bb**) products.

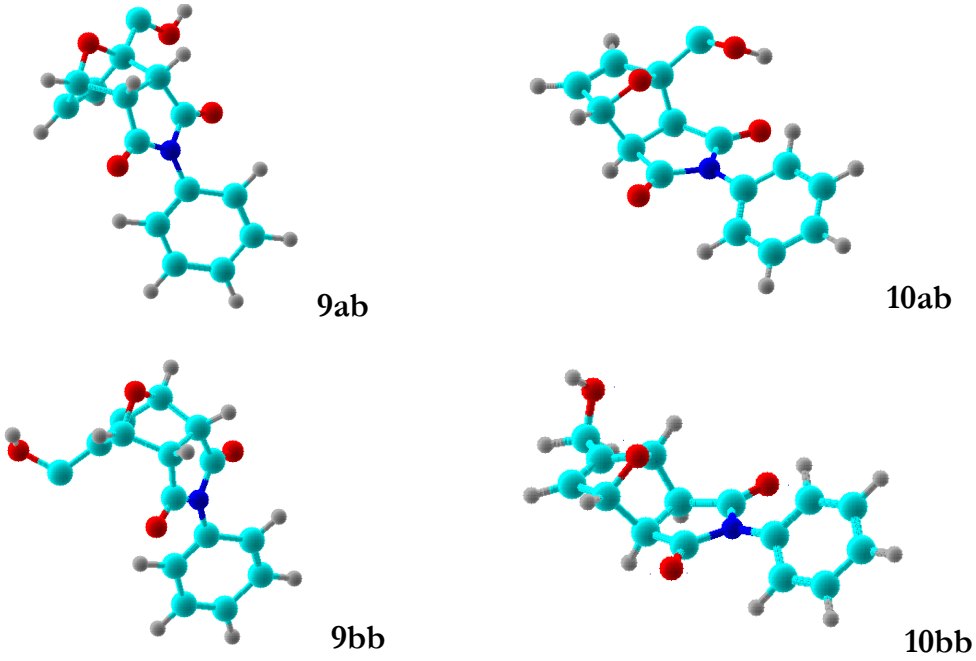

Figure 3-5: Minimized structures for the *endo* (**9**) and *exo* (**10**) products of the reactions of 2-furylmethanol (**7a**) and 3-furylmethanol (**7b**) with *N*-phenylmaleimide (**8b**).

From Table 3-V it is clear that the ΔV for the reaction of 2-furylmethanol (**7a**) is much more negative than for the corresponding reaction with 3-furylmethanol (**7b**). The hydroxymethyl group at C-3 results in a less compact structure (Figure 3-5, **9bb** and **10bb**). Therefore the reactions of **7b** were not affected by pressure, while the reactions of **7a** were.

Table 3-V: Reaction volumes (ΔV), in $cm^3\ mol^{-1}$, for the reactions of 2- (**7a**) and 3-furylmethanol (**7b**) with the maleimides (**8a-c**).

	7a		**7b**	
8	*endo* (**9a**)	*exo* (**10a**)	*endo* (**9b**)	*exo* (**10b**)
a	-6.9	-7.9	-5.3	-4.6
b	-13.5	-14.4	-8.6	-6.3
c	-7.1	-10.1	-5.3	-5.2

The stereochemistry of the reaction products is mainly *endo* because of the overlap in the transition state of the *p* orbitals of the maleimides with the *p* orbitals of the new double bond formed in the diene. However, for the reaction of **7a** with **8a-c** at 600 bar, the *endo*/*exo* ratio slightly changes to a lower preference for the *endo* isomer.

Apparently, in this case the steric effect of the hydroxymethyl group at C-2 in **7a** influences the *endo*/*exo* ratio. This trend is in line with their reaction volumes. The *exo* structure (**10a**) has a higher negative ΔV value than the *endo* (**9a**) (Table 3-V), which means that the *exo* isomer is preferentially affected by pressure.

3.3 Conclusions and Outlook

To the best of our knowledge, the simple silica fiber microreactor is the first example of a miniaturized platform in which a reaction can be monitored on-line up to 600 bar. In addition, reactions under pressure can be studied without the extensive safety precautions that are required for conventional high pressure instrumentation.

The effectiveness of this platform was illustrated by the determination of the rate constants as well as the activation volumes at pressures up to 600 bar for different organic reactions: the nucleophilic aromatic substitution reaction of three p-halonitrobenzenes with secondary amines and an aza-Diels-Alder reaction of the Danishefsky's diene with benzylidenaniline. In addition, the microsystem was successfully used for studying the influence of pressure on the conversion and the stereochemistry of the Diels-Alder reactions of 2- (**7a**) or 3-furylmethanol (**7b**) with methyl-, benzyl- and phenylmaleimide (**8a-c**). 1.7-fold higher conversions were observed in the reaction of 2-furylmethanol (**7a**) at 600 bar while not in the case of 3-furylmethanol (**7b**). Additionally, in the reaction of 2-furylmethanol (**7a**) slight increases in the *exo* product formation were obtained. This effect was explained considering the reaction volumes where the exo shows higher negative values than the *endo* isomers.

The system does not operate in a continuous flow mode, so the simple incorporation of a pressure actuator at the outlet, will make this possible by controlling the fluid flow. Furthermore, the capillary microreactor can be incorporated in more sophisticated devices like glass microreactors. The next goal is to build a microsystem based on lab-on-a-chip concept,[44] for studying organic reactions under pressure in continuous flow operation as will be shown in the subsequent Chapters.

3.4 Experimental

3.4.1 Materials

Pyrrolidine (**2a**), piperidine (**2b**) and morpholine (**2c**) were purchased from Acros Organics (Geel, Belgium). 1-Fluoro-4-nitrobenzene (**1a**), 1-chloro-4-nitrobenzene (**1b**), 1-bromo-4-nitrobenzene (**1c**), 2-furylmethanol (**7a**), 3-furylmethanol (**7b**), 1-methyl-1*H*-pyrrole-2,5-dione (**8a**), 1-phenyl-1*H*-pyrrole-2,5-dione (**8b**) and 1-benzyl-1*H*-pyrrole-2,5-dione (**8c**) were purchased from Aldrich (Zwijndrecht, The Netherlands). *Trans*-1-methoxy-3-(trimethylsilyloxy)-1,3-butadiene (**4**) was purchased from Sigma Chemical Co. (Zwijndrecht, The Netherlands). *N*-Benzylidenaniline (**5**), tetrahydrofuran (THF), dioxane, HCl and absolute methanol (analytical reagent grade) were obtained from Fisher Scientific ('s Hertogenbosch, The Netherlands). THF was freshly distilled from sodium benzophenone ketyl immediately before use. Acetone-d_6 was purchased from Aldrich (Zwijndrecht, The Netherlands). For sample preparation, microliter syringes 1725RN (Hamilton Bonaduz AG, Switzerland) were used.

^{1}H NMR spectra were recorded using a Varian Inova 400 MHz spectrometer, equipped with a CapNMR™ microprobe that has a 7 μL flow cell and a 1.5 μL active volume (capillary microreactor experiments) and a Varian Inova 300 MHz spectrometer (characterization of the products). Mass spectra were recorded with an AccuTOF JMS-T100LC (JEOL) mass spectrometer. Elemental analyses were carried out with a model 1106 Carlo Erba Strumentazione elemental analyzer.

3.4.2 Microreactor set-up

Figure 3-1 shows a schematic drawing of the set-up. It consists of a fused silica capillary microreactor with 100 μm I.D. (375 μm O.D.) (Polymicro Technologies, LLC, Phoenix, Arizona) with an optical window burned into the coating. The capillary, with an estimated volume of about 3 μL, runs through a stainless steel cross and fittings (Silica SealThight Kit, Upchurch Scientific, Inc., Oak Habor, Washington). The optical fiber (FC-UV600-2, Avantes B.V., Eerbeek, The Netherlands) used for this work has a 600 μm thick high OH- silica core surrounded by silica cladding and a polyimide buffer with a total outer diameter of 710 μm and a numerical aperture of 0.22. The fiber is connected to a spectrometer (S2000, Ocean Optics, Inc., Duiven, The Netherlands) and a UV/Vis light source (Fiberlicht DTM6/1, Germany). Absorption measurements on the reacting mixtures were carried out in intervals of 10 or 20 seconds.

The sample was injected into the microreactor *via* a valve (6 post 2-post valve-XH System, manual 1/16″, 25 mm 50 °C/10000 psi liq., N60/X, sn 04N-0007, Valco Instruments Co. Inc., Schenkon, Switzerland), which enabled the capillary reactor to be switched in or out of the flow path without the need to depressurize the entire system. A high-pressure pump (Model 100DM, Isco, Lincoln, Nebraska) equipped with a high-precision pressure transducer was used as a pressure source.

3.4.3 Nucleophilic aromatic substitution reaction

A mixture of 1-halo-4-nitrobenzene (**1**) (100 μL, 0.25 M) and amine (**2**) (100 μL, 2.5 M) in THF, Scheme 3-1, was injected into the capillary reactor through the six-port valve and the absorbance at 391 nm was measured on-line in the pressure range of 1 to 600 bar. The reaction products (**3**) have a maximum absorbance at about 391 nm, while that of the reactants is virtually zero at this wavelength.

The rate constants (k) of the different reactions at the mentioned pressures were calculated, from the increase of the absorption peak, using a pseudo-first order kinetic equation 3-1:

$$A_t = A_\infty\left[1-\exp\left(-k_{obs}t\right)\right] \qquad \text{eq. (3-1)}$$

where A_t is the absorbance at time t and A_∞ is the absorbance after infinite time.

As an example, the reaction of 1-chloro-4-nitrobenzene (**1b**) with pyrrolidine (**2a**) at different pressures is displayed in Figure 3-6 and the activation volume calculation using equation 3-2 is shown in Figure 3-7.

$$\left(\partial \ln k/\partial p\right)_T = -\Delta V^{\neq}/RT \qquad \text{eq. (3-2)}$$

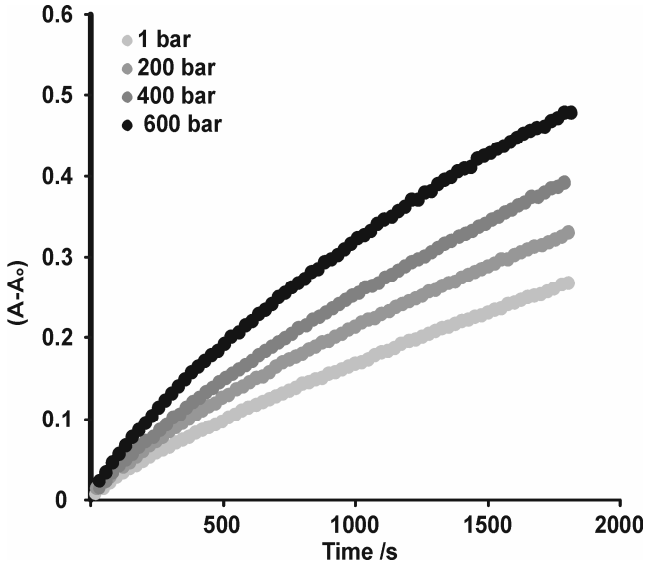

Figure 3-6: Plot of the change of the absorbance at 391 nm versus time (10 s intervals) for the product (**3b**) formation of the reaction of 1-chloro-4-nitrobenzene (**1b**) with pyrrolidine (**2a**) at different pressures (1-600 bar).

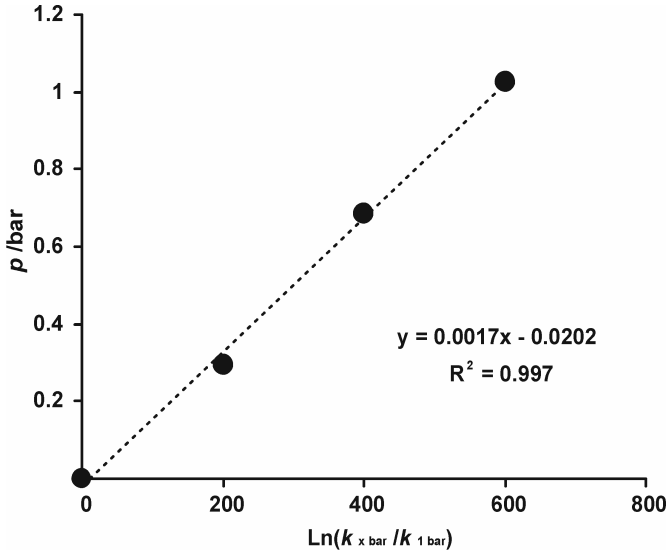

Figure 3-7: Plot of the pressure (*p*) *vs.* the logarithm of the rate constants (*k*) for the reaction of 1-chloro-4-nitrobenzene (**1b**) with pyrrolidine (**2a**) at different pressures (1-600 bar) to calculate $\Delta V^{\neq}$ using equation 3-2 ($\Delta V^{\neq}$= -41.7 $cm^3\,mol^{-1}$).

3.4.4 Aza-Diels-Alder reaction

To a solution of *N*-benzylidenaniline (**5**) in methanol (200 µL, 12 mM) and HCl in water (30 µL, 100 mM), was added a solution of Danishefsky's diene (**4**) in methanol (100 µL, 50 mM) *via* a micro liter syringe. This mixture was introduced into the capillary microreactor and the UV absorbance at 335 nm was measured at different time intervals. Reactions were carried out in the pressure range of 1 to 300 bar at ambient temperature (22 °C).

3.4.5 Pressure influence on the stereoselectivity of the reaction of 2- and 3-furylmethanol with methyl-, benzyl- and phenylmaleimide

3.4.5.1 Microreactor reactions

A mixture of 2- (**7a**) or 3-furylmethanol (**7b**) (100 µL, 0.05 M) and the different maleimides (8a-c) (100 µL, 0.05 M) in acetone-d_6, was injected into the capillary microreactor through the six-port valve. The reaction was performed at 50 °C for 20 hours at 1 and 600 bar. The product formation and their *endo*/*exo* ratio were determined by ^{1}H NMR spectroscopy.

3.4.5.2 Batch reactions

General Method: Batch reactions using the same concentrations, temperature and time conditions as in the capillary microreactor were carried out for the complete characterization of the products. A solution of **7a,b** (0.025 M) and maleimides **8a-c** (0.05 M) in acetone (100 mL) was heated at 50 °C during 20 h. The solvent was evaporated and the residue was separated by preparative TLC (SiO_2/acetonitrile/CH_2Cl_2 1:9). The ^{1}H NMR spectra of the crude reaction mixtures showed the same conversions as of those performed in the capillary microreactor. The pure products **10ab**, **10ac** and **9bb** were isolated and characterized. The rest of the products were obtained with a small impurity of the accompanying *endo* or *exo* isomer.

***Endo* 1-hydroxymethyl-4-methyl-10-oxa-4-aza-tricyclo[5.2.1.0^{2,6}]dec-8-ene-3,5-dione (9aa):** ^{1}H NMR (300 MHz, acetone-d_6) Colorless oil. δ 6.39 (dd, 1H, *J* = 5.8 and 1.5 Hz, CH=C*H*-C), 6.31 (d, 1H, *J* = 5.8 Hz, C*H*=CH-C), 5.21 (dd, 1H, *J* = 1.5 and 5.5 Hz, =CH-*CH*-O), 3.8-3.95 (m, 2H, CH_2-OH), 3.62 (dd, 1H, *J* = 5.5 and 7.7 Hz, -CH-C=O), 3.46 (d, 1H, *J* = 7.7 Hz, CH-C=O), 2.70 (s, 3H, CH_3). ESI-MS *m*/*z* = 210.1 ([M+H]$^+$, calcd. 210.21).

***Exo* 1-hydroxymethyl-4-methyl-10-oxa-4-aza-tricyclo[5.2.1.0^{2,6}]dec-8-ene-3,5-dione (10aa):** White solid. ^{1}H NMR (300 MHz, acetone-d_6) δ 6.58 (s, 2H, CH=CH), 5.10 (s, 1H, =CH-*CH*-O), 4.05-4.2 (m, 2H, CH_2-OH, overlap with CH_2-O*H*), 3.05 (d, 1H, *J* = 6.5 Hz, -CH-C=O), 2.96 (d, 1H, *J* = 6.5 Hz, -CH-C=O), 2.85 (s, 3H, CH_3). ESI-MS *m*/*z* = 210.1 ([M+H]$^+$, calcd. 210.21).

***Endo* 1-hydroxymethyl-4-phenyl-10-oxa-4-aza-tricyclo[5.2.1.0^{2,6}]dec-8-ene-3,5-dione (9ab):** White solid. ^{1}H NMR (400 MHz, acetone-d_6) δ 7.5-7.7 (m, 3H, ArH), 7.15-7.25 (m, 2H, ArH), 6.62 (dd, 1H, *J* = 5.8 and 1.4 Hz, CH=C*H*-C), 6.53 (d, 1H, *J* = 5.8 Hz, C*H*=CH-C) 5.36 (dd, 1H, *J* = 1.6 and 5.3 Hz, =CH-*CH*-O), 3.9-4.3 (m, 2H, CH_2-OH), 3.7-3.9 (m, 2H, -CH-C=O, overlap with CH_2-O*H)*, 3.66 (d, 1H, *J* = 7.7 Hz, -CH-C=O). ESI-MS *m*/*z* = 272.32 ([M+H]$^+$, calcd. 272.27).

***Exo* 1-hydroxymethyl-4-phenyl-10-oxa-4-aza-tricyclo[5.2.1.0^{2,6}]dec-8-ene-3,5-dione (10ab):** White solid. Mp: 121-122 °C. ^{1}H NMR (400 MHz, acetone-d_6) δ 7.5-7.7 (m, 3H, ArH), 7.3-7.4 (m, 2H, ArH), 6.75-6.65 (m, 2H, CH=CH), 5.33 (d, 1H, *J* = 1.5 Hz, =CH-*CH*-O), 4.29 (AA'X, 1H, *J* = 6.5 and 13.0 Hz, C*H*H'-OH), 4.08 (AA'X, 1H, *J* = 6.5 and 13.0 Hz, CH*H'*-OH), 3.29 (d, 1H, *J* = 6.5 Hz, -CH-C=O), 3.16 (d, 1H, *J* = 6.5 Hz, -CH-C=O, overlap with CH_2O*H*) 3.16 (t, 1H, *J* = 6.5 Hz, CH_2O*H*). ESI-MS *m*/*z* = 272.04 ([M+H]$^+$, calcd. 272.27). Anal. Calcd. for $C_{15}H_{13}NO_4$: C, 66.41; H, 4.83; N, 5.16. Found: C, 66.54 H, 4.88; N, 5.08.

***Endo* 1-hydroxymethyl-4-benzyl-10-oxa-4-aza-tricyclo[5.2.1.0^{2,6}]dec-8-ene-3,5-dione (9ac):** Yellow oil. ^{1}H NMR (400 MHz, acetone-d_6) δ 7.2-7.35 (m, 5H, ArH), 6.20 (dd, 1H, *J* = 5.8 and 1.4 Hz, CH=C*H*-C), 6.10 (d, 1H, *J* = 5.8 Hz, C*H*=CH-C), 5.22 (dd, 1H, *J* = 1.4 and 5.4 Hz, =CH-*CH*-O), 4.40 (s, 2H, CH_2-Ar), 4.0-4.2 (m, 3H, CH_2-OH, overlap with CH_2-O*H*), 3.65 (dd, 1H, *J* = 7.6 and 5.4 Hz, -CH-C=O), 3.50 (d, 1H, *J* = 7.6 Hz, -CH-C=O). ESI-MS *m*/*z* = 286.31 ([M+H]$^+$, calcd. 286.30).

***Exo* 1-hydroxymethyl-4-benzyl-10-oxa-4-aza-tricyclo[5.2.1.0^{2,6}]dec-8-ene-3,5-dione (10ac):**
Yellow oil. ^{1}H NMR (400 MHz, acetone-d_6) δ 7.2-7.35 (m, 5H, ArH), 6.55-6.65 (m, 2H, CH=CH), 5.17 (d, 1H, J = 1.5 Hz, =CH-*CH*-O), 4.60 (s, 2H, CH_2-Ar), 4.19 (AA'X, 1H, J = 6.5 and 13.0 Hz, C*H*H'-OH), 3.90 (AA'X, 2H, J = 6.5 and 13.0 Hz, CH*H*'-OH), 3.14 (d, 1H, J = 6.5 Hz, CH-C=O, overlap with CH_2-O*H*) 3.06 (d, 1H, 6.5 Hz, -CH-C=O). ESI-MS m/z = 286.21 ([M+H]$^+$, calcd. 286.30). Anal. Calcd. for $C_{16}H_{15}NO_4$: C, 67.36; H, 5.30; N, 4.91. Found: C, 67.41; H, 5.37; N, 4.88.

***Endo* 2-hydroxymethyl-4-methyl-10-oxa-4-aza-tricyclo[5.2.1.0^{2,6}]dec-8-ene-3,5-dione (9ba):**
White solid. ^{1}H NMR (300 MHz, acetone-d_6) δ 6.06 (d, 1H, J = 1.5 Hz, C=CH), 5.21 (dd, 1H, J = 1.5 and 3.7 Hz, =CH-C*H*), 5.18 (d, 1H, J =3.7 Hz, =C(CH_2OH)-C*H*), 4.0-4.4 (m, 2H, CH_2-OH), 3.5-3.7 (m, 2H, -CH-C=O) 2.70 (s, 3H, CH_3). ESI-MS m/z = 210.33 ([M+H]$^+$, calcd. 210.21).

***Exo* 2-hydroxymethyl-4-methyl-10-oxa-4-aza-tricyclo[5.2.1.0^{2,6}]dec-8-ene-3,5-dione (10ba):**
White solid. ^{1}H NMR (300 MHz, acetone-d_6) δ 6.26 (d, 1H, J = 1.5 Hz, C=CH), 5.05-5.15 (m, 2H, =CH-*CH* and =C(CH_2OH)-C*H*), 4.0-4.4 (m, 2H, *CH*$_2$-OH), 2.9-3.0 (m, 2H, -CH-C=O), 2.85 (s, 3H, CH_3). ESI-MS, m/z = 210.12 ([M+H]$^+$, calcd. 210.21).

***Endo* 2-hydroxymethyl-4-phenyl-10-oxa-4-aza-tricyclo[5.2.1.0^{2,6}]dec-8-ene-3,5-dione (9bb):**
White solid. Mp: 130-131 °C. ^{1}H NMR (300 MHz, acetone-d_6) δ 7.35-7.5 (m, 3H, ArH), 7.20 (d, 2H, J= 7.5 Hz, ArH), 6.30 (d, 1H, J = 1.5 Hz, C=CH), 5.34 (dd, 1H, J = 1.5 and 5.7 Hz, =CH-*CH*), 5.28 (d, 1H, J = 5.7 Hz, =C(CH_2OH)-C*H*), 4.35-4.45 (m, 1H, CH*H*-OH), 4.15-4.25 (m, 2H, C*H*H-OH, overlap with CH_2-OH), 3.7-3.8 (m, 2H, -CH-C=O). ESI-MS m/z = 272.12 ([M+H]$^+$, calcd. 272.27). Anal. Calcd. for $C_{15}H_{13}NO_4$: C, 66.41; H, 4.83; N, 5.16. Found: C, 66.51 H, 4.88; N, 5.21.

***Exo* 2-hydroxymethyl-4-phenyl-10-oxa-4-aza-tricyclo[5.2.1.0^{2,6}]dec-8-ene-3,5-dione (10bb):**
^{1}H NMR (300 MHz, acetone-d_6) δ 7.35-7.5 (m, 3H, ArH), 7.20 (d, 2H, J = 7.5 Hz, ArH), 6.38 (d, 1H, J = 1.6 Hz, C=C*H*), 5.25-5.3 (m, 1H, =CH-*C*H), 5.2-5.25 (m, 1H, =C(CH_2OH)-*CH*), 3.35-4.4 (m, 1H, C*H*-OH,), 4.2-4.3 (m, 2H, *CH*H-OH, overlap with CH_2-O*H*), 3.19-3.23 (m, 1H, -CH-C=O), 3.15-3.2 (m, 1H, -CH-C=O). ESI-MS m/z = 272.32 ([M+H]$^+$, calcd. 272.27).

***Endo* 2-hydroxymethyl-4-benzyl-10-oxa-4-aza-tricyclo[5.2.1.0^{2,6}]dec-8-ene-3,5-dione (9bc):**
White solid. ^{1}H NMR (300 MHz, acetone-d_6) δ 7.15-7.4 (m, 5H, ArH), 5.96 (d, 1H, J = 1.4 Hz, C=CH), 5.2-5.35 (m, 1H, =CH-*CH*), 5.18 (d, 1H, J = 3.3 Hz, =C(CH_2OH)-*CH*), 4.30 (s, 2H, CH_2-Ar), 3.3-3.6 (m, 3H, *CH*$_2$-OH, overlap with CH_2-O*H*), 3.7-3.8 (m, 2H, -CH-C=O). ESI-MS m/z = 286.17 ([M+H]$^+$, calcd. 286.30).

***Exo* 2-hydroxymethyl-4-benzyl-10-oxa-4-aza-tricyclo[5.2.1.0^{2,6}]dec-8-ene-3,5-dione (10bc):**
White solid. ^{1}H NMR (300 MHz, acetone-d_6) δ 7.15-7.4 (m, 5H, ArH), 6.28 (d, 1H, J = 1.5 Hz, C=CH), 5.1-5.2 (m, 2H, CHOCH), 4.65 (s, 2H, CH_2-Ar), 4.3-4.4 (m, 1H, C*H*-OH), 4.1-4.2 (m, 1H, *CH*H-OH), 3.0-3.1 (m, 2H, -CH-C=O). ESI-MS m/z = 286.16 ([M+H]$^+$, calcd. 286.30).

3.4.5.3 Calculation of reaction volumes (ΔV)

An estimation of the reaction volumes for the reactions of 2-furylmethanol (**7a**) and 3-furylmethanol (**7b**) with the maleimides (**8a-c**) was performed using PCModel V.8.00.1 for Windows (Gilbert K., Serena Software: Bloomington, Indiana) using the MMX force field (Table 3-V).

3.5 References

1. Van Eldik, R.; Klärner, F. G., *High Pressure Chemistry*. Wiley-VCH: Weinheim (Germany), **2002**; p 239-283.
2. Basheer, C.; Shahitha, F.; Hussain, J.; Lee, H. K.; Valiyaveettil, S., *Tetrahedron Lett.* **2004**, *45*, 7297-7300.
3. Kiwi-Minsker, L.; Renken, A., *Catal. Today* **2005**, *110*, 2-14.
4. Licklider, L.; Kuhr, W. G., *Anal. Chem.* **1998**, *70*, 1902-1908.
5. Schulze, P.; Ludwig, M.; Kohler, F.; Belder, D., *Anal. Chem.* **2005**, *77*, 1325-1329.
6. Ceriotti, L.; Weible, K.; De Rooij, N. F.; Verpoorte, E., *Microelectron. Eng.* **2003**, *67-8*, 865-871.
7. Lee, G. B.; Lin, C. H.; Chang, G. L., *Sens. Actuators, A* **2003**, *103*, 165-170.
8. Wu, C. H.; Scampavia, L.; Ruzicka, J., *Analyst* **2003**, *128*, 1123-1130.
9. Lippert, J. A.; Xin, B. M.; Wu, N. J.; Lee, M. L., *J. Microcolumn Sep.* **1999**, *11*, 631-643.
10. Carrott, M. J.; Wai, C. M., *Anal. Chem.* **1998**, *70*, 2421-2425.
11. Paradkar, R. P.; Williams, M. L.; Drews, M. J., *Am. Lab.* **2000**, *32*, 26-28.
12. Hunt, F.; Ohde, H.; Wai, C. M., *Rev. Sci. Instrum.* **1999**, *70*, 4661-4667.
13. Maharrey, S. P.; Miller, D. R., *AIChE J.* **2001**, *47*, 1203-1211.
14. Stishov, S. M.; Petrova, A. E., *Inst. Exp. Tech.* **2003**, *46*, 719-720.
15. Ibata, T.; Isogami, Y.; Toyoda, J., *Bull. Chem. Soc. Jpn.* **1991**, *64*, 42-49.
16. Ibata, T.; Shang, M. H.; Demura, T., *Bull. Chem. Soc. Jpn.* **1995**, *68*, 2941-2949.
17. Bunnett, J. F.; Zahler, R. E., *Chem. Rev.* **1951**, *49*, 273-412.
18. Bartoli, G.; Todesco, P. E., *Acc. Chem. Res.* **1977**, *10*, 125-132.
19. Brynner, G. P.; Miller, J.; Leveris, M.; Lutz, P. G., *J. Chem. Soc.* **1954**, 1265-1266.
20. Ibata, T.; Zou, X. Z.; Demura, T., *Tetrahedron Lett.* **1993**, *34*, 5613-5614.
21. Brower, K. R., *J. Am. Chem. Soc.* **1958**, *80*, 2105-2107.
22. Emokpae, T. A.; Isanbor, C., *Int. J. Chem. Kinet.* **2004**, *36*, 188-196.
23. Bunnett, J. F.; Garst, R. H., *J. Am. Chem. Soc.* **1965**, *87*, 3875-3878.
24. Bernasconi, C. F.; Schmid, P., *J. Org. Chem.* **1967**, *32*, 2953-2956.

25. Bunnett, J. F.; Bernasconi, C. F., *J. Org. Chem.* **1970**, *35*, 70-75.
26. Brower, K. R., *J. Am. Chem. Soc.* **1959**, *81*, 3504.
27. Isanbor, C.; Emokpae, T. A.; Crampton, M. R., *J. Chem. Soc., Perkin Trans. 2* **2002**, 2019-2024.
28. Matsumoto, K.; Sera, A., *Synthesis* **1985**, *11*, 999-1027.
29. Matsumoto, K.; Sera, A.; Uchida, T., *Synthesis* **1985**, *11*, 981-999.
30. Ciobanu, M.; Matsumoto, K., *Liebigs Ann. Recl.* **1997**, 623-635.
31. Klärner, F. G.; Diedrich, M. D., *The Effect of Pressure on Reactions of Dienes and Polyenes*. Wiley-Interscience: New York (USA), **1997**.
32. McCabe, J. R.; Eckert, C. A., *Acc. Chem. Res.* **1974**, *7*, 251-257.
33. Brun, C.; Jenner, G.; Deluzarche, A., *Bull. Soc. Chim. Fr.* **1972**, *6*, 2332-2337.
34. Yuan, Y.; Li, X.; Ding, K. L., *Org. Lett.* **2002**, *4*, 3309-3311.
35. Drljaca, A.; Hubbard, C. D.; Van Eldik, R.; Asano, T.; Basilevsky, M. V.; Le Noble, W. J., *Chem. Rev.* **1998**, *98*, 2167-2289.
36. Jenner, G., *Tetrahedron* **1997**, *53*, 2669-2695.
37. Seguchi, K.; Sera, A.; Maruyama, K., *Tetrahedron Lett.* **1973**, *17*, 1585-1588.
38. Jenner, G., *New J. Chem.* **1991**, *15*, 897-899.
39. Arjona, O.; Iradier, F.; Manas, R. M.; Plumet, J.; Grabuleda, X.; Jaime, C., *Tetrahedron* **1998**, *54*, 9095-9110.
40. Calculation of the dihedral angle H_A-C-C-H_B (Scheme 3-3, *exo*) using PCModel (79.8 °) explained the absence of a coupling between the two adjacent protons. The Karplus equation predicts a coupling of 0.01 °
41. D'Auria, M.; Emanuele, L.; Racioppi, R., *J. Photochem. Photobiol., A* **2004**, *163*, 103-111.
42. Anslyn, E. V.; Dougherty, D. A., *Modern Physical Organic Chemistry*. University science books Sausalito, California (USA), **2006**; p 877-935.
43. http://ocw.mit.edu/index.html.
44. Oosterbroek, R. E.; Berg, A. v. d., *Lab-on-a-Chip: Miniaturized Systems for (Bio)Chemical Analysis and Synthesis*. Elsevier: Enschede, (The Netherlands), **2003**.

4

Fabrication and Mechanical Testing of High Pressure Glass Microreactor Chips*

The design, fabrication and performance of several in-plane fiber-based interface geometries to microreactor chips for high pressure chemistry are discussed. The investigated parameters are the fabrication of the inlet/outlet structure, *i.e.* powderblasting and/or etching with hydrofluoric acid, the post annealing process, the geometry of the inlet/outlet structure, the manner in which top and bottom wafer are bonded and the way the inlets/outlets develop into the microfluidic channels. Destructive pressure experiments with H_2O and liquid CO_2 showed that the optimal geometry for high pressure microreactor chips is an in-plane tubular structure that is etched with hydrofluoric acid and that is suitable for fibers with a diameter of 110 μm and pressures up to at least 690 bar.

---

* Parts of this Chapter have been published in: Oosterbroek, R. E.; Hermes, D. C.; Kakuta, M.; Benito-López, F.; Gardeniers, J. G. E.; Verboom, W.; Reinhoudt, D. N.; Van den Berg, A., Fabrication and mechanical testing of glass chip for high-pressure synthetic or analytical chemistry, *Microsyst. Technol.* **2006**, *12*, 450-454.

Parts of this Chapter have been accepted for publication in *Chem. Eng. J.*: Tiggelaar, R. M.; Benito-López, F.; Hermes, D. C.; Rathgen, H.; Egberink, R. J. M.; Mugele, F. G.; Reinhoudt, D. N.; Van den Berg, A.; Verboom, W.; Gardeniers, J. G. E., Fabrication, mechanical testing and application of high-pressure glass microreactor chips.

4.1 Introduction

In Chapter 2 an overview was presented of the most commonly used equipment for high pressure chemistry, like autoclaves[1] and NMR-probes.[2] High pressure chemistry requires specialized, complicated and expensive equipment due to the strict safety precautions. The miniaturization of chemical reaction vessels down to the micrometer scale offers a number of interesting advantages, including increased heat and mass transfer.[3-5] A simple miniaturization step is the construction of capillary microreactors, as described in the previous Chapter.[4] A step further is the incorporation of high pressure techniques into the microreactor itself. A feature of microreactors that is currently exploited is the presumption that "smaller is safer",[6] *i.e.* chemical reactions at extreme pressure and temperature conditions and with toxic or explosive species can be studied without the safety issues associated with larger scale systems.[4,7,8]

In the literature there is only limited information on microfluidic devices (*i.e.* microreactors) for high pressure chemistry, where the term "high pressure" is already used for pressures of 4 bar. In case of metal-plate based microreactors, working pressures are up to 5 bar for gas-phase reactions,[9] and up to 150 bar for two- and three-phase reactions.[10,11] For glass-based microreactors, working pressures of ~90 bar have been achieved.[12] In fact, the limiting factor when performing chemistry in microreactors at pressures above 150 bar is the quality of the connections to the microreactors as reviewed in Chapter 2.[13] All the fiber-based interface methods presented in Chapter 2 are based on an out-of-plane connection of the fiber to the chip, in which the connections are made on the top surface of the chip, which lead to a rather fragile combination. By using an in-plane connection of the fiber to the chip a much more robust connection can be obtained.

In this Chapter the design, fabrication and performance of several in-plane fiber-based interface geometries to microreactor chips for high pressure chemistry are discussed. By implementing different improvements in fabrication of the dead-end channels chips, the maximum pressure (p_{max}) that a chip can resist in stop flow or continuous flow is increased.

4.2 Results and Discussion

4.2.1 First generation of in-plane fiber-based chip interfaces

4.2.1.1 Design and fabrication

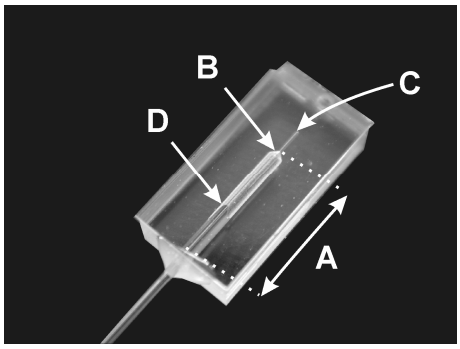

Figure 4-1: Glass chip to examine the maximum working pressure: A inlet/outlet geometry, B transition area towards microchannel, C microchannel, D glue front (meniscus).

The first generation of dead-end channel chips (Figure 4-1) was fabricated in two different ways, as shown in Figure 4-2. In the first design process (Figure 4-2**a**) chips are realized by processing of two wafers. In the bottom wafer, rather large access holes, 600 μm wide and 400 μm deep, are made by powderblasting. These access holes, inlets/outlets, are suitable for connecting fused silica capillaries with an outlet diameter of 360 μm to the chips using glue. By means of wet isotropic etching with HF, the channels are defined in the top wafer. In the second design process (Figure 4-2**b**), however, only one wafer is processed. Powderblasting is used for making the access holes, same dimensions as in the first design and in the same wafer the channel structure is defined by HF etching. Owing the etching of the channels, the side walls of the powderblasted inlet/outlets are smoothened by the HF. Thus, by applying this process sequence the microcracks, present at the rough side walls of the powderblasted structures are removed, since they are a few micrometers in size. The HF etched channels were 20 μm deep (90 μm width) and thus a shell of 20 μm, including the microcracks, was removed during this etching step. This sequence is implemented in the test-chip since it is assumed that fiber-based interfaces with smoother surfaces can resist higher pressures than structures with a rough surface.

In both designs the wafer pairs (roughness R_a = 0.232 nm/R_q = 0.301 nm) were directly bonded after stripping the chromium/gold mask in chromium etchant, an ultrasonic cleaning step with DI water (10 min) and a cleaning step in 100% HNO_3 (5 min). After establishing a pre-bond, both designs were annealed at 600 °C for 1 hour, after which the wafer packages were diced.

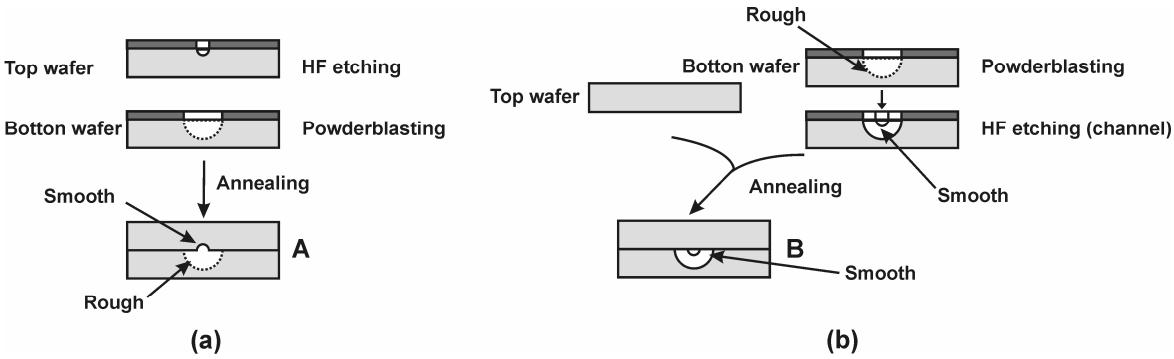

Figure 4-2: Two process sequences **a** and **b** to fabricate the dead-end channel chips. In structure **A**, the channel structure and access holes interfaces are HF etched and powderblasted in two wafers, while in structure **B**, the channel structure and access holes interfaces are realized in one wafer.

4.2.1.2 Post annealing procedure and pressure tests

The dead-end channel chips of type **A**, made with process sequence **a** (Figure 4-2), failed at pressures in the range of 10-100 bar and the maximum working pressures showed a large deviation. The main reason for the chip failure at these relatively low pressures is the microcracks on the surface of the powderblasted inlet/outlet structures.

Microscopic inspection revealed that at these microcracks, the large ones were initiated (see Figure 4-3**a**), resulting in chip failure at elevated pressures. During pressure experiments these microcracks grew substantially and finally resulted in the macrocracks/fracture pattern shown in Figure 4-3**b**.

This indicates that the surface roughness of the powderblasted interface-structure limits the p_{max}. Reduction of this roughness might result in increased maximum working pressures and can probably be obtained by additional annealing steps. This assumption is confirmed by p_{max} tests of chips fabricated with sequence **b** (Figure 4-2) with lower surface roughness, where p_{max} is 120-150 bar (Figure 4-3**c**).

These dead-end channel chips were subjected to an additional annealing step, to investigate whether this second annealing step yields higher p_{max} values.

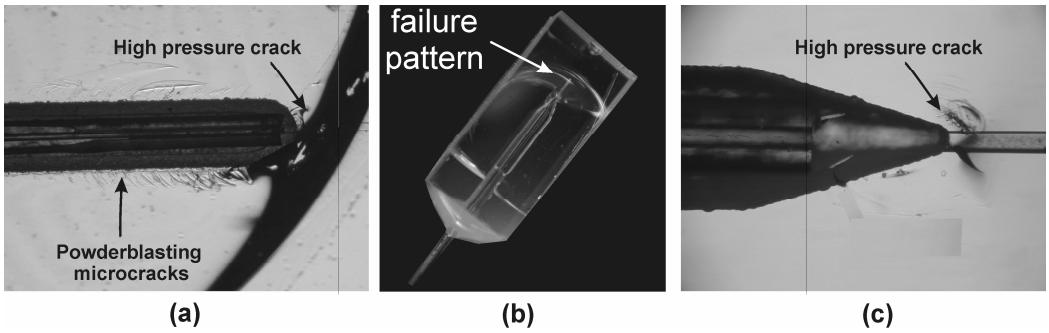

Figure 4-3: Grown microcracks, observed after pressure testing in chips with rough channel walls **a** and with smoothened (post-etched) walls **c**. In figure **b** a fractured chip is shown.

After dicing, the dead-end channel chips of type **B**, made with process sequence **b** (Figure 4-2), were individually treated with different additional annealing steps, as summarized in Table 4-I. During these annealing steps the temperatures were as high as possible without obtaining any channel deformation of the chips due to softening of the glass (softening temperature of Borofloat is 820 °C). To be sure that chip deformation did not occur, such that the chip position during annealing plays a role, these chips were positioned facing channel up- and downward.

Table 4-I: List of additional annealing conditions. The first annealing step was 1 hour at 600 °C (experiment 1).

Experiment number	Description
1	1 h 600 °C (first annealing step)
2	6 h 600 °C
3	6 h 680 °C
4	6 h 700 °C
5	10 h 680 °C
6	1:30 h 700 °C + 10 h 680 °C
7	3 h 680 °C; channel down during annealing
8	3 h 680 °C; channel up during annealing
9	6 h 680 °C

The effect of the different annealing processes on the p_{max} values of the dead-end channel chips **B** is presented in Figure 4-4. The chips of experiments 2-9 present larger p_{max} values than that of experiment 1 showing the positive effect of an additional annealing step. However, per chip the variation in the p_{max} is very large. In addition,

there are problems with the reproducibility, for example, the experiments 3 and 9 were done with chips exposed to the same additional annealing conditions, but the difference in p_{max} was about 100 bar.

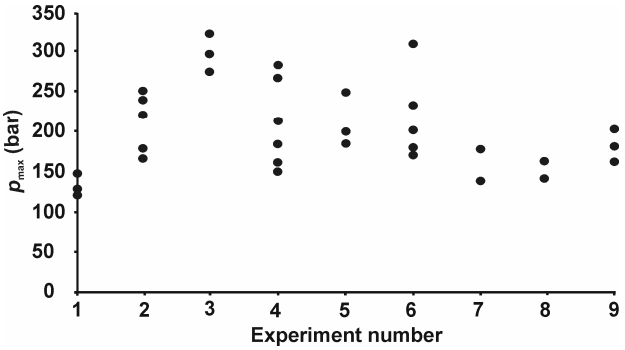

Figure 4-4: Maximum pressures (p_{max}) obtained for different additional annealing conditions of dead-end channels made with fabrication sequence **b**. Experiment 1 shows the pressure tests of dead-end channel chips with a single annealing step.

4.2.1.3 First generation high pressure microreactor

Based on the p_{max} results of the dead-end channel chips (Figure 4-4) the first glass microreactors for high pressure chemistry were fabricated and tested at high pressures (Figure 4-5).

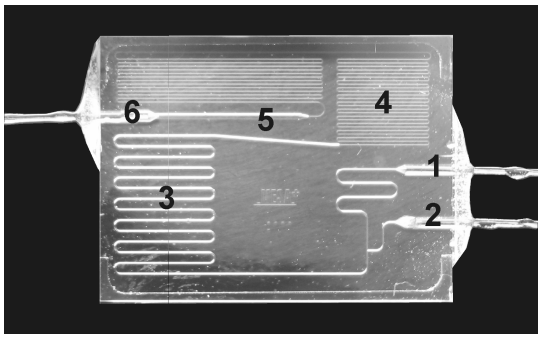

Figure 4-5: Glass microreactor for high pressure chemistry: **1**, **2** inlets, **3** reaction zone, **4** fluidic resistor, **5** expansion zone, **6** outlet.

The microreactor has two inlets (**1**, **2**) for the introduction of pressurized fluids. After mixing in the first part of the microchannel, the fluid runs into a serpentine **3** (length 13.5 mm, width × height: 70 µm × 30 µm). Subsequently, the fluid enters a flow restriction **4** with a length of 177 mm and a smaller cross-section (20 µm × 5 µm), which ensures a virtually constant pressure in the reaction section (**3**) upstream and

ends in a wider zone with outlets **5**, **6** in which the fluid mixture gradually expands to atmospheric conditions. The silica fibers used for these continuous flow microreactors have an outer diameter of 360 μm (with inner diameters of 40 μm and 10 μm for the inlet and outlet fibers, respectively) and epoxy glue was used for fixation.[14] The complete fabrication is presented in the Experimental section of this Chapter.

During the first experiments in continuous flow mode it turned out that the microreactor failure at pressures in the range of 80 - 100 bar mostly occurred at one of the inlets. It seems that continuous flow operation decreases the p_{max}. Therefore another series of dead-end channel-based structures/interfaces was designed and implemented in test chips (see section 4.2.4).

4.2.2 Second generation of in-plane fiber-based chip interfaces

4.2.2.1 Design and fabrication

The second generation of dead-end channel test-chip designs focused on different inlet/outlet configurations and bonding procedures to investigate which design results in the highest working pressures. Two main design parameters were studied:

- The geometry of the in-plane inlet/outlet structure combined with the manner in which top and bottom wafers are connected (Figure 4-6 **C**-**F**).
- The manner in which the in/outlets connect to the microchannels (Figure 4-7).

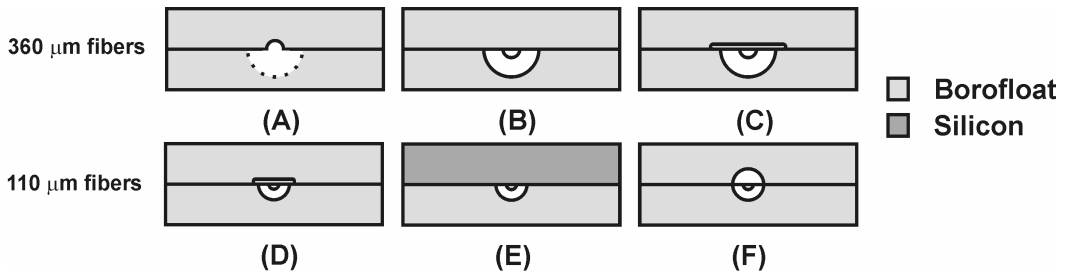

Figure 4-6: Cross-sectional views of the six different in-plane inlet/outlet geometries. Geometries **A** and **B** from the first dead-end channel chip generation are shown for comparison with the second generation.

Figure 4-6 shows the cross-sectional side view of the basic in-plane inlet/outlet geometry. The p_{max} this geometry can withstand can be improved by avoiding sharp corners where stress concentrations occur.[14] The latter can be reduced by implementing small cappings in the top wafer (Figure 4-6**C**). Alternatively, the use of smaller fibers (outer diameter 110 μm instead of 360 μm), second chip generation and thus smaller inlet/outlet holes, reduces the load on bond edges, resulting in higher p_{max} values (Figure 4-6**D**-**F**). The shape that should withstand the highest pressure is a perfectly circular one, Figure 4-6**F**,[15] however, in practice this situation is extremely difficult to achieve.[14] In Figure 4-6**F** a circular cross-section is shown, which is theoretically the shape that can withstand the highest pressures. The inlet/outlet geometries shown in Figure 4-6**A**-**D** and **F** are based on direct bonding of two glass wafers. Since it is well-known that this bond is less strong than an anodic bond (glass-silicon), also a geometry based on anodic bonding was tested (Figure 4-6**E**).

As it can be seen in Figure 4-1, the inlet/outlet geometry turns into a microchannel. Three different transitions towards this channel, which is etched with HF (70 μm wide, 10 μm deep and 2 mm long), are implemented in the geometries that were made with powderblasting and HF-etching (Figure 4-6, **B**-**E**). Top views of these different transitions are shown in Figure 4-7. Due to the fact that geometry **F** is fabricated with isotropic etching only, for this inlet/outlet structure only a (near) flat transition is realized. The fabrication details of the different in-plane inlet/outlet geometries are summarized in the Experimental part.

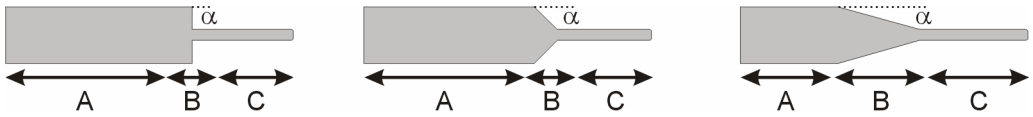

Figure 4-7: Top views of three transitions from inlet/outlet to microchannel: flat tip (left, α = 90°), tapered tip (middle, α = 45°) and sharp tip (right, α = 15°); A inlet/outlet geometry, B transition area towards microchannel, C microchannel.

For direct bonding of the borofloat wafers two procedures were used. The first bonding procedure is standard (i) while the second (upgraded) procedure (ii) is the same as (i), but with an additional cleaning step to remove organic contaminants. The complete bonding procedures are described in the Experimental section.

After dicing, fibers were glued in the different in-plane inlet/outlet geometry test chips. Two types of epoxy resin, Araldite Rapid™ and Loctite®, were used to glue the fibers (outer diameters 360 μm and 110 μm, respectively). Both glues are resistant

to commonly used solvents and have a relatively high viscosity, which is necessary to avoid capillary filling of the fibers and/or microchannels with the resin. Gluing was done at least 8 h before pressure testing.

4.2.2.2 Bond inspection

Comparison of the results of wafer-scale inspection revealed a rather striking difference: after the standard procedure (i), some large bubbles and blisters (diameter up to 3 mm) were observed as well as voids and small (white) particles. Only a few voids and particles were seen near wafer edges after procedure (ii), giving a nearly 100% yield in bonded chips. In Figure 4-8 the measured reflection across the interface between the glass wafers is shown for three different cases: a wafer-stack bonded with standard bonding procedure (i), the upgraded procedure (ii) and a stack exposed to the upgraded procedure excluding the final annealing step at 600 °C.

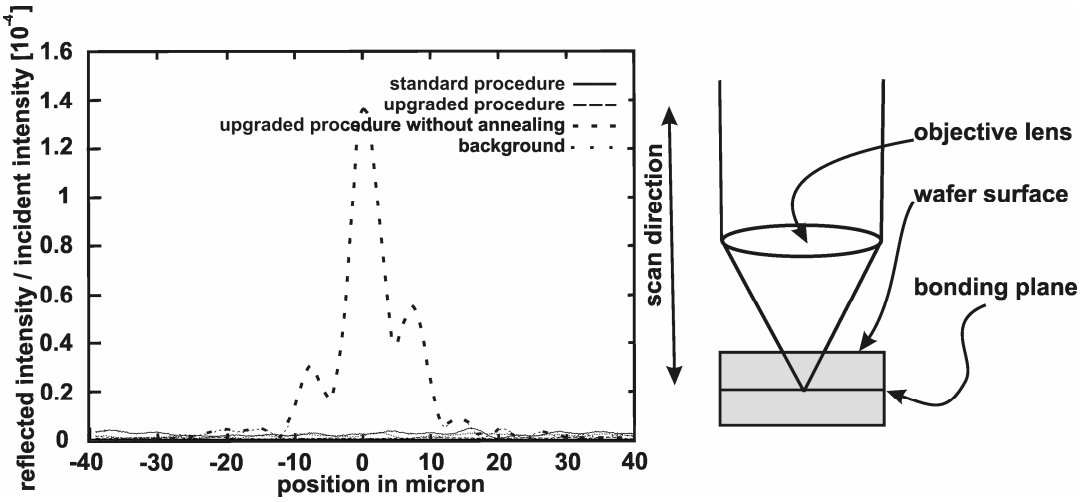

Figure 4-8: Measured reflection at bond interfaces after performing the standard bond procedure (solid line), the upgraded bonding recipe (dashed line) and after the upgraded procedure excluding annealing at 600 °C (broken line). The background signal corresponding to the residual reflection from the surface of the stack is represented by the dotted line.

For wafer stacks exposed to bonding procedures (i) and (ii), the reflectivity of the bond interface is smaller than 10^{-6}, while for the wafer stack that was not annealed the reflectivity was 1.4×10^{-4}. A wafer stack bonded with the standard procedure (i) excluding the final annealing step also showed a high reflectivity at the interface (not shown here). Using thin film optics calculations (see the Experimental), it was found that a reflectivity of 1.4×10^{-4} corresponds to a dielectric layer of air with a thickness

of 1 nm, or, alternatively, a layer of water with a thickness of about 5 nm. It is assumed that gas or residual water that is trapped in the nanometer-sized roughness of the bond interface is not present anymore at this interface after the final annealing step at 600 °C.

Based on the results of Figure 4-8 it can be concluded that it is crucial to perform the annealing step at 600 °C. In that case no interface between the wafers can be distinguished, whereas the interface is clearly perceptible when the annealing step is not carried out. The reflectance measurements do not show a difference between the two bonding procedures of section 4.4.3, no noticeable difference in reflection is found between the stacks (Figure 4-8, measurements reproducible at locations without voids/particles). Nevertheless, when the results of visual inspection are combined with the confocal microscopy results (see section 4.4.4), it can be concluded that the upgraded bonding procedure (ii) yields the best glass-glass direct bond.

4.2.2.3 Pressure tests

Figure 4-9 shows the maximum pressure p_{max} obtained with pressurized CO_2 (**a**) and H_2O (**b**) of all inlet/outlet geometries described in Figures 4-5 and 4-6.

From the graphs in Figure 4-9 several conclusions can be drawn. Overall, geometries with small cross-sections (**B-F**) are significantly stronger than structures with a larger cross-section (**B**, **C**) and show less spreading in p_{max}. The use of a capping in the top wafer to reduce high local stresses slightly increases p_{max} (**C** *vs.* **B**), whereas reduction of the cross-sectional area results in a significant increase in p_{max} (**D**, **E** *vs.* **C**). Moreover, in case of small inlets that are fabricated with powderblasting and HF-etching (**D**, **E**), there is a trend that a more gradual transition from the inlet to the microchannel (Figure 4-7, sharp tip) results in a higher p_{max} value. For configurations with these small cross-sections, Loctite resin resulted in somewhat higher maximum pressures than Araldite Rapid. Since Loctite is slightly less viscous than Araldite Rapid, this glue fills a larger area between the fiber and the inlet/outlet structure, giving a lower 'dead volume' around the fiber (Figure 4-1) and a higher p_{max}. The highest maximum pressures were obtained with geometry **F**, *i.e.* tubular structures made with HF-etching only. Independent of the glue type, chips with geometry **F** did not fail up to the maximum pressure of the HPLC pump, 690 bar.

A remarkable difference in the type of failure was found between the direct-bonded glass-glass chips and the anodic bonded glass-silicon chips. For the majority of the direct bonds (~95%), failure occurred due to release of the bond, as could clearly be seen from the position where liquid droplets formed when the chips failed. However, for the anodic bonded chips failure was always due to out-of-plane cracking of the glass part of the chips, showing that not the bond was the limiting factor, but the mechanical strength of the glass.

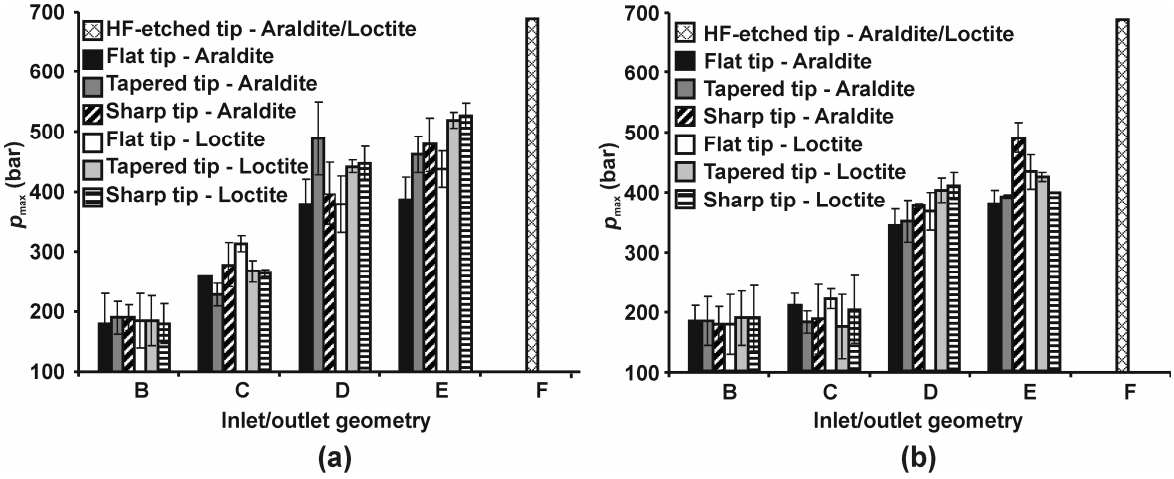

Figure 4-9: Maximum pressures (p_{max}) obtained with dedicated test chips containing in-plane geometries as described in Figures 4-5 and 4-6 using the CO_2 (*l*) (**a**) or H_2O (**b**) as medium. Data points are averages over at least three experiments.

The obtained p_{max} values were 30-70 bar lower in case of H_2O compared to CO_2(*l*). This is a well-known effect, since due to the passivation of a freshly created glass surface with silanol groups, a crack in the glass (or a rupturing interface) will be stabilized in CO_2. This process will not occur in H_2O.[16]

From the pressure experiments it can be seen that the optimal inlet geometry for microreactor chips for high pressure chemistry is the tubular structure etched with HF. Beside that, this geometry (**F**) has the optimal cross-section to obtain high pressures,[15] this structure also does not suffer from microcracks that are due to powderblasting.[14] On the other hand, small powderblasted inlets/outlets with a sharp transition towards the flow channels (geometry **D**) are adequate for working pressures up to 300 bar.

4.3 Conclusions and Outlook

In this Chapter the design, fabrication and high pressure performance of several in-plane fiber-based interface geometries to microreactor chips for high-pressure chemistry have been discussed. The main investigated parameters have been the roughness of the side walls surface of the interfaces, the post annealing procedure, the geometry of the inlet/outlet structure (*i.e.* cross-sectional shape and size), the way in which top and bottom wafer are bonded and the way in which the inlets/outlets turns over into the microfluidic channels of the chip.

Yield strength, that is the maximum pressure before failure, can be increased by reducing the roughness of the sidewalls of powderblasted geometries with isotropic wet chemical HF etching (removes microcracks). Improving the yield strength by a second annealing step slightly increases p_{max}, but is difficult to reproduce.

From visual inspection (wafer-scale) and confocal microscopy, it was found that a bonding procedure including an additional cleaning step with HNO_3 and a step during which the wafer stack is compressed with a high force (~11 metric tons) yields the best glass-glass direct bond.

Pressure tests revealed that the optimal inlet geometry for microreactor chips for high-pressure chemistry is a tubular structure that is etched with HF and suitable for fibers with an outer diameter of 110 μm. These inlet/outlet geometries can withstand pressures up to 690 bar. Small powderblasted inlets/outlets that are smoothened with HF and with a sharp transition towards the flow channels are adequate for working pressures up to 300 bar.

Future generations of such a microfluidic set-up may provide a convenient high-throughput experimentation platform for (automated) parallel synthesis and analysis of large numbers of "leads" for the development of specialty chemicals where pressure can be used as a standard tool in any synthetic step.

4.4 Experimental

4.4.1 Materials

For the pressure experiments DI water was used, as well as liquid CO_2 with a purity ≥ 99.7% and < 150 vpm of water purchased from Hoek Loos.

A high-pressure syringe pump (model 100DM; Teledyne Isco, Inc. Lincoln, USA) was used for the pressure tests.

4.4.2 General procedure for the fabrication of the high pressure microreactor

The microchannels in the microreactors (Figure 4-5) were made by means of wet chemical etching in two separate 1.1 mm thick borosilicate glass wafers (Borofloat 33, Schott Technical Glasses, Germany) and direct bonding. The in- and outlets were fabricated by powderblasting and the microchannels were etched with 25 vol.% HF. The HF solution also smoothens the surface of powderblasted in- and outlets reducing the surface roughness of the powderblasted channels. Upon stripping the chromium/gold mask layer in chromium etchant (Merck 111547.2500) and cleaning in 100% nitric acid (HNO_3) and DI water, a pre-bond was established and the wafer stack was annealed in air at 600 °C for 1 h, followed by dicing of the individual chips. Capillary fused silica fibers (Polymicro Technologies, USA) were connected to the chips using two-component glue (Araldite Rapid™, Ciba-Geigy, Switzerland or Loctite®, Henkel, Dortmund, Germany), *via* in-plane inlet/outlet structures.

4.4.3 Second generation of in-plane fiber-based chip interfaces: fabrication

In the chip geometries shown in Figure 4-6, the capping that covers the powderblasted and HF-smoothened geometry **C** is made with HF (depth 5 μm, width 430 μm). Geometries **D**-**E** are designed to be used in combination with smaller fibers (outer diameter 110 μm instead of 360 μm). The fabrication of geometries **D** and **E** is identical to the procedure for geometry **B**, but the powderblasted (and HF-smoothened) inlet/outlet is smaller: geometry **D** was 180 μm wide and 135 μm deep after powderblasting, whereas these values were 580 μm and 390 μm for geometry **C**, respectively. Following on powderblasting the depth of the in/outlet is increased to 400 μm (geometries **B**, **C**) or 145 μm (geometries **D**-**E**) by HF-etching (25 vol.%). The capping covering geometry **D** is 5 μm deep and 210 μm wide (fabricated using HF). Geometry **F** is realized with HF-etching only. In this case, in both wafers a half-circular structure was revealed (isotropic etch profile: width 120 μm, depth 55 μm) that after alignment and bonding results in a tubular inlet/outlet structure.

The two direct bonding procedures of the borofloat wafers are:

(i) After processing, the substrates are cleaned in HNO_3 (10 min) and DI water, immersed in KOH (75 °C, 25 wt.%, 1 min), rinsed in DI water (10 min) and spin dried. After alignment and pre-bonding, the wafer sandwich is annealed at 600 °C (1 h, ramp up 6 h, ramp down 12 h).

(ii) The same as (i), but with an additional cleaning step to remove organic contaminants, which consists of immersion in HNO_3 (5 min) and DI water rinsing, followed by dry spinning. In

addition to this, after alignment and pre-bonding the wafer-stack is compressed with a force of 11 metric tons (approx. 137 bar) for 30 min using a hydraulic flat-plate system. During this compression the temperature is ~343 °C. Finally, the wafer stack is annealed at 600 °C (1 h, ramp up 6 h, ramp down 12 h).

Procedure (ii) is implemented to further reduce the influence of contaminants (probably organic residues)[17] that are responsible for the appearance of voids/bubbles/blisters on the interface during annealing.[18]

The silicon-glass stack is bonded anodically at 400 °C under a nitrogen atmosphere (bonding potential 400 V for 20 min).

4.4.4 Bond inspection

Prior to dicing the bond interfaces were inspected at wafer-scale to verify the presence of voids, blisters or bubbles on the interface: these bond errors can easily be seen with a microscope or by eye. Subsequently, with confocal microscopy the quality of the bond was investigated directly at the interface. A home-built sample scanning confocal microscope was used that is adapted for the quantitative measurement of reflection coefficients down to 10^{-6}. The measurements are based on the so-called z-scan of a confocal microscope. During the movement of a flat interface with reflectivity R through the focus of a beam (*i.e.* along the optical z-axis; see inset Figure 4-8), the detector intensity I is recorded. The intensity can be expressed as equation 4-1.[19]

$$I(u) \approx R \cdot \left(\frac{\sin(u)}{u} \right)^2 \qquad \text{eq. (4-1)}$$

where u is a normalized coordinate on the optical axis (u is related to the real axial z-coordinate *via* $u = z\ \pi\ NA^2/\lambda$, with NA the numerical aperture of the objective lens and λ the wavelength of the light). Usually the quantity of interest is the full-width at half-maximum (FWHM) of this center peak, which determines the capability of distinguishing two objects (point like) that are located behind each other on the optical axis and this determines the superior depth discrimination of the confocal microscope.

When a bonded wafer-stack is illuminated with visible light about 4% of the incident light is reflected from the surface of the stack, whereas only less than 10^{-4}% of the incident light is reflected from the bonding interface (this interface is assumed to be a single dielectric layer with a thickness much smaller than the wavelength. For such thin layers, the reflectivity scales quadratically with its thickness). As a consequence, optical inspection of the interface is only possible if a method is available to discriminate between the (small) reflection from the bonding plane and the (large) reflection from the surface of the stack. This can be accomplished by using a feature of eq. (4-1), namely that $I(u)$ decreases with z^2 for large z-values (the intensity I of defocused objects decreases quadratically with z).

The wafers used in this work have a thickness of 1.1 mm. Thus, if the bond interface is in focus, the surface of the stack is 1.1 mm out-of-focus. This leads to a suppression of the reflection from the surface by a factor of approx. 10^{-6}, as can be calculated with eq. (4-1) (NA used in the set-up

is 0.33; λ of the light source is 488 nm). The corresponding residual intensity signal (background) determines the resolution of the set-up and is plotted in Figure 4-8 (dotted line).

At the bond interface the z-value is defined as zero. From eq. (4-1) it follows that for $z = 0$ $I(u)$ equals R, which means that the magnitude of the center peak of the z-scan directly yields the reflectivity. The reflectivity R of the bond interface is related to its optical thickness nd (eq. 4-2).[20]

$$R = \left(\frac{4\pi}{\lambda} nd\right)^2 \cdot \frac{(n-n_0)^2}{(n+n_0)^2} \qquad \text{eq. (4-2)}$$

with n the refractive index of the interface material, d the thickness of the interface and n_0 the refractive index of the surrounding medium (borofloat glass).

Thus, when bonded glass-glass interfaces show a reflectivity (significantly) larger than the background signal, the thickness of the interface can be estimated. In other words, this method can be used to verify the quality of direct bonds. The method is described in detail elsewhere.[21]

4.4.5 Pressure tests

The p_{max} that the proposed in-plane inlet/outlet geometries (Figures 4-6 and 4-7) can withstand was tested with H_2O and CO_2. The fused-silica capillaries were used to connect the chips to a high-pressure syringe pump (model 100DM; Teledyne Isco, Inc. Lincoln, USA) using stainless steel fittings (F-140 & A-318, Upchurch Scientific, USA). The chips were cooled to 10 °C *via* a home-built Peltier element (CP 0.8-7-06L, Melcor, USA). After filling the chip with liquid CO_2 (starting pressure 65 bar) or H_2O, the pressure in the chip was increased using a constant flow rate (2000 μL/min). During these destructive experiments the pressure was monitored with a PC. A sudden pressure drop indicated chip failure (Figure 4-10). Failure is accompanied by the formation of a small H_2O-droplet or ice formation due to CO_2 expansion: no explosions occur when a microreactor chip of such a small size fails.

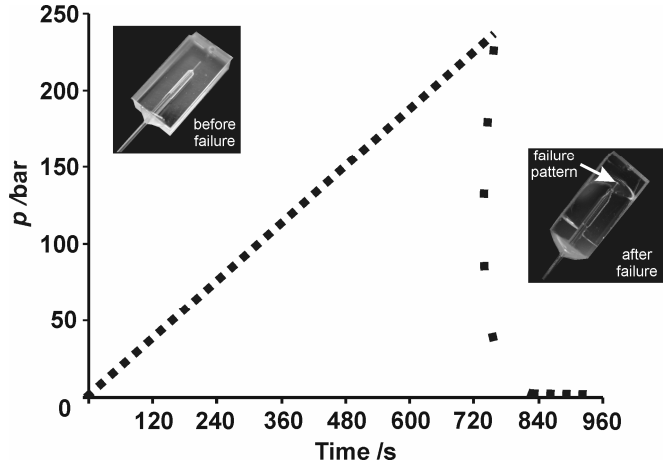

Figure 4-10: Example of a pressure log during a destructive experiment (H_2O used as pressure medium) and pictures of the test chip before and after the destructive pressure test.

4.5 References

1. Kotowski, M.; Van Eldik, R., *Coord. Chem. Rev.* **1989**, *93*, 19-57.
2. Amita, F.; Oka, H.; Mukaide, M.; Urasaki, Y.; Takegoshi, K.; Terao, T.; Kajimoto, O., *Rev. Sci. Instrum.* **2004**, *75*, 467-471.
3. Jensen, K. F., *Chem. Eng. Sci.* **2001**, *56*, 293-303.
4. Benito-López, F.; Verboom, W.; Kakuta, M.; Gardeniers, J. G. E.; Egberink, R. J. M.; Oosterbroek, E. R.; Van den Berg, A.; Reinhoudt, D. N., *Chem. Commun.* **2005**, 2857-2859.
5. Brivio, M.; Verboom, W.; Reinhoudt, D. N., *Lab Chip* **2006**, *6*, 329-344.
6. Hendershot, D. C., *Chem. Eng. Prog.* **2000**, *96*, 35-40.
7. Jensen, K. F., *AIChE J.* **1999**, *45*, 2051-2054.
8. Ehrfeld, W.; Hessel, V.; Löwe, H., *Microreactors: New Technology for Modern Chemistry*. Wiley-VCH: Weinheim (Germany), **2000**.
9. Franz, A. J.; Jensen, K. F.; Schmidt, M. A. In *Palladium Membrane Microreactors*, in: Tech. digest 3nd Int. Conf. on Microreaction Technology (IMRET 3), Frankfurt am Main, Germany, April 18-21, **1999**, p 267-276.
10. Chattopadhyay, S.; Veser, G., *AIChE J.* **2006**, *52*, 2217-2229.
11. Stoll, N.; Hawali, I.; Thurow, K., *J. Autom. Methods Manage. Chem.* **2005**, 230-234.
12. Kobayashi, J.; Mori, Y.; Kobayashi, S., *Chem. Commun.* **2005**, 2567-2568.
13. Stishov, S. M.; Petrova, A. E., *Instr. Exp. Tech.* **2003**, *46*, 719-720.
14. Oosterbroek, R. E.; Hermes, D. C.; Kakuta, M.; Benito-Lopez, F.; Gardeniers, J. G. E.; Verboom, W.; Reinhoudt, D. N.; van den Berg, A., *Microsyst. Technol.* **2006**, *12*, 450-454.
15. Doremus, R. H., *Glass Science*. Wiley: New York (USA), **1973**.
16. Wiederhorn, S. M.; Freiman, S. W.; Fuller Jr., E. R.; Simmons, C. J., *J. Mater. Sci.* **1982**, *17*, 3460-3478.
17. Plossl, A.; Krauter, G., *Mater. Sci. Eng. R.* **1999**, *25*, 1-88.
18. Hermes, D. C.; Heuser, T.; van der Wouden, E. J.; Gardeniers, J. G. E.; van den Berg, A., *Microsyst. Technol.* **2006**, *12*, 436-440.
19. Wilson, T., *Confocal Microscopy*. Academic Press: London (UK), **1990**.
20. Born, M.; Wolf, E., *Principles of Optics*. Cambridge University Press: Cambridge (UK), **1973**.
21. Rathgen, H.; Mugele, F., *Confocal reflectometry: a new tool for studying buried interfaces*, unpublished results.

5

Microfluidic Study of Flow Phenomena in CO_2-Alcohol Mixtures at High Pressures

By implementing microfluidic chips in a high pressure set-up, fluid phase transitions in flowing multi-component mixtures (CO_2-alcohol) under conditions close to the critical point of the mixtures were studied by optical microscopy. Two different flow patterns were observed; the well-known boiling process at low pressure-temperature conditions and a mist flow pattern consisting of nanodroplets at higher pressures and temperatures. Both flow patterns can be related to a liquid-vapor phase transition. This set-up was used to determine the liquid-vapor pressure-temperature locus for 50/50 v/v methanol-CO_2 and ethanol-CO_2 mixtures, for pressures between 60 and 140 bar and temperatures between 35 and 95 °C.

5.1 Introduction

Knowledge of the phase behavior of solvent or reaction mixtures is crucial for chemical applications. For example, in supercritical fluid chromatography detailed knowledge of the phase conditions of mixtures is required, to avoid the use of unnecessary harsh conditions meant to maintain the homogeneity of the mobile phase.[1] Modeling of phase behavior cannot be done using simple thermodynamics because extreme non-ideality occurs in and near the supercritical region. Experimental determination of critical points of pure substances or mixtures is usually performed using a variable-volume high pressure view cell,[2] which is equipped with a sapphire window through which the disappearance of the liquid-gas meniscus if the fluid (mixture) reaches supercritical conditions can be observed by means of a mirror or a video camera.[3] Recently developed alternative methods, which use a similar type of high pressure cell, apply shear mode piezoelectric sensing and fiber-optic reflectometry[4] or ultrasonic time-delay.[5]

As it was mentioned briefly in Chapter 2, fluids close or above their critical point are used as "green" alternatives for organic solvents in separation processes, *e.g.* in food industry, (nano)particle production, cleaning and drying and biological processes.[6-12] They are also attractive media for synthetic chemistry,[7,10] leading to higher selectivity,[13-15] better yields[16] or orders of magnitude higher reaction rates.[17] What makes supercritical fluids so special is that they have densities similar to those of liquids, while viscosity and diffusivity are closer to those of gases.[8,10] Slight changes in temperature and pressure close to the critical point give rise to large variations in solubility, a property exploited in supercritical fluid chromatography. [1,11] Carbon dioxide (CO_2) is of particular interest because of its low critical temperature of 31.1 °C and moderate critical pressure of 73.9 bar. It is non-flammable, non-toxic and environmentally friendly, miscible with a variety of organic solvents and readily recovered after processing. It is also a small molecule with high diffusivity, a property of interest for extraction processes. A drawback is that supercritical CO_2 is not a very good solvent for high molecular weight and polar compounds. To increase the solubility of such compounds, small amounts (0 to 20%) of co-solvents are usually added. The co-solvent, often an alcohol,[11] interacts strongly with the solute and significantly increases its solubility, in particular close to the critical point of CO_2.

Miniaturization based on micromachining can be used to obtain microflow and microreaction systems with internal volumes in the picoliter to microliter range, in which near-critical pressure and temperature conditions (conditions (p,T)) can be reached without applying the special safety precautions required for conventional, larger high pressure systems. If such systems are made of a transparent material, they constitute attractive research tools to study phase behavior directly by microscopy. Here, this approach is followed and a microscopic set-up containing a microfluidic glass chip is used to study phase change dynamics in CO_2-alcohol mixtures under high pressure conditions and temperatures. Rhodamine B, a fluorescent dye, is used to visualize the different phases.

5.2 Results and Discussion

5.2.1 Chip layout and fabrication

The chip, Figure 5-1, has two inlets (**1**, **2**) for introduction of pressurized fluids (liquid CO_2 and alcohol-rhodamine B solutions). In the first part of the connected channel, **a-c** mixing of the fluids takes place. In one of the chip designs this channel section contained herringbone mixers with >>>, <<<, / / / and \ \ \ designs similar to the ones used by Stroock *et al.*[20] These mixers continue in the next section **d-e**, which is at high temperatures in order to initiate phase transitions and runs into a serpentine, located in the heated zone. Subsequently, the fluid enters a flow restriction **3** with a length of 177 mm and a smaller cross-section (20 μm × 5 μm). This channel section ensures a virtually constant pressure in the channel section upstream, the section where phase transitions occur. The hydraulic resistor ends in a wider zone with outlets (**4**, **5**) in which the fluid mixture gradually expands to atmospheric conditions. The complete fabrication procedure is based on the first generation of chips described in Chapter 4.

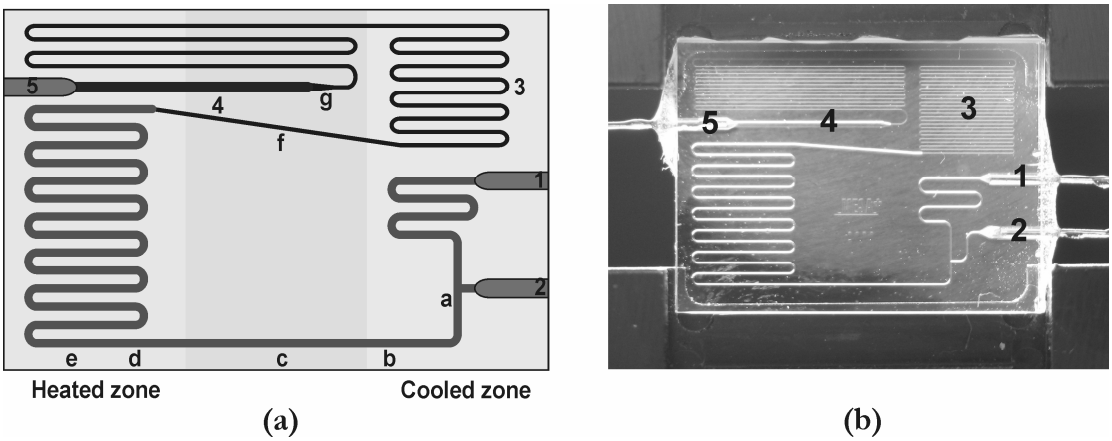

Figure 5-1: Microfluidic chip: Layout (**a**) and photograph (**b**) of chip for visualization of phase transitions. The labels **a** to **g** are used to facilitate the description of the microscope images in Figures 5-2 and 5-3. Legend: **1** inlet CO_2, **2** inlet alcohol-dye mixture, **3** fluidic resistor, **4** expansion zone, **5** outlet.

In order to initiate and control phase transitions in mixtures of ethanol-CO_2 and methanol-CO_2, the left side of the chip is heated and the right side cooled. In all experiments, the cooled side was kept at 10 °C to maintain the CO_2 in the liquid phase. The temperature of the heated side was regulated to a temperature between 35 and 95 °C, see the Experimental. It was calculated that a small temperature gradient exists on the chip at the edge of the heated zone, but at 200 μm from the edge the temperature of the chip is within 0.1 °C of that of the heater. Due to the small channel dimensions and thin glass layer between heater and fluid in the channel, the temperature of the fluid, at the used flow rates, is virtually the same as that of the heater (or cooler). To avoid condensation of moisture at the outside of the chip in the area where the CO_2 becomes a gas and to limit thermal stresses in the glass due to excessive heat absorbance in that area, the last part of the back pressure channel and the expansion zone are heated.

5.2.2 Microscopic observation of phase changes

Instead of the variable-volume high pressure view cells which are frequently used to determine the appearance of sub- to supercritical phase transitions by visual observation of the resulting turbidity or the (dis)appearance of a meniscus,[3,21] a glass chip was used for *in-situ* studies of the hydrodynamics and phase behavior of dense fluids by optical microscopy. The chip contains a microfluidic channel network

through which a 50/50 v/v mixture of two fluids can be pumped, Figure 5-1. The design is such that pressurized liquid CO_2 from inlet **1** after mixing with a second pressurized liquid, added *via* inlet **2**, passes at virtually constant pressure through a heated, isothermal zone. At a specific location close to position **d** in Figure 5-1, which depends on local pressure and temperature, a phase change occurs, which is monitored by optical microscopy. After the heated zone, the fluid flows through the rest of the channel.

Compared to the visual determination of phase transitions in the conventionally used variable-volume view cell,[2,3] which is a static method in which the pressure at constant temperature is increased in time with the aid of a piston, the microfluidic system presented here has the advantage that the image can be viewed over a relatively long channel section, where experimental conditions (p,T) can be gradually varied. This facilitates the interpretation of observed patterns and, provided that the pressure and temperature gradients in the chip are known, helps to pinpoint the exact experimental conditions where transitions occur.

Figure 5-2 shows a sequence of microscope pictures taken at different locations on the chip during an experiment with a 50/50 v/v mixture of ethanol (EtOH) and CO_2 (calculated CO_2 mol fraction: 0.54). Since these liquids are colorless and therefore their liquid-liquid and even their liquid-gas interfaces were difficult to observe by microscope, the fluorescent dye rhodamine B was added to the EtOH (or methanol (MeOH), see below) in a concentration of 0.1 mM. This concentration corresponds to a mol fraction of 1.7×10^{-6}. The addition of such a small amount of rhodamine B is assumed not to cause significant changes of the phase diagram of the mixtures used in this study (although no literature data exists to substantiate this assumption). Moreover the rhodamine B concentration is in the range of the impurities in the liquid CO_2 (N_2 ~60 ppm).

During the experiment of Figure 5-2 the inlet pressure was maintained at 100 ± 0.5 bar, the temperature of the heated and cooled zone were kept at 60 ± 0.5 °C and 10 ± 0.5 °C, respectively. Image **a** shows the injection of the EtOH + rhodamine B mixture (yellow) into the colorless liquid CO_2 stream. The fluids mix downstream due to diffusion enhanced by advection caused by "herringbone" mixers[20] embedded in the wall of the microchannel. The initial lamella flow pattern (Figure 5-2 **b**) turns into a homogeneous, uniformly colored liquid mixture of CO_2 and EtOH (Figure 5-2 **c**). When the mixture reaches the 60 °C zone on the chip, an abrupt change in the flow

pattern is visible (Figure 5-2 **d**), characterized by a bright-red mist. Downstream, a two-phase system forms with the liquid flowing along the walls (yellow in Figure 5-2 **e**) and a vapor in the middle of the channel. When the two-phase system enters the fluidic resistor, a uniform red-colored liquid mixture is seen again, Figure 5-2 **f**. Finally, the liquid mixture enters the expansion zone, where CO_2 becomes gaseous (formation of vapor bubbles, Figure 5-2 **g**).

Figure 5-3 shows snapshots taken from a microscope movie recorded at a fixed location (position **d** in Figure 5-1; camera speed: 25 frames per second) of experiments at different temperatures and pressures, for a 50/50 v/v mixture of methanol and CO_2. The microscope photographs give a clear view of two different phase change phenomena, *i.e.* boiling with vapor bubbles (**C** and **D**) and an event characterized by a red mist (images **A** and **B**).

Based on reported phase diagrams,[22-26] a 50/50 v/v MeOH-CO_2 mixture (CO_2 mol fraction 0.45) will be in the liquid state at the pressure and temperature conditions that exist upstream of the heated zone. Upon temperature increase the bubble-point line in the phase diagram will be crossed, after which the mixture will de-mix in a liquid consisting mainly of MeOH with dissolved CO_2 (here also with dissolved rhodamine B) and vapor CO_2 saturated with MeOH. For pressures and temperatures below 50 °C and 80 bar indeed, the typical gas-liquid two-phase flow of the slug type,[27] which is characteristic for a boiling process in a microchannel was observed. At higher pressures and temperatures the mist pattern mentioned above was observed. Further downstream of the mist pattern, annular flow[28] (Figure 5-2 **e**), was observed. The film that separates and collects on the surface walls of the channel shows yellow-orange fluorescence, typical of rhodamine B in ethanol. The location where the mist pattern starts was observed to fluctuate in time over a distance of 100 - 120 μm. It was calculated that this displacement corresponds to less than 0.1 °C temperature difference. The observed fluctuations are probably due to small pressure perturbations caused by nucleation of bubbles or droplets somewhere downstream in the microchannel.

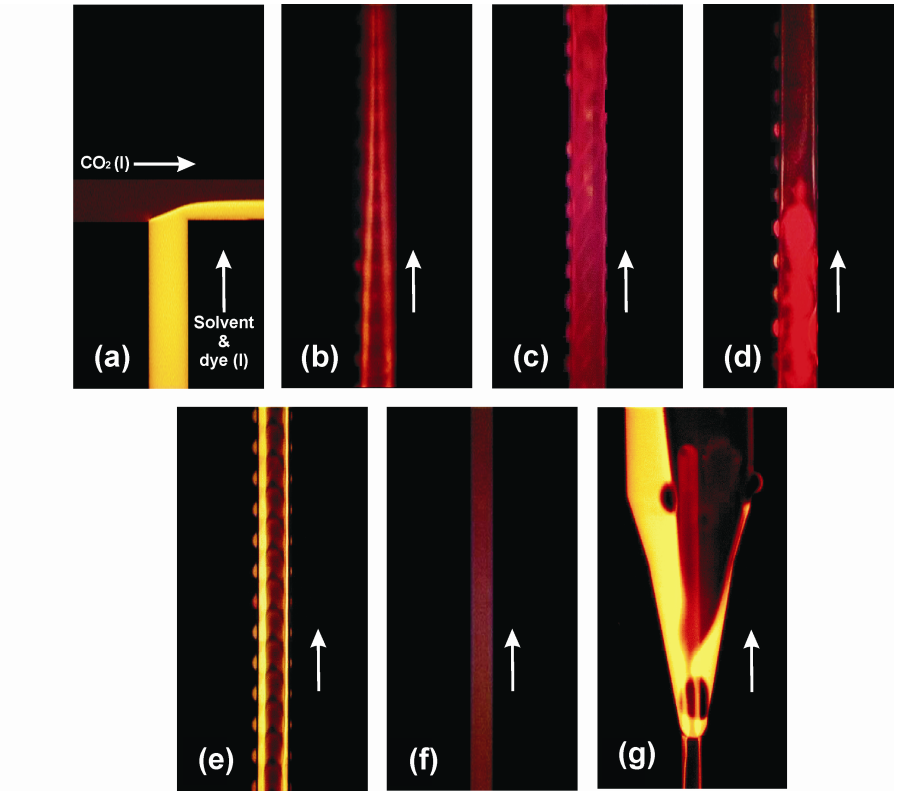

Figure 5-2: Microscopic visualization of phase transitions. Images of a 50/50 v/v mixture of CO_2 and EtOH with rhodamine B at different positions in the chip (letters correspond to locations in Figure 5-1).

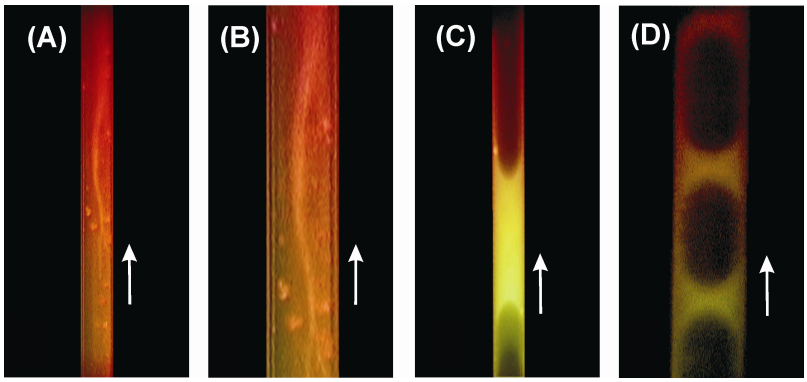

Figure 5-3: Comparison of boiling and mist flow. Images of a 50/50 v/v mixture of CO_2 and MeOH with rhodamine B were taken in the heated zone of the chip (location **d** in Figure 5-1). Images **B** and **D** show identical flow patterns as **A** and **C**, respectively, but at higher magnification. The flow direction is indicated by arrows. Experimental conditions for images **A** and **B**: pressure 100 ± 0.5 bar, temperature heated zone 61 ± 0.5 °C; for images **C** and **D**: pressure 70 ± 0.5 bar, temperature heated zone 39 ± 0.5 °C. This chip did not contain herringbone mixers.

An additional experiment was performed with a chip configuration that allowed heating up and pressurizing the pure CO_2 stream to supercritical conditions first, before it reached the T-junction at which it was combined with the stream of liquid ethanol with dissolved rhodamine B. Starting only a small distance down-stream of the T-junction where the two streams joined, exactly the same mist pattern was observed as was described above and as shown in Figure 5-3 **A** and **B**.

5.2.3 Construction of phase diagrams

The phase changes described above were studied for a wider range of temperatures and pressures, for 50/50 v/v mixtures of EtOH-CO_2 and MeOH-CO_2, by continuously monitoring the flow pattern at a fixed position (**d** in Figure 5-1) for a constant inlet pressure, while the temperature of the heated zone was varied in small steps of half degree. For a range of pressures, up to 140 bar, the temperature was recorded at which a characteristic change in flow pattern occurred. The results are plotted in Figure 5-4. For each mixture a p,T-point exists, above which only the mist pattern of Figure 5-3 **b** is found. These points are 50 °C/85 bar for the MeOH-CO_2 mixture and 47 °C/82 bar for EtOH-CO_2. Slightly below these p,T-points, within a narrow temperature range of 3 to 7 degrees, during an increase of temperature first tiny gas bubbles appear, whereas at a slightly higher temperature the mist pattern arises. The mist flow pattern and the vapor bubbles were never observed simultaneously. All these effects and the corresponding conditions (p,T) at which they occurred were perfectly reproducible.

For EtOH-CO_2 mixtures above 82 °C/115 bar the characteristic flow pattern of image **A**/**B** in Figure 5-3 was not observed. Instead the precipitation of a red powder was found in the channel, leaving a homogeneous colorless fluid. Precipitation reproducibly occurred at the position of the herringbone mixers. In the liquid collected during two hours at the outlet of a chip operated at 100 °C/120 bar, no traces of rhodamine B or of possible decomposition products could be detected by Matrix-Assisted Laser Desorption Ionization (MALDI) Time-Of-Flight (TOF) Mass Spectrometry (MS). However, in a sample collected at 65 °C/100 bar rhodamine B was clearly identified by MALDI-MS. This indicates that the powder consists of rhodamine B.

The graphs show that the observed transitions coincide with the bubble-point lines for the 50/50 v/v mixtures as derived from literature data.[2,22-26,28] Unfortunately, for the literature data in refs. 29, 30 the exact mixture compositions for the critical points have not been specified. Based on interpolation of the data of ref. 20, the critical point of the MeOH-CO_2 mixture with the composition studied in our work should be close to 150 °C/160 bar. By extrapolation of the data of Galicia-Luna *et al.*,[31] the critical point of the 50/50 v/v EtOH-CO_2 mixture studied by us should be near 130 °C/150 bar. These temperatures were however beyond the range of our experimental set-up.

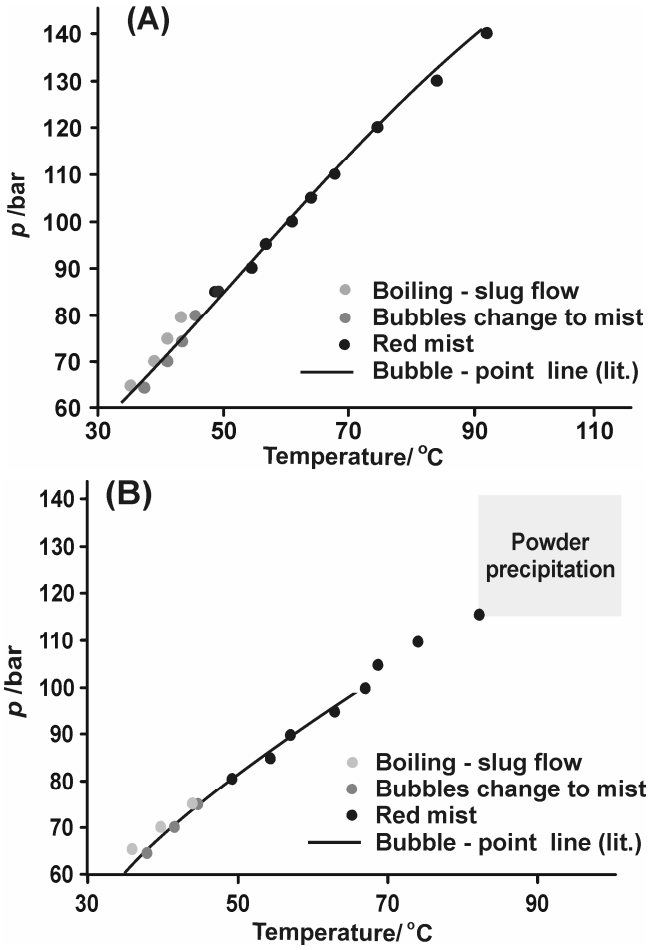

Figure 5-4: Phase diagrams derived from microscopic observation of flow patterns in a microfluidic chip. **A**; 50/50 v/v MeOH-CO_2, **B**; 50/50 v/v EtOH-CO_2. Data points are averages of at least three experiments. Estimated experimental error in transition temperatures is about 2% (on Celsius scale).

5.2.4 High speed camera investigation of phase changes

The dynamics of bubble formation followed by slug flow as well as the mist formation were studied with the aid of a microscope equipped with a high-speed camera, recording 1000 frames per second. Figure 5-5 shows a number of frames extracted from these movies, taken at different temperature-pressure conditions. Due to low contrast, the stills do not clearly show details of the mist pattern (Figure 5-5 **a**) nor of the contours of the vapor bubble (Figure 5-5 **b**), but they could be observed clearly in the movies. The low contrast is mainly due to the fact that the light intensity during video recording had to be limited in order to avoid heating of the liquid, which led to a shift of the location of phase changes in the microchannel. Furthermore, due to the relatively high fluid velocity in combination with the large microscope magnification, a particular bubble was only visible in three consecutive movie frames at the most. But although bubble images were blurry, they allow the determination of the linear velocity of the bubbles at 100 bar, which was found to be 5 ± 1 cm s^{-1} for the conditions under which slug flow occurs.

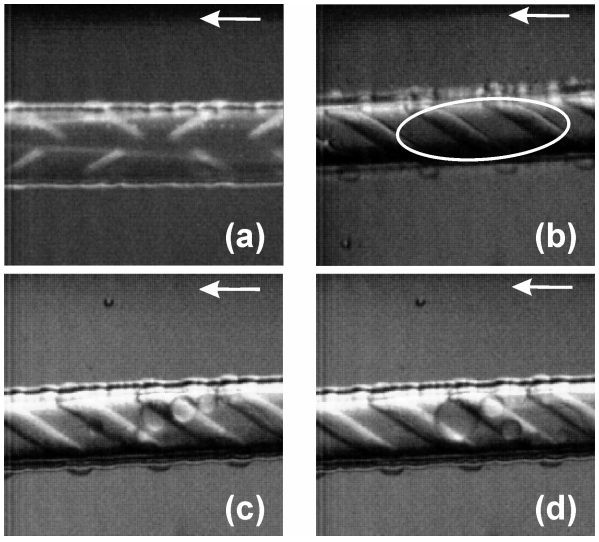

Figure 5-5: Snap-shots of high-speed camera recordings of droplet condensation. White arrows show the direction of the flow. (**a**). Mist pattern (the white streaks running at the top side and the center of the channel), 60 °C, 100 bar; (**b**). Vapor bubble (white ellipsoid), conditions: 40 °C, 70 bar. (**c**) and (**d**). Droplets condensing in the microchannel downstream of the mist pattern; conditions: 100 bar and 65 °C. All pictures are for a MeOH-CO_2 mixture in a microchannel with herringbone mixers integrated in the channel wall.

The stills in Figure 5-5 **c** and **d** show how the mist pattern ends up in liquid droplets that slowly grow in size further downstream and finally connect to establish the liquid film on the walls that was shown in Figure 5-2 **e**.

5.2.5 Interpretation of the flow patterns

Ample literature exists on two-phase flow phenomena in tubes and other fluidic structures of a wide variety of dimensions, but most of the literature on two-phase flow in microchannels is concerned with mixed streams of air and water, with separately controlled flow rates, at atmospheric and isothermal conditions.[29,32,33] Only few experiments similar to those performed here, *i.e.* microscopic observations of pressurized fluids passing from a cold to a hot zone and therewith going through a phase change, have been reported.

The mist flow pattern showed in Figure 5-2 **d** and images **A**/ **B** of Figure 5-3 is different from most two-phase flow phenomena reported for microchannels,[33] including the ones observed for boiling liquids,[34] and at first sight seems to be characterized by the total absence of a meniscus. In studies using variable-volume view cells, a mist phenomenon is observed when a supercritical mixture approaches the dew point.[2] Because of these characteristics, one may speculate whether the observed pattern represents a phase transition involving a supercritical phase. However, according to literature,[22] the conditions (p,T) are not sufficient for reaching critical conditions of the mixture. Furthermore, mist flow is not an exclusive characteristic of supercritical fluids. In the literature on two-phase flow in minichannels (hydraulic diameter in the order of 1 mm) and larger tubes, one may find situations described, namely at the high vapor velocity side of the flow regime plot, where a pattern called "annular-droplet",[33] "annular mist",[35] or "droplet" flow[32,36] is encountered. In these cases, the liquid flows as a thin film on the channel wall, while the gas flows in the core, therewith forming an annulus. Most of the liquid, however, is entrained in the gas in the form of droplets, constituting a mist.[35]

In microchannels, or more specifically channels with hydraulic diameter much smaller than the Laplace constant (which scales surface tension to gravitational forces and which is of order 1 mm for water at atmospheric conditions and room temperature), two-phase flow characteristics are known to become significantly different from characteristics in larger channels.[27] The flow patterns will be dominated

by surface tension. Since liquid surface tension is low in near-critical fluids and even vanishes at the critical point,[37,38] one may expect that the formation of entrained droplets, *i.e.* a mist, is enhanced for a fluid approaching its critical point. In this respect the work of Pettersen[36] deserves special attention. As part of a heat exchanger study Pettersen has investigated flow vaporization of CO_2 in microchannel tubes with 0.81 mm ID, uniformly heated by a water jacket. Observation of two-phase flow patterns was performed in the heated zone of a transparent tube, mainly at 20 °C, so close to the critical temperature. At the higher mass fluxes (corresponding to vapor velocities close to 2 m s^{-1}), he observed flow patterns with a mist flow of liquid droplets in the core and a very thin annular liquid film flowing along the wall, with a notable difference in velocity between the film and the mist. The author states that even at 99% vapor there was a notable amount of entrained liquid droplets, indicating a non-equilibrium situation where the vapor phase had become superheated. Transitions in flow patterns occurred at much lower vapor velocities than the ones reported by others for water/air flow in tubes of similar dimensions.

For channels of the dimensions as investigated here (*i.e.* with a hydraulic diameter below 100 μm), mist patterns have not been reported, see *e.g.* the flow regime maps obtained in studies in 224 μm wide microchannels,[39] and channels formed by spacings between micropillars of ~50 μm.[40] The reason for this may be that the studied fluid velocities, in particular the superficial gas velocity, were not high enough to achieve mist flow. What is observed in Figure 5-2 **d** and the images **A** and **B** of Figure 5-3 is a jet of nanodroplets of MeOH with concentrated rhodamine B entrained in a stream of very dense CO_2 vapor. Ziegler *et al.* speculate about the presence of such an aerosol at conditions close to the critical point of a 1-propanol-CO_2 mixture in supercritical fluid chromatography in 50 μm ID capillaries, in order to explain their spiked detector signals.[29] Extrapolating the trends reported in literature to the small dimensions of the channels and adding to that the conditions close to the critical point of the mixture, where the surface tension becomes low, ca explain the mist pattern observed at fluid velocities of about 0.5 m s^{-1} (see Experimental), which are much lower that the ones reported in literature.[36]

We have elaborated on the observation that the CO_2-alcohol mixture upon reaching the heated zone form a mist of small droplets entrained in a background of pressurized CO_2-alcohol vapor. Interpretation of the phase diagrams that correspond to this situation learns that the vapor phase is enriched in CO_2, while the liquid phase

has an increased alcohol content compared to the original mixture composition.[22-26] Such a mist or spray may have important implications for the chemistry proceeding in the fluid.

5.2.6 Interpretation of the rhodamine B behavior

One effect of the droplet formation as discussed in the previous section is that the concentration of low-volatility species which dissolve more easily in the liquid alcoholic phase, will increase compared to the original concentration. This is in fact what is used in the so-called "supercritical anti-solvent" or "gas anti-solvent" process,[41] in which a solution of a specific chemical is nebulized into CO_2 fluid (sub- or supercritical), which will lead to rapid supersaturation of the fluid and formation of ultra-fine particles with a narrow size distribution. This is also what was observed with the dye rhodamine B. Namely, a bright-red color as observed for the mist pattern is uncommon for a rhodamine B solution. Normally in ethanol or methanol rhodamine B fluorescence is observed at 570 - 590 nm for the complete temperature range studied here.[42] Red shifts in fluorescence have been attributed to aggregate formation in solution, occurring at high dye concentrations.[43,44] Eventually, the concentration of rhodamine B will exceed the solubility limit, because the amount of ethanol is decreasing due to evaporation (or rather, dissolution in the CO_2-rich vapor phase) and the dye will precipitate, as was indeed observed for the higher temperatures during the experiments (Figure 5-4 diagram **B**).

Another implication for the course of chemical reactions in a system like described here is that internal mixing in the liquid phase is enhanced due to the small size of the droplets. Mixing under these conditions can be assumed to be mainly by diffusion, although some advection occurring within the droplet cannot be excluded. The situation resembles that in the segmented gas-liquid flow microfluidic systems that were used by Jensen and co-workers to form well-defined quantum dots[45] or silica particles.[46] The small liquid slugs that compose the segmented flow not only ensure a narrow residence time distribution[47] but also experience enhanced mixing due to recirculating flows within the slug.[48] In the literature on the droplet diffusion model for micromixing,[49] a characteristic mixing time in a (hypothetical in the original work, but real in this study) droplet is of the order of R^2/D, with R the droplet radius and D the diffusivity of the reacting species. Judging from the movie from which Figure 5-3

B was taken and other movies of the mist pattern, droplets in our case are typically much smaller than a percent of the channel width, *i.e.* a few hundred nm at most, so that for a typical diffusivity of 10^{-5} cm^2 s^{-1} a mixing time of the order of 0.5 ms is achieved for homogenization of the concentration within the droplet. This may lead to enhanced reaction kinetics or changes in selectivities.

5.3 Conclusions and Outlook

In summary, in this Chapter the feasibility of a simple table-top set-up for studying fluid mixtures under conditions of high pressure and temperature under continuous flow fashion was demonstrated. Very specific flow patterns were observed in the microfluidic chip, which can be attributed to a liquid-vapor phase transition. The set-up was used to determine high pressure phase diagrams of two different alcohol-CO_2 mixtures, which were in agreement with literature data. A specific flow pattern type was observed, which was identified as an annular mist pattern. The conditions under which this pattern was observed differ greatly from those reported in literature, which was attributed to the smaller microchannel dimensions in this case and the fact that the conditions are close to the critical point of the fluid mixture ($p/p_c \sim 1$, $T/T_c \sim 0.7$ - 0.9) where the surface tension vanishes. The implications of the formation of liquid droplets entrained in a CO_2-alcohol vapor were discussed and it was anticipated that reaction kinetics under these conditions may become enhanced due to fast homogenization of the mixture in the droplet and the increased concentration of non-volatile components of the droplets.

The set-up as described here will be valuable to study phase change events in supercritical fluid chromatography, where knowledge of the exact fluid conditions and corresponding flow profiles is essential.[11,30] The chip itself could be used as a chromatograph. Beside that direct observation of the separation process may be performed, integration of injectors and detectors, as is almost common practice in chip-based capillary electrophoresis,[50] is feasible. It will also have its value in the study of heat exchangers for transcritical refrigeration cycles[51] and more importantly, in chemical applications like synthesis and analysis, exploiting the characteristic features (improved heat management and large surface-to-volume ratio) that make microreactors beneficial, in particular, for heterogeneous catalysis.[52,53]

5.4 Experimental

5.4.1 Materials

Methanol was purchased from Fisher Scientific, analytical reagent grade (< 0.015% water) and ethanol was purchased from Merck (Amsterdam, The Netherlands) (< 0.1% water). Both solvents were dried with molecular sieves beads (0.3 nm). Rhodamine B was purchased from Sigma-Aldrich (Zwijndrecht, The Netherland), purity ≈ 95%. CO_2 was purchased from Hoek Loos (2.7), (Schiedam, The Netherlands) with a purity ≥ 99.7% and < 150 ppm of water.

The characterization of the Rhodamine B was done using a Voyager (Applied Biosystems) Matrix Assisted Laser Desorption Ionization Time-of-Flight Mass Spectrometer.

5.4.2 Set-up

Figure 5-6 shows a schematic representation of the set-up used for the phase transition observations.

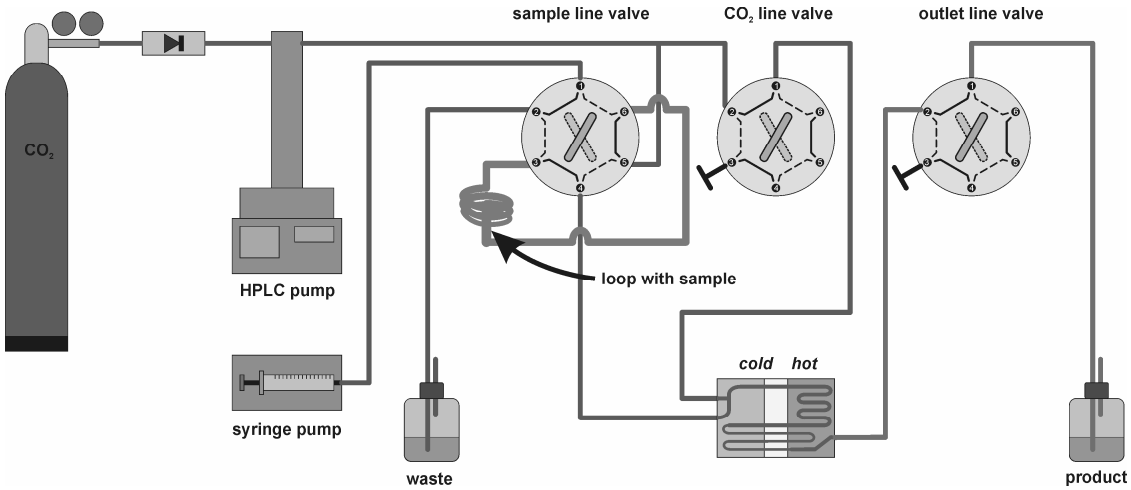

Figure 5-6: Schematic view of the set-up used during the visualization of phase transitions in alcohol-CO_2 mixtures.

The fused-silica capillaries that were attached to the chips and stainless steel fittings (F-140 & A-318, Upchurch Scientific, USA) were used to connect the chips to a high-pressure syringe pump (model 100 DM; Teledyne Isco, Inc. Lincoln, USA.). In Figure 5-7 a picture of the set-up is shown. Liquid CO_2 (purity ≥ 99.7%) was supplied from a cylinder and further pressurized with the high pressure pump. The CO_2 flow was split into two streams (50/50 v/v), to both directly feed the chip *via* the CO_2 inlet and/or to drive the sample liquid EtOH or MeOH with dissolved rhodamine B from a looping (600 μL volume) into the sample inlet. A set of valves (Rheodyne C6W, Valco Instruments Co. Inc., USA) was used to control the flows to/from the chip (injection of liquid CO_2, injection of

sample *via* the looping, as well as closing/opening of the inlets and outlet), whereas in-line filters (type A-102, Upchurch Scientific, USA) prevented the channels in the chip from clogging.

In order to control the temperature of the fluids in the chip, two zones were defined of which the temperatures could be individually controlled *via* home-built Peltier elements (CP 0.8-7-06L, Melcor, USA), glued pair wise onto two copper blocks. The temperature of these blocks was measured with miniature Pt-100 temperature sensors. The Peltier elements were mounted on top of the chip, for removal of the excess heat generated by the Peltier elements a heat sink was used (Figure 5-8). Optical inspection of the microchannel was done from below *via* an inverted microscope (Olympus CK40M).

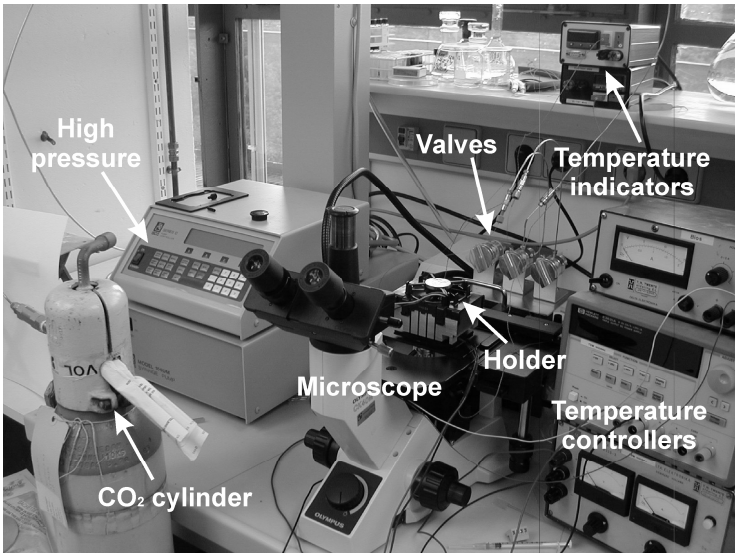

Figure 5-7: Picture of the set-up used for visualization of phase transitions of fluidic mixtures.

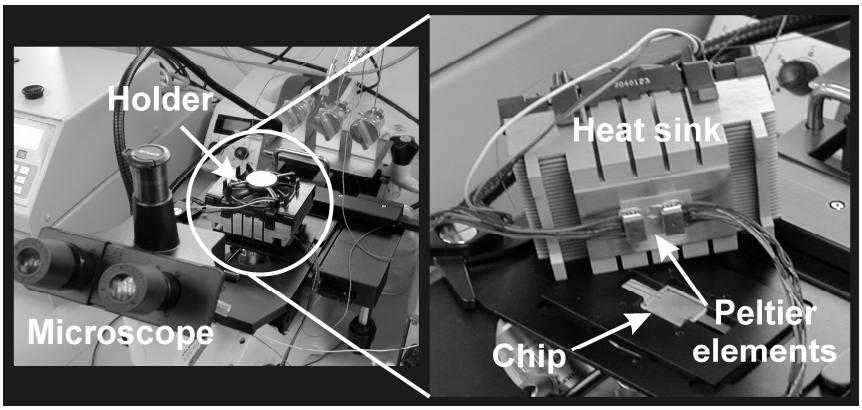

Figure 5-8: Picture of the holder used for visualization of phase transitions of fluidic mixtures.

5.4.3 Temperature, pressure and fluid velocity conditions in the chip

The original idea behind this work was to study phase changes of a fluid flowing in a microchannel, under conditions of high pressures and temperatures near the critical point of the fluid. To this end, a system was constructed in which the flowing fluid is kept at constant pressure in a microchannel section on which a spatial temperature gradient is imposed. The actual fluid temperature and pressure conditions during the experiments have to be determined. Information about these parameters at the exact location of interest is difficult to access through a local measurement. Only information about the inlet pressure, which is the pressure generated by the HPLC pump (Figure 5-6) the outlet pressure, which is atmospheric and the temperature at the outside of the chips, measured by thermocouples inserted between chip and Peltier elements (Figure 5-8) is available.

The dimensions of the flow restrictor were chosen to ensure that the pressure drop is entirely over the restrictor. Assuming that the liquid velocity is the same as that of the measured bubble velocity (see above) it can be calculated that the Reynolds number for the situation of slug flow in the wider channel section is of order 1, indicating that the flow in the microchannel is laminar. For fully developed laminar flow and assuming that the entire channel on the chip is filled either with liquid or with vapor, it is calculated that the hydraulic resistance of the wider channel section is $1.15 \times 10^{19}\ \eta\ m^{-3}$, with η the viscosity of the fluid, while that of the narrower channel of the flow restrictor is $9.73 \times 10^{22}\ \eta\ m^{-3}$. This gives a hydraulic resistance ratio of 8430, which means that indeed nearly all of the pressure drop will be over the flow restrictor. The latter is true even in the extreme case that the wider channel section would be filled with liquid and the restrictor would be filled with gaseous CO_2, which constitutes a situation with a viscosity ratio of about 10 at the most.[54,55]

Based on the fluid velocity of 5 ± 1 cm s^{-1} determined above and an approximate viscosity of the mixture of 1 mPa s, for a pressure drop of 100 bar a flow rate of 50 ± 10 μL min^{-1} is calculated. This fits quite well with the value of 40 ± 5 μL min^{-1} indicated by the HPLC pump for the flow rate at the inlet of the chip, where the fact that the measured velocity in this flow regime is slightly higher than one would expect on the basis of the inlet flow can be explained by the increase in average volume per mole of material due to the evaporated liquid that has formed vapor bubbles. The velocity of the completely evaporated fluid, with an approximate viscosity of 0.1 mPa s, would be ~10 times higher than that calculated above for the liquid and thus would be about 0.5 m s^{-1}.

Taking the measured fluid velocity and the smallest channel dimension of 30 μm at the high pressure section of the microchannel and assuming a constant glass temperature (in the heated zone), constant flow rate and fluid viscosity can be calculated[56] for liquid CO_2. The temperature profile in the microchannel will adapt to the higher temperature within a distance of ~35 μm after entering the heated zone (Figure 5-1; CO_2 heat transfer data taken from reference 57). The real situation in our experiments is that the CO_2 of the liquid mixture starts to evaporate when the heated zone is reached, leading to a less dense fluid with a higher fluid velocity due to the expansion that occurs during evaporation. Therefore the entrance length will be different and very difficult to calculate for the non-equilibrium two-phase flow studied here. The viewpoint for fluidic phase transitions (**d** in Figure 5-1) in our experiments was chosen at a distance of about 300 μm far from the edge of the heater.

5.5 References

1. Luo, Z.; Xiong, Y.; Parcher, J. F., *Anal. Chem.* **2003**, *75*, 3557-3562.
2. Reighard, T. S.; Lee, S. T.; Olesik, S. V., *Fluid Phase Equilib.* **1996**, *123*, 215-230.
3. Poliakoff, M.; King, P., *Nature* **2001**, *412*, 125-125.
4. Ke, J.; Oag, R. M.; King, P. J.; George, M. W.; Poliakoff, M., *Angew. Chem., Int. Ed.* **2004**, *43*, 5192-5195.
5. Aguiar-Ricardo, A.; Temtem, M.; Casimiro, T.; Ribeiro, N., *Rev. Sci. Instrum.* **2004**, *75*, 3200-3202.
6. Leitner, W., *Nature* **2000**, *405*, 129-130.
7. Jessop, P. G.; Leitner, W., *Chemical Synthesis Using Supercritical Fluids*. Wiley VCH: Weinheim (Germany), **1999**.
8. DeSimone, J. M., *Science* **2002**, *297*, 799-803.
9. Adam, D., *Nature* **2000**, *407*, 938-940.
10. Arai, Y.; Sako, T.; Takebayashi, Y., *Supercritical Fluids: Molecular Interactions, Physical Properties and New Applications*. Springer: Berlin (Germany), **2002**.
11. Wells, P. S.; Zhou, S.; Parcher, J. F., *Anal. Chem.* **2003**, *75*, 18A-24A.
12. Jung, J.; Perrut, M., *J. Supercrit. Fluids* **2001**, *20*, 179-219.
13. Clifford, A. A.; Pople, K.; Gaskill, W. J.; Bartle, K. D.; Rayner, C. M., *Chem. Commun.* **1997**, 595-596.
14. Licence, P.; Gray, W. K.; Sokolova, M.; Gray, W. K., *J. Am. Chem. Soc.* **2005**, *127*, 293-298.
15. Hyde, J. R.; Licence, P.; Carter, D.; Poliakoff, M., *Appl. Cat. A* **2001**, *222*, 119-131.
16. Prajapati, D.; Gohain, M., *Tetrahedron* **2004**, *60*, 815-833.
17. Ellington, J. B.; Park, K. M.; Brennecke, J. F., *Ind. Eng. Chem. Res.* **1994**, *33*, 965-974.
18. Wensink, H.; Elwenspoek, M. C., *Sens. Actuators A* **2002**, *102*, 157-164.
19. Oosterbroek, R. E.; Hermes, D. C.; Kakuta, M.; Benito-Lopez, F.; Gardeniers, J. G. E.; Verboom, W.; Reinhoudt, D. N.; Van den Berg, A., *Microsyst. Technol.* **2006**, *12*, 450-454.
20. Stroock, A. D.; Dertinger, S. K. W.; Ajdari, A.; Mezic, I.; Stone, H. A.; Whitesides, G. M., *Science* **2002**, *295*, 647-651.
21. Dohrn, R.; Brunner, G., *Fluid Phase Equilib.* **1995**, *106*, 213-282.
22. Brunner, E.; Hültenschmidt, W.; Schlichthärle, G., *J. Chem. Thermodyn.* **1987**, *19*, 273-291.
23. Ohgaki, K.; Katayama, T., *J. Chem. Eng. Data* **1976**, *21*, 53-55.
24. Suzuki, K.; Sue, H., *J. Chem. Eng. Data* **1990**, *35*, 63-66.
25. Jennings, D. W.; Lee, R. J.; Teja, A. S., *J. Chem. Eng. Data* **1991**, *36*, 303-307.
26. Day, C. Y.; Chang, C. J.; Chen, C. Y., *J. Chem. Eng. Data* **1996**, *41*, 839-843.

27. Triplett, K. A.; Ghiaasiaan, S. M.; Abdel-Khalik, S. I.; Sadowski, D. L., *Int. J. Multiphase Flow* **1999**, *25*, 377-394.
28. Joung, S. N.; Yoo, C. W.; Shin, H. Y.; Kim, S. Y.; Yoo, K. P.; Lee, C. S.; Huh, W. S., *Fluid Phase Equilib.* **2001**, *185*, 219-230.
29. Ziegler, J. W.; Dorsey, J. G.; Chester, T. L.; Innis, D. P., *Anal. Chem.* **1995**, *67*, 456-461.
30. Chester, T. L., *J. Chromatogr. A* **2004**, *1037*, 393-403.
31. Galicia-Luna, L. A.; Ortega-Rodriguez, A.; Richon, D., *J. Chem. Eng. Data* **2000**, *45*, 265-271.
32. Spedding, P. L.; Nguyen, V. T., *Chem. Eng. Sci.* **1980**, *35*, 779-793.
33. Xu, J. L.; Cheng, P.; Zhao, T. S., *Int. J. Multiphase Flow* **1999**, *25*, 411-432.
34. Xu, J. L.; Shen, S.; Gan, Y. H.; Li, Y. X.; Zhang, W.; Su, Q. C., *J. Micromech. Microeng.* **2005**, *15*, 1344-1361.
35. Mandhane, J. M.; Gregory, G. A.; Aziz, K., *Int. J. Multiphase Flow* **1974**, *1* 537-553.
36. Pettersen, J., *Exp. Therm. Fluid Sci.* **2004**, *28*, 111-121.
37. Dittmar, D.; Oei, S. B.; Eggers, R., *Chem. Eng. Technol.* **2002**, *25*, 23-27.
38. Sun, Y. D.; Shekunov, B. Y., *J. Supercrit. Fluids* **2003**, *27*, 73-83.
39. De Mas, N.; Günther, A.; Schmidt, M. A.; Jensen, K. F. In Proc. 12th IEEE Int. Conf. Solid-State Sensors, Actuators and Microsystems (Transducers '03), Boston, MA, (USA), 8-12 June, Boston, MA, (USA), **2003**; pp 655-658.
40. Losey, M. W.; Jackman, R. J.; Firebaugh, S. L.; Schmidt, M. A.; Jensen, K. F., *J. Microelectochem. Syst.* **2002**, *11*, 709-717.
41. Dixon, D. J.; Johnston, K. P.; Bodmeier, R. A., *AIChE J.* **1993**, *39*, 127-139.
42. Ali, M. A.; Moghaddasi, J.; Ahmed, S. A., *J. Opt. Soc. Am. B: Opt. Phys.* **1991**, *8*, 1807-1810.
43. Bindhu, C. V.; Harilal, S. S.; Varier, G. K.; Issac, R. C.; Nampoori, V. P. N.; Vallabhan, C. P. G., *J. Phys. D: Appl. Phys.* **1996**, *29*, 1074-1079.
44. Bindhu, C. V.; Harilal, S. S., *Anal. Sci.* **2001**, *17*, 141-144.
45. Yen, B. K. H.; Gunther, A.; Schmidt, M. A.; Jensen, K. F.; Bawendi, M. G., *Angew. Chem., Int. Ed.* **2005**, *44*, 5447-5451.
46. Khan, S. A.; Gunther, A.; Schmidt, M. A.; Jensen, K. F., *Langmuir* **2004**, *20*, 8604-8611.
47. Trachsel, F.; Gunther, A.; Khan, S.; Jensen, K. F., *Chem. Eng. Sci.* **2005**, *60*, 5729-5737.
48. Gunther, A.; Jhunjhunwala, M.; Thalmann, M.; Schmidt, M. A.; Jensen, K. F., *Langmuir* **2005**, *21*, 1547-1555.
49. Nauman, E. B., *Chem. Eng. Sci.* **1975**, *30*, 1135-1140.
50. Vandaveer, W. R.; Pasas-Farmer, S. A.; Fischer, D. J.; Frankenfeld, C. N.; Lunte, S. M., *Electrophoresis* **2004**, *25*, 3528-3549.
51. Pettersen, J.; Hafner, A.; Skaugen, G.; Rekstad, H., *Int. J. Refrig.* **1998**, *21*, 180-193.

52. Kobayashi, J.; Mori, Y.; Okamoto, K.; Akiyama, R.; Ueno, M.; Kitamori, T.; Kobayashi, S., *Science* **2004**, *304*, 1305-1308.
53. Kobayashi, J.; Mori, Y.; Kobayashi, S., *Chem. Commun.* **2005**, 2567-2568.
54. Herreman, W.; Grevendonk, W.; De Bock, A., *J. Chem. Phys.* **1970**, *53*, 185-189.
55. Tilly, K. D.; Foster, N. R.; Macnaughton, S. J.; Tomasko, D. L., *Ind. Eng. Chem. Res.* **1994**, *33*, 681-688.
56. Bird, R. B.; Stewart, W. E.; Lightfoot, E. N., *Transport Phenomena*. John Wiley & Sons: New York (USA), **1960**.
57. Pitla, S. S.; Robinson, D. M.; Groll, E. A.; Ramadhyani, S., *HVAC & R Res.* **1998**, *4*, 281-301.

6

Rate Enhancements at High Pressure and Supercritical CO_2 Conditions in a Glass Microreactor

The esterification reaction of phthalic anhydride with methanol was performed in a continuous flow microreactor at pressures up to 110 bar or using supercritical CO_2 as co-solvent. The design is such that supercritical CO_2 can be generated inside the microreactor. Spectacular rate enhancements were obtained, *viz* a 53-fold increase was obtained at 110 bar and 60 °C, while using supercritical CO_2 as co-solvent a 5400-fold increase was obtained, both with respect to batch experiments at 1 bar and at the same temperature.

6.1 Introduction

Microreactors have proven to be a very useful tool to optimize organic reactions, as described in detail in Chapter 2.[1-3]

Supercritical fluids as solvents or reaction media are more and more applied in industrial processes like separations or extractions.[4-7] However, working at supercritical conditions in synthetic chemistry is complicated since elevated pressures are required. Due to its quite easily accessible supercritical conditions, supercritical carbon dioxide (scCO$_2$) has great potential for achieving these goals. In Chapter 5 a first attempt was made for a better understanding of the behavior of liquid mixtures involving CO$_2$ close to their critical point.[8-10]

In this Chapter a new microreactor platform is described for studying pressure chemistry near or under supercritical conditions. The development and performance of this platform is presented. A simple reaction, that was studied before by Ellington *et al.*[11] at scCO$_2$ conditions in a stop flow autoclave, the esterification of phthalic anhydride (**1**) with methanol (**2**) (Scheme 6-1), was chosen to study the effects of pressure as well as scCO$_2$ on the reaction rate. This reaction answers all the requirements imposed by the microreactor. It has fast reaction kinetics, min range, according with the short residence times in the microreactor. Methanol (**2**) is a good solvent for phthalic anhydride (**1**) and product (**3**), avoiding clogs in the channel. Furthermore, the reaction is known to be positively affected by pressure and scCO$_2$.[11]

The unique design of this system is such that supercritical conditions can be generated in the microreactor by controlling both the pressure and the temperature. The microreactor design allows studying the influence of different conditions (p, T) on the reaction rate in an easy and safe way.

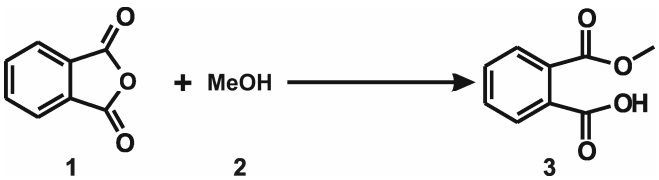

Scheme 6-1: Esterification reaction of phthalic anhydride (**1**) with methanol (**2**) at pressures up to 110 bar and also under scCO$_2$.

In the first part of this Chapter the esterification reaction of phthalic anhydride (**1**) with methanol (**2**) carried out at pressures of 90 and 110 bar in a microreactor in continuous flow mode is discussed. The obtained rate constants are compared with those of the batch experiments at 1, 90 and 110 bar carried out in stop-flow mode. In the second part, *sc*CO_2 is used as a co-solvent for the reaction in the microreactor. The obtained rate constants are compared with those of the microreactor experiments at 90 and 110 bar.

6.2 Results and Discussion

6.2.1 Microreactor layout

The design of the microreactor used for the experiments in this Chapter is slightly different from that of the microreactor presented in Chapter 5. In this case the two reagent channels arrive separately to the heated zone of the microreactor, where they join and mix, (Figure 6-1). In this way, CO_2 can reach its supercritical phase lengthwise the channel (p and T are above p_c and T_c) and mix with the reagents at *sc*CO_2 conditions.

The inlet-side of the microreactor is cooled to 10 °C and the temperature of the reaction zone can be regulated for 20 – 120 °C. For a detailed description of the microreactor fabrication see Chapters 4 and 5.

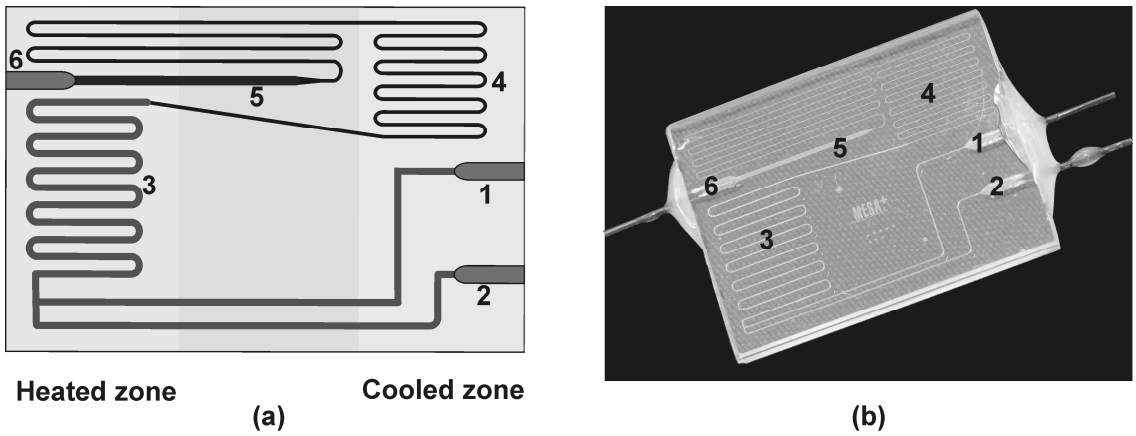

Figure 6-1: Microreactor microreactor: Layout (**a**) and photograph (**b**) (20 × 15 × 2.2 mm). **1** inlet liquid-CO_2, **2** inlet reagents, **3** reaction zone, **4** fluidic resistor, **5** expansion zone, **6** outlet.

6.2.2 Set-ups

Microreactor for working pressures up to 10 bar. The microreactor cannot be operated at atmospheric pressure. The high-resistance channel (**4**) causes that a minimum pressure (~ 2.5 bar) is required to obtain continuous flow in the microreactor, as a consequence of its hydrodynamic resistance. Experiments at pressures up to 10 bar were done using a syringe pump system at fixed flow rates (0.125 and 0.075 μL min^{-1}, Figure 6-2).

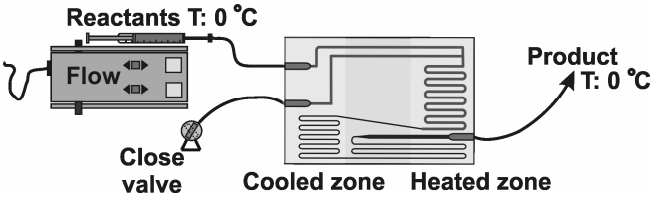

Figure 6-2: Schematic drawing of the set-up for the esterification reaction of phthalic anhydride (**1**) with methanol (**2**) at pressures up to 10 bar.

Microreactor for working pressures of 90 and 110 bar. In Figure 6-3 the set-up for pressures above 70 bar is shown. Pressurized liquid CO_2 and/or the reagents are introduced in the microreactor *via* two inlets (**1, 2**). The pressure experiments were done with valve **9** in closed position, while the experiments using *sc*CO_2 as a co-solvent were performed with valve **9** in open position allowing a 50:50 mixture of methanol and liquid CO_2 in the microreactor.

The reagents are kept in a pressurized loop (**7**) at 0 °C. The pressure is controlled/measured by the pressure sensor of the high pressure pump. The reagents are introduced in the microreactor *via* inlet **1** and valve **8**. Both fluids are heated along the channels and mix and react in the reaction zone (**3**). Subsequently, the mixture enters in a high-resistance channel (**4**) (fluidic resistor). Since this zone has a much smaller cross-section than the channel in the reaction zone, this channel ensures a constant pressure in the reaction zone. The high-resistance channel ends in an expansion zone (**5**) and the combination of these two structures guarantees that the fluid mixture gradually expands towards atmospheric conditions. The expansion zone ends in an outlet (**6**).

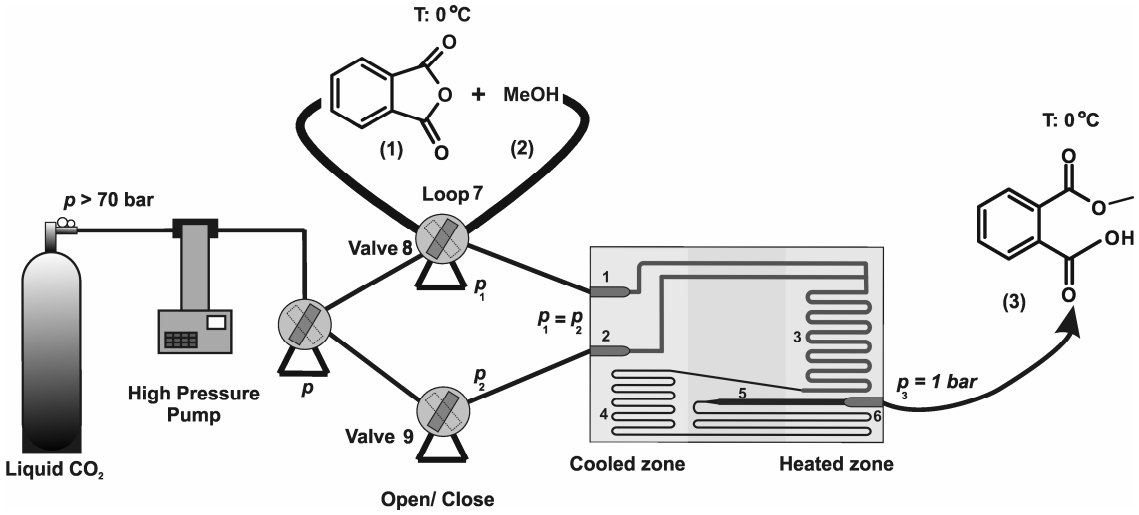

Figure 6-3: Schematic drawing of the set-up for the esterification reaction of phthalic anhydride (**1**) with methanol (**2**) at high pressure and/or *sc*CO_2 conditions (90 and 110 bar). **1** inlet reagents, **2** inlet liquid CO_2, **3** reaction zone, **4** fluidic resistor, **5** expansion zone, **6** outlet, **7** loop that contains the reagents, **8** valve that regulates the access of the reagents to the microreactor and **9** valve that regulates the access of CO_2 to the microreactor.

6.2.3 Batch reaction of phthalic anhydride with methanol

Temperature influence. For comparison, the esterification reaction of phthalic anhydride (**1**) with methanol (**2**) was performed in a 25 mL vessel at 0, 25, 50 and 60 °C at atmospheric pressure. The product formation was monitored by following the intensity of the absorption peak at 229 nm in the UV/Vis spectra. The rate constants (k_{obs}) were calculated using a pseudo-first order kinetic equation (see the Experimental section 6.4.3). The second-order rate constants (k) were calculated by dividing k_{obs} by the methanol concentration at each temperature. The values are summarized in Table 6-I. Analysis of these data using the Arrhenius equation (6-1), gave an activation energy (E_a) of 40.1 kJ mol^{-1} and a pre-exponential factor (A) of 128.7 M^{-1} s^{-1}.

$$k = A \cdot e^{\frac{-E_a}{RT}} \qquad \text{eq. (6-1)}$$

Table 6-I: Rate constants of the esterification reaction of phthalic anhydride (**1**) with methanol (**2**) at different temperatures at atmospheric pressure.

T /°C	k_{obs} /s^{-1} [a]	k /M^{-1} s^{-1} [a]
0	6.20×10^{-5}	2.45×10^{-6}
25	3.60×10^{-4}	1.46×10^{-5}
50	1.09×10^{-3}	4.56×10^{-5}
60	1.34×10^{-3}	5.66×10^{-5}

[a] Mean values from duplicate experiments.

Pressure influence. Using a stainless steel loop as a reaction vessel (Figure 6-4), the same calculation procedure as above was followed to obtain the rate constants at 90 and 110 bar and at 0 °C. The rate constants were 2.43×10^{-6} and 2.43×10^{-6} at 90 and 110 bar, respectively.

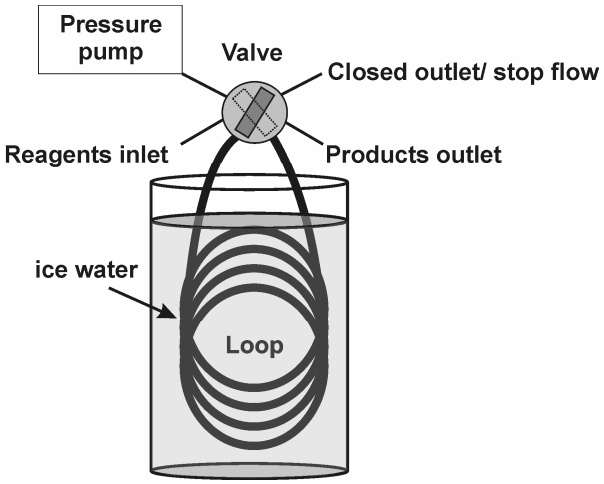

Figure 6-4: Stainless steel loop used for the determination of the rate constants at pressures of 90 and 110 bar.

Based on these data, an activation volume ($\Delta V^{\neq}$) of approximately 0 cm^3 mol^{-1} was calculated. Thus, these experiments show that pressures up to 110 bar do not influence the reaction kinetics of the esterification reaction of phthalic anhydride with methanol at batch reaction.

6.2.4 Esterification reaction at pressures up to 10 bar in a microreactor

In the glass microreactor (see Figure 6-1b) experiments at two different flow rates, 0.075 and 0.125 μL min^{-1} and four temperatures were performed. A certain time (t_{total}) was needed to collect enough sample volume to be analyzed by UV-Vis spectroscopy; t_{total} depends on the applied flow. The reagents and the product were kept at 0 °C during operation of the microreactor since the reaction proceeds only slowly at this temperature (k = 2.45 × 10^{-6} M^{-1} s^{-1}). The rate constants were calculated from equations (6-2) and (6-3) that exclude the product formed outside the microreactor in the syringe and the collecting vessel. Pseudo-first order reaction kinetics were assumed ($C_{methanol} >> C_A$), described by k_{obs}^T, $t_{microreactor}$ is the residence time in the microreactor. The deduction of equation (6-2) is explained in detail in the Appendix of this Chapter.

$$k_{obs}^T \cdot t_{microreactor} = \ln\left(\frac{C_{A\,total}^{0\,°C}}{C_{A\,microreactor}^T}\right) \text{ when } t_{microreactor} << t_{total} \qquad \text{eq. (6-2)}$$

$$k^T = \frac{k_{obs}^T}{C_{methanol}^T} \qquad \text{eq. (6-3)}$$

In equation (6-2), $C_{A\,total}^{0\,°C}$ is the concentration of phthalic anhydride (**1**) after a batch experiment at 0 °C, taking into account t_{total}. $C_{A\,microreactor}^T$ is the concentration of phthalic anhydride (**1**) after an experiment in the microreactor (also includes product formed in the syringe and the collecting vessel) at each temperature (for the same t_{total}).

The rate constants (k) are graphically represented in Figure 6-5. According to the batch experiments, pressure should not influence the rate constants under the conditions used. However, it was found that a pressure of 5-9 bar in the microreactor does already influence the reaction rate.

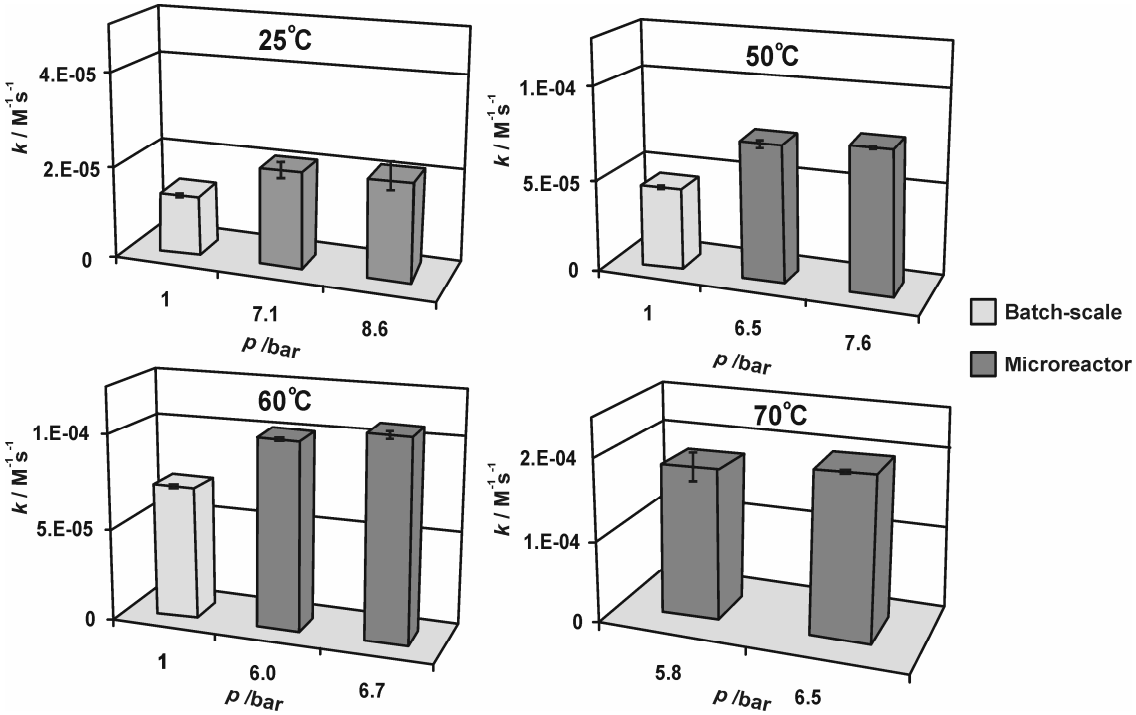

Figure 6-5: Second-order rate constants (*k*), at four temperatures, for the reaction of phthalic anhydride (**1**) with methanol (**2**) performed in the microreactor, at pressures up to 10 bar. The microreactor experiments are compared with the batch experiments carried out at 1 bar. At 70 °C and 1 bar the rate constant cannot be measured, because this temperature is above the boiling point of methanol (Experimental section 6.4.4).

The influence of the microreactor was found over the entire temperature range that was investigated. For instance at 25 °C the ratio in the *k* values between 1 and 7.1 bar is 1.3. This ratio goes to almost 1.9 at higher temperatures (50 and 60 °C). Based on the batch experiments at elevated pressures (section 6.2.3) this is a surprising result since batch experiments showed that even a pressure of 110 bar does not influence the esterification reaction kinetics.

From the experiments in the microreactor at pressures below 10 bar an activation energy (E_a) of 38.8 kJ mol^{-1} and a pre-exponential factor (A) of 142.6 M^{-1} s^{-1} was calculated. Although the E_a value is slightly smaller than that for the batch experiments, it can be assumed that batch and microreactor experiments up to 10 bar have the same E_a (within experimental error). The pre-exponential factor (A) for the reaction up to 10 bar is substantially larger than that at batch experiments.

6.2.5 Esterification reaction at 90 and 110 bar in the microreactor

Experiments in the glass microreactor at pressures of 90 and 110 bar were performed at five temperatures. As for the experiments at pressures up to 10 bar, a certain time (t_{total}) was needed to collect enough sample volume to be analyzed by UV-Vis spectroscopy, t_{total} depends on the applied pressure. The reagents and the product were kept at 0 °C during operation of the microreactor. The rate constants were calculated with equations (6-2) and (6-3) that exclude the product formed outside the microreactor, *e.g.* in the loop (**7**) and the collecting vessel.

The rate constants (k) for the experiments in the microreactor at 90 and 110 bar are shown in Table 6-II. A pressure increase of 20 bar yields a 2.2-fold increase of the rate constants (k_{110}/k_{90}). In section 6.2.4 it was already shown that the use of a microreactor for this esterification reaction enhances the rate constants, even at low pressures. The ratio $k_{microreactor}/k_{batch}$ at 90 and 110 bar is exceptionally large, *viz.* 17 and 32, respectively, at 20 °C. This $k_{microreactor}/k_{batch}$ ratio increases when the temperature is increased.

The calculated activation energies (E_a) are 34.6 and 33.9 kJ mol^{-1} and the pre-exponential factors (A) are 468.7 and 690.9 M^{-1} s^{-1} at 90 and 110 bar, respectively.

Table 6-II: Rate constants for the esterification reaction of phthalic anhydride (**1**) with methanol (**2**) at five temperatures and at 90 and 110 bar (microreactor experiments).

T /°C	k /M^{-1} s^{-1} (90 bar) [a]	k /M^{-1} s^{-1} (110 bar) [a]
20	3.5×10^{-4}	6.7×10^{-4}
40	7.6×10^{-4}	1.4×10^{-4}
60	1.6×10^{-3}	3.1×10^{-3}
80	3.5×10^{-3}	6.4×10^{-3}
100	7.5×10^{-3}	1.3×10^{-2}

[a] Mean values from duplicate experiments (Experimental section 6.4.5)

6.2.6 Influence of the microreactor on the esterification reaction

At pressures up to 10 bar the activation energy (E_a) is similar to that of batch experiment (Figure 6-6 and Table 6-III). For this reason, the increase of the rate constants when the reaction is carried out in the microreactor will be due to the increase of the pre-exponential factor (A). Theoretically, the A factor is associated with a steric factor (f) that includes the local properties of the reaction, the required orientations of the species and the details of how close they have to come to one another in order to react and the collision rate (Z_{AB}), which is called encounter rate in solution.[12] In the *collision theory*[13] for gases, Z_{AB} is defined as the frequency of encounters between molecules (entropy) and the probability that these encounters result in a reaction.[14] In general, when pressure increases, molecules get closer to one another, thereby increasing the number of encounters, resulting in an increase of the pre-exponential factor (A) and thus increase in the rate constants.[12,15]

The collision theory[13] for gases is used here as an indication of which parameters may affect the esterification reaction carried out in solution in the microreactor. The continuous flow in the microreactor, as well as pressure, provides experimental conditions that positively influence the encounter rate between molecules (Z_{AB}) and the steric factor (f) thus, the rate constant of the reaction. Equation (6-4) shows that Z_{AB} is proportional to the diameter of the molecules ($d = 1/2 \cdot (d_A + d_B)$) and its velocity $\langle u \rangle = (8kT/\pi\mu)^{1/2}$ in which $\mu = m_A m_B/(m_A + m_B)$, calculated using the Maxwell distribution, but inversely proportional to the volume of the system (V).[14,16,17]

$$Z_{AB} = \pi d^2 \langle u \rangle \cdot \left(\frac{N_A N_B}{V^2} \right) \qquad \text{eq. (6-4)}$$

The increase in the A factor and thus the rate constants, is mainly caused by the quite high flow rate of the fluid and the very small microreactor volume. Burns *et al.*[18] studied the influence of flow velocity on the reaction rate of the nitration of benzene in microdevices, *e.g.* 2.0, 4.1 and 8.6 min^{-1} for 2.0, 7.7 and 18.5 cm s^{-1} flow velocity respectively. They observed an increase of the rate constant when the flow speed was increased. In this study it was assumed that improved mixing at higher

flow velocities results in an increase in mass transfer, which has the strongest influence in the region with the fastest kinetics.

It is known that at high flow velocities, the formation of a longer Taylor cone[19,20] can also result in better mixing. For increased flow rates, the length of the cone increases, resulting in higher concentration gradients, thereby enhancing the diffusive mixing of species, leading to larger rate constants.[21]

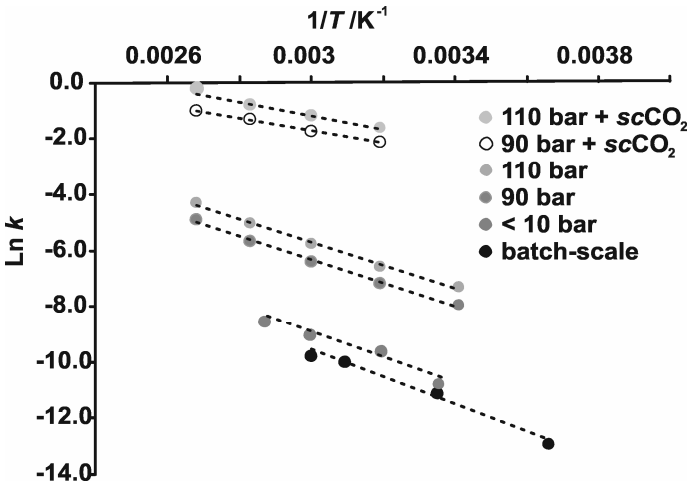

Figure 6-6: Ln*k* values *vs.* 1/*T* plot for the activation energy calculation for all the experiments carried out in the microreactor and at batch.

When higher pressures are applied, the activation energy (E_a) is lower than in the batch reactions; this difference in E_a is more pronounced at higher pressures (Figure 6-6 and Table 6-III). A possible catalytic process occurring at the sidewalls of the microreactor could be the reason for the decrease in the activation energy. The glass material of the microreactor, *i.e.* silanol groups, may play a role, since the esterification reaction is acid-catalyzed. This catalytic property of the channel walls of glass microreactors has been shown before by Brivio *et al.*[22] and similar effects have also been demonstrated using silica particles as catalysts.[23-26] However, this effect was not observed for the experiments carried out at pressures up to 10 bar, which have the same E_a values as at batch reactions, section 6.2.4. At higher pressures (90 and 110 bar) the catalytic effect is visible, based on the decrease in the E_a values at these pressures with respect to those at 1 and 10 bar. The rate acceleration at higher pressures might also be attributed, based on the *collision theory*[13] for gases, to the substantial increase of the averaged encounter rate with the walls (Z_W), equation (6-5):

$$Z_w \propto \frac{N}{V} \cdot \langle u \rangle \cdot \theta \qquad \text{eq. (6-5)}$$

In equation 6-5 the encounter rate Z_W should increase for small volumes (V), high speed of molecules $\langle u \rangle$ or very high surface area (θ).[16,17]

It seems that in the microreactor the combination of pressure and catalytic channel walls induces a synergetic effect. The number of encounters (Z_W) of the reagents with the channel wall increases at high pressures, partially due to the high flow speed and the high surface-to-volume ratio of the microreactor (θ/V). So, since E_a decreases, the rate constants are much higher than in batch reactions and/or pressures up to 10 bar.

Table 6-III: Activation energies (E_a) and pre-exponential factors (A).

Experiment	E_a /kJ mol^{-1}	A /M^{-1} s^{-1}
Batch	40.1	128.1
Microreactor < 10 bar	38.8	142.6
Microreactor 90 bar	34.6	468.7
Microreactor 110 bar	33.9	690.9
Microreactor 90 bar + *sc*CO_2	18.0	120.1
Microreactor 110 bar + *sc*CO_2	19.9	411.6

Clearly, the results of this study show that glass microreactors in continuous flow mode operated at elevated pressure conditions give rise to significant rate enhancements. Higher yields and lower reaction times have previously also been observed by Hessel *et al.*[27] for the Kolbe-Schmitt reaction carried out in a metallic "miniaturized system" (millimeter scale) operated in continuous flow mode and at pressures up to 74 bar, although no explanations were given for the increases. Here it is shown that in a continuous flow glass microreactor, the rate enhancements may be explained by a possible catalytic effect of the wall surface, observed by an activation energy (E_a) decrease and by the high flow velocity and the elevated pressures that enhance the diffusive mixing of species and thus increase the pre-exponential factor (A).

6.2.7 Esterification reaction in a microreactor using $scCO_2$

Experiments using *sc* CO_2 as a co-solvent (CO_2 mol fraction 0.45) were carried out in the microreactor. The methanol concentration, $C_{Methanol}$, is about half of the concentration of the experiments done at different pressures and temperatures, using only methanol as a solvent.

Based on literature, it is known that the density of this mixture is similar to that of pure methanol.[28,29] For instance, at 100 °C/91 bar a 50/50 v/v mixture has a density of 0.718 g mL^{-1} and under these conditions the density of pure methanol is 0.72 g mL^{-1}. Tilly *et al.* published viscosity correlations for binary mixtures of CO_2 and methanol (< 5%).[30] By extrapolation, it is possible to make an estimation of the viscosity values of our experimental mixture at different temperatures (Table 6-IV). The well-known Poiseuille equation (6-6) was used for the calculation of the flows in the microreactor for all conditions (p,T). The obtained flows are in the same range as the flows shown on the display of the high pressure syringe pump. Finally, the $t_{microreactor}$ was calculated.

$$Flow = V/t = \frac{\pi r^4}{8\eta} \cdot \frac{(p_1 - p_2)}{l} \qquad \text{eq. (6-6)}$$

In this equation r is the channel radius, l the channel length and η is the fluid viscosity.

Table 6-IV: Viscosity values, estimated from reference 30, for a methanol/scCO_2 mixture with 55% methanol; flow and reaction time of the microreactor at 90 and 110 bar.

T /°C	90 bar			110 bar		
	Viscosity /Pa s	Flow /μL min^{-1}	$t_{microreactor}$ /s	Viscosity /Pa s	Flow /μL min^{-1}	$t_{microreactor}$ /s
40	1.63×10^{-4}	49.5	0.39	1.81×10^{-4}	54.6	0.35
60	1.61×10^{-4}	50.1	0.38	1.79×10^{-4}	55.2	0.35
80	1.59×10^{-4}	50.7	0.38	1.77×10^{-4}	55.8	0.34
10	1.57×10^{-4}	51.4	0.37	1.75×10^{-4}	56.4	0.34

The reagent solution is introduced *via* inlet **1** and liquid CO_2 *via* inlet **2** (Figure 6-3). The fluids come together in the reaction zone of the microreactor (**3**), where the conditions (p, T) are sufficiently high for generating *sc*CO_2. This concept

differs from Kobayashi's studies where *sc*CO_2 as such was introduced in a micro-reactor.[31] Here, an on-chip phase transition of CO_2 was used to generate *sc*CO_2. Table 6-V shows the rate constants at different temperatures.

Due to the low viscosity of the methanol/*sc*CO_2 mixture, the flow rates in the microreactor are very high at pressures of 90 and 110 bar. The residence time, $t_{microreactor}$, is approximately 0.35 s for all experimental conditions.

For example, the rate constants are 160 and 300 times higher than those of the experiments described in Table 6-II at 90 and 110 bar and at 40 °C, respectively. This difference decreases at higher temperatures. However, it is evident that by using *sc* CO_2 in the microreactor the highest reaction rates are obtained. This effect can be attributed to the unique properties of *sc*CO_2. Close to its critical conditions CO_2 was proven to have a positive effect on the cluster formation between phthalic anhydride (**1**) and methanol (**2**) molecules[11,32] resulting in localized regions of high densities and high concentrations of the reactants which can serve as microscopic pockets for reaction which leads to higher reaction rates.[33-35]

Table 6-V: Second-order rate constants *k*, at four temperatures for the reaction of phthalic anhydride (**1**) with methanol (**2**) performed in the microreactor using *sc*CO_2 as a co-solvent.

T /°C	*k* /M^{-1} s^{-1} (90 bar) [a]	*k* /M^{-1} s^{-1} (110 bar) [a]
40	1.2×10^{-1}	2.0×10^{-1}
60	1.8×10^{-1}	3.1×10^{-1}
80	2.7×10^{-1}	4.6×10^{-1}
100	3.6×10^{-1}	6.9×10^{-1}

[a] Mean values from duplicate experiments.

The calculated activation energies (E_a) are 18.0 and 19.9 kJ mol^{-1} and the pre-exponential factors (A) 120.1 and 411.6 M^{-1} s^{-1} at 90 and 110 bar, respectively (Figure 6-6 and Table 6-III). Similar to what happened in the experiments at 90 and 110 bar without *sc*CO_2, the pre-exponential factor significantly increases from 128.1 M^{-1} s^{-1} at batch experiments to 411.6 M^{-1} s^{-1} at 110 bar, thereby positively affecting the rate constants. Nevertheless, when *sc*CO_2 is used as co-solvent, the influence of E_a on the *k* values is dominant.

The same arguments used for explaining the *k* values at high pressure in the microreactor can be applied for the *sc*CO_2 experiments. In addition, the low E_a values suggest that *sc*CO_2 as reaction medium might result in a change of the reaction mechanism, where CO_2 is actively involved as a solvent or even playing a role in the reaction itself, although it is not clear how. This influence on (catalyzed) reactions at supercritical conditions and continuous flow operation, in autoclaves, has been recently reviewed.[23]

6.3 Conclusions and Outlook

In this Chapter the first example of a glass-based microreactor platform is described for studying the influence of pressure as well as *sc* CO_2 on the rate constants of the esterification reaction of phthalic anhydride with methanol. The results of this study show that microreactors in continuous flow mode combined with pressure operation give rise to significant rate enhancements for this specific reaction when compared to conventional conditions. Since temperature and pressure can be regulated and their influence on continuous flow reactions can be observed easily, microreactors have a great potential for performing high pressures reactions.

At high pressures the rate constant enhancement is mainly caused by the high velocity flow and the elevated pressures that enhance the diffusive mixing of species, increasing the pre-exponential factor (*A*). The unique properties of *sc*CO_2 in the high pressure microreactor substantially decrease the activation energy of the reaction, probably caused by a change in the reaction mechanism, thereby increasing the rate constants.

Implementation of high-pressure reactions in microreactors offers important advantages in terms of safety and therefore makes high pressure research more easily accessible. Further improvement of the system could be the incorporation of on-line analysis such as UV-Vis,[36] Nuclear Magnetic Resonance spectroscopy,[37] and/or (confocal) Raman microscopy.[38]

6.4 Experimental

6.4.1 Materials

Methanol was purchased from Fisher Scientific, analytical reagent grade (< 0.015% water). The solvent was dried with 3 Å molecular sieves beads. Phthalic anhydride (≥ 99.0%) was bought from Sigma-Aldrich. CO_2 was obtained from Hoek Loos (2.7) with a purity ≥ 99.7% and < 150 ppm of water.

The complete set-up for the microreactor experiments used in this Chapter is basically the same as that in Chapter 5. UV-Vis spectra were measured on a Varian Cary 3E UV-spectrophotometer in 100 μm cuvettes (8 μL).

The experiments at pressures up to 10 bar were performed using a Microdialysis CMA/102, (type 8713) syringe pump flow rate 0.1-20 $\mu L \cdot min^{-1}$ for 1 mL syringes, with Hamilton syringes of 250 μL. The experiments at pressures of 90 and 110 bar were done using a high pressure syringe pump (model 100DM; Teledyne Isco, Inc. Lincoln, USA).

6.4.2 Set-up calibration: residence time calculation

Microreactor working at pressures up to 10 bar. The pressure gradient over the microreactor varies with the (applied) temperature. Since the flow through the microreactor is constant (using a syringe pump at a fixed flow rate), the residence time ($t_{microreactor}$) in the microreactor is constant, but the pressure in the reaction zone of the microreactor (**3**) depends on the temperature. In Table 6-VI, the calculated pressures in the microreactor at different temperatures are shown. The residence times in the microreactor are 256 and 154 s for 0.075 and 0.125 μL min^{-1} flows, respectively. The microreactor volume is 0.32 μL.

Table 6-VI: Calculated pressures in the reaction zone (**3**) of the microreactor for flows of 0.075 and 0.125 μL min^{-1} at different temperatures.

T /°C	p /bar (Flow: 0.075 μL min^{-1})	p /bar (Flow: 0.125 μL min^{-1})
25	7.1	8.6
50	6.5	7.6
60	6.0	6.7
70	5.8	6.5

Microreactor working at pressures of 90 and 110 bar. During the pressure experiments, a constant pressure (90 or 110 bar) was applied with the high pressure syringe pump. The residence time in the microreactor ($t_{microreactor}$) for each experiment was calculated using equation (6-7):

$$t_{microreactor\ x\ °C,\ p} = \frac{V_{microreactor}}{Flow_{x\ °C,\ p}} \qquad \text{eq. (6-7)}$$

where the flow varies with pressure and temperature. The microreactor volume is 0.32 μL.

The flow is determined for each condition (*p*, *T*). An example at 20 °C and pure methanol as solvent is shown in Figure 6-7. The data are the average of three experiments using different microreactors (max. error < 1.3%).

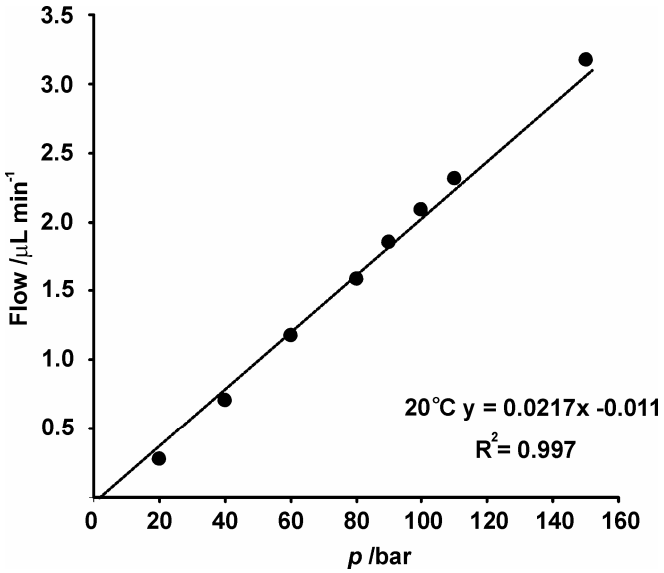

Figure 6-7: Relation between the applied pressure and the flow for the calculation of the residence time in the microreactor at 20 °C.

Since the microreactor is operated in a continuous flow mode, the $t_{microreactor}$ depends on the pressure applied in the microreactor (*p*) and, *via* the viscosity, on the temperature (*T*). At 40 °C and a pressure of 6.5 bar, the residence time is around 4 min, while it is only 11.4 s for a pressure of 110 bar. Due to the fact that the viscosity of the solvent depends on the temperature, the residence time decreases about 16 s (at a pressure of 90 bar) when the temperature is raised from 20 to 100 °C. The $t_{microreactor}$ was calculated for each pressure and temperature and *via* a calibration curve of the applied pressure *vs*. flow, Figure 6-8.

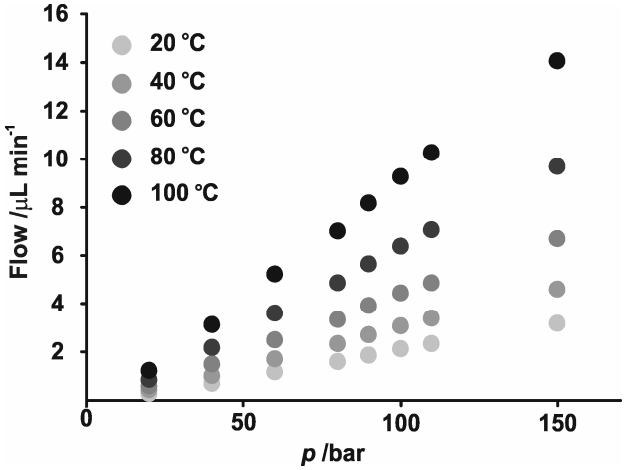

Figure 6-8: Relation between applied pressure and flow for the calculation of the residence time in the microreactor at various conditions (*p*, *T*). Data points are mean values from triplicate experiments using different microreactors (flow error 0.05 µL min^{-1}).

In Table 6-VII the residence times in the microreactor at two different pressures (90 and 110 bar) and five temperatures are shown. These values are calculated using the microreactor volume and the flows obtained experimentally for each pressure and temperature using the microreactor shown in Figure 6-1 (b).

Table 6-VII: Reaction time in the microreactor at 90 and 110 bar at different temperatures.

Temperature /°C	$t_{microreactor}$ /s (*p:* 90 bar)	$t_{microreactor}$ /s (*p:* 110 bar)
20	20.8	16.6
40	14.3	11.4
60	9.9	7.9
80	6.8	5.4
100	4.7	3.8

6.4.3 Batch reaction at pressures of 1, 90 and 110 bar

During the batch experiments at 1 bar, 25 mL of methanol (**2**) was heated at the desired temperature in a vessel and then 37 mg of phthalic anhydride (**1**) was added and stirred strongly. An UV/Vis spectrum of the solution was recorded every 30 s. At t = 0 s the phthalic anhydride concentration is 0.0098 M (< 0.5% error).

The methanol concentration varies with temperature. The experimental pressure used in this Chapter does not affect the methanol concentration. The rate constants, k, were calculated

using the corrected methanol concentration. The observed pseudo first-order rate constants (k_{obs}) were calculated using equation (6-8).

$$(A - A_0) = (A_\infty - A_0) \cdot [1 - \exp(-k_{obs} \cdot t)] \qquad \text{eq. (6-8)}$$

During the batch experiments at 90 and 110 bar and at 0 °C, the esterification reaction was performed in a stainless steel looping (Figure 6-4) with an inner diameter of 500 μm and a volume of 500 μL. A 0.01M phthalic (**1**) anhydride cool solution in methanol (**2**) is introduced in the loop. UV/Vis spectra are recorded every 1 min for 2 h. The rate constants were calculated using equation (6-8) as well.

6.4.4 Esterification reaction in a microreactor at pressures up to 10 bar

A vessel containing methanol (**2**) (25 mL) was placed in a Dewar flask filled with dry CO_2 (-79 °C) and after three minutes (time enough to cool the methanol down) 37 mg of phthalic anhydride (**1**) was added. The solution was sonicated 30 s to be sure that (**1**) was dissolved. A UV/Vis spectrum was recorded to ensure that the initial concentration of **1** is 0.01M. The reaction is quenched by the temperature of the dry CO_2.

During these pressure experiments, the flow was kept constant with a syringe pump at 0.075 and 0.125 μL/min. The pressure was induced *via* the fluidic resistor of the microreactor. The temperature was regulated by heaters and Peltier elements, which are controlled by temperature sensors. In Table 6-VIII, the calculated experimental error and the values of $Ln\left(\frac{C^{0\ °C}_{A\ total}}{C^{T}_{A\ microreactor}}\right)$ are shown for both flows.

Table 6-VIII: Logarithm of the difference in concentrations between the experiment at batch (0 °C) and the same experiment using the microreactor, for the esterification reaction of phthalic anhydride (**1**) in methanol (**2**) at pressures up to 10 bar.

T /°C	$Ln\left(\frac{C^{0\ °C}_{A\ total}}{C^{T}_{A\ microreactor}}\right)$ Flow: 0.075 μL min^{-1}				
	1	2	3	Average	Error /%
25	0.120	0.119	---	0.120	4.5
50	0.417	0.411	0.417	0.412	1.6
60	0.616	0.618	0.610	0.618	0.3
70	1.028	0.988	---	1.092	5.1

T /°C	$Ln\left(\frac{C_{A\,total}^{0\,°C}}{C_{A\,microreactor}^{T}}\right)$ Flow: 0.125 µL min^{-1}				
	1	2	3	Average	Error /%
25	0.079	0.073	---	0.076	5.1
50	0.252	0.251	0.252	0.252	0.3
60	0.382	0.392	---	0.387	1.7
70	0.649	0.642	0.653	0.648	0.9

6.4.5 Esterification reaction in a microreactor at pressures of 90 and 110 bar

A 0.01 M phthalic anhydride solution in methanol was introduced in the loop (**7**) (Figure 6-3) kept at 0 °C. The solution was injected into the microreactor at the desired pressure when open valve (**8**). The microreactor was heated at the desired temperature of the experiment using the Peltier elements. The product was collected in a small vessel maintained at 0 °C at the microreactor outlet. In Table 6-IX, the calculated experimental error and the values of $Ln\left(\frac{C_{A\,total}^{0\,°C}}{C_{A\,microreactor}^{T}}\right)$ are shown for both pressures.

Table 6-IX: Logarithm of the difference in concentrations between the experiment at batch (0 °C) and the same experiment but using the microreactor, for the esterification reaction of phthalic anhydride (**1**) in methanol (**2**) at pressures of 90 and 110 bar.

T /°C	$Ln\left(\frac{C_{A\,total}^{0\,°C}}{C_{A\,microreactor}^{T}}\right)$ Pressure: 90 bar			
	1	2	Average	Error /%
20	0.183	0.181	0.182	0.6
40	0.265	0.261	0.263	1.1
60	0.378	0.378	0.378	0.1
80	0.546	0.543	0.545	0.4
100	0.795	0.784	0.789	1.0

T /°C	$Ln\left(\frac{C^{0\ °C}_{A\ total}}{C^{T}_{A\ microreactor}}\right)$ Pressure: 110 bar			
	1	2	Average	Error /%
20	0.276	0.278	0.277	0.7
40	0.402	0.380	0.391	4.0
60	0.572	--		
80	0.800	--		
100	1.126	--		

6.4.6 Esterification reaction in a microreactor using $scCO_2$

The experimental procedure was the same as in section 6.4.5 except for maintaining the valve **9** opened (Figure 6-3). This valve ensured that CO_2 was introduced in the microreactor *via* inlet (**2**) at the desired pressure. In Table 6-X, the calculated experimental error and the values of $Ln\left(\frac{C^{0\ °C}_{A\ total}}{C^{T}_{A\ microreactor}}\right)$ are shown for both pressures.

Table 6-X: Logarithm of the difference in concentrations between the experiment at batch (0 °C) and the same experiment but using the microreactor, for the esterification reaction of phthalic anhydride (**1**) in methanol (**2**) at pressures of 90 and 110 bar and using *sc*CO_2 as a co-solvent.

T /°C	$Ln\left(\frac{C^{0\ °C}_{A\ total}}{C^{T}_{A\ microreactor}}\right)$ Pressure: 90 bar			
	1	2	Average	Error /%
40	0.567	0.572	0.569	0.6
60	0.819	0.800	0.809	1.7
80	1.173	1.220	1.197	2.8
100	1.542	1.629	1.585	3.9

T /°C	$Ln\left(\frac{C_{A\ total}^{0\ °C}}{C_{A\ microreactor}^{T}}\right)$ Pressure: 110 bar			
	1	2	Average	Error /%
40	0.856	0.834	0.845	1.9
60	1.227	1.300	1.263	4.1
80	1.803	1.800	1.802	0.1
100	2.623	2.620	2.622	0.1

6.5 References

1. Brivio, M.; Verboom, W.; Reinhoudt, D. N., *Lab Chip* **2006**, *6*, 329-344.
2. Ehrfeld, W.; Hessel, V.; Löwe, H., *Microreactors: New Technology for Modern Chemistry*. Wiley-VCH: Weinheim (Germany), **2000**.
3. Jensen, K. F., *AIChE J.* **1999**, *45*, 2051-2054.
4. DeSimone, J. M.; Tumas, W., *Green Chemistry Using Liquid and Supercritical Carbon Dioxide*. Oxford university press: New York (USA), **2003**.
5. Hauthal, W. H., *Chemosphere* **2001**, *43*, 123-135.
6. Van Eldik, R.; Klärner, F. G., *High Pressure Chemistry*. Wiley-VCH: Weinheim (Germany), **2002**.
7. Noyori, R., *Chem. Rev.* **1999**, *99*, 353-354.
8. Giddings, J. M.; Myers, M. N.; McLaren, L.; Keller, R. A., *Science* **1968**, *162*, 67-73.
9. Angus, S.; Armstrong, B.; De Reuck, K. M., *Carbon Dioxide (on the Basis of Surveys and Equations Produced by V. V. Altunin)*. Oxford University Press: New York (USA), **1976**.
10. Beckman, E. J., *J. Supercrit. Fluids* **2004**, *28*, 121-191.
11. Ellington, J. B.; Park, K. M.; Brennecke, J. F., *Ind. Eng. Chem. Res.* **1994**, *33*, 965-974.
12. Atkins, P. W., *Physical Chemistry, 2nd Edition*. Oxford University Press: Oxford (UK), **1982**; p 859-1041.
13. McNaught, A. D.; Wilkinson, A., *IUAPC (Gold Book) Compendium of Chemical Terminology, 2nd Edition*. Blackwell Science: Cambridge (UK), **1997**.
14. Levenspiel, O., *Chemical Reaction Engeneering*. John Wiley and Sons, Inc.: New York (USA), **1976**; p 23-24.
15. Levine, N. I., *Physical Chemistry (4th Ed.)*. McGraw-Hill, Inc.: New York (USA), **1995**.

16. Child, M. S., *Molecular Collision Theory*. Academic Press: London and New York (UK and USA), **1974**.
17. Meyers, R. A., *Encyclopedia of Physical Science and Technology*. Academic Press: London (UK), **2001**.
18. Burns, J. R.; Ramshaw, C., *Chem. Eng. Res. Des.* **1999**, *77*, 206-211.
19. Taylor, G., *Proc. R. Soc. London, A* **1953**, *219*, 186-203.
20. Taylor, G., *Proc. R. Soc. London, A* **1954**, *225*, 473-477.
21. Bühler, B.; Fröhlich, D.; Haake, H. M.; Brecht, A.; Gauglitz, G., *TrAC, Trends Anal. Chem.* **2001**, *20*, 186-194.
22. Brivio, M.; Oosterbroek, R. E.; Verboom, W.; Goedbloed, M. H.; Van den Berg, A.; Reinhoudt, D. N., *Chem. Commun.* **2003**, 1924-1925.
23. Hamminga, G. M.; Mul, G.; Moulijn, J. A., *Catal. Lett.* **2006**, *109*, 199-206.
24. Deng, Q.; Wilkie, C. A.; Moore, R. B.; Mauritz, K. A., *Polymer* **1998**, *39*, 5961-5972.
25. Pelmenschikov, A. G.; Morosi, G.; Gamba, A.; Zecchina, A.; Bordiga, S.; Paukshtis, E. A., *J. Phys. Chem.* **1993**, *97*, 11979-11986.
26. Natal-Santiago, M. A.; Dumesic, J. A., *J. Catal.* **1998**, *175*, 252-268.
27. Hessel, V.; Hofmann, C.; Lob, P.; Lohndorf, J.; Lowe, H.; Ziogas, A., *Org. Process Res. & Dev.* **2005**, *9*, 479-489.
28. Smith Jr., R. L.; Lee, S. B.; Suzuki, S.; Saito, C.; Inomata, H.; Arai, K., *J. Chem. Eng. Data* **2002**, *47*, 608-612.
29. Brunner, E.; Hültenschidt, W.; Schlichthärle, G., *J. Chem. Thermodynamics* **1987**, *19* 273-291.
30. Tilly, K. D.; Foster, N. R.; Macnaughton, S. J.; Tomasko, D. L., *Ind. Eng. Chem. Res.* **1994**, *33*, 681-688.
31. Kobayashi, J.; Mori, Y.; Kobayashi, S., *Chem. Commun.* **2005**, 2567-2568.
32. Ellington, J. B.; Brennecke, J. F., *J. Chem. Soc. Chem. Commun.* **1993**, 1094-1095.
33. Mantell, C.; Rodriguez, M.; De la Ossa, E. M., *J. Supercrit. Fluids* **2003**, *25*, 57-68.
34. Ferrieri, R. A.; Garcia, I.; Fowler, J. S.; Wolf, A. P., *Nucl. Med. Biol.* **1999**, *26*, 443-454.
35. Bai, S.; Taylor, C. M. V.; Liu, F.; Mayne, C. L.; Pugmire, R. J.; Grant, D. M., *J. Phys. Chem. B* **1997**, *101*, 2923-2928.
36. Schulze, P.; Ludwig, M.; Kohler, F.; Belder, D., *Anal. Chem.* **2005**, *77*, 1325-1329.
37. Wensink, H.; Benito-Lopez, F.; Hermes, D. C.; Verboom, W.; Gardeniers, J. G. E.; Reinhoudt, D. N.; Van den Berg, A., *Lab Chip* **2005**, *5*, 280-284.
38. Kazarian, S. G.; Chan, K. L. A., *Analyst* **2003**, *128*, 499-503.

Appendix

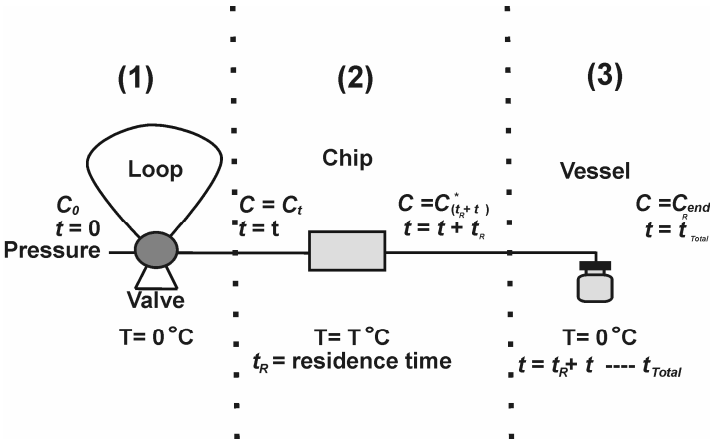

Figure 6-9: Scheme of the set-up used for the equation calculation.

The system is divided in three parts (Figure 6-9):

- Loop (**1**), where the reagents are stored before introducing them in the microreactor, the temperature is 0 °C.
- Microreactor (**2**), where the reaction mostly takes place. This part of the set-up is where the temperature is varied for each experiment (20-100 °C).
- Vessel (**3**), the collector vessel at 0 °C.

At $t = 0$:

Loop: t = 0: C = C_0

Microreactor: $t = 0$: C = C_0

$t = t_R$: C= $C^*(t_R)$

$$\boxed{Ln\left(C^*_{(t+t_{Total})} \Big/ C_t\right) = -k^T(t_R)}$$

Vessel: $$Ln\left(C_{end}(t_{Total}) \Big/ C^*_{(t_R)}\right) = -k°(t_{Total} - t_R) \qquad \text{eq. (1)}$$

At $t = t$

Loop: $$Ln\left(C_t \Big/ C_0\right) = -k° \cdot t \text{ where } C_t = C_0 \cdot Exp(-k° \cdot t)$$

Microreactor: $t = t$: C= C_t

$t = t + t_R$: C= $C^*(t + t_R)$

Vessel: $$Ln\left(C_{end}(t_{Total}) \Big/ C^*(t + t_R)\right) = -k°(t_{Total} - t - t_R)$$

The system is working in continuous flow mode. The total amount converted is:

$$V(C_0\text{-}C_{end})$$

$$FR \cdot t_{Total} = V$$

Amount converted at 0 °C: $\int_0^V (C_0 - C_t)dV = \int_0^{t_{Total}-t_R} C_0 \cdot (1 - Exp(-k^\circ \cdot t)) \cdot FRdt$ eq. (2)

a volume element dV exists in loop at $t = t$.

$$C(t) = C_0 \exp(-k^\circ \cdot t) \quad \text{eq. (3)}$$

$$C^*(t + t_R) = C(t) \cdot Exp(-k^T \cdot t_R) \quad \text{eq. (4)}$$

From equation (1) it is possible to calculate the $C_{end}(t_{Total})$:

$$C_{end}(t_{Total}) = C^*(t + t_R) \cdot Exp(-k^\circ \cdot (t_{Total} - t - t_R) \quad \text{eq. (5)}$$

using eq.(3) and (4)

$$C_{end}(t_{Total}) = C_0 \exp(-k^\circ \cdot t) \cdot Exp(-k^T \cdot t_R) \cdot Exp(-k^\circ \cdot (t_{Total} - t - t_R) =$$

$$C_0 \exp(-k^\circ \cdot (t_{Total} - t_R) - k^T \cdot t_R) \quad \text{eq. (6)}$$

Vessel: is empty at the beginning but it is filled with the applied flow.

At $t^* = 0$:

$$C_{in}^o = C_0 \cdot Exp(-k^T \cdot t_R)$$

V°=0

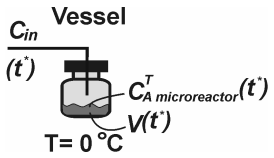

At $t^* = t^*$

$$C_{in}(t^*) = C_0 \cdot Exp(-k^\circ \cdot t^*) \cdot Exp(-k^T \cdot t_R) \quad \text{eq. (7)}$$

$$\left.\begin{aligned} V(t^*) &= FR \cdot t^* \\ C^T_{A\ microreactor}(t^*) & \end{aligned}\right\} \quad \text{eq. (8)}$$

$$n(mol): \quad n(t^*) = V(t^*) \cdot C^T_{A\ microreactor}(t^*)$$

At $t^* = t^* + dt^*$

$$C_{in}(t^* + dt^*) = C_0 \cdot Exp(-k^\circ \cdot (t^* + dt^*) \cdot Exp(-k^T \cdot t_R) \approx C_0 \cdot Exp(-k^\circ \cdot t^*) \cdot Exp(-k^T \cdot t_R)$$

$$dV = FR \cdot dt^*$$

$$n(t^* + dt^*) = n(t^*) + dn$$

The value of dn depends on the flow but also on the batch reaction that is taking place in the vessel: $dn = dn_1(flow) + dn_2(reaction)$ eq. (9)

$$dn_1 = C_{in}(t^*)dV = C_{in}(t^*) \cdot FR \cdot dt^*$$

$$dn_2 = V(t^*)dC^T_{A\ microreactor}(t^*) = V(t^*) \cdot C^T_{A\ microreactor}(t^*) \cdot dExp(-k^\circ \cdot t^*) =$$

$$-V(t^*) \cdot C^T_{A\ microreactor}(t^*) \cdot k^\circ \cdot dt^* = -k^\circ \cdot n(t^*) \cdot dt^*$$

Where $C^T_{A\ microreactor}(t^*)$ is the concentration of **A** in the microreactor.

$$dn = dn_1 + dn_2 = C_{in}(t^*) \cdot FRdt^* - k^\circ \cdot n(t^*)d(t^*)$$

$$\frac{dn}{dt*} = C_{in}(t*)\mathrm{FR} - k^{\circ} \cdot n(t*) \qquad \text{eq. (10)}$$

From equation (7) the equation (10) becomes:

$$\frac{dn}{dt*} = C_0 Exp(-k^{\circ} \cdot t*) \cdot Exp(-k^T \cdot t_R) = A \cdot Exp(-a \cdot t*) - B \cdot n(t*)$$

where $a = B = k^{\circ}$ and $A = C_0 \cdot Exp(-k^T \cdot t_R) \cdot FR$

So equation (8) is now:

$$n(t*) = A \cdot t* \cdot Exp(-k^{\circ} \cdot t*)$$

$$V(t*) = FR \cdot t*$$

$$C^T_{A\ microreactor}(t*) = \frac{A \cdot t* \cdot Exp(-k^{\circ} \cdot t*)}{FR \cdot t*} = C_0 Exp(-k^{\circ} \cdot t*) \cdot Exp(-k^T \cdot t_R)$$

In conclusion at $t = t_{Total}$ and $t^* = t_{Total} - t_R$

$$C^T_{A\ microreactor} = C_0 Exp(-k^{\circ} \cdot (t_{Total} - t_R) \cdot Exp(-k^T \cdot t_R) =$$

$$C_0 Exp(-k^{\circ} \cdot (t_S) \cdot Exp(-k^T \cdot t_R)$$

for $t_S = t_{Total} - t_R$ The comparison with the experiment done at 0 °C which runs til t_S is

$$C^{0\ ^{\circ}C}_{A\ Total} = C_0 \cdot Exp\ (-k^{\circ} \cdot t_S) \qquad Exp(-k^T \cdot t_R) = \frac{C^T_{A\ microreactor}}{C^{0\ ^{\circ}C}_{A\ Total}}$$

$$k^T_{obs} \cdot t_{microreactor} = \ln\left(\frac{C^{0\ ^{\circ}C}_{A\ Total}}{C^T_{A\ microreactor}}\right) \qquad \text{eq. (11)}$$

where $t_{microreactor}$ is the residence time that reagents are in the microreactor. This relation is correct when $t_{\mathrm{microreactor}} << t_{0\ ^{\circ}C}$. Subsequently, the second-order rate constants (k) were calculated by dividing the observed rate constants (k_{obs}) by the methanol concentration (eq. (12)).

$$k^T = \frac{k^T_{obs}}{C^T_{Methanol}} \qquad \text{eq. (12)}$$

7

Influence of Pressure on Diels-Alder Reactions in Glass Microreactors

A microreactor platform that resists pressures up to 150 bar has been constructed and used to study the influence of pressure on the Diels-Alder reaction of cyclopentadiene with methyl-, phenyl- and benzylmaleimides. The reaction of cyclopentadiene with phenylmaleimide and benzylmaleimide showed 1.7-fold and 1.3-fold higher conversions, respectively, compared with batch experiments, while the reaction of cyclopentadiene with methylmaleimide was not accelerated.

7.1 Introduction

Diels-Alder reactions show a large pressure-induced acceleration.[1] The most recent examples of this are summarized by Jenner[2,3] and were discussed in detail in Chapter 2.[4]

Cyclopentadiene (**1**) is extensively used as a dienophile in Diels-Alder reactions, because it provides fast reaction rates and gives rise to high yields.[5] Its reactivity toward maleimides has been studied by several groups. For instance, Meijer *et al.* showed the positive influence of water on the reaction of cyclopentadiene (**1**) with methylmaleimide (**2a**)[6] and Xu *et al.* described the Diels-Alder reaction of **1** with phenylmaleimide (**2b**) in the presence of carbon-bridged (diphenolato)lanthanide complexes as Lewis acids.[7]

In Chapter 3 the influence of pressure on the conversion and the stereoselectivity of the Diels-Alder reaction, carried out in a capillary microreactor, of 2- and 3-furylmethanol with methyl-, benzyl- and phenylmaleimide was described.[8] To our best knowledge, there is only one other example of a Diels-Alder reaction performed in a miniaturized system.[9] A domino reaction, a Knoevenagel condensation reaction of a 1,3-diketone and an aldehyde giving an alkylidene-1,3-dicarbonyl intermediate, which immediately undergoes an intramolecular hetero-Diels–Alder reaction, was carried out in a glass microreactor using pressure driven flow by Fernandez-Suarez *et al.*[9]

In this Chapter, a glass microreactor is used to study the influence of pressure, up to 150 bar, on the Diels-Alder reaction of cyclopentadiene (**1**) with methyl (**2a**), benzyl- (**2b**) and phenylmaleimide (**2c**), (Scheme 7-1).

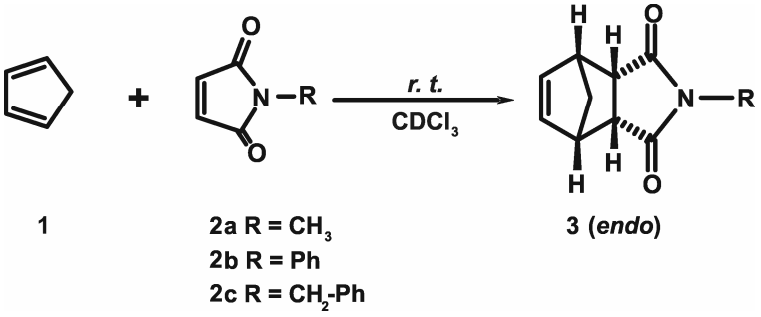

Scheme 7-1: Diels-Alder reaction of cyclopentadiene (**1**) with maleimides (**2a-c**).

7.2 Results and Discussion

7.2.1 Microreactor layout

The design of the microreactor used for the experiments in this Chapter is similar to that described in Chapter 6. The main difference is that the inlet/outlet structures of the chip have a circular shape and are suitable for fibers with an external diameter of 110 μm (cross-section **F**, in Figure 4-6, Chapter 4) for the connection to the HPLC pump and the valve system. As shown in Chapter 4, this inlet/outlet geometry can withstand high working pressures. In Figure 7-1 a picture of the microreactor chip is shown. The two reagent channels **1** and **2** lead separately to the reaction zone (**3**), where they join, mix and react at high pressures.

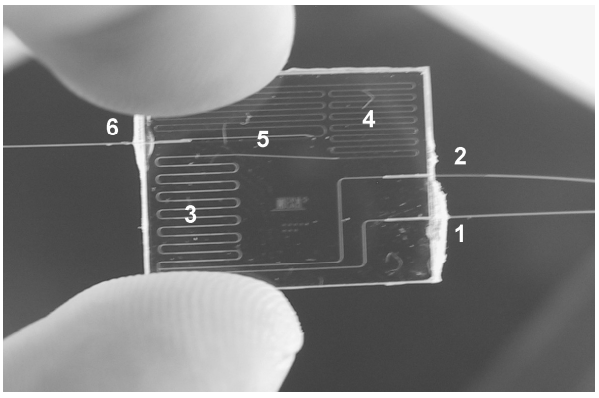

Figure 7-1: Photograph of the microreactor chip. **1** inlet for cyclopentadiene, **2** inlet for maleimides, **3** reaction zone, **4** fluidic resistor, **5** expansion zone, **6** outlet. The fibers have an internal diameter of 50 μm and an external diameter of 110 μm.

Since the microreactor is operated under continuous flow and constant pressure, the residence time in the chip depends on the applied pressure (see Chapter 6 for details). The residence time in the microreactor ($t_{microreactor}$), which is defined as the total reaction time minus the residence time in the outlet fiber before the quenching vessel ($t_{outlet\text{-}fiber}$), was calculated for each pressure (Table 7-I); see the Experimental section 7.4.4.

Table 7-I: Pressures, flows and corresponding residence times in microreactor ($t_{microreactor}$) and outlet-fiber ($t_{outlet\text{-}fiber}$) and the total reaction time.

Pressure /bar	Flow /μL min^{-1}	$t_{microreactor}$ /s	$t_{outlet\text{-}fiber}$ /s	Reaction time /s
90	1.8	8.4	1.6	10.0
100	2.1	7.5	1.5	9.0
110	2.3	6.8	1.3	8.1
150	3.2	4.9	1.0	5.9

7.2.2 Set-up

In contrast to Chapters 5 and 6, where the reagents were pre-mixed in a loop before introduction in the microreactor, here two independent loops were used to flow the reactants in the microreactor.

These loops are pressurized and contain the reagents; 6-port valves are used to flow the reagents independently and simultaneously into the microreactor, Figure 7-2.

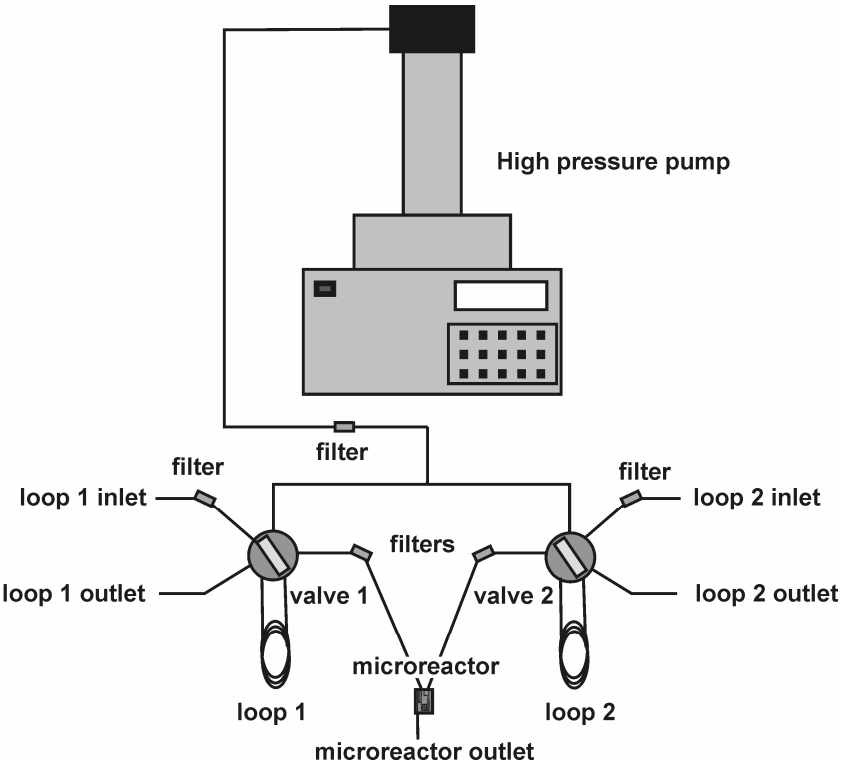

Figure 7-2: Set-up for the continuous flow operation of a glass microreactor at high pressures.

7.2.3 Diels-Alder reaction at high pressures in a microreactor

A 0.01 M solution of cyclopentadiene (**1**) in deuterated chloroform ($CDCl_3$) was injected in loop 1, while the same concentration of maleimide (**2a-c**) was injected in loop 2. After pressurizing both loops, the reagents were led into the microreactor. When the fluid flowed out of the outlet fiber the reaction was quenched by sample dilution at low temperature (-20 °C) to inhibit further reaction.

Because of the quenching, the reaction-to-analysis "delay" time, which is inherent to off-line microreactor analysis, was considerably reduced. The conversions were determined by comparing the intensities of the two signals of the four double bond protons of cyclopentadiene (**1**) at 6.40 and at 6.50 ppm with those of the signals of the double bond protons of the products (**3**) at 5.90-6.30 ppm in the ^{1}H-NMR spectra of the reaction mixtures. The *endo* isomers were exclusively formed under these conditions, no *exo* isomer was detected in the ^{1}H-NMR spectra, in line with the results reported in literature for these reactions.[6,7,10]

In Figure 7-3 the second order rate constants are plotted *vs.* the applied pressure. This graph shows that the reaction of **1** with **2a-c** is affected by pressure in the order: methylmaleimide (**2a**) < phenylmaleimide (**2b**) < benzylmaleimide (**2c**). These results are in agreement with the estimated reaction volumes (ΔV) presented in Table 7-II estimated with the PCModel, a molecular modeling program. In Chapter 3 a different order of reactivity of the maleimides (**2a-c**) was observed when reacting with 2-furylmethanol at 600 bar, phenylmaleimide (**2b**) < benzylmaleimide (**2c**) < methylmaleimide (**2a**), with respect to the same experiments at 1 bar. This was explained based on their different reactivity with 2-furylmethanol and its hydroxymethyl group which varies the ΔV.

Table 7-II: Reaction volumes (ΔV) for the reactions of cyclopentadiene (**1**) with the maleimides (**2a-c**) as estimated with PCModel for Windows.

2	ΔV /cm^3 mol^{-1}
a	-11.0
b	-12.7
c	-13.4

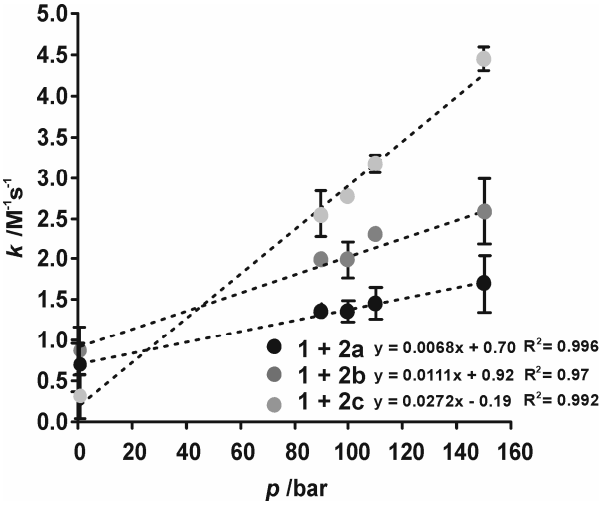

Figure 7-3: Second order rate constants as function of pressure for the Diels-Alder reaction of cyclopentadiene **1** with the maleimides **2a-c** carried out in the microreactor at pressures up to 150 bar. Data at 1 bar are the batch reactions carried out in the silica fiber. Data points are mean values from duplicate experiments.

The order of reactivity of **1** with the **2a-c** was phenylmaleimide (**2b**) > methylmaleimide (**2a**) > benzylmaleimide (**2c**) in batch experiments (1 bar) with rate constants of 0.87, 0.70 and 0.31 M^{-1} s^{-1}, respectively. For these experiments the batch reactions were carried out in a silica fiber, connected to a pump that controls the residence time in the fiber. The same order of reactivity for the reaction of phenyl- (**2b**) and methylmaleimide (**2a**) with thiophene as dienophile was found by Margetic *et al.*[11] In a study of the copolymerization of styrene with the maleimides (**2b**-**c**) Butz *el al.*[12] explained the same order of reactivity by a different electronegativity of the maleimide C=C double bond (3.23 (**2b**)[13] >> 1.47 (**2c**)[14]).

The high pressure microreactor influences the three reactions differently. These effects can be explained taking into account two main parameters: the pressure, as it was mentioned before and the very efficient and fast mixing that takes place in the microreactor which improves the reaction rates.

The reaction of cyclopentadiene (**1**) with methylmaleimide (**2a**) was hardly affected in the microreactor. Taking into account the three reactions, the reaction of cyclopentadiene (**1**) with methylmaleimide (**2a**) has the less negative ΔV value. Only a 1.1-fold increase was obtained compared to batch experiments.

The reaction of **1** with phenylmaleimide (**2b**) shows 1.7-fold higher conversions compared to batch experiments. The reaction has a high negative ΔV value, thus it is positively influenced by pressure.

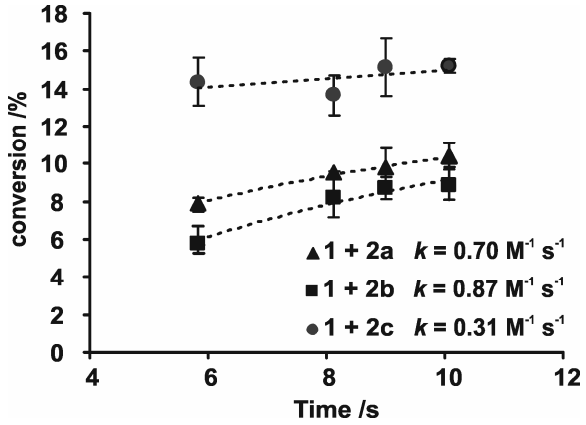

Figure 7-4: Diels-Alder reaction of cyclopentadiene (**1**) with methyl- (**2a**), phenyl- (**2b**) and benzylmaleimide (**2c**) carried out in batch experiments at 1 bar. Data points are mean values from duplicate experiments.

A 1.3-fold higher conversion compared to batch experiments was obtained for the reaction of cyclopentadiene (**1**) with benzylmaleimide (**2c**). Although, it has the highest negative ΔV value, its reaction kinetics is slower than that of the reaction of **1** with **2b**, thus the difference in conversion between batch and microreactor experiments is less marked than in the previous reaction.

It is known that microreactors can influence organic reactions,[15] and that the integration of mixing structures in microfluidic devices[16] can positively influence the reaction rates.[17,18] In these high pressure microreactors, the residence time ($t_{microreactor}$) is very short, max. 8.4 s for 90 bar and depends on the applied pressure. As a consequence, it is difficult to determine whether the increase in product formation of the reactions carried out in the microreactor is exclusively due to the applied pressure or partly also to the efficient mixing that takes place.[19] Nevertheless, in Chapter 5 it is shown that the mixing dynamics in these high pressure microreactors is very fast due to the mixers incorporated in the channels.[20] Thus this fast mixing may also positively affect the Diels-Alder reactions presented here.

7.3 Conclusions and Outlook

A set-up to study organic reactions in continuous flow at pressures up to 150 bar was constructed, in which the pressurized reagents can be introduced in the microreactor independently and/or simultaneously. It was used to study the influence of pressure on the Diels-Alder reaction of cyclopentadiene (**1**) with methyl- (**2a**), phenyl- (**2b**) and benzylmaleimide (**2c**).

The effect of pressure and/or the fast and efficient mixing of the reagents in the microreactor are believed to be the reasons for the 1.3-fold and 1.7-fold higher conversions, with respect to batch experiments, for the reaction of **1** with **2b** and **2c**, respectively.

The rather short residence times in the microreactor only allow studying the influence of pressure on fast reactions. Increasing the length of the reaction channel or the hydraulic resistance channel, will result in larger residence times ($t_{microreactor}$) and consequently, will allow to study less fast reactions. Implementing heaters in the set-up, as presented in Chapter 5, opens new possibilities for chemistry at high pressure and high temperatures in the microreactor chip.

Further improvement of the system could be the incorporation of on-line analysis such as UV-Vis[21] and/or NMR spectroscopy[22] to give a complete Micro Total Analysis System (μTAS).

7.4 Experimental

7.4.1 Materials

Cyclopentadiene (**1**) was directly used upon cracking and distillation at 170 °C of dicyclopentadiene. 1-Methyl-1*H*-pyrrole-2,5-dione (**2a**), 1-phenyl-1*H*-pyrrole-2,5-dione (**2b**), 1-benzyl-1*H*-pyrrole-2,5-dione (**2c**) were purchased from Aldrich (Zwijndrecht, The Netherlands).

Chloroform-*d* was purchased from Aldrich (Zwijndrecht, The Netherlands). For sample preparation micro liter syringes 1725RN (Hamilton Bonaduz AG, Switzerland) were used.

^{1}H-NMR spectra were recorded using a Varian Inova 300 MHz spectrometer. The complete characterization of the products **3a-c** can be found in references 6 (**3a**), 7 (**3b**) and 10 (**3c**).

An estimation of the reaction volumes for the reactions of cyclopentadiene (**1**) with the maleimides (**2a-c**) was performed using PCModel V.8.00.1 for Windows (Gilbert K., Serena Software:

Bloomington, Indiana) using MMX force field (Table 3-II). The obtained values are not entirely accurate but they are good enough to draw conclusions over the three different reactions involved in this study.

7.4.2 Microreactor set-up

Figure 7-2 shows a schematic drawing of the set-up. It consists of two fused silica fiber loops (100 µm inner diameter, 120 cm length) (Polymicro Technologies, LLC, Phoenix, Arizona), two valves, a microreactor chip and a HPLC pump. The loops, with an estimated volume of about 9.4 µL, are connected to two valves (6 post 2-post valve-XH System, manual 1/16″, 25 mm 50 °C/10000 psi liq., N60/X, sn 04N-0007, Valco Instruments Co. Inc., Schenkon, Switzerland) that enable the loops to be switched in or out of the flow path without the need of depressurizing the entire set-up. A high-pressure pump (Model 100DM, Isco, Lincoln, Nebraska) equipped with a high-precision pressure transducer was used as a pressure source.

The microreactor is protected against particles with in-line microfilter assemblies, inline, M-520, 0.5 mm PEEK™, Microtight® (Upchurch Scientific, Harbor, Washington).

7.4.3 Batch experiments set-up

To compare the reactions performed in the microreactor with batch experiments, a method to have identical reaction times was developed. The setup of Figure 7-5 consists of three fibers connected to a U-428 Stainless Steel Tee (volume 0.57 µL). Two of these fibers are connected to a pumping system (CMA /102 Microdialysis pump) with two syringes (1 mL Hamilton Gastight®) containing the reactants.

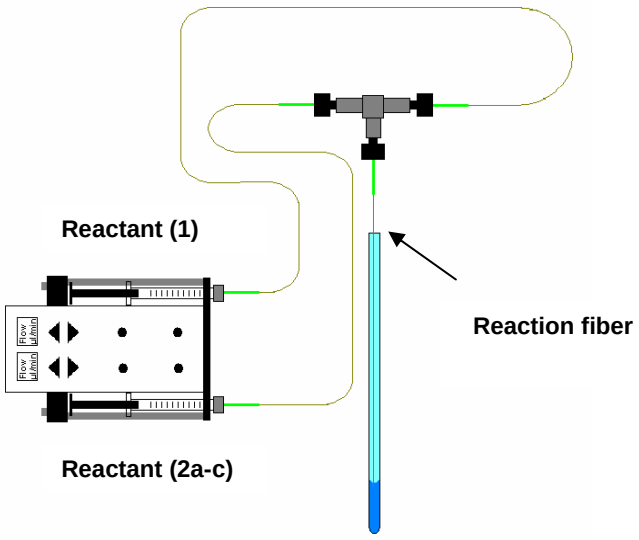

Figure 7-5: Set-up for continuous flow analysis at batch experiments at 1 bar.

7.4.4 Batch experiments

A 0.01 M solution of cyclopentadiene (**1**) in $CDCl_3$ was injected in the main fiber using one of the syringe pumps, while the same concentration of maleimide (**2a-c**) was injected in the same fiber by the other syringe pump. The reagents mix and react at the stainless steel tee and fiber for 10.0, 9.0, 8.1 and 5.9 s, respectively. The reaction fiber is positioned in a NMR tube to collect the sample. The NMR tube is cooled (-20 °C) and filled with 0.6 mL of $CDCl_3$ such that the sample is quenched in the same way as the microreactor sample. The determination of the rate constants at batch experiments was performed using the integrated form of a second order rate equation, eq. (7-1):

$$\frac{1}{[A]} - \frac{1}{[A]_0} = k \cdot t \qquad \text{eq. (7-1)}$$

where $[A]_0$ is 0.01 M of cyclopentadiene (**1**) and [A] is the amount of cyclopentadiene remained at time (*t*), (Figure 7-4).

Due to a reproducibility problem at 5.9 seconds reaction time for the reaction of cyclopentadiene (**1**) with benzylmaleimide (**2c**), the rate constant could not be precisely determined. Nevertheless, the different trend with respect to the other reactions is clearly visible, (Figure 7-4).

7.4.5 Calibration of the set-up

A calibration curve of the applied pressure *vs.* flow was made for the determination of the residence time in the microreactor ($t_{microreactor}$) at each pressure. The procedure is equal to that presented in Chapter 6. The calibration is done for four microreactors (Figure 7-6). Except for the first microreactor that was damaged, all of them gave identical linear relations between the applied pressure and the observed flow.

$$\text{Flow} = 0.0225 \cdot p - 0.1773 \quad R^2 = 0.996$$

The residence time in the microreactor for each experiment was calculated using equation (7-2)

$$t_{microreactor\ x,\ p} = \frac{V_{microreactor}}{Flow_{x,\ p}} \qquad \text{eq. (7-2)}$$

The microreactor volume is 0.26 μL. Values of $t_{microreactor}$ are shown in Table 7-I. The time that the reagents are in the outlet fiber (4 cm) of the microreactor have also to be considered for the reaction time.

During the experiments carried out in the microreactor, a 0.01 M solution of cyclopentadiene (**1**) in $CDCl_3$ was injected in loop 1, while the same concentration of maleimide (**2a-c**) was injected in loop 2. After pressurizing both loops, the reagents were flown into the microreactor using the valves 1 and 2 of Figure 7-2. When the fluid flowed out of the outlet fiber (4 cm) the reaction was quenched by sample dilution at low temperature -20 °C to inhibit further reaction. The temperature of the microreactor is kept constant at 22 °C during the experiments.

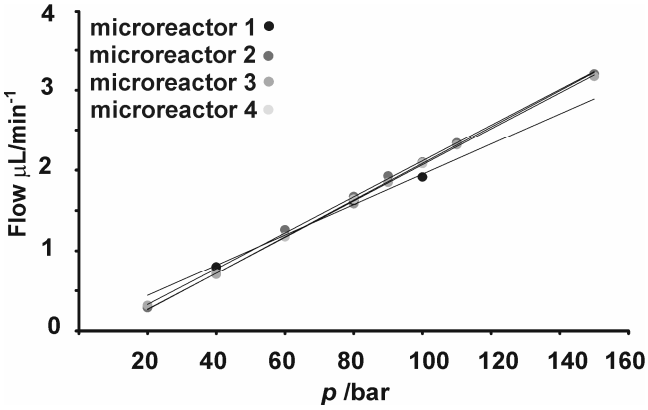

Figure 7-6: Relation between the applied pressure and the flow for the calculation of the residence time in the microreactor at various pressures (flow error 0.05 µL min^{-1}) using $CDCl_3$ at 22 °C.

7.5 References

1. Klärner, F.-G.; Diedrich, M. K., *The Chemistry of Dienes and Polyenes, 1*. Wiley-VCH: New York (USA), **1997**; p 547-617.
2. Jenner, G., *Mini-Rev. Org. Chem.* **2004**, *1*, 9-26.
3. Jenner, G., *New J. Chem.* **1991**, *15*, 897-899.
4. Matsumoto, K.; Hamana, H.; Iida, H., *Helv. Chim. Acta* **2005**, *88*, 2033-2234.
5. Van Eldik, R.; Klärner, F.-G., *High Pressure Chemistry*. Wiley-VCH: Weinheim (Germany), **2002**; p 45-96.
6. Meijer, A.; Otto, S.; Engberts, J. B. F. N., *J. Org. Chem.* **1998**, *63*, 8989-8994.
7. Xu, X. P.; Ma, M. T.; Yao, Y. M.; Zhang, Y.; Shen, Q., *Eur. J. Inorg. Chem.* **2005**, 676-684.
8. Benito-Lopez, F.; Verboom, W.; Kakuta, M.; Gardeniers, J. G. E.; Egberink, R. J. M.; Oosterbroek, E. R.; Van den Berg, A.; Reinhoudt, D. N., *Chem. Commun.* **2005**, 2857-2859.
9. Fernandez-Suarez, M.; Wong, S. Y. F.; Warrington, B. H., *Lab Chip* **2002**, *2*, 170-174.
10. Morgan, M. S.; Tipson, R. S.; Lowy, A.; Baldwin, W. E., *J. Am. Chem. Soc.* **1944**, *66*, 404-407.
11. Margetic, D.; Butler, D. N.; Warrener, R. N., *Arkivoc* **2002**, 234-256.
12. Butz, S.; Baethge, H.; Schmidt-Naake, G., *Macromol. Chem. Phys.* **2000**, *201*, 2143-2151.
13. Schmidt-Naake, G.; Bierlich, M., *Kautsch. Gummi Kunstst.* **1997**, *50*, 470-476.
14. Schmidt-Naake, G.; Drache, M.; Leonhardt, K., *Macromol. Chem. Phys.* **1998**, *199*, 353-361.
15. Brivio, M.; Verboom, W.; Reinhoudt, D. N., *Lab Chip* **2006**, *6*, 329-344.
16. Jensen, K., *Nature* **1998**, *393*, 735-737.

17. De Bellefon, C.; Pestre, N.; Lamouille, T.; Grenouillet, P.; Hessel, V., *Adv. Synth. Catal.* **2003**, *345*, 190-193.

18. Hertzog, D.; Michalet, X.; Jager, M.; Kong, X. X.; Santiago, J.; Weiss, S.; Bakajin, O., *Biophys. J.* **2005**, *88*, 376.

19. The unique design of the high pressure microreactor prevents to work at 1 bar, thus it is impossible to determine quantitatively the mixing effect. A microreactor that is capable to operate at 1 bar and has the same design and mixing characteristics as the high pressure microreactor presented in this Chapter could be used to quantify this effect.

20. Stroock, A. D.; Dertinger, S. K. W.; Ajdari, A.; Mezic, I.; Stone, H. A.; Whitesides, G. M., *Science* **2002**, *295*, 647-651.

21. Schulze, P.; Ludwig, M.; Kohler, F.; Belder, D., *Anal. Chem.* **2005**, *77*, 1325-1329.

22. Wensink, H.; Benito-Lopez, F.; Hermes, D. C.; Verboom, W.; Gardeniers, J. G. E.; Reinhoudt, D. N.; Van den Berg, A., *Lab Chip* **2005**, *5*, 280-284.

8

Measuring Reaction Kinetics in a Microreactor by Microcoil NMR*

In this Chapter the fabrication of a microreactor with an integrated microcoil for NMR spectroscopic analysis as well as the holder for the incorporation of such a microreactor in a 60 MHz NMR apparatus is presented. Pressure experiments revealed that the system functions very well for pressures up to 60 bar. Moreover, the rate constant of the imine formation of benzaldehyde with aniline was determined with this NMR microreactor operated in continuous flow mode.

---

* Parts of this Chapter have been published in: Wensink, H.; Benito-López, F.; Hermes, D.C.; Verboom, W.; Reinhoudt, D. N.; van den Berg, A., Measuring reaction kinetics in a lab-on-a-chip by microcoil NMR, *Lab Chip* **2005**, *5*, 280–284.

8.1 Introduction

It is still common to use off-line detection techniques for the analysis of product streams from microreactors, but the integration of on-line methods allows faster analyses on smaller amounts of sample and better process control. The search for on-line measurement techniques for microfluidic systems (microreactors) have resulted in the development of new (sophisticate) microreactor instrumentation.

Incorporation of miniaturized Nuclear Magnetic Resonance (NMR) coils in microfluidic systems is one of the new on-line techniques. For example, the group of Sweedler reported the development of a micromachined mixer coupled to a microcoil NMR probe to study the kinetics of protein conformational changes.[1] In this work the integration of planar metal film microcoils for the excitation and detection of NMR signals in a microreactor is described. In parallel, microfabricated small-volume NMR probes with a planar microcoil integrated onto a glass substrate with microfluidic channels were fabricated and tested by Massin *et al.*[2] The main advantage of coupling NMR microcoils direct to a microreactor is that in this way direct spectroscopic information is obtained that allows the identification and quantification of chemical species in continuous flow mode, as well as on-line (real time) kinetic studies.

Over the last 50 years, NMR spectroscopy has developed enormously as a powerful analytical tool to probe the atomic structure and molecular dynamics of proteins, polymers and biomolecular assemblies. In the high pressure research area in particular, reaction kinetics and/or chemical mechanisms are commonly studied using NMR spectroscopy,[3] where the design and the construction of sophisticated probes for new applications are ongoing.[4,5] The implementation of this powerful analytical technique in high pressure microreactors will open new information windows on chemical reactions. For example, the influence of pressure on a reaction can be studied on-line for continuous flow operation of the microreactor.

In previous Chapters, where microreactors have been used for chemical purposes, the detection was done by an off-line technique. Here, a microreactor with an integrated microcoil for on-line NMR spectroscopic analysis is presented. As a proof of principle, the rate constant of the imine formation of benzaldehyde with aniline was determined with this NMR microreactor.

8.1.1 Design aspects of a microreactor with an integrated microcoil NMR

A drawback of NMR is that it is inherently insensitive, requiring special measures in case it is applied to the very small sample volumes present in a microreactor. NMR performed on small sample volumes, down to 5 nL, was first demonstrated in capillaries, in which case a solenoidal coil for excitation and detection of the NMR signals was wrapped around the capillary.[6] In this form, NMR has been used as an on-line detection method for capillary separation techniques like High-Performance Liquid Chromatography (HPLC) and Capillary Electrophoresis (CE).[7] An extra feature of being able to work with small sample volumes is the possibility to insert multiple probes into a single NMR magnet, which allows high-throughput NMR analysis.[8] The combination of microreactor-based microfluidics with NMR was (to our knowledge) first demonstrated by Trumbull *et al.*,[9] who integrated a planar NMR coil on a CE microreactor. These authors reported ^{1}H NMR spectra of a 30 nL water sample acquired at 250 MHz with a frequency-domain signal-to-noise ratio (SNRf) of 23.5 per scan and a minimal line width of 1.39 Hz. Comparable results have been obtained by Massin *et al.*,[10] *viz.* a SNRf of 117 per scan but with a line width of 30 Hz for 30 nL water in a micromachined glass microreactor with integrated microcoil, acquired at 300 MHz. The main factor that limits the performance of micromachined NMR probes in terms of sensitivity and spectral resolution was identified to be probe-induced static magnetic field inhomogeneity and routes for improvement were suggested to be in the areas of probe design and materials, magnetic field shimming and signal processing.[2]

8.2 Results and Discussion

8.2.1 Microreactor layout and fabrication

Two 1.1 mm thick Borofloat wafers were powder blasted,[11] to obtain a 450 μm deep channel structure in one and through holes in the other. The channel width is 500 μm underneath the detection coil and the cross-section has a rounded

V-shape; the channels that connect the through holes to the detection channel are slightly smaller. The wafers were bonded and annealed (600 °C for 1 h). About 570 μm of glass was removed from one side of the wafer stack by etching in 33 wt.% HF which left about 80 μm of glass between the NMR detection coil and the bottom of the channel (Figure 8-1). The coil fabrication is described in the Experimental part of this Chapter.[12]

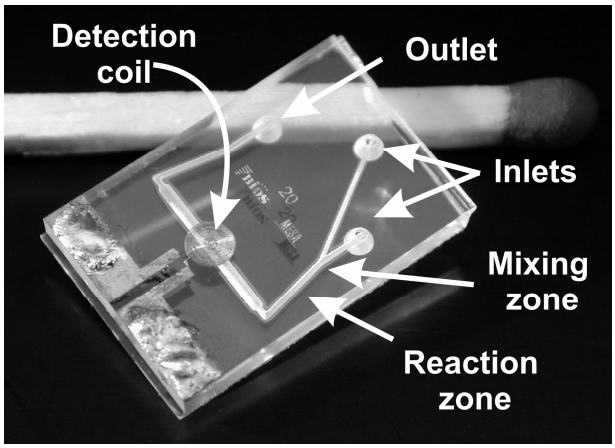

Figure 8-1: The glass NMR microreactor with planar microcoil. Microreactor size is 1 by 1.5 cm; the channel width underneath the coil is 500 μm.

8.2.2 Set-up

A modification of the probe head of a 60 MHz NMR spectrometer allowed fixing a holder that supports the microreactor. The holder enabled the incorporation of microfluidic connections to the chip (Figure 8-2). The connections, fibers and holder interfered with the magnetic field, reducing the spectral resolution to approximately 0.1 ppm, indicating that fluidic connections should be located further away from the NMR coil in future microreactor designs. Nevertheless, the new set-up allowed solutions to be pumped into the microreactor by syringes and thus continuous flow operation of the microreactor.

The electrical set-up is similar to that of Massin *et al.*,[13] and is presented in detail in the Experimental section of this Chapter.

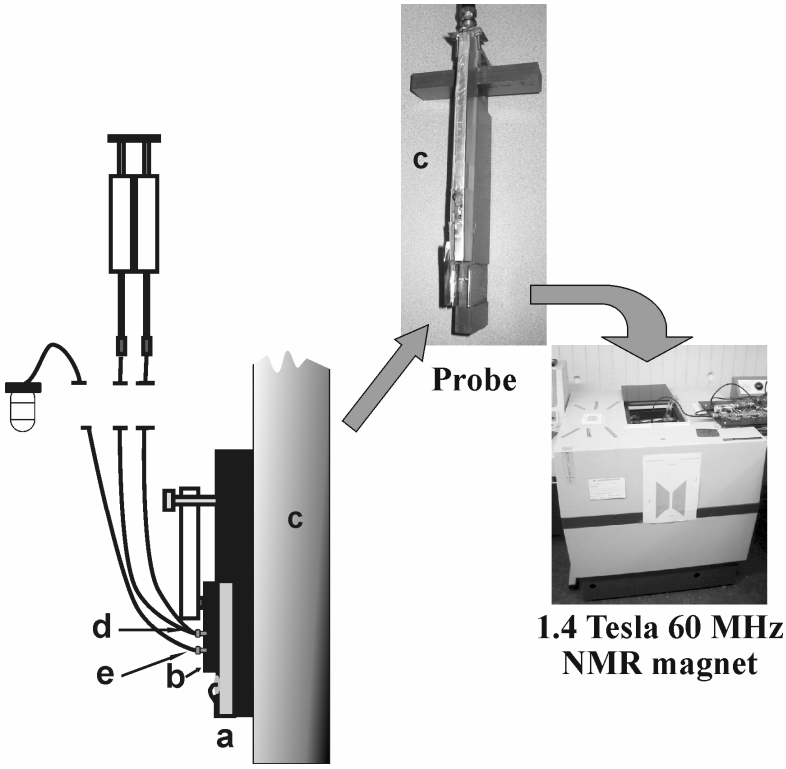

Figure 8-2: Set-up for continuous flow operation and on-line analysis by NMR spectroscopy in a microreactor. The microreactor (**a**) is placed into the holder (**b**) where microfluidic connections (inlets **d**, outlet **e**) are adjusted with commercially available connectors. This system is incorporated in the modified probe (**c**) of a 60 MHz NMR spectrometer.

8.2.3 Imine formation: microreactor experiments

In the NMR microreactor the total channel volume between the mixing point, *i.e.* the point where the two inlet channels join and the detection coil is approximately 0.57 μL (Figure 8-1), the detection volume (the channel volume under the coil) is estimated to be 56 nL. The residence time in this volume ranges from 0.9 s to 30 min, depending on the flow rate. It has to be taken in to account that if the flow rate is too high (20 μL min^{-1}), the excited sample volume will be removed from the detection region before NMR signal acquisition is completed, which will reduce the spectral resolution. However, for the settings used in this Chapter such an effect was not observed.

Imine (Schiff base) formation was chosen as a model reaction (Scheme 8-1). This reaction has been performed in a microfluidic microreactor before and was analyzed by mass spectrometry[14] or laser-induced Raman microscopy.[15] Here a

different approach was followed. The microreactor inlets were connected to two 100 μL syringes containing 4.95 M benzaldehyde (**1**) and 4.95 M aniline (**2**) in deuterated nitromethane (CD_3NO_2), respectively, with tetramethylsilane (TMS) as internal standard.

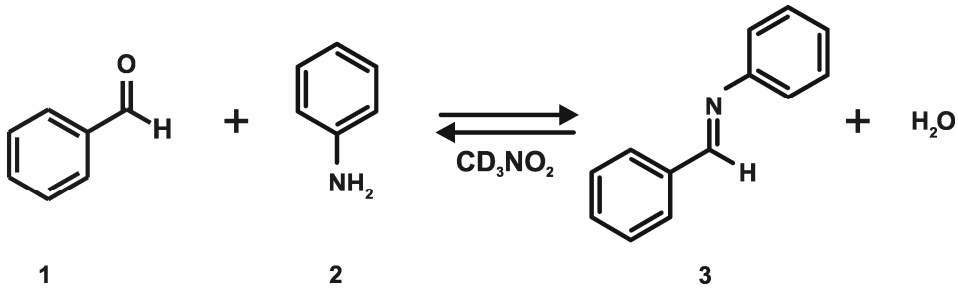

Scheme 8-1: Imine formation (**3**) from benzaldehyde (**1**) and aniline (**2**).

Figure 8-3 shows the ^1H NMR spectra of the individual reagent solutions measured with the microcoil of the microreactor.

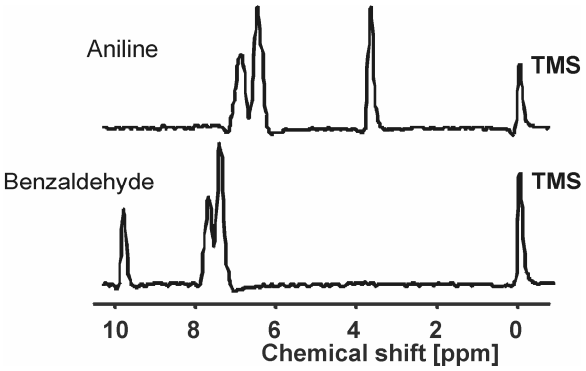

Figure 8-3: ^1H NMR spectra of the two reagent solutions in CD_3NO_2. TMS is used as internal reference.

Due to the high reagent concentrations, a substantial amount of water was formed during the reaction, which is immiscible with the organic solution and remained stuck at the channel walls, particularly at the corners. Therefore, a high flow rate flush was applied between the scans to prevent the dominance of water resonance in the spectra. After flushing, the flow rate was set to a lower value to achieve the desired residence time.

The measurement procedure was as follows: the two reagents (**1**, **2**) were pumped into the microreactor after which the flow rate was adjusted to have the desired residence time in the channel section between the mixing point and the detection coil. This time is defined as the reaction time. An NMR scan was taken

(acquisition time 0.2 s, 2000 data points), after which a delay time was taken before the next scan was recorded. The delay time between two consecutive scans was scaled with the flow rate to ensure complete refreshment of the detection volume; a maximum delay time of 10 s was taken. Per reaction time 32 NMR scans were measured and the average resulted in the different spectra of Figure 8-4.

For analysis of the reaction kinetics, we focused on two peaks, *viz.* the aldehyde peak of benzaldehyde (**1**) at 9.9 ppm and the imine peak (**3**) of the product at 8.4 ppm. Figure 8-4 shows the increase of the imine peak and decrease of the aldehyde signal with increasing residence time. The area of the two peaks of interest was calculated to follow the course of the reaction.

In Figure 8-5, the conversion of the reaction is plotted as the ratio of each peak area to the sum of both peak areas, as a function of the residence time. The curves in this figure are a fit with a second order rate equation with a rate constant of 5.8 x 10^{-2} M^{-1} min^{-1}, with an error of 0.64%. The reaction was also carried out in a conventional probe in a 400 MHz NMR apparatus using the same concentration as in the microreactor, but not in a continuous flow mode. The reaction was followed by taking a single scan every 5 s and the experiment was performed three times, (see the Experimental). The second order rate constant was found to be (5.0 $\pm$ 0.05) x 10^{-2} min^{-1}. This value is in the same range as values measured by Raman spectroscopy for imine formation in chloroform.[16] The reaction rate constant found in the microreactor is slightly higher than at batch approximately 1.2 times, both values are within the experimental error.

The degree of mixing may be characterized by the penetration depth for diffusion of a species from one liquid into the other, which in a simple 1-dimensional diffusion model without chemical reaction is equal to the square root of *2Dt*, with *t* the time of contact of the two liquids and *D* the diffusivity of the species of interest. The diffusivity of the reagents benzaldehyde and aniline is 1.5 x 10^{-9} m^2 s^{-1} and 1.96 x 10^{-9} m^2 s^{-1}, respectively.[17,18] Thus, the time needed for complete mixing in a 160 μm wide channel is approximately 2 s, from which it can be concluded that mixing can be considered to be instantaneous for most of the time range in which we have measured the reaction kinetics (Figure 8-5). The reaction time range that is available for study in our microreactor is comparable to that obtained by Kakuta *et al.*,[1] who mentioned a mixing time of 1.4 s for a Y-connector included in their system and could measure reaction times down to 3.8 s.

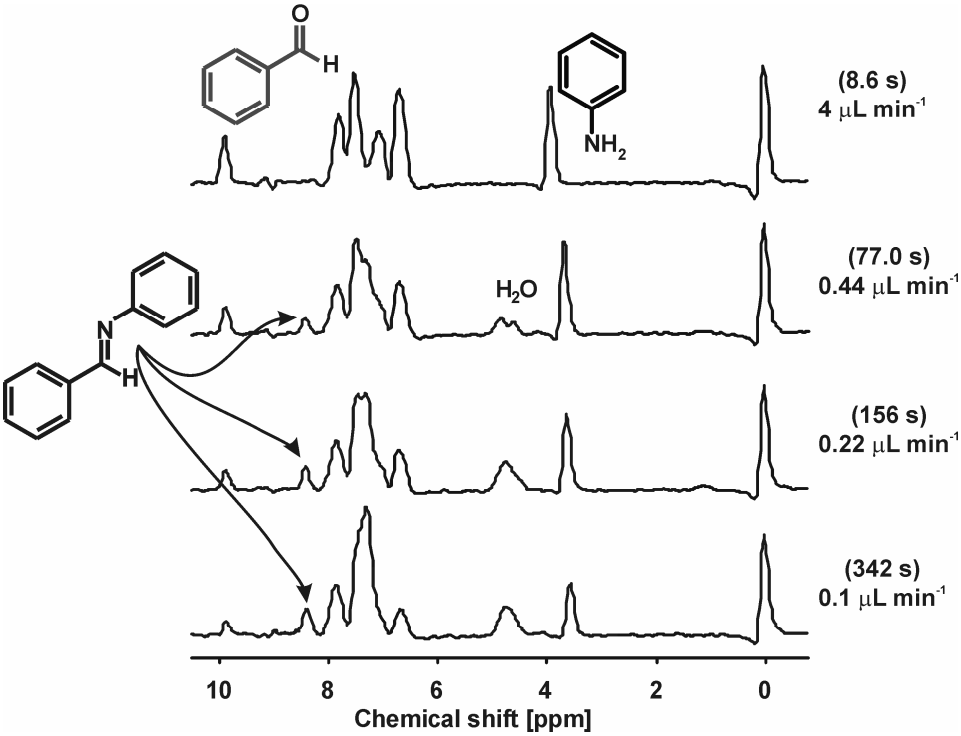

Figure 8-4: ^{1}H NMR spectra taken at different residence times.

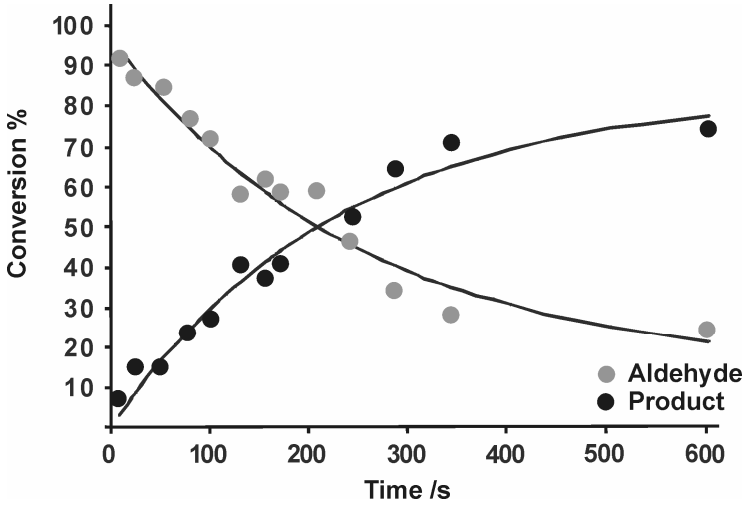

Figure 8-5: Time dependence of imine formation measured in the microreactor by ^{1}H NMR.

8.3 Conclusions and Outlook

In this Chapter we have demonstrated the design, fabrication and testing of a microreactor with an integrated microcoil for NMR measurements. The microreactor system is optimized for low-field NMR in a conventional NMR magnet. It can be used in continuous flow mode for pressures up to 60 bar using commercially available microfluidic connections. Higher pressures can be obtained by using different connections; *e.g.* gluing of fibers in the chip (Chapter 4). Moreover these glue connections will have a lower interference on the magnetic field, since a holder is not needed.

With the microreactor the reaction kinetics of the imine formation from benzaldehyde (**1**) and aniline (**2**) was determined by NMR spectroscopy at 60 MHz. The rate constants are slightly larger than those determined in a conventional tube in a 400 MHz NMR spectrometer nevertheless; both values are within the experimental error.

The mixing time in the microreactor was calculated to be approximately 2 s, while the reaction times can be set from 30 min down to only 0.9 s, therewith enabling monitoring of relatively fast reactions.

More complex pulse sequences, like COSY and NOESY,[19] are in principle possible with the developed set-up and in fact a simple COSY experiment with ^{13}C-labeled acetic acid on a microfluidic microreactor with an integrated Helmholtz microcoil (*i.e.* a dual microcoil) has been demonstrated.[20] Additional functionality that aids in the measurement of reaction kinetics could be the implementation of a fast mixer or heaters, or the use of two or more coils at different positions along a microchannel, a configuration that was used by Ciobanu *et al.*, who wrapped several solenoidal microcoils at different locations around a flow-through capillary.[21]

The performance of the microreactor for NMR spectroscopy was adequate for the kinetic study presented here, in which relatively simple, low molecular weight species at high concentrations were studied. However, to work at more practical concentrations or with more complex molecules, a much better spectral resolution is required. Since in the present design the spectral resolution is completely determined by magnetic field imhomogeneity in the microreactor, improving the design of the microreactor is the main step to be taken. Microreactor designs other than the planar coil (*e.g.* striplines[22]) are currently under investigation.

8.4 Experimental

8.4.1 Materials

Benzaldehyde (**1**) (freshly distilled), aniline (**2**), tetramethylsilane (TMS) and deuterated nitromethane were purchased from Aldrich (Zwijndrecht, The Netherlands).

8.4.2 Microreactor coil fabrication

A 25 nm titanium adhesion layer and a 150 nm copper seed layer were sputtered over the whole wafer. AZ9240 resist was patterned on the wafer with a thickness of 25 μm to define the NMR detection coil. 18 μm of copper was electroplated on the wafer using the resist as a mould. After the resist was removed, the remaining seed layer was removed by ion beam etching to avoid electrical shorting between the windings. The coil has 24 windings with a width and separation of 20 μm and an inner diameter of 200 μm. Simulations showed that at 60 MHz, this coil has a self induction of 500 nH, a resistance of 4.5 Ω and a quality factor of 42.[12]

8.4.3 Pressure test of the system

The microfluidic system with integrated micro-NMR coil was subjected to pressure tests to verify its resistance. These tests were done using commercially available nanoports (Upchurch) connections. These connections are the most common ones used in microdevices and create reliable fluidic connections to microdevices. If the assembled parts are connected directly to the microdevice (using a nanoport, a gasket and a preformed adhesive ring) the fluidic connections can withstand pressures up to 103 bar (Upchurch) like it was explained in more detail in Chapter 2, section 2.5.3.3.[23] However, for flexibility reasons, a home-made microreactor holder was used. The capping part of this holder contains screw-threaded holes, through which fittings and ferrules can be connected to the powderblasted inlets/outlet of the microdevices.

Via the holder and fittings (F-123H), fibers (250 μm i.d.) can be connected by means of ferrules (biocompatible PEEK polymer) (Figure 8-6). Three different types of ferrules are available, depending on the type/size of microreactor hole:

- N-123-03 is a flat bottom ferrule, for holes of 1 mm diameter (or less)
- N-123-04 is a ferrule with a 'tip' at the bottom (tip lowered in the hole, to obtain a smaller dead volume), for holes of 1 mm diameter (or less) and a depth of 1 mm
- N-123-05 is a ferrule with a 'tip' at the bottom (tip lowered in the hole, to obtain a smaller dead volume), for holes of 1 mm diameter (or less) and a depth of 1.5 mm.

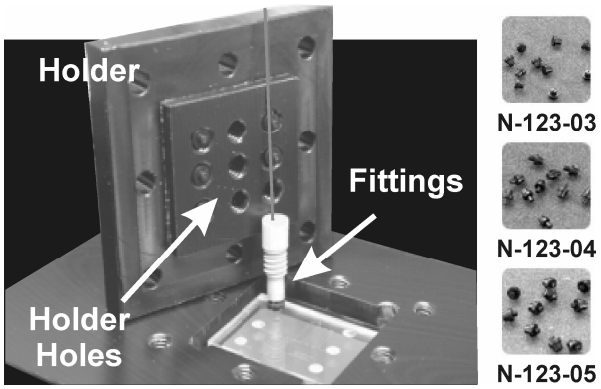

Figure 8-6: Picture of a holder similar to that used for pressure tests and the three ferrules: N-123-03, N-123-04 and N-123-05 used for the tests.

Since the microreactors have inlets/outlet with a depth of ~1.1 mm, for the experiments ferrules N-123-03 and N-123-04 were used. The fittings were hand-tight connected to the microreactor, but not over tightened. The connection between pump and fiber was done with 'cream-colored' connections (F-120 PEEK fitting, F-240 (green) sleeve, reliable up to ≈ 414 bar). An HPLC-pump (Isco-100 DM) was used to introduce the water in the microreactor at a constant flow rate. Subsequently, the flow rate was increased step-wise until leakage at the ferrule/ microreactor interface was observed by eye.

The pressure tests were done for two types of ferrules and two microreactors (Figure 8-7).

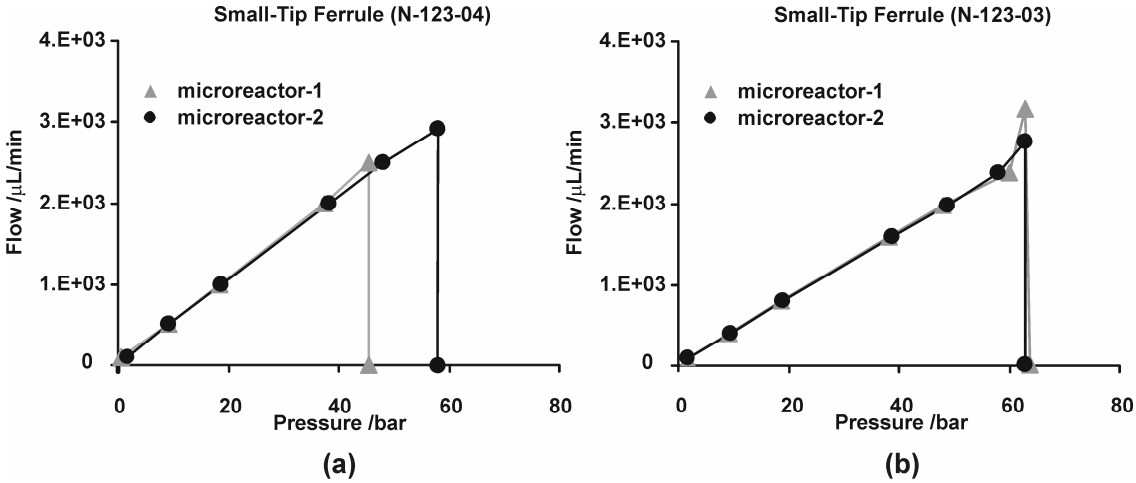

Figure 8-7: Pressure reliability test of the microreactors with the fluidic ferrules N-123-04 (**a**) and N-123-03 (**b**).

From Figure 8-7 it is clear that these connections (home-built holder and ferrules to access holes) can withstand approximately 50-60 bar, whereas ferrules of type N-123-03 are slightly stronger than of type N-123-04. With these connectors the NMR microreactor can be operated up to 60 bar in a continuous flow mode. However, for higher pressures other types of connections like those showed in Chapter 4 (glued fibers) should be used.

8.4.4 Imine formation: batch experiments

Batch experiments were performed using conventional NMR spectroscopy (Varian Inova 400 MHz).

The reactions were performed with the same concentrations as in the microreactor, 4.95 M benzaldehyde (**1**) and 4.95 M aniline (**2**) in deuterated nitromethane. In Figure 8-8 the imine concentration *vs.* reaction time is shown.

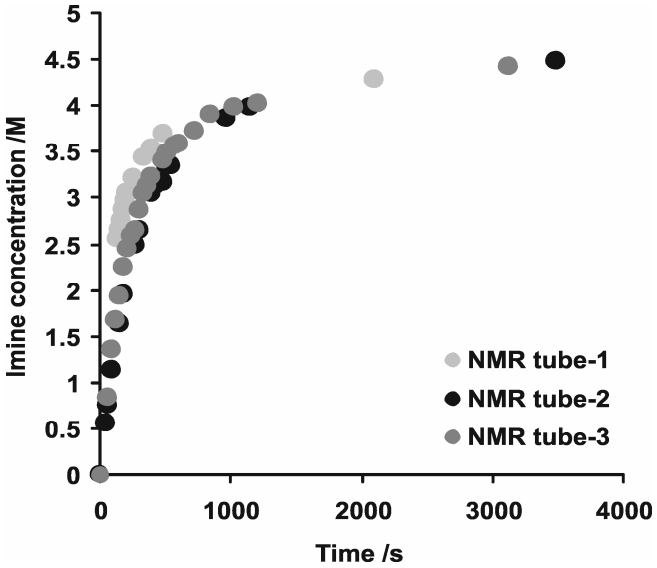

Figure 8-8: Imine concentration (M) (**3**) as function of time for three experiments performed in an NMR tube using ^{1}H NMR (400 MHz).

The second order rate constants were calculated using equation (8-1),[15] and are k_1 = 5.22 × 10^{-2}, k_2 = 4.65 × 10^{-2} and k_3 = 5.46 × 10^{-2} M^{-1} min^{-1}.

$$\frac{1}{[A]} - \frac{1}{[A_0]} = k \cdot t \qquad \text{eq. (8-1)}$$

where [*A*] is the aldehyde concentration and [A_0] is 4.95 M.

8.4.5 Signal-to-noise ratio

For an optimal signal-to-noise ratio, the planar microcoil has to be properly designed, *i.e.* the parameter set that defines the coil (Figure 8-9) *viz.* the number (*N*), width (*w*), height (*h*) and separation (*s*) of the windings and the inner diameter (r_i), has to be optimized. Different effects play a role in this optimization. For example, increasing the number of windings will increase the signal level but will also increase the coil resistance and therewith the noise level (the main source is Johnson noise that scales with the square root of the coil resistance). It is difficult to calculate analytically which parameters yield the maximum SNR, since the coil resistance depends non-

linearly on *e.g.* the amount of windings, due to the frequency-dependent skin effect and the proximity effect caused by neighboring windings. In previous work[12] it has been shown how to find the optimum coil geometry using finite element simulations.

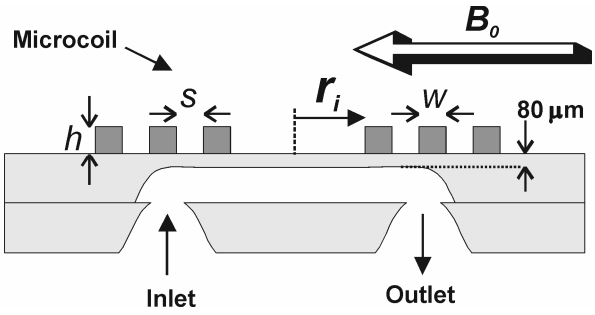

Figure 8-9: Schematic cross-section of the microcoil with three windings on top of the microreactor.

The design rules that can be derived from this work and that of others are as follows: (1) The windings and the separations between the windings should be as small as possible; this puts demands on the tolerances of the microfabrication process; (2) The coil height has only a small influence on the resistance and should be about 20 to 50 µm (*i.e.* at least twice the skin depth[24]); (3) The inner coil radius should match the average radius of the sample volume to obtain a high filling factor; [4] (4) There is no general rule to determine the optimal number of windings, it should be determined by simulations for specific coil shapes (examples of optimized coils can be found in ref. 12); (5) For a simple model of a planar microcoil it can be derived[25] that SNR scales with the inverse of the distance between NMR detection coil and sample, which distance should therefore be as small as possible.

8.4.6 Spectral resolution

Spectral resolution mainly depends on the homogeneity of the magnetic fields over the interrogated NMR sample volume. Commercial high-resolution NMR equipment is designed to have a homogeneous magnetic field over a sufficiently large area. Any material introduced in the homogeneous area distorts the magnetic field, unless the magnetic permeability of the material matches with that of the magnetic field area. Although the permeability of *e.g.* glass and copper differs only slightly from that of air, it still disturbs the homogeneity and therewith decreases the spectral resolution. This is a typical problem for NMR detection in a microreactor since, in contrast to conventional NMR probes, the volume of glass surrounding the sample is relatively large. To avoid these field distortions, abrupt changes in material geometry near the NMR detection area can best be avoided. Consequently, electrical and fluidic connections should not be placed in the neighborhood of the detection area. The fluidic channel that contains the sample will also disturb the magnetic field, but for reasons of sensitivity this has to be close to the detection coil. Two approaches can be followed to maintain a homogeneous field inside the sample volume of interest. The first approach becomes clear from the simulation result in Figure 8-10a: in a

spherical or cylindrical volume, the field inside the volume will be very homogeneous. This approach was followed by others.[13,20] The second approach, the one followed in this work, is to place a straight channel (which could have arbitrary cross section) in line with the magnetic field. Any disturbances created by the ends of the channel part will have faded out in the central region of the channel, where the detection coil is placed (Figure 8-10b). With state-of-the-art microfabrication techniques this configuration is easier to achieve than perfectly spherical or cylindrical channels.

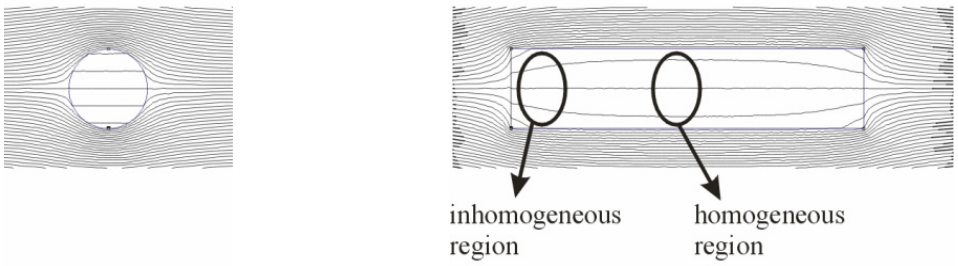

(**a**) (**b**)

Figure 8-10: The effect of the cross-sectional channel shape on the B_0 magnetic field lines. (**a**), spherical or cylindrical channel and (**b**), a long straight channel in line with the field lines.

8.4.7 Electrical NMR set-up

A conventional NMR magnet was used for the measurements (1.4 Tesla, 60 MHz, Varian EM360L), with the original probe head removed. A microreactor was placed on a plastic bar (the probe head) that allowed it to be positioned in the magnet. The probe head could be moved to position the microreactor exactly in the center of the two magnetic heads, where the homogeneous region of the magnetic field is located. Two adjustable capacitors were mounted on the probe head at 3.5 cm from the microreactor and electrically connected to the coil. This allows the coil to be matched to 50 Ω impedance and tuned to resonate at 60 MHz for a maximum power transfer to the electrical set-up. The electrical set-up is shown in Figure 8-11. Switches (ZYSW-2-50DR), amplifiers (ZFL-500LN), mixer (ZAD-1) and power splitter (ZSC-2-1) were obtained from Mini-Circuits Europe, Surrey, United Kingdom. The filter is a simple RC-network with a cut-off frequency of 1500 Hz. The 60 MHz RF-source is an Agilent 33250A function generator, the pulse length was determined by an HP33120A function generator. The NMR signal was acquired by an Agilent oscilloscope 54621A and Fourier transformed by Agilent VEE Pro 6.0 software that also controlled the set-up. The acquisition parameters (acquisition time, number of data points, electronic filter settings) were kept constant for all measurements. The correct power for a 90° pulse was determined by gradually increasing the power till maximum NMR signal was obtained. The pulse typically had an amplitude of 0.5 V (top) at a length of 28 μs.

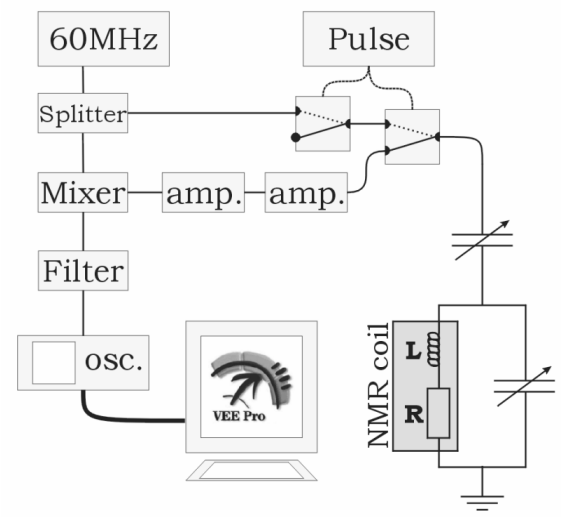

Figure 8-11: Electrical scheme of the NMR set-up.

8.5 References

1. Kakuta, M.; Jayawickrama, D. A.; Wolters, A. M.; Manz, A.; Sweedler, J. V., *Anal. Chem.* **2003**, *75*, 956-960.
2. Massin, C.; Vincent, F.; Homsy, A.; Ehrmann, K.; Boero, G.; Besse, P. A.; Daridon, A.; Verpoorte, E.; De Rooij, N. F.; Popovic, R. S., *J. Magn. Reson.* **2003**, *164*, 242-255.
3. Maiwald, M.; Fischer, H. H.; Kim, Y. K.; Albert, K.; Hasse, H., *J. Magn. Reson.* **2004**, *166*, 135-146.
4. Amita, F.; Oka, H.; Mukaide, M.; Urasaki, Y.; Takegoshi, K.; Terao, T.; Kajimoto, O., *Rev. Sci. Instrum.* **2004**, *75*, 467-471.
5. Zahl, A.; Neubrand, A.; Aygen, S.; Van Eldik, R., *Rev. Sci. Instrum.* **1994**, *65*, 882-886.
6. Olson, D. L.; Peck, T. L.; Webb, A. G.; Magin, R. L.; Sweedler, J. V., *Science* **1995**, *270*, 1967-1970.
7. Jayawickrama, D. A.; Sweedler, J. V., *J. Chromatogr. A* **2003**, *1000*, 819-840.
8. Macnaughtan, M. A.; Hou, T.; Xu, J.; Raftery, D., *Anal. Chem.* **2003**, *75*, 5116-5123.
9. Trumbull, J. D.; Glasgow, I. K.; Beebe, D. J.; Magin, R. L., I*EEE Trans. Biomed. Eng.* **2000**, *47*, 3-7.
10. Massin, C.; Daridon, A.; Vincent, F.; Boero, C.; Besse, P. A.; Verpoorte, E.; De Rooij, N. F.; Popovic, R. S. In Proc. of Micro Total Analysis Systems (MicroTAS), Monterey, CA, USA, Oct. 21-25, Piscataway NJ., USA, **2001**, pp. 438.
11. Wensink, H.; Elwenspoek, M. C., *Sens. Actuators A* **2002**, *102*, 157-164.

12. Wensink, H.; Hermes, D. C.; Van den Berg, A., In Proc. of: Micro Electro Mechanical Systems (MEMS), January 25–29, Maastricht, The Netherlands, **2004**, pp 407-410.
13. Massin, C.; Boero, C.; Vincent, F.; Abenhaim, J.; Besse, P. A.; Popovic, R. S., *Sens. Actuators A* **2002**, *97-8*, 280-288.
14. Brivio, M.; Fokkens, R. H.; Verboom, W.; Reinhoudt, D. N.; Tas, N. R.; Goedbloed, M.; Van den Berg, A., *Anal. Chem.* **2002**, *74*, 3972-3976.
15. Lee, M.; Lee, J. P.; Rhee, H.; Choo, J.; Chai, Y. G.; Lee, E. K., *J. Raman Spectrosc.* **2003**, *34*, 737-742.
16. Lee, M.; Kim, H.; Rhee, H.; Choo, J., *Bull. Korean Chem. Soc.* **2003**, *24*, 205-208.
17. Terazima, M.; Okamoto, K.; Hirota, N., *J. Chem. Phys.* **1995**, *102*, 2506-2515.
18. Landolt-Börnstein, *Numerical Data and Functional Relationships in Science and Technology*. 6th Edn. Engl., Springer-Verlag: Berlin (Germany), 1969, Vol. vol. II/5a.
19. Derome, A. E., *Modern NMR Techniques for Chemistry Research*. Pergamon Press: Oxford (UK), 1987.
20. Walton, J. H.; De Ropp, J. S.; Shutov, M. V.; Goloshevsky, A. G.; McCarthy, M. J.; Smith, R. L.; Collins, S. D., *Anal. Chem.* **2003**, *75*, 5030-5036.
21. Ciobanu, L.; Jayawickrama, D. A.; Zhang, X. Z.; Webb, A. G.; Sweedler, J. V., *Angew. Chem., Int. Ed.* **2003**, *42*, 4669-4672.
22. Van Bentum, P. J. M.; Janssen, J. W. G.; Kentgens, P. M., *Analyst* **2004**, *129*, 793-803.
23 *http://www.upchurch.com.*
24. Massin, C., *Microfabricated Planar Coils in Nuclear Magnetic Resonance*. Hartung-Gorre Verlag: Konstanz (Germany), 2004, Vol. 15.
25. Webb, A. G., *Prog. Nucl. Magn. Reson. Spectrosc.* **1997**, *31*, 1-42.

Summary

The realization of microreactors, in which chemical reactions can be carried out in continuous or stop flow mode under pressure conditions, is the main topic of this thesis.

Chapter 1 gives a general introduction to high pressure chemistry and describes the principles of lab-on-a-chip technology.

High pressure is usually generated in very sophisticated, expensive and closed systems and it is regarded as a technique that requires specialized equipment with strict safety precautions. In Chapter 2 the trend of high pressure technology towards miniaturization is described. Particular emphasis is given to potential advantages of small and portable systems that will allow relaxing safety issues, saving costs, materials and increasing the performance of high pressure systems by integrating miniaturized sensors and actuators.

Chapter 3 deals with a capillary based microreactor platform with fiber-optics for on-line UV/Vis spectroscopy. The reaction rate constants and the activation volumes for a nucleophilic aromatic substitution and an aza-Diels-Alder reaction were determined at different pressures. The influence of pressure on the conversion and the stereoselectivity of the Diels-Alder reactions of 2- and 3-furylmethanol with methyl-, benzyl- and phenylmaleimide was also studied by ^{1}H-NMR spectroscopy. The silica fiber microreactor is the first example of a miniaturized platform in which a reaction can be monitored on-line for pressures up to 600 bar.

The design, fabrication and performance of several in-plane fiber-based interface geometries to glass microreactor chips for high pressure chemistry are described in Chapter 4. The yield strength, defined as the maximum pressure before failure, can be increased by reducing the roughness of the sidewalls of powderblasted geometries with isotropic wet chemical etching with hydrofluoric acid. Moreover, it is demonstrated that small powderblasted inlets/outlets (suitable for 110 μm fibers) that

are smoothened with hydrofluoric acid and with a sharp transition towards the flow channels are adequate for working pressures up to 300 bar. Nevertheless, the optimal inlet-geometry for high pressure microreactors was found to be a tubular structure, etched with hydrofluoric acid and suitable for fibers with an outer diameter of 110 μm. These inlet/outlet geometries can withstand pressures up to at least 690 bar, which is the limit of the high pressure pump.

In Chapter 5 microfluidic high pressure microreactors were used to study fluid phase transitions in mixtures of 50%-50% carbon dioxide and alcohol (methanol and ethanol) under conditions near the critical point of the mixtures by means of optical microscopy. Very specific flow patterns were observed that can be attributed to a liquid-vapor phase transition. The set-up was used to determine phase diagrams of two different alcohol-carbon dioxide mixtures in an easy and fast way at pressures up to 140 bar. The obtained diagrams are in excellent agreement with data reported in the literature.

The esterification reaction of phthalic anhydride with methanol was performed in a continuous flow microreactor at pressures up to 110 bar and temperatures up to 100 °C as well as with supercritical CO_2 as a co-solvent. The results of this study, presented in Chapter 6, show that microreactors in continuous flow mode combined with pressure operation give rise to significant rate enhancements for this specific reaction. For example, a 53-fold increase was obtained at 110 bar and 60 °C, while using supercritical carbon dioxide as co-solvent yielded a 5400-fold increase, with respect to batch-experiments at 1 bar and identical experimental temperatures. The rate enhancement is mainly caused by the high velocity flow and the elevated pressures that improve the diffusive mixing of species in the microreactor. The unique properties of supercritical CO_2 in the microreactor substantially decrease the activation energy of the reaction, probably caused by a change in the reaction mechanism, thereby increasing the rate constant.

Chapter 7 describes a set-up to study organic reactions in continuous flow at pressures up to 150 bar, in which pressurized reagents can be introduced in the microreactor independently and/or simultaneously. This set-up was used to study the influence of pressure on the Diels-Alder reaction of cyclopentadiene with methyl-,

phenyl- and benzylmaleimide. The effect of pressure and/or the fast and efficient mixing of the reagents in the microreactor are believed to be the reasons for the 1.3-fold and 1.7-fold higher conversions, with respect to batch-experiments, for the reaction of cyclopentadiene with phenyl- and benzylmaleimide, respectively.

Chapter 8 deals with the fabrication of a microreactor with an integrated microcoil NMR for on-line NMR spectroscopic analysis (60 MHz NMR apparatus). The rate constant of the imine formation of the reaction of benzaldehyde and aniline was determined with this NMR microreactor operated in continuous flow mode, being 5.8×10^{-2} M^{-1} min^{-1}. This rate constant is slightly larger than in a conventional tube in a 400 MHz NMR spectrometer; both values are within the experimental error.

The mixing time in the microreactor was calculated to be approximately 2 s, while the reaction times can be set from 30 min down to only 0.9 s, therewith enabling monitoring of relatively fast reactions. This micro Total Analysis System (μTAS) is meant to be used for on-line monitoring of high pressure organic reactions. Preliminary pressure experiments revealed that the system functions very well for pressures up to 60 bar.

The advantages of microreactor technology for pressure chemistry are clearly demonstrated in this thesis. Organic reactions were successfully carried out at micro- to nanoliter scale at pressures up to 600 bar, thus safety regulations are not an issue anymore. The combination of pressure and the small characteristic dimensions of microreactors give rise to rate enhancements compared to conventional batch operation. In addition, on-line detection techniques like NMR and UV-Visible spectroscopy were successfully incorporated in the microreactors, resulting in the development of a μTAS.

Samenvatting

In dit proefschrift zijn de resultaten beschreven van de ontwikkeling en toepassing van 'lab-on-a-chip' systemen, microreactorchips, waarin chemische reacties onder (hoge) druk uitgevoerd kunnen worden onder stationaire condities of onder continue doorstroming van de reactanten.

In hoofdstuk 1 wordt een algemene introductie in hogedrukchemie gegeven en worden de basisaspecten van de 'lab-on-a-chip' technologie beschouwd.

In het algemeen worden hoge drukken gegenereerd in geavanceerde, dure en gesloten systemen. Het wordt beschouwd als een techniek waarvoor speciale apparatuur nodig is, waarbij strikte veiligheidsmaatregelen in acht genomen moeten worden. In hoofdstuk 2 is de miniaturisering van de hogedruktechnologie beschreven. Middels kleinere en draagbare systemen kunnen de veiligheids-risico's (gedeeltelijk) verminderd worden, en kan de 'performance' van hogedruksystemen vergroot worden door het integreren van geminiaturiseerde sensoren en actuatoren.

In hoofdstuk 3 wordt een microreactorplatform behandeld dat gebaseerd is op capillairen en dat is voorzien van fiberoptica voor 'online' UV/Vis spectroscopie. Met dit platform zijn voor verschillende drukken de reactiesnelheidsconstanten en activeringsvolumes bepaald van een nucleofile aromatische substitutie en een aza-Diels-Alderreactie. De invloed van druk op de omzetting en de stereoselectiviteit van de Diels-Alderreactie van 2- en 3-furylmethanol met methyl-, benzyl- en fenylmaleimide is tevens bestudeerd met ^{1}H-NMR spectroscopie. De silicafibermicroreactor is het eerste voorbeeld van een geminiaturiseerd platform waarin reacties 'online' gevolgd kunnen worden voor drukken tot 600 bar.

Het ontwerp, de fabricage en de 'performance' van een aantal op fibers gebaseerde "in-het-vlak" verbinding geometrieën voor glazen microreactorchips voor hogedrukchemie worden behandeld in hoofdstuk 4. De 'yield strength', gedefinieerd als de maximale druk die de verbinding kan weerstaan, kan verhoogd worden door de

ruwheid van de zijwanden van gepoederstraalde geometrieën te reduceren met behulp van nat chemisch etsen met waterstoffluoride. Er is aangetoond dat kleine gepoederstraalde ingangen/uitgangen (geschikt voor fibers met een buitendiameter van 110 μm) waarvan de zijwanden behandeld zijn met waterstoffluoride en met een scherpe overgang naar het vloeistofkanaal toereikend zijn voor werkdrukken tot 300 bar. Echter, de optimale ingangsgeometrie voor hogedrukmicroreactoren is een buisvormige structuur die volledig geëtst is met waterstoffluoride, en die geschikt is voor fibers met een buitendiameter van 110 μm. Deze geometrie kan drukken weerstaan tot minimaal 690 bar, de maximale druk die de gebruikte hogedrukpomp kon leveren.

De microfluidische hogedrukmicroreactoren zijn gebruikt voor het bestuderen van faseovergangen. In hoofdstuk 5 worden de resultaten beschreven van 50%-50% mengsels van koolstofdioxide en alcohol (methanol en ethanol) voor condities nabij het kritische punt van de mengsels, en welke verkregen zijn middels optische microscopie. De waargenomen stromingspatronen zijn zeer kenmerkend/specifiek en kunnen toegeschreven worden aan een vloeistof-gas faseovergang. De opstelling is gebruikt voor het op een snelle en veilige manier bepalen van de fasediagrammen voor twee verschillende alcohol-koolstofdioxide mengsels voor drukken tot 140 bar. De verkregen diagrammen komen zeer goed overeen met data uit de literatuur.

De veresteringsreactie van ftaalzuuranhydride met methanol is uitgevoerd in een microreactor voor drukken tot 110 bar en temperaturen tot 100 °C onder condities van continue stroming van de reactanten, en tevens met superkritisch koolstofdioxide als oplosmiddel. De resultaten, beschreven in hoofdstuk 6, tonen aan dat in microreactoren de combinatie van continue stroming van de reactanten en hoge druk voor deze specifieke reactie leidt tot een significante toename van de reactie-snelheidsconstanten. Bijvoorbeeld voor een druk van 110 bar en een temperatuur van 60 °C is de toename in reactieconstante een factor 53; deze factor is 5400 bij het gebruik van superkritisch koolstofdioxide als oplosmiddel (berekeningen ten opzichte van 'batch'-experimenten uitgevoerd bij een druk van 1 bar en een identieke temperatuur). Deze toename in reactieconstanten is voornamelijk het gevolg van de hoge stromingssnelheden en de verhoogde druk: deze twee aspecten verbeteren het diffusieve mengen van de reactanten in de microreactor. Bij het gebruik van super-

kritisch koolstofdioxide in de microreactor dragen de unieke eigenschappen van superkritisch koolstofdioxide wezenlijk bij aan het verlagen van de activeringenergie van de reactie. Dit laatste is mogelijkerwijs het gevolg van een verandering in het reactiemechanisme, met als gevolg dat de reactieconstanten toenemen.

In hoofdstuk 7 wordt een opstelling beschreven die gebruikt kan worden voor het onderzoeken van organische reacties onder continue stromingscondities voor drukken tot 150 bar. In de opstelling kunnen reactanten onafhankelijk en/of tegelijkertijd onder druk in de microreactor worden gepompt. Met deze opstelling is de invloed van druk op de Diels-Alderreactie van cyclopentadieen met methyl-, fenyl- en benzylmaleimide onderzocht. Voor de laatste twee reacties werd een toename in omzetting gevonden van respectievelijk 1.3 en 1.7 in vergelijking met 'batch'-experimenten. Dit kan toegeschreven worden aan de druk en/of het snel en efficiënt mengen van de reactanten in de microreactor.

In hoofdstuk 8 wordt de fabricage van een microreactor met een geïntegreerde microspoel voor 'online' NMR spectroscopische analyse behandeld (60 MHz NMR apparaat). De snelheidsconstante van de iminevorming van de reactie van benzaldehyde met aniline is met deze NMR microreactor bepaald voor continue stroming van de reactanten en bedraagt 5.8×10^{-2} M^{-1} min^{-1}. Deze constante is iets hoger in vergelijking met de reactie in een NMR- buis in een 400 MHz NMR spectrometer.

De mengentijd is ongeveer twee seconden en de reactietijd kan worden ingesteld van 30 minuten tot slechts 0.9 seconden; het is dus mogelijk om relatief snelle reacties nauwkeurig te volgen. Het is de bedoeling deze μTAS te gaan gebruiken voor het 'online' onderzoeken van organische reacties onder hoge druk. Met behulp van een serie inleidende experimenten is aangetoond dat het systeem goed functioneert voor drukken tot 60 bar.

In dit proefschrift is duidelijk aangetoond dat microreactortechnologie vele voordelen heeft voor het uitvoeren van hoge druk chemie. Een aantal organische reacties is met succes uitgevoerd voor drukken tot 600 bar in volumes in het gebied van microliters tot nanoliters, waarbij veiligheidsmaatregelen geen probleem meer zijn. De combinatie van druk en de kleine karakteristieke dimensies van microreactoren leidt tot toename van de reactiesnelheidconstanten in vergelijking met die bepaald in

conventionele apparatuur. Tevens zijn 'online' detectietechnieken zoals NMR en UV-Vis spectroscopie geïntegreerd in de microreactoren, resulterend in de ontwikkeling van een geminiaturiseerd Totaal Analyse Systeem (μTAS).

Resumen

En esta tesis se investiga la fabricación de microreactores diseñados para llevar a cabo en su interior reacciones químicas a alta presión en condiciones de flujo continuo.

El Capítulo 1 es una introducción al concepto de alta presión aplicado a la química, así como a los principios de la tecnología lab-on-a-chip.

Habitualmente, alta presión es generada en sofisticados, caros y casi exclusivamente sistemas cerrados. Se considera como una técnica que requiere equipamiento especializado y que necesita estrictas medidas de seguridad. En el Capítulo 2, alta presión se presenta en su camino a la miniaturización. Se enfatiza el potencial y las posibles ventajas que tienen nuevos sistemas más pequeños y portátiles; los cuales no sólo permiten disminuir las medidas de seguridad, reducen costes y materiales, sino que además mejoran las prestaciones del sistema a alta presión gracias a la integración de pequeños actuadotes y sensores.

En el Capítulo 3 se muestra un microsistema para alta presión, basado en un capilar (de vidrio) conectado a un sistema de fibras ópticas para análisis de reacciones químicas en tiempo real, con espectroscopia UV / Visible. Con este microsistema se determinaron, las constantes cinéticas y los volúmenes de activación de diferentes substituciones nucleofílicas aromáticas, así como de una reacción aza-Diels-Alder, a diferentes presiones. En el mismo capítulo se incluye el estudio, por espectroscopía de RMN, del efecto de la presión en la conversión y en la estereoselectividad de la reacción de Diels-Alder, entre 2- o 3-furilmetanol con metil-, bencil- y fenilmaleimida, llevada a cabo en dicho capilar. Este microsistema, un simple capilar de vidrio, es el primer ejemplo en literatura que permite monitorizar a tiempo real una reacción química que tiene lugar a una presión de 600 bares a microescala.

El diseño, la fabricación y la evaluación de diferentes geometrías, que darán lugar a la fabricación de microreactores para el estudio de reacciones químicas a alta

presión se describe en el Capítulo 4. La resistencia que opone cada geometría a la presión, puede ser mejorada reduciendo la rugosidad de la superficie de los canales, gracias al uso de la técnica conocida como "powderblasted" en combinación con el uso de ácido fluorídrico. En este Capítulo se investiga la fabricación de las entradas y salidas del microreactor, adecuadas para fibras de 110 μm. Se ha demostrado que la fabricación de dichas entradas (en el mismo plano que los canales), mediante la técnica de "powderblasted", con una geometría terminada en pico y con un posterior tratamiento de éstas con ácido fluorídrico, permite que estos microreactores puedan trabajar a presiones de hasta 300 bares. Aún así, los mejores resultados fueron obtenidos con geometrías circulares, validas para fibras de 110 μm, creadas con ácido fluorídrico. Estas geometrías pueden resistir presiones de más de 690 bares, siendo este el límite del sistema de presión utilizado.

En el Capítulo 5 microreactores para alta presión se utilizaron para el estudio de transiciones de fase de mezclas 50% - 50%, de dióxido de carbono líquido y alcohol (metanol o etanol) en condiciones de presión y temperatura cercanas al punto crítico de la mezcla, usando microscopia óptica. Patrones específicos fueron observados y caracterizados como transiciones de fase líquido-gas. El sistema fue utilizado para determinar diagramas de fases de mezclas de dos componentes como metanol - dióxido de carbono líquido y etanol - dióxido de carbono líquido a presiones de hasta 140 bares. Los diagramas obtenidos coinciden exactamente con los diagramas de publicados previamente en literatura.

El microreactor descrito en el Capitulo 5 se utilizó para el estudio de la reacción de esterificación del anhídrido phtálico con metanol a presiones de hasta 110 bares y temperaturas de hasta 100 °C. La mismas reacción fue también llevada a cabo usando dióxido de carbono supercrítico ($sc CO_2$) como co-disolvente. Los resultados de este estudio, presentados en el Capítulo 6, muestran que microreactores en flujo continuo combinados con elevadas presiones incrementan significativamente la cinética de la reacción. Por ejemplo, se ha observado que la cinética de la reacción se incrementa unas 53 veces a 110 bares y 60 °C, mientras que usando $sc CO_2$ el incremento es de unas 5400 veces, comparando los resultados con los valores a 1 bar a las mismas condiciones de temperatura en un sistema convencional. El incremento de los valores cinéticos es causado por las altas velocidades del flujo de fluidos en el canal a elevadas

presiones, las cuales mejoran la mezcla por difusión de los compuestos introducidos en el microreactor. Las propiedades únicas del *sc*CO_2 reducen significantemente la energía de activación de la reacción en el microreactor, probablemente este efecto es causado por un cambio en el mecanismo de la reacción, el cual incrementa la constante cinética.

El Capítulo 7 describe un nuevo sistema para estudiar reacciones orgánicas en flujo continuo y presiones de hasta 150 bares. En este sistema, los reactivos pueden ser introducidos y controlados independientemente o consecutivamente. Este sistema se ha utilizado para estudiar la influencia de la presión en la reacción de Diels-Alder del ciclopentadieno con metil-, bencil- y fenilmaleimida. El efecto de la presión y / o de la rápida y eficaz mezcla de los reactivos en el microreactor se cree que es la causa por la cual se han observado conversiones 1.3 y 1.7 veces mayores, comparando estos resultados con experimentos fuera del microreactor, para la reacción del ciclopentadieno con fenil- y bencilmaleimida respectivamente.

El Capítulo 8 describe la fabricación de un microreactor con bobina integrada para el estudio en flujo continuo de reacciones químicas mediante espectroscopía de RMN (en un instrumento de 60 MHz). La constante cinética de la formación de la imina, desde el benzaldehído y anilina, fue determinada con este RMN-microreactor operando en flujo continuo, siendo 5.8×10^{-2} M^{-1} min^{-1}. Esta constante es algo mayor que la determinada en un espectrómetro de RMN (400 MHz).

El tiempo de mezcla en el microreactor fue calculado en 2 s, mientras que los tiempos de reacción pueden ser variados desde 30 min hasta 0.9 s, siendo posible el monitorizar reacciones relativamente rápidas. Este "micro Total Analysis System" (μTAS) ha sido construido con la intención de llevar a cabo en él reacciones químicas a alta presión. El examen preliminar del sistema, a elevadas presiones, muestra que se puede trabajar con él a una presión de hasta 60 bares.

En esta tesis se demuestran claramente las ventajas del uso de la tecnología de microreactores en química a alta presión. Diferentes reacciones orgánicas han sido llevadas a cabo con éxito a micro- y a nanoescala, a presiones de hasta 600 bares, donde las medidas de seguridad ya no son necesarias. La combinación de la alta presión y las características pequeñas dimensiones de los microreactores, dan lugar a

incrementos del los valores cinéticos de las reacciones, en comparación con experimentos llevados a cabo en sistemas convencionales. Además, sistemas de análisis a tiempo real como espectroscopías de RMN y UV-Visible han sido incorporadas con éxito en los microreactores, dando lugar al desarrollo de un completo μTAS.

Acknowledgments

It is an incredible sensation that I have today… I am writing the acknowledgments!!!! (Even though this is a word that I have to check twice to be sure that I have written it correctly). Wikipedia, in its first denotation defines this word as follows: "*a statement of gratitude for assistance in producing a work*". Therefore, I would like to express here my sincere gratitude to all the people that have made this thesis possible in by both, assisting me on my work and supporting me during my free time.

My love story with SMCT began more than four years ago in Madrid, when I decided to start a new Ph.D. project abroad. Thanks Lourdes for sending me information on an available position at your group (SMCT…of which I had never heard about before). I read about the group and about the project and it seemed very interesting, "High Pressure Organic Chemistry in Microreactors" (what a name!) Although I wondered what could an Inorganic Chemist offer to such a challenging project. I am greatly indebt to my Spanish supervisors at Universidad Autónoma de Madrid, Dr. Rosa María Medina and Dr. María José Macazaga for all their support and help at that time. If it had not been for you, I would have never made such an important step in my life. Muchísimas gracias, he aprendido mucho con vosotras. I also would like to thank here everyone who worked with me at the inorganic department and in particular those who are still in contact with me offering their friendship: Avi, ¡casi terminamos la tesis el mismo año ☺!, Lola, cómo lo pasabamos en el "labo" disfrazando al santo, y Ana, con una eterna sonrisa pese a las adversidades.

I sent my CV to SMCT and two weeks later I was at the Universiteit Twente for a job interview. Ohh Wim, it was so difficult to understand you!... But I can not even imagine how difficult it was for you to understand me☺. Thanks to Monica, who told me *-don't worry Fernando, I studied Food and Science Technology and now I am doing lab-on-a-chip, you will also be able to do it!-*, all my fears faded, and when Wim and David said yes to me so did I. I accepted the position and since that day I became a SMCT member.

David you have always told me -*Fernando, you can do everything you want!* -but for a Spanish person like me, it was difficult to assimilate the real meaning of *everything*. My beginning was very hard and my progress was slower than it was expected for such a challenging project; nevertheless, you believed in me and in my project (sometimes even more than I did). Thank you very much for a lot of scientific discussions and for pushing me with -*and now? What is the next thing you want to do?* - Once I learnt what the meaning of *everything* was, I used it. However, in the end, it was hard to cover *everything* we did under the same thesis title. -Do you remember what you told me fifteen days before submitting my concept thesis? -Fernando, *Chapter 8 has nothing to do with your thesis, put it as an appendix!* -You almost killed me. Luckily we could work it out. Hartelijk bedank David for the opportunity you gave me to be part of such a magnificent group. I really appreciate the way the group is structured and all the freedom you have given me to perform my research.

Beste Wim, ik probeer het dankwoord voor jou in het Nederlands te zeggen. Het was een grote uitdaging en moeilijk om met jou te werken; zowel jij als ik hebben een sterk temperament, dus wij altijd veel discussie, maar uiteindelijk vormen we een goed team. Ik wil je bedanken voor de samenwerking van de afgelopen vier jaar en ook voor het consciëntieus corrigeren van mijn artikelen en thesis hoofdstukken.

This project was written for two Ph.Ds. one should work at SMCT and other one at BIOS-The lab on a chip group. Dear Masaya (crazy scientist!), we worked together during the first year in very close collaboration. Sometimes you drove me crazy with your new ideas and broken chips. I have learnt very much from you. It was a real loss when you decided to leave the group. Thank you for all the time together and as well for all your help in Chapter 3 and 4.

After Masaya left, I was waiting for a new partner for the project. During that time I met Henk Wensink at the MESA+ day and I proposed to him -*why don't we do on-line reaction kinetic on your NMR-chip?* -David said, "*everything"*, so, -let's work on that! It was very exciting to work with you. We did a very nice job together; we did a Lab on chip! and fortunately that work became my Chapter 8. I thank here Rob Duwell for helping us with the chip-holder and Dorothee Hermes for the fabrication of the new chip generation (sorry but we couldn't use them yet).

Unfortunately, as it happened to me before, I lost my project partner, Henk decided to leave. -what to do next? – I wondered. Then EdwinO, who has been always involved in the project, decided to fabricate the first functional high pressure chip. Only 110 bar was not enough pressure, nevertheless 110 bars is enough pressure to do supercritical fluids! David said "*everything"*, so -let's work on that! -It was so exciting when we saw the first phase transition in the chip, unforgettable. Thank you very much for your help in Chapter 4 and 5 and thanks for listening to me when the work was not going as expected. After a few months working together… EdwinO also left me ☹ …-what to do next?

Lucky me, soon after Roald Tiggelaar came across. The last two years of my Ph.D. could not have been possible without his help. Roald, you gave my hopes back; thanks to you I still love research. I think we made the perfect team, Netherlands and Spain together for ever! You are a very good scientist and a better friend. I am very proud of having you as a friend. Scientifically speaking, I thank you for the work done in Chapter 4, 5, 6 and 7, the correction of my thesis (our thesis ☺) and the never-ending scientific discussions in front of the microscope at BIOS, it was very funny.

I also would like to thank Han Gardeniers for being always there for a scientific discussion and for all his help during these four years. You take care of your Ph.Ds. and also of me. Personally, I considered you as the perfect staff member but luckily University of Twente considered you as a perfect Professor, Congratulations!

From the BIOS I would also like to thank Professor Albert van den Berg, for giving me all the freedom to be in his group. Albert, I considered myself part of your team. I would like to thank Helmut Rathgen and Frieder Mugele from Physics of Complex Fluids for their help in Chapter 4.

I would like to thank to all my STW committee members for all their good tips and support during the pass four years. To have an industrial point of view of the situation has helped me a lot in my research.

Coming back to SMCT, more people were involved in the pressure project. Richard thanks for your help during these four years. You helped me every time with my continuous computer problems (we drove the SGA crazy many many times, didn't we?) You were my personal psychiatrist, cooling me down before going to Wim. Thanks to Kasia Salbut my Socrates student; you did a great job in Chapter 6, in four month you did a lot of work! David Veurink (the talking driller), Hugo Renkema (NMR guy) and of course Steven Kettelarij. Steven, you were an incredibly good student, independent and precise; Chapter 7 exists thanks to you.

But what is a lab-on-a-chip guy without a team? At SMCT the lab-on-a-chip people are special. We are doing something completely different than the rest of the group and we are always going away to BIOS, to the clean room… (poor Wim!) We are a family inside another family. We have always helped and supported each other, making our own "illegal" group meetings in the corner of the lab. Monica, you were the first and the leader of the team. I deeply thank you for all your help and kindness. You were my guardian angel. Menglin, you could not make it. I was sorry to see an extremely intelligent person and a very good friend leaving us to make a new life in Denmark. I hope all your dreams and wishes come true. Kristianto, also gone, I wish you good luck in Indonesia. And also to Francesca, a cyclone in the lab; good luck! You will make it. But I recommend you to drink a lot chamomile during the last year of your Ph.D.

The technical work could not be possible without the help of some of our technicians, Marcel and Tieme, my volleyball mates. At the end I was not such bad player, was I? (¡¡Aunque nadie lo crea, he hecho deporte aquí y todo!!) Tieme, it has been very funny to work with you at the mass spectrometry room. We laughed a lot during Mr Ikami visits. Marcel you have been always there smiling and willing to help me every time, thank you.

A good working atmosphere is essential (it is said by the people how know about working conditions). In my lab, the 2701, the conditions were perfect because of the people who worked there. We had a lot of fun. Thanks to Monica Che palle Brivio (Grazie per aver corretto la mia tesi), Menglin, Richard (once upon a time in the SMCT…), Christiaan, Christian, Jurien, Olga (se me nota, se me nota?) It has been a real pleasure to be you, although the tights almost killed me. Michel (te quiero tío pero…I don't need you anymore!!!), Mattijs (Matias, the borrels left with you), Jessica, Kim, Francesca, Kristianto, Huub, Steven, David, Amela (I made you believe I was able to speak in Dutch, ah ah ah!!), Gena, Alart (do not accept a dropje from him, disgusting!), Paolo and many others.

This good atmosphere is also present in the other labs and of course during the coffee breaks and lunches. Thanks to Emiel (Emilio, you are a good friend and the only one who made my mum cook vegetarian; now she knows that tuna is not consider vegetarian food, bedank voor mij proefschrift corrigeren), Marta (la Reinoso!) and Francesca (mi araña favorita) it was very nice the time

we spent together inside and outside the labs. Soco (pura energía y alegría en el bar), Rob (together we are the best "deejays" in town), Xing-Yi (¿por qué?) and InnYee (you are my favorite borracho) phenomenal people and great friends. Deborah (sorry, I did not mean what I said to you, I was learning Italian ☺); Pascale, together with Manon and Menglin formed the "SMCT Charlie Angels". Tommaso Auletta, we had too much fun during Juanjo's wedding -¡*se le ve el pavo*!, -Andrea (our first SMCT-production), Choon Woo, Tian, András, Dorota (aha!) and Barbara (la aguela).

Alessio, Henkino and Marloes (friends forever, we enjoyed a lot the parties in Santa Cruz del Retamar). Sachin, Becky (very understanding and willing to listen), Dominik, Wojciech, Mrinal, Fijs (thanks for mentioning me in your acknowledgments). Juanjo and Floren (what a weeding!), Maryana, Hans (Hansito, you are always ready for a bierje); Veera, Janet (super smile-girl), Xuemei, Duan, Elisabetta, Roberto Fiammengo (sei sempre disposto a sciare con noi). Ricardo, Alberto, Shu-Han (the beamer), Srinidhi, Albert (uomo megafono), Chien-Ching, Moira, Oktay, Umbretta, Fabio, Marco, Maria Peter, Ruben, Joris, Frederieke, Steffen, Jurjen, Martine (the duck you prepare is delicious, sigue hablando en español que lo haces genial), Laura, Rolf, Victoria (¡viva Castilla la Mancha!), Huaping, Ben, Bianca… I am sure I forgot somebody, sorry about that.

One amazing thing at SMCT is that fun does not only come from the Ph.Ds., Post Docs or students. We have incredible staff members ready for parting any time, but at the same time always willing to help you unconditionally. I want to thank specially Jurriaan, who has always has had time to answer my questions and even to correct my thesis. Thank you for being part of my committee and showing me that Brand beer is also an option. Merce muchas gracias por escucharme cuando lo necesitaba, darme apoyo moral para continuar en los momentos duros y por cuidar tan bien de mi niña. Aldrick and Bart Jan, you made the work-weeks unforgettable. Thanks to Roel Fokkens who helped me a lot during the first month at SMCT, it is a pity that he disappeared for ever from one day to the other.

For such an important group, one secretary is not enough, SMCT has had three! Carla, Marieke and Izabel. You helped me a lot with the bureaucracy. You made me feel that a simple Ph.D. can have a secretary! Especial thanks to Izabel, who has helped me with all the thesis papers and calls without losing her smile.

But SMCT did not offer me only science and research, here I have found very good friends as well. I would like to thank Miko Faccini for all the enjoyment we had together. Since the day I met you with "il salame" and the "caracoles" I knew we would be good friends. Querida Olgueta…cuando estabas en tu Sabadell profunda nunca hubieras pensado que tendrías un amigo Madrileño verdad?, pues aquí lo tienes y para sempre; gracias por escucharme cuando lo necesitaba. Caro Alessio, we have many things in common: we met each other during our interviews and then we arrived at the same time to the group. Later we went to live to the same house. Our characters are similar and we both enjoy and make fun of everything, nevertheless there is a big difference between you and I… AGE!! ☺ …Sei il mio fratello italiano. Sono orgoglioso e mi sento fortunato di essere tuo amico. Voglio

ringraziare tutta la tua famiglia perché mi sono sentito uno di voi ogni volta che sono venuto a Roma. Michel amazingly funny man!!!, en Enschede has sido mi confidente y amigo, me has ayudado siempre y lo hemos pasado genial; wij kleuren de stad!! ¡Qué sepas que solamente he hecho el ninya contigo, con nadie más! Marina, siempre te recordaré en Javastraat la noche de la promoción de Steffen, ese día pensé: ¡esta chica vale!! Por cierto… ¿cuándo vamos a ir a Argentina?

Marloes en Henkino zijn een erg speciaal stel voor me. Altijd was jullie huis voor me open net zoals jullie harten. Jullie zijn ongelofelijke vrienden van me. Ik hou van jullie jongens!

From BIOS I can not forget you Ana. Lo hemos pasado muy bien juntos, cenas, saliendo de marcha y cotilleando en la coffee room de BIOS. Neither could I forget some other BIOS and Mesofluidic members: Jan Eijkel, Erik Faber, Dragana, Anil, Jacob, Alfons, Wim, Séverine, Regina, Egbert, Paul, Jurjen, Erik Krommenhoek, Kevin, Floor, Vincent and Sebastiaan.

Many house warming parties, dinners and events in Enschede like Thursdays at the Beiaard, allowed me to know people from other groups, with who I have enjoyed a lot. Monique, Edi, la medimueta, Denis, Oya, Melba, Cristiano, Vittorio, Shanga-la-morte, Frederic, Monse, Joao, la carogna,… I especially would like to mention, Laura and Francesca Romana: eravate sempre disposti a fare una cena o una festa. Charu, I thank you for introducing me to hot spices and the Indian cuisine. Mónica y Marco siempre teníais un ratito para pasaros por la fiesta aunque vuestras agendas estaban mas ocupadas que las del presidente del gobierno. Marco, the Lord of the Rings marathondag was onvergetelijk. Bas, ik heb nog nooit iemand zoveel zien eten… aunque Yanina, ¡tú no te quedas corta!!

In Lipperkerkstraat there was a person who I would like to thank for being my flat mate for more than two years. Richard, it was great to live with you, I enjoyed a lot our afternoons on the sofa chatting and watching TV, do you remember the life of St. Maria Goretti?

But what is a Ph.D., in The Netherlands without trying to learn Dutch…how many of you have been 100% successful? I haven't sorry, maar Ik probeerde. Azita, together we were a good team, nevertheless an Iranian and a Spanish learning Dutch from an Italian was a little bit unconventional. Graziella, your Dutch lessons have been very helpful for me…at least I can talk with the CWI assistants.

Javastraat house is a place that I will never forget. There, we have enjoyed dinners, lunches, parties…and it is where I have spent the most of my free time (thanks to Lourdes of course ☺). From the earliest times I want to remember Maria Cadic and Irene Mazzitelli. Irene, conoscerti é stato un piacere. Sei divertente e molto pungente allo stesso tempo, come me… insieme a te ho riso tantissimo.

The writing period has been very stressful for me, I would like to thank my mates in room 1717 for the terrific moments we have had together. Kim (inaudible!), Christian (Kim is asking you not to me… thanks god!), Alessio (… Paris Hilton forever!!), Henkino (bachata is not Spanish music!!) and Manon (together we did the most amazing barbeque speech ever).

Henkino and Alessio thank you for being my paranimfen. Four years ago destiny joined us in room 1719 during our literature report period, only space will separate us in the future, our friendship is for ever.

Gracias a mis amigos de España, los cuales han estado siempre allí apoyándome, animándome cuando lo necesitaba y disfrutando conmigo al máximo el poco tiempo que pasaba con ellos. Mis amigas del pueblo Yoana y Pili (nunca me faltó un mailito tuyo cada semana, gracias de verdad). Mis compis del McDonalds, Noemí y Carol petándome el mail de porquerías. Del instituto Jorge y Minerva, amigos verdaderos. De la universidad, Almu (nuestras vidas han cambiado mucho desde aquel día en que nos conocimos, aún sonrío cuando lo pienso; pero nuestra amistad no cambiará jamás) Bea (que no me falte nunca tu mensajito cuando vuelvo a casa después de una noche de juerga) Miguel (siempre dispuesto a salir por ahí, disfruto mucho tu compañía) e Itxarín (¡¡qué decirte corazón!! Si estas más en Enschede que en Madrid…que regalo te hice con ese pedazo novio que te busque ☺). En mi barrio hay una familia a la que quiero agradecer lo bien que siempre me tratan cuando estoy allí, María Luisa, Alejandro, Raúl y Marta Sánchez Carrascalejo. Y como no, mi más sincera gratitud a mis mejores amigos, los que han estado en mi vida desde siempre, Iván y David. Sin vosotros esto no podría haber sido posible, os quiero chicos.

Lo más importante para mi ha sido, es y será siempre mi familia. Muchas gracias por todo el apoyo incondicional que me habéis dado durante estos cuatro años. Papas y tía, siempre con una gran sonrisa cuando llego y otra cuando me voy, se que es duro para vosotros, pero sabéis que es lo mejor para mi. A mi hermano, cuñada y mi queridísimo sobrinito, no sabéis lo mucho que disfruto el tiempo que pasamos juntos. Y como no, a mi cuñado y mi ¡¡¡hermaaaanaaaa!!! Deseando llegar a casa para ir de compras y charlar largo y tendido, realmente echo tanto de menos nuestros momentos. Esta tesis os la dedico a todos vosotros, sin vuestro cariño no hubiera sido posible.

El último párrafo de esta tesis esta dedicado a ti Lourdes. Amor, has estado junto a mi en todo momento. Me has apoyado en cada cosa que he decidido hacer y siempre has tenido un buen consejo o sugerencia que darme cuando lo veía todo negro. Esta tesis ha sido posible gracias a tu paciencia y serenidad, que me han iluminado hasta el final. Eres la persona mas especial que he conocido nunca. Gracias por ser como eres, por todo tu amor y cariño. Te quiero.

Fernando Benito López.

About the author

Fernando Benito López was born in Madrid, Spain, the 30th of May 1978. He studied chemistry at the Universidad Autónoma de Madrid (UAM) from 1996 till 2000. During that period he specialized in Inorganic Chemistry. In October 2000 he started his master thesis at the Inorganic Department of the UAM under the supervision of Dr. M. J. Macazaga Porlan and Dr. R. M. Medina Martinez on "Synthesis and Electrochemical study of Alkinyl Cobalt and Osmium Complexes". In September 2002 he finished his master thesis.

In October 2002 he joined the Supramolecular Chemistry and Technology group of Prof. Dr. Ir. David N. Reinhoudt at the University of Twente, the Netherlands, as a Ph.D candidate. The results of his research are described in this thesis.